

**MEMORANDO DE ENTENDIMIENTO ENTRE LA FREIE
UNIVERSITÄT BERLIN (FUB) ALEMANIA, EL ALFRED WEGENER
INSTITUT (AWI) POTSDAM (ALEMANIA), LA UNIVERSIDAD DE
GRANADA (ESPAÑA), Y EL INSTITUTO GEOLÓGICO Y MINERO
DE ESPAÑA PARA LA COOPERACIÓN EN EL DESARROLLO DE
TÉCNICAS DE HIDROLOGÍA ISOTÓPICA Y DE MODELIZACIÓN
HÍDRICA HIDROGEOQUÍMICA Y SU APLICACIÓN A LOS
ACUÍFEROS DE ANDALUCÍA.**

**INTERACTION BETWEEN SALT LAKE AND
GROUNDWATER. A HYDROGEOCHEMICAL,
ISOTOPEGEOCHEMICAL AND SEDIMENTOLOGICAL
STUDY IN FUENTE DE PIEDRA BASIN, SPAIN.**

*Revisado por C.M. Abreu el 20-12-07. Lo firmó J.C. Rubio pero ya no se
guardan en formato papel.*



MINISTERIO
DE EDUCACIÓN
Y CIENCIA



Instituto Geológico
y Minero de España



*Pasado por
C.M. Narrete el 20-12-07
que lo hizo hace tiempo J.C. Rubio al archivar, pero
ya no se archivan físicamente
en papel.*

INFORME	Identificación: DIRG - H - 002 - 07
	Fecha: 2007
TÍTULO	
MEMORANDO DE ENTENDIMIENTO ENTRE LA FREIE UNIVERSITÄT BERLIN (FUB) ALEMANIA, EL ALFRED WEGENER INSTITUT (AWI) POTSDAM (ALEMANIA), LA UNIVERSIDAD DE GRANADA (ESPAÑA), Y EL INSTITUTO GEOLÓGICO Y MINERO DE ESPAÑA PARA LA COOPERACIÓN EN EL DESARROLLO DE TÉCNICAS DE HIDROLOGÍA ISOTÓPICA Y DE MODELIZACIÓN HÍDRICA HIDROGEOQUÍMICA Y SU APLICACIÓN A LOS ACUÍFEROS DE ANDALUCÍA.	
PROYECTO	
INTERACTION BETWEEN SALT LAKE AND GROUNDWATER. A HYDROGEOCHEMICAL, ISOTOPEGEOCHEMICAL AND SEDIMENTOLOGICAL STUDY IN FUENTE DE PIEDRA BASIN, SPAIN.	
RESUMEN	
Se aporta numerosa información hidrogeoquímica, isotópica y sedimentológica en el marco de la relación Laguna salada de Fuente de Piedra acuífero que aporta agua a la Laguna.	
* Continuar al dorso en caso necesario	
Revisión	Autores: Christian Menz, Cord Fenk, A Pekdeger.
Nombre: Juan Antonio López Geta	
Unidad: Hidrogeología y Aguas Subterráneas	
Fecha: 2007	Responsable: Juan Carlos Rubio Campos

**INTERACTION BETWEEN SALT LAKE AND
GROUNDWATER –
A HYDROGEOCHEMICAL, ISOTOPEGEOCHEMICAL
AND SEDIMENTOLOGICAL STUDY IN FUENTE DE
PIEDRA BASIN, SPAIN**

**DIPLOMA THESIS
(DIPLOMARBEIT)**

AND

**GEOLOGICAL MAPPING
(GEOLOGISCHE KARTIERUNG)**



Submitted to:
Freie Universität Berlin (FUB)
Prof. Dr. A. Pekdeger

Submitted by:
Christian Menz
&
Cord Fenk

Berlin, February 2007

Resumen

Este estudio trata de la interacción entre lagos salados y las aguas subterráneas en ejemplo de la laguna de Fuente de Piedra, situada en Andalucía, sur de España. La cuenca de Fuente de Piedra constituye una cuenca cuaternario, endorreica y INTRAMONTAN. Con una extensión máxima de 13 km² y 148,5 km² de la cuenca hidrográfica la laguna es una de las mayores de Europa.

Abstract

The aim of this study is the characterization of surface water and groundwater interaction in the Fuente de Piedra Salt Lake and its environment. The Fuente de Piedra Basin is an intramontane, endorheic, Neogene Basin, located close to Antequera (Andalusia). The Lake shows a maximum flooding area of 13 km² and an appropriate catchment area of 148.5 km² and is one of the largest ephemeral salt lakes in Europe.

Karstification of Triassic evaporites lead to the development of the Fuente de Piedra Basin. Today the Triassic materials constitute the impermeable basement of the basin. Micocene sediments and Quaternary alluvial deposits form the main aquifer.

To identify interactions of surface and groundwater hydrogeochemical and isotopegeochemical investigations were realized by sampling of 18 wells and piezometers and of surface waters from 2004 to 2006. Samples were analysed for Na⁺, K⁺, Mg²⁺, Ca²⁺, Li⁺, Sr²⁺, Mn²⁺, Fe²⁺, Br⁻, Cl⁻, SO₄²⁻, NO₃⁻ (FU Berlin) and stable isotopes of H₂O (AWI Potsdam) and aqueous SO₄²⁻ (TU Freiberg). Additionally electric conductivity and temperature logs were recorded to detect salinity stratifications and their distribution and to characterize the spatial and seasonal variation of a transition zone between salt- and freshwater. Furthermore the distribution and character of lake sediments were investigated with regard to the extension of former lake stages. For this purpose an in situ sediment characterisation were realized for 28 borehole profiles with a mean depth of 5 m. The chemical analysis of sediments is the purpose of further investigations by FU Berlin and University of Malaga.

Recent lake deposits are dominated by grey clays with interbedded organic layers and gypsum crystals. In the northern lake vicinity these clays turn into red clays with an increase of interbedded sand layers to the edges. Mapping of lake sediments in the northern vicinity of the salt lake indicates a former lake terrace with differing sedimentation conditions and an additional extension of 2 km northwards.

For the salt lake and its proximate vicinity Na-Cl-type water are observed, whereas Ca-Cl-type water is dominating the eastern basin and indicate a salinisation of the aquifer by intruding salt water. Ca-HCO₃-type water is only observed at the north-eastern edge of the basin.

The spatial variability of evaporite deposits in the basin is as well represented in the hydrogeochemical conditions of the aquifer. Sediments and water chemistry are

significant varying for north and south/west lake edges and the development of a well-defined brine/freshwater transition zone is only observed in the northern lake vicinity.

A leaching of Triassic halite and gypsum as the main source for groundwater salinisation of the aquifer is suggested by ion ratio analyses of Cl^-/Na^+ and $\text{Cl}^-/\text{SO}_4^{2-}$. But also evaporative enrichment, observed due to Cl^-/Br^- ratios and isotope data, is supposed to be involved in the salinisation of the aquifer.

Super saturation of brines with Calcite, Dolomite and Magnesite within the maximum flooding area and at the south and north shore, is indicated by saturation indices, whereas gypsum precipitates only in shallow depths at the east shore of the lake.

Isotope signatures of H_2O show a strong evaporative trend for groundwater in the salt lake and the associated aquifer. Heavy isotope enriched groundwaters are observed below the lake and in greater depth beyond the lake edges and suggest a descent of brines originated at the lake surface. Furthermore a recycling of brines due to convection is indicated. Sulphate isotopes point to a leaching of Triassic evaporites as source of salinization.

Conductivities reach up to 205 mS/cm below the lake. Salinity stratification between high and low mineralized groundwater is developed below and around the lake. With decreasing distance towards the lake conductivity increases and the high/low mineralized groundwater transition zone is ascending. The distribution of conductivity shows the formation of a cone-shaped brine body beneath the Salt Lake. The salinity stratification and the position of the transition zone are developed in constant states as shown by EC-logs. Seasonal variation occurs partially and only in low depths.

Recovering times of salinity stratifications indicate a main groundwater inflow at the lake's eastern margin due to relatively good permeable sediments. Because of almost impermeable sediments (coefficient of hydraulic conductivity from 10^{-6} to 10^{-8} m/s) in the northern lake area and beyond, upraise of brines have to be slow and is supposed to be partly driven by diffusion.

Triassic evaporites situated towards the north-eastern basin edge are supposed to be the source of the initial salinisation of the aquifer. A hydraulic closed basin and high evaporation rates caused a predominantly reprecipitation and deposition of evaporite sediments in the northern part of the lake. This is indicated by greater sediment thicknesses. Due to density driven flows a recycling of brines and their intrusion into the eastern basin is observed.

Acknowledgement	1
Abstract	2
List of Figures	6
List of Tables	9
1 INTRODUCTION	10
1.1 Research Framework	10
1.2 Endorheic basins and Salt lakes in General (CM)	10
1.3 Study site	14
1.3.1 Location and history of the natural reserve (CF)	14
1.3.2 Geomorphology and catchment area (CF)	16
1.3.3 Geology (CM/CF)	17
1.3.4 Climate and Hydrology (CF)	28
1.3.5 Hydrogeology (CF)	36
1.3.6 Water supply (CF)	37
1.3.7 Previous studies in Fuente de Piedra Basin (CF)	38
1.4 Topics and aims of this study	42
2 MAPPING	44
2.1 Methods	44
2.1.1 Definition of mapping area (CF)	44
2.1.2 Drilling network (CM)	47
2.1.3 Borehole drillings (CM)	47
2.1.4 Sediment characterization (CM)	49
2.1.5 Sediment analysis (CM)	50
2.2 Results	54
2.2.1 Sediment characterization (CM)	54
2.2.1.1 Borehole logs (CM)	54
2.2.1.2 Cross sections (CF/CM)	71
2.2.1.3 Relation to stratigraphic units (CF)	77
2.2.1.4 Stages of lake development (CM)	77
2.2.1.5 Proveniences (CF)	79
2.2.2 Sediment analysis (CF)	80
2.3 Conclusions	84
3 DIPLOMA THESIS	85
3.1 Basic Principles and methods	85
3.1.1 Hydrogeochemistry	85
3.1.1.1 Sampling network, campaigns and parameters (CF)	85
3.1.1.2 Sampling methods (CF)	85
3.1.1.3 Laboratory analytical methods (CM)	88
3.1.2 Basic Principles	92
3.1.2.1 Hydrochemistry (CF)	92
3.1.2.2 Stable isotopes (CM)	102
3.1.3 Constructing monitoring wells - multilevel piezometer (CM)	109
3.1.3.1 Levelling (CM)	109

3.1.4 Hydraulics	110
3.1.4.1 Piezometer network (CM)	110
3.1.4.2 Freshwater head and salt correction (CM)	111
3.2 Results	112
3.2.1 Hydrogeochemistry	112
3.2.1.1 Major and minor ions (CF)	112
3.2.1.2 Temperature logs (CM)	134
3.2.1.3 Electric conductivity logs (CF)	136
3.2.2 Stable isotopes	139
3.2.2.1 H ₂ O isotopes (CM)	139
3.2.2.2 Sulphate isotopes (CM)	144
3.2.3 Hydraulic pattern (CM)	145
3.3 Conclusions	148
4 FUTURE PROSPECTS	150
Abbreviations	151
References	152

5 APPENDIX

- I. Tables (CF)
- II. Location register (CM)

Author:

CF – Cord Fenk

CM – Christian Menz

5. Appendix

I

- Table A1: Monthly mean temperature in [°C] at la Herriza. Grey shaded data is completed by correlation with data from Bobadilla (LINARES, 1990; IGME, 2001). Mean-, max- and min-values are calculated without completed data.
- Table A2: Monthly mean precipitation in [mm] at la Herriza. Grey shaded data is completed by correlation with data from Bobadilla (LINARES, 1990; IGME, 2001). Mean-, max- and min-values are calculated without completed data.
- Table A3: Monthly mean Evapotranspiration (Thornthwaite method) in [mm] at la Herriza. Grey shaded data is calculated with completed data from Bobadilla. Mean-, max- and min-values are calculated without completed data.
- Table A4: Monthly mean Evaporation in [mm] at la Herriza (Piché-type atmometer) (IGME, 2001).
- Table A5: Monthly mean temperature in [°C] at Bobadilla estación (ALMECIJA RUIZ, 1997).
- Table A6: Monthly mean precipitation in [mm] at Bobadilla estación (ALMECIJA RUIZ, 1997).
- Table A7: Monthly mean Evapotranspiration (Thornthwaite method) in [mm] at Bobadilla estación.
- Table A8: Monthly mean Evaporation in [mm] at Bobadilla estación (Piché-type atmometer) (LINARES, 1990).
- Table A9: Basic data of the sampling sites. Altitude reference - L: leveling; RL: relative leveling to neighbored piezometer/well; I: IGME reference height; M: estimation by topographic map 1:10 000.
- Table A10: Hydraulic heads, freshwater heads and vertical flow gradients for sampling campaigns 2005 and 2006.
- Table A11: Levelling of piezometers and drillings in Fuente de Piedra Basin.
- Table A12: Density calculation after McCain (1991).
- Table A13: Sieving and sedimentation data.

II

1. Location registers of sampling sites
 - Field site data
 - Field master data
 - Borehole profiles (construction schemes)
 2. Borehole profiles of drilling sites
-

1. Introduction

1.1 Research Framework

This diploma thesis was carried out within the scope of a cooperation between the University of Granada, Spain (Universidad de Granada), the Geological Survey of Spain (Instituto Geológico y Minero de España) the AWI Potsdam (Alfred-Wegener-Institut Potsdam) and the Free University of Berlin (Freie Universität Berlin).

1.2 Endoheric basins and Salt lakes in general

Salt lakes generally appear in arid climes like subtropical and polar regions of our planet (Fig. 1.1).

The normal spread of Salt lakes is situated around the desert belts of the Northern and southern hemisphere (STRAHLER & STRAHLER, 1994).

After HOLZBECHER (2005) the occurrence of Salt lakes in arid regions requires certain conditions:

- 1) A closed basin. Saline lakes are defined by endoheric drainage basins, which originated often in relation to karstic structures.
- 2) Arid climatic conditions induce high potential evaporation and result in a negative climatic balance.
- 3) A permanent water flux. (Water supply by sufficient precipitation and/or percolating groundwater).

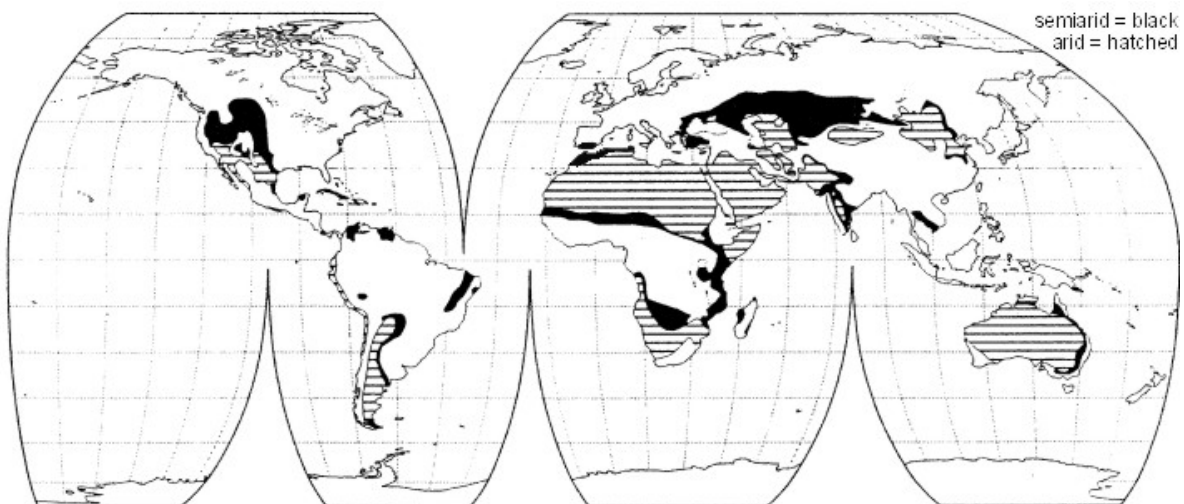


Figure 1.1: Arid and semiarid areas (saline systems) on earth (modified after STRAHLER & STRAHLER, 1994).

Playa lake systems develop in arid to semi-arid climates, where water tables are very close to the surface. High evapotranspiration causes groundwater to be evaporated through the thin unsaturated zone, forming highly saline brines beneath the surface

of the Salt lakes (LE GAL LA SALLE ET AL., 2006). Upward groundwater flow stabilizes the dense brines formed near the surface in closed basins, or causes instability and sinking of brines, if regional groundwater systems are associated. (LE GAL LA SALLE ET AL., 2006)

On closer examination, two main types of Salt lakes can be distinguished for their attributes: The perennial and the ephemeral salt lake (FÜCHTBAUER, 1988).

The perennial salt lake is mainly supplied by rivers and precipitation and rarely by groundwater. This type of Salt lake tends to be deeper than ephemeral lakes and therefore underlie only episodic dry outs. Due to water supply by rivers and precipitation sedimentation is characterized by interbedded evaporites and clastic materials, developed as varves. The development of a "tear drop" zoning of evaporites is given for Salt lakes supplied by single influx (FÜCHTBAUER, 1988).

Ephemeral Salt lakes are characterized by lower depths and yearly episodic dry outs. The terms playa, playa lake and sabkha are often used in this context. After BRIERE (2000) a playa is a discharging intracontinental basin with a negative water balance (remaining dry 75% of the year), often associated with evaporites and equivalent to a continental sabkha. Playa Lakes are essentially termed as flooded playas. For one thing periodic flooding due to strong rainfall events provides the lakes water supply. For another the lake can be supplied by groundwater rise. After FÜCHTBAUER (1988) episodic flooding conditions a bisection of sedimentation area. Lateral distributed bedded evaporites (salt pan) in the center in contrast to fine grained clastic materials in the marginal (external) area. For groundwater supplied salt lakes a bull eye zoning of evaporites is occurring as shown in Fig. 1.2.

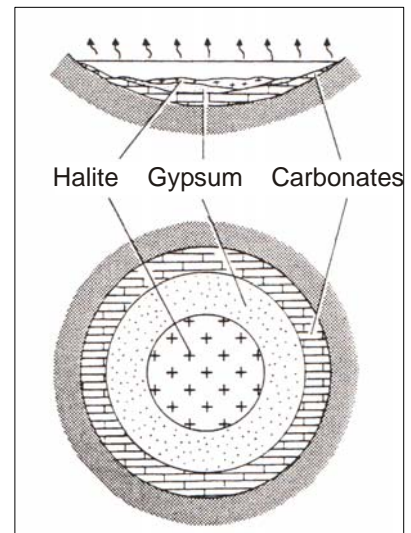


Figure 1.2: Bull eye structure (modified after FÜCHTBAUER, 1988).

YECHIELI & WOOD (2002) is giving a review of water and solute fluxes in saline systems based on a conceptual model of a coastal sabkha. The model indicates local rainfall as the main source of water in saline systems, whereas upward flux of groundwater from underlying formations is expected as the major source of solutes. For hydrological closed systems the solute composition of the brine depends largely on the composition of the input water. Seasonal changes in temperature and a loss

of moisture due to evaporation in the unsaturated zone are the decisive parameters controlling the precipitation of minerals. Because the suite of minerals and their relative abundance are depending on the leakage of the brine, the distinction of hydrological open and closed systems is evident.

After YECHIELI & WOOD (2002) following factors can affect the chemistry and mineralogy in playas: (1) the recycling of brines (Fig. 1.3) where they gravitate at the centre of the playa as a result of evaporation and ascend at the playas margins (SMOOT & LOWENSTEIN, 1991). While recycling of brines changes the salt composition due to the

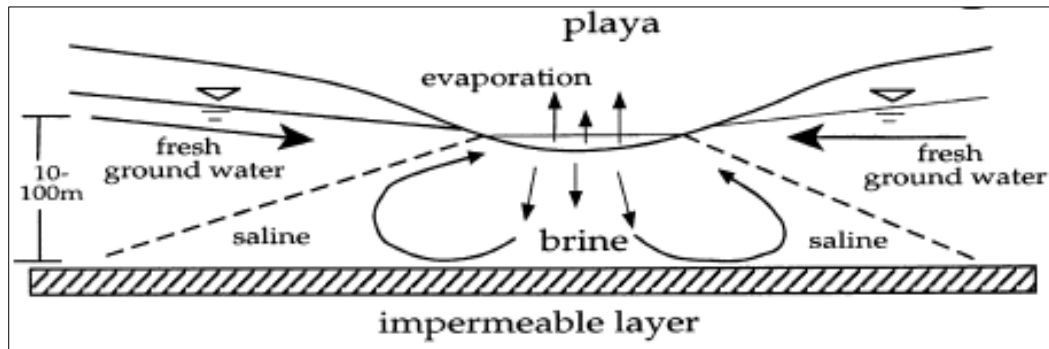


Figure 1.3: Schematic cross-sections of a playa lake showing the flow regime and the recycling of the brines (YECHIELI & WOOD, 2002).

precipitation of various salts, it does not affect significantly the general water and solute balance of the playa, it; (2) water–rock interaction, which affect the chemistry but will not increase the salinity significantly; and (3) geothermal fluids which may ascend from great depth.

In general, the basic relationship between fresh groundwater and saltwater is defined by the approximation of GHYBEN (1889) and HERZBERG (1901). YECHIELI & WOOD (2002) assumes a shallower position and slope of the fresh/brine water interface relative to the fresh/seawater interface because of the greater density difference between the fresh/brine water bodies.

FAN ET AL. (1997) investigate the groundwater processes of closed basins and the significance of free convection and the conditions when it occurs. For the Great Basin (USA) they ascertain, that besides diffusion as the dominant solute transport mechanism, also free convection of the brine occurs. This is dependent on geological and climatic conditions like playa wetness, the permeability of sediments, the regional climate and climate history. Heterogeneity in hydraulic conductivity induces a change in flow pattern by creating multiple convection cells. FAN ET AL. (1997) assume that free convection evolve when 1) brine density is high (lake centre), 2) free convective

flow penetrates surface sediments and migrates laterally in more permeable alluvium layers and 3) brines pond on surface for extended periods.

HOLZBECHER (2005) examines interactions of saline water and groundwater near salt lakes. Hence both fluids have different density and viscosity which leads to density driven flows. Due to these properties the flow patterns in the groundwater that result from mixing are more complex than from diffusion only. After HOLZBECHER (2005) the flow patterns change as an effect of salinisation, when high mineralized saline water lies over low mineralized groundwater. Due to this unstable situation convective motions may pertain. In a homogenous porous medium, a front of highly saline water penetrates the ambient fresh water layer and can build a steady state with convection rolls. These circulate over the entire depth of the aquifer (HOLZBECHER, 2005). Though, models have been developed in several studies to investigate the connection between salt lakes and groundwater. But until today the hydraulic processes in natural environment are poorly understood (SIMMONS & NARAYAN, 1997; SIMMONS ET AL., 1999; WOODING ET AL., 1997).

LAST (1997) investigated bedding characteristics in Salt lakes and ascertained that physical laminations are uncommon in salt lakes because of the dominance of chemical sedimentary processes.

Because of the absence of sediment penetrating organisms due to anoxic conditions in ephemeral, hypersaline playas, depositional laminations are often well preserved and provide information about past brine compositional changes and salinity fluctuations.

SMOOT & LOWENSTEIN (1991) specify difficulties in investigations of Salt lake sequences due to the susceptibility of chemical sediments in Salt lakes to syndepositional dissolution, remobilization and reprecipitation. GREER (1977) amend that ephemeral Salt lakes often contain in succession of periodic subaerial exposure, desiccation and erosion hiatuses in their stratigraphic records.

After MEES (1999) distribution patterns of evaporite minerals in ephemeral systems that form as groundwater precipitates can be explained by referring to mechanisms of water and solute movement in soils that are subjected to evaporation. The decisive factors affecting the distribution pattern are the groundwater depth and the lithological composition and the hydraulic conductivity respectively. Crystalline gypsum occurs as 1) Subaqueous precipitates and crystals that developed within a brine-saturated surface layer; 2) crystals that formed within brine-filled macropores 3) crys-

tals produced by intrasediment growth in the vadose zone, and 4) recrystallized gypsum within a nearly permanently waterlogged interval in lower parts of the deposits.

1.3 Study site

1.3.1 Location and history of the natural reserve

The investigated area, the Fuente de Piedra Basin, is located 15 km northwest of Antequera in the province of Málaga, Andalusia, Spain (see Fig. 1.4).

The Fuente de Piedra Basin contains one of the largest ephemeral Salt lakes in Spain and is located in an intramontane, Neogen basin in the Betic Cordilleras of southern Spain (LINARES, 1990; BENAVENTE ET AL., 1996a). Due to its comparatively small catchment area and its complex hydrogeological situation, this study area provides excellent conditions for studying hydraulic and geochemical processes related to salinisation processes in endoheric basins. Great differences of density and strongly transient hydrologic conditions (LINARES, 1990) lead to a complex mechanism of salinisation which is at present poorly understood.

This salt lake and its environment is a protected humid zone at national and international levels (RENDÓN MARTOS, 1996). Similar to the Camargue (France) this biotope constitutes an important breeding ground for flamingos in the western Mediterranean (RENDÓN MARTOS, 1996).

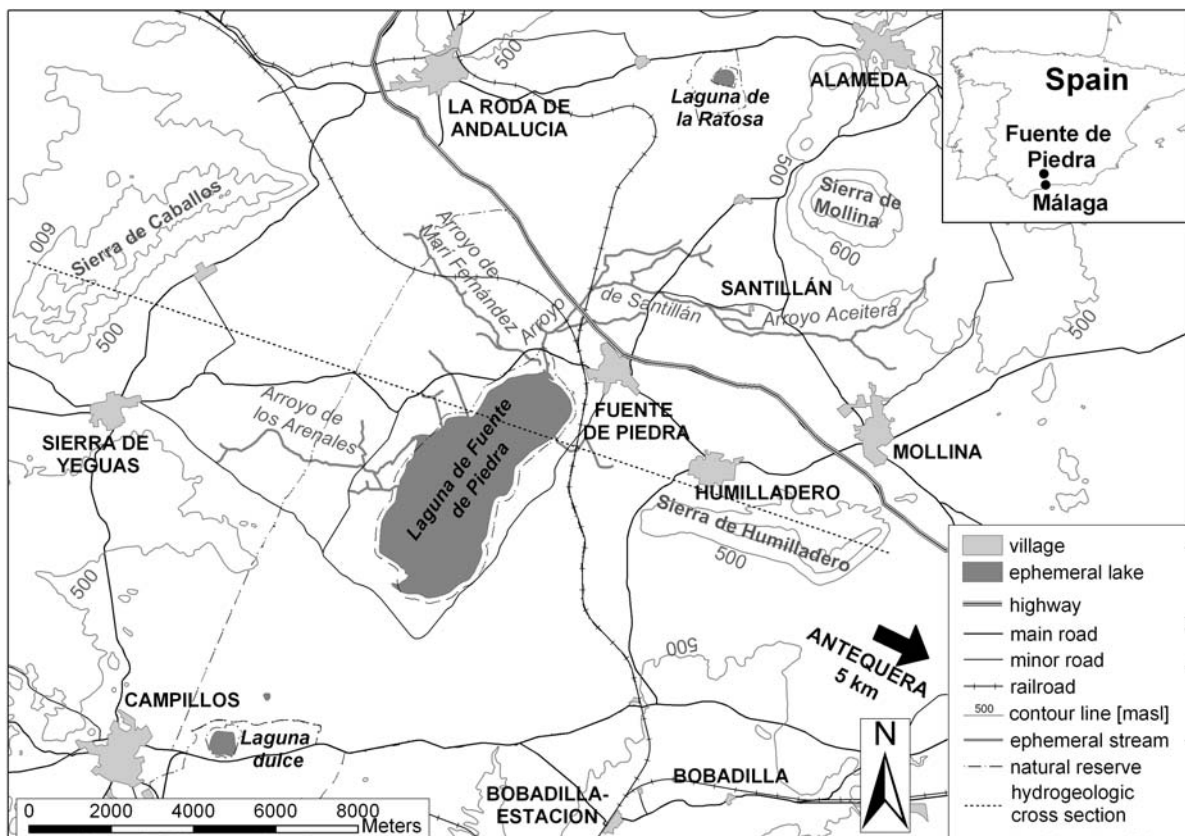


Figure 1.4: Situation of the study area.

This type of ecosystems is unique in Europe and is therefore of great hydrologic, ecologic and geomorphologic interest (HEREDIA ET AL., 2004).

Owing to the strong annual and interannual hydrologic changes in response to the climatic cycles of the western Mediterranean (ITGE, 1998), this small catchment area is considered an excellent natural laboratory for quantitative studies of different processes to hydrologic balances and even climatic changes at larger scale (RODRIGUEZ-RODRIGUEZ ET AL., 2005).

As the largest salt lake in this area it was investigated several times and therefore provides the highest density of hydrogeochemical data in this area (ITGE, 1998).

Fuente de Piedra is situated on a practically flat area, surrounded by the Sierras de Molina mountain range, whose highest peaks reach to almost 800 meters. The first settlements here date back a long way, to the 5th century B.C., although the first written reference to the place dates from Roman times: "The reference is to the water with its curative powers, and which gives the name to the town, in that those who drink it will be cured of their 'mal de la piedra', illness of the stone, meaning gall stones." (MUÑOZ & GARCIA, 1983).

The history of the town itself has always been closely linked with the history of the salt lake. This refers to the extraction of salt from Roman times until 1951, but now the source of income is mainly constituted by the production of olive oil (MUÑOZ & GARCIA, 1983). The lake is fed by three small rivers, by rainfall and by highly mineralized groundwater (ITGE, 1998). The most important surface inflow is the Arroyo de Santillán (6 to 8 hm³ per year) in the northern part of the lake (LINARES, 1990). In times when salt was extracted from the lake, the Arroyo de Santillán was directed in a canal through the lake in order to prevent dilution of the highly mineralized solution (MUÑOZ & GARCIA, 1983). Flora and fauna have adapted themselves to grow here in the salt water and they form an ecosystem in which a large number of birds and animals live (RENDÓN MARTOS, 1996). For further information about zoology and vegetation see RENDÓN MARTOS (1996).

Although Fuente de Piedra is the best known case of salt lakes in southern Spain, due to its extension and its ornithological interest this is not by far the only of these aquatic ecosystems in the surrounding area (ALMECIJA RUIZ, 1997).

At present the Nature Reserve (see Fig. 1.4) is managed by the Environmental Agency of the autonomous government of Andalusia which supervises the natural resources of the Fuente de Piedra Basin (ITGE, 1998). The operative figure of man-

agement of this area is a Patronage, where most of environmental impacts – and, particularly, those related with water resources exploitation – are considered, as well as scientific research is carried out. Different social and administrative instances form a part of this Patronage (ITGE, 1998).

1.3.2 Geomorphology and catchment area

Due to the karstification of Triassic evaporites, in the Antequera region numerous Endorheic basins appeared. With a size of 148.5 km² the Fuente de Piedra Basin is the largest in the region (CARRASCO, 1986; BENAVENTE ET AL., 1996b; GUTIÉRREZ ET AL., 2002). LHÉNAFF (1981) has attributed this anomalous size to the situation at the border of the Atlantic-Mediterranean hydrographic watershed.

Fuente de Piedra Salt Lake is situated in an intramontane, Neogene basin (GUTIÉRREZ ET AL., 2002). The altitude of the basin bottom is 410 m above sea-level, which is considered the deepest part of the basin. Average altitude is about 450 masl. Surrounding mountain ranges are Sierra de Mollina in the northeast, Sierra de Humilladero in the east and Sierra de Caballos in the west. Sierra de Mollina (798 masl) and Sierra de Humilladero (680 masl) constitute the border to the Guadalquivir and the Guadalhorce basin respectively. Only at this mountain ranges relieve is abrupt. These ranges are constituted by Jurassic limestones. Along the southern border of the lake or rather the basin abrupt relieve appears at smaller scale (10 meters). In the rest of the basin moderate relieve is typical. Landslide bodies like “Cerro del Palo”, on which the Visitors Center of the natural reserve in Fuente de Piedra was built, interrupt this moderate relieve. Gradients are directed to the lake with small amplitudes.

The ground of the lake is nearly horizontal. But in the interior small elevations appear above the water-level, with a few centimeter of height (Fig. 1.5). Their contours change due to sedimentation and erosion (ITGE, 1998).

From ancient times to the almost recent (1951) salt was exploited in the lake (MUÑOZ & GARCIA, 1983). This led to the graving of shallow pools and peripheral canals (ITGE, 1998). These appear until today and make up the present morphology of the lake (Fig. 1.5) to avoid an intrusion of low mineralized water into the lake. Regarding this, the Santillán Creek (Arroyo de Santillán) was canalized in the middle of the lake (ITGE, 1998). Due to erosion and sedimentation this canal has almost disappeared today. In addition to intrusion of low mineralized water two to three meter wide trenches were dug at the edges around the lake (LINARES, 1990). Nowadays these

canals and the lock gate system are used for management of artificial water supply (LINARES, 1990).

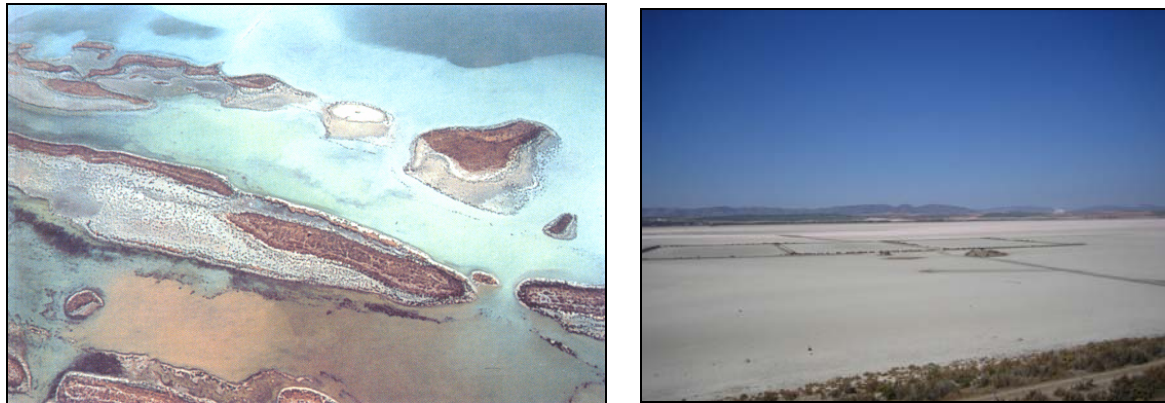


Figure 1.5: Left: Elevations interior the lake at the southwest shore, picture taken in direction E (ITGE 1998). Right: Evaporation pools inside the lake, picture taken in direction W.

The shape of the lake is more or less elliptic, the long axis strikes SW-NE with a length of 6.8 km, maximum width is 3 km (Fig. 1.4). The perimeter is about 18 km, with a maximum flooding area of 13 km².

The surface catchment area, with an extension of 148.5 km², is about ten times bigger than the maximum area of the flooded lake with 13 km². The Drainage Divide is adequate to the basin-border (LINARES, 1990; ITGE, 1998; ALMECIJA RUIZ, 1997).

The so-called “Betic endorheism” comprises subsidence caused by subsurface dissolution of evaporites may result in, or take part in, the generation of lacustrine basins (GUTIÉRREZ ET AL., 2002). Lake systems in depressions generated by dissolution induced subsidence are relatively frequent in the Triassic evaporite outcrops of some alpine ranges. The so-called “Betic endorheism” corresponds to a large number of ephemeral lakes of great environmental interest developed in the extensive Antequera Triassic outcrops in Cadiz, Sevilla, Cordoba and Malaga provinces (DÚRAN & VAL, 1984). The Fuente de Piedra Lake, together with Gallocanta Lake, is the largest lacustrine system in Spain. Its genesis is related to large-scale subsidence caused by the removal of evaporites by means of underground rising flows (LINARES & RENDON MARTOS, 1998).

1.3.3 Geology

1.3.3.1 Geology of Andalusia

GIBBONS & MORENO (2002) give a comprehensive review of the geology of the Iberian Peninsula and in particular of the Betic orogenesis. The Betic and the Moroccan Riff Cordilleras form an arc-shaped mountain belt north and south of the Alboran Sea

(Fig. 1.6). The Betic Cordilleras range from the Spanish Atlantic coast in the southwest along the Mediterranean Sea to Alicante for a distance of 600 km. The Guadalquivir basin on the western and the Iberian basement on the eastern site are defining the borders of the Cordillera. Three pre-Mesozoic domains can be distinguished. The first major zone, the External Zone, forms the northern part of the Betic and represents the former margins of the Iberian and African plate and is of low-metamorphic character. The External zone can be divided in Prebetic and Subbetic. The Prebetic is located in the northeast and is built up by Mesozoic sediments. In the south, the Prebetic is overthrust by Subbetic sediments which mainly exist of Triassic gypsum.

After GIBBONS & MORENO (2002) the Subbetic can be divided into four main groups:

- a) Triassic Sediments building up by evaporite-bearing clays and marls and a lesser occurrence of sandstones, limestones, dolomites and volcanic rocks.
- b) lower Jurassic limestones and dolomites
- c) Sediments from the lower Jurassic to the Oligocene. Mainly build by marls interbedded with thin limestone strata.
- d) In the central part of the basin quaternary alluvial deposits from the Guadalorce cover an area of 250 km² and form the Antequera plain.

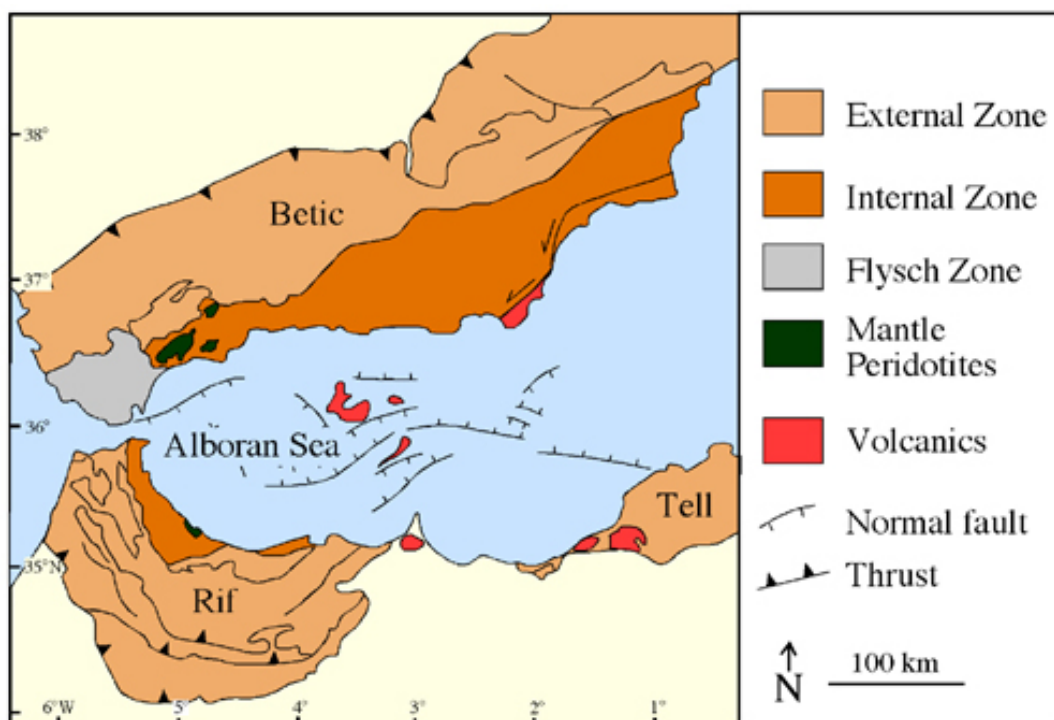


Figure 1.6: Geological map of the Alboran Sea and the Rif-Betic cordillera (after PLATT & VISSERS, 1989).

The Internal Zone comprises three nappe complexes of variable metamorphic grade including the Sierra Nevada Mountains with the highest altitude, the Mulhacen (3481 masl). This zone is dominated by Flysch and molasses (GIBBONS & MORENO, 2002). The Nevado-Filabride complex as lowermost unit comprises large anticline structures that form the Sierra Nevada. After this folding period the Palaeozoic Sierra Nevada has been overthrust by the Mesozoic Nappe complexes of the present surrounding Alpujarride Complex. The nappes of the Alpujarride complex are mainly composed by Mesozoic schists and Triassic carbonates and sulphates. The topmost nappes complex, the Malaguide complex, is dominated by high-grade metamorphic Palaeozoic rocks, but also Mesozoic sediments, termed as “dorsal” unit, appear.

The third zone, the Gibraltar Flysch zone, is situated in the Southwest and consists of flysch sediments deposited in a basin between African and Iberian plate.

1.3.3.2 Geology of Fuente de Piedra

The Fuente de Piedra Basin is part of the External Zone (Subbetic Zone) in the Betic Cordilleras (GIBBONS & MORENO, 2002). Systems (Formations) are described from oldest to youngest. Numbers in brackets () constitute the lithology Id.-number of the geological map Antequera 16-42: 1023 (IGME, 1986).

Four main-lithologies can be found: Triassic materials, made up by evaporite bearing clays and marls; Lower Jurassic limestones and dolomites; Miocene marls with thin interbedded limestone strata and Quaternary alluvial deposits (IGME, 1986). As shown in the simplified geological cross section (Fig. 1.8) the basins substratum is made up by Triassic deposits while Jurassic and Cretaceous carbonates constitute the surrounding mountain ranges and limit the hydrologic catchment area. Miocene and Quaternary loose sediments are deposited on the above mentioned formations.

The Fuente de Piedra section of the geological map 1023 and the stratigraphic chart are shown in Fig. 1.7.

The following descriptions for geological units in the Fuente de Piedra Basin are given after IGME (1986).

(A) *Subbético indiferenciado*

Triassic

A distinction by tectonic criteria into two formations is commonly made: Trias de Antequera and Trias Subbético. Trias Subbético occurs in the south and northeast of the working area. The Trias de Antequera is situated in the south is situated south of

the working area and is tectonically overlying the Trias Subbético. Both formations have similar, homogenous lithologies and can be combined as Trias Subbético undifferentiated. The local substratum is made up by Triassic sediments.

Colorful spotted massive claystone with varying shares of marl (1). These claystones are in interbedded strata with reddish, greenish or greyish sandstones and colorful spotted Gypsum. Gypsum is the most significant material in these interbedded strata (IGME, 1986). The Triassic formations contain interbedded Halite, although it is not present at the surface due to solution processes. Due to the existence of sodium water springs there must be sufficient amounts of halite to solute (BENAVENTE HERRERA & CARRASCO CANTOS, 1985).

Small amounts of Halite occur furthermore in dolomites mostly breccia, limestone and marble (2), which can be found locally in small outcrop dimensions. These layers are interpreted as interbedded strata. Isolated volcanic rocks (3), ophites, are distributed locally in Triassic formations (ITGE, 1998).

Dissolution of contained evaporites and transformation of Anhydrite into Gypsum caused Gypsum Karst features like recent dolines, subsidence and karstification (ITGE, 1998; DURAN & VAL, 1984; GUTIÉRREZ ET AL., 2001 and 2002; CALAFORRA & PULIDO-BOSCH, 1999).

(B) *Subbetic Zone*

Jurassic

Jurassic deposits are predominantly carbonates. The Jurassic's substratum is made up by grey or light yellow dolomites (4) (breccia) of Lower Lias with a thickness of 100 - 250 m (Sierra de Humilladero and Nacimiento del Santillán). The contact to the overlying unit is irregular and dominated by a dolomitization front. This formation is followed by massive, light colored limestones of Lower and Middle Lias (5) with a thickness of 200 m which occur at Sierra de Humilladero and Cortijo de la Herriza.

Upper Lias to Upper Dogger constitute a heterogeneous, 50 m thick, alternated stratification of (a) limestone and calcareous marl with silex and (b) greenish or light colored marl which occur at the borders of Sierra de Humilladero and south of Cortijo de la Herriza (6).

Upper Dogger to Middle Malm (Kimmeridgian) is made up by calcareous sandstones with silex and light colored marls northwest of Sierra de Humilladero (7).

Paleogene

Calcareous sandstone, sandstone and marl of turbiditic origin appear 12 km east of Mollina in the east of Fuente de Piedra Basin (11).

Neogene formations are below mentioned

(C) *Circumbetic Zone*

Lower Miocene

Green-brownish shaly marl (Flysch sediment) lies in interstratification with detritic limestone (12). These limestones are of turbidite origin and therefore allochthon. Lower Miocene formations superposition the Triassic sediments and occur in strip elongation east of Campillos and southwest of Bobadilla in the south of Fuente de Piedra Basin.

(D) *Postorogenic Formations*

Quaternary¹ sediments cover large areas in Fuente de Piedra Basin; they show a wide heterogeneity in lithology. The major parts of quaternary sediments are made up by alluvial deposits in valley ground and at mountain sides and clay padding in depressions. These loose, heterogenic sediments build up of clay, sand and gravel. At mountain sides of important relieve, for example at the east border of Sierra de Caballos, slight cementated formations appear (ITGE, 1998).

Upper Miocene

Occurrence is discordant to older formations. Upper Miocene sediments are of molassic character. Main lithology is coarse, calcareous sand (14) with inter beddings of grey marls and conglomerates (15). Contained fossils are Lamellibranchia, Bryozoa and alga. The sediments are of Tortonian to Messinian age (PEYRE, 1974), although appearing fauna is not characteristic. Miocene deposits appear in bad outcrop conditions which complicates the stratigraphic description. They are covered by red soils and other superficial formations. Thickness varies from 30 to 100 m, due to deposition on a paleo-relief. Thicknesses of 30 – 40 m were found in boreholes east of Fuente de Piedra and between the recent Salt lake and Sierra de Caballos Mountain range 50 – 75 m (LINARES, 1990).

¹ antiquated for Paleogene and Neogene Periods, in this case used for postorogenic formations, which are younger than Lower Miocene

Pleistocene

- (a) Lower Pleistocene: Constituted of higher terrace (above 460 masl) sediments (red clays and sub rounded limestone fragments (16/17) and glacial deposits. Glacial deposits (18) constitute of sub rounded limestone or calcareous sandstone fragments (Jurassic) in a marly matrix. Thicknesses are up to 2 m.
- (b) Middle Pleistocene: Powdery crust with red clay fragments (19). Situated NW of La Herriza between 450 – 460 masl. Formation (23) consists of clay, red sand and crusts and can be found between 420 to 450 masl. Lithologies (20), (21), (22) and (24) are not present in the study area and are therefore not described.
- (c) Upper Pleistocene: Sinkhole fillings made up by decalcified reddish clay, which develops by subsidence processes (27). This formation is associated with the lithologies (14), (18) and (19) NW of la Herriza and west of Nacimiento de Santillán. Sand, clay and subrounded calcareous fragments build up fluvial terrace materials which occur south and north of Fuente de Piedra Salt Lake (29). Recent detrital fan consist mainly of clay and sand (angular grains) deposits (30). Occurrence at hill slopes. Solution-depression fillings are made by fine sediments like clay and red sand (32); they are wide spread around the lake. Grey or light colored marl and organic loam made up former lake terraces (33) and are up to 15 m higher elevated than the salt lake. Occurrence is at nearly the whole east shore and north of Fuente de Piedra lake. Recent glacial at light slope is presented by brown-red clay and red sand (angular grains) (34). Formation (34) covers, with thin thicknesses, anterior glacial or Upper Miocene sediments.

Holocene

Brown-greyish, sandy loam with fragments constitutes sediments from terraces and flood plains of Guadalquivir River (35). These sediments constitute the last terrace level of Guadalquivir River.

Light colored clay and fuscous sand appear in valley grounds, areas without sufficient de-watering and sporadic water supply, above the ultimate terrace level (36). Typical profile (Laguna Salada) is grey, marly, organic loam followed by 20 cm light colored marl with small carbonate parts and covered by 30 cm clayey, organic-rich soil.

Sandy clay with fragments, occur at alluvial fans, e.g. submontane Sierra de Caballos mountain range (37).

At Salt lake bottoms or tarns sandy ooze with sapropel which is covered by salt crusts, appear (38). The salt crust evolves due to desiccation of lake water in sum-

mer and shows salt ridges and marks the present sedimentation. Below the salt crust a black, organic layer in decomposition of few centimeters occur. The organic material derives from algae, bird feathers and fauna relicts. Under the organic layer grey, water saturated sandy ooze can be found.

Alluvial deposits in valley grounds are generally fine grained, sandy, clayey sediments with sub rounded fragments (39). A grouping of all alluvial sediments which cover the valley grounds was made regardless the type of origin.

Sedimentation in the lake was investigated by CASTELLÓN SERRANO (1970); he found a homogeneous distribution of minerals (quartz, feldspars, phyllosilicates, calcite, dolomite, gypsum, halite and hexahydrate) except for Montmorillonite. Furthermore the actual salt deposits are mainly of continental type while only few can be associated with marine origin. RODRÍGUEZ-JIMÉNEZ ET AL. (1993) sampled the salt crust and sediments from two shallow holes for minerals. Minerals are mainly quartz, feldspars, phyllosilicates, calcite, dolomite, gypsum, halite and hexahydrate. They suggest besides a vertical zoning, a lateral zoning of these minerals with increasing salt contents towards the lake.

At present the Geological Survey of Spain (Instituto Geológico y Minero de España, IGME) Madrid carries out geological investigation at the Fuente de Piedra Basin (briefed by J. Benavente, 10.04.2006) to design a new geological map – 16-42: 1023 Antequera (actual map: IGME, 1986).

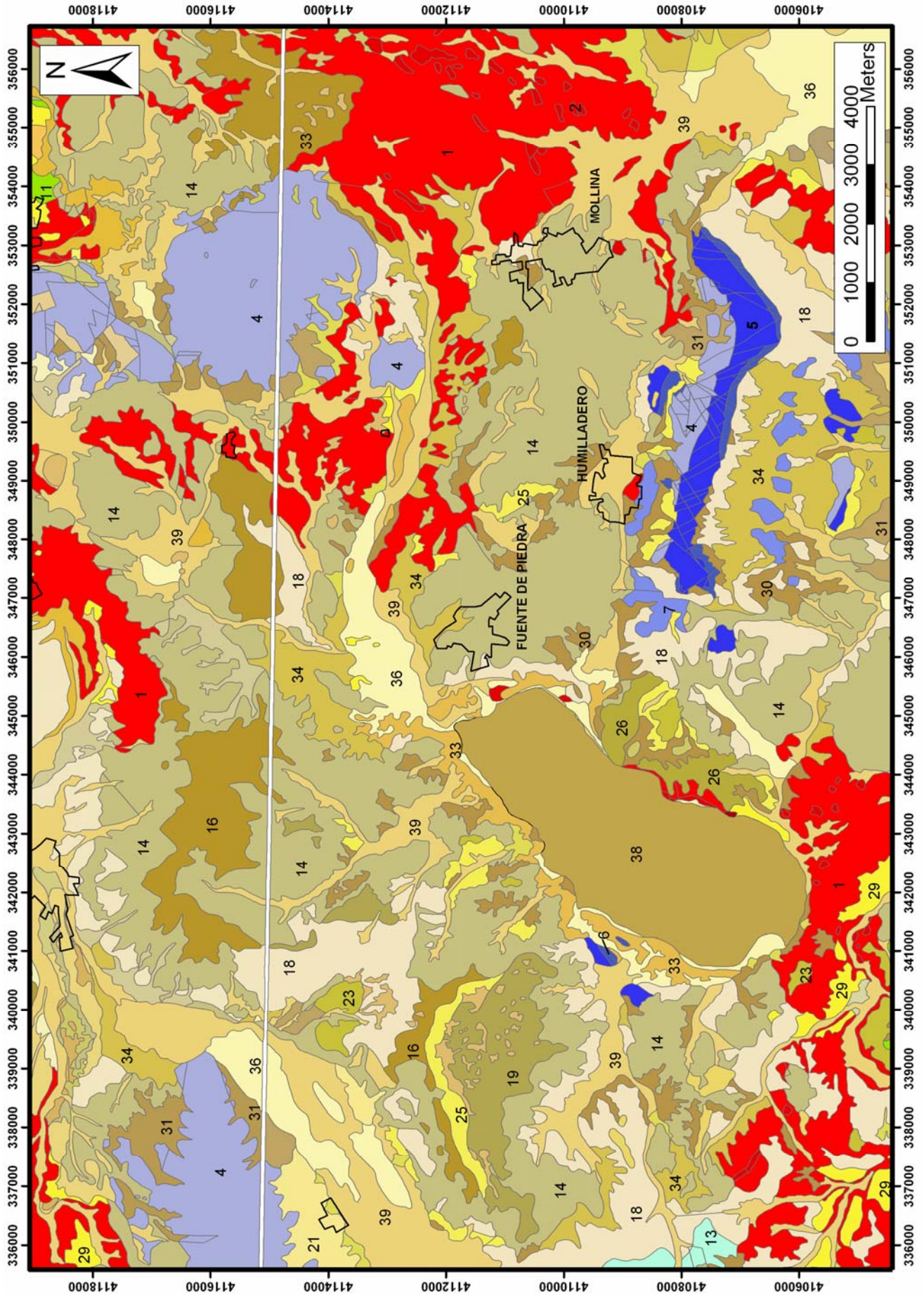


Figure 1.7a: Geologic map of Fuente de Piedra. Derived from IGME (1986).

Legend










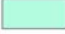














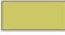






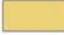
Triassic			(1) Claystone with interbedded Halite	
			(2) Dolomites mostly breccia, limestone and marble, interbedded Halite	
			(3) Ophite	
Jurassic	Dogger Lias		(4) Dolomites (breccia)	
			(5) Massive, light colored limestones	
			(6) Alternated stratification of limestone and calcareous marl	
			(7) Calcareous sandstone with silex and marl	
Paleogene			(11) Calcareous sandstone, sandstone and marl	
Neogene	Tertiary — Miocene — Upp. Low.		(12) Shaly marl, detritic limestone	
			(13) Marl and calcerous marl	
			(14) Coarse, calcareous sandstone	
			(15) Grey marls and conglomerates	
		Quaternary	Pleistocene — Lower —	
	(17) Red clay and sub rounded limestone fragments			
	(18) Limestone or calcareous sandstone fragments in shaly matrix			
	(19) Powdery crust with red clay fragments			
Middle				(21) Wackestone, limestone and dolomite fragments
				(23) Clay, red sand and crust
				(25) Breccia crust
Upper				(26) Calcerous fragments in red clay matrix
				(27) Decalcified reddish clay
			(28) Calcerous fragments in marl-sand matrix	
			(29) Sand, clay and calcareous fragments	
			(30) Clay and sand, recent detrital fan	
			(32) Clay and red sand	
			(33) Organic loam	
				(34) Brown-red clay and red sand
				(35) Brown-greyish, sandy loam
				(36) Light colored clay and fuscous sand
				(37) Sandy clay with fragments
				(38) Salt crust, recent lake sedimentation
			(39) Sandy, clayey sediment with fragments	

Figure 1.7b: Legend for the geological map Fig. 1.7a. Derived from IGME (1986).

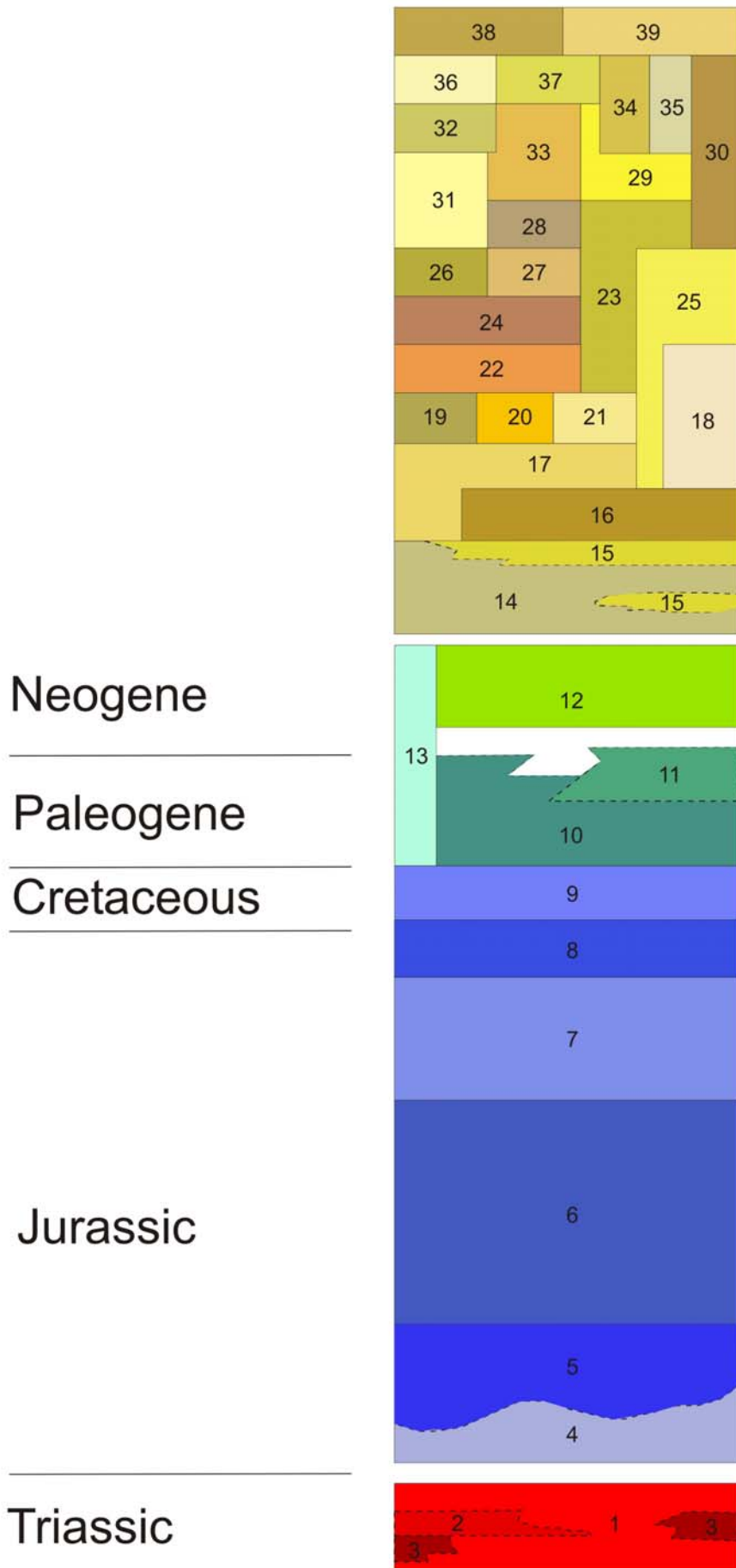


Figure 1.7c: Stratigraphic chart for geological map 1023 (IGME, 1986).

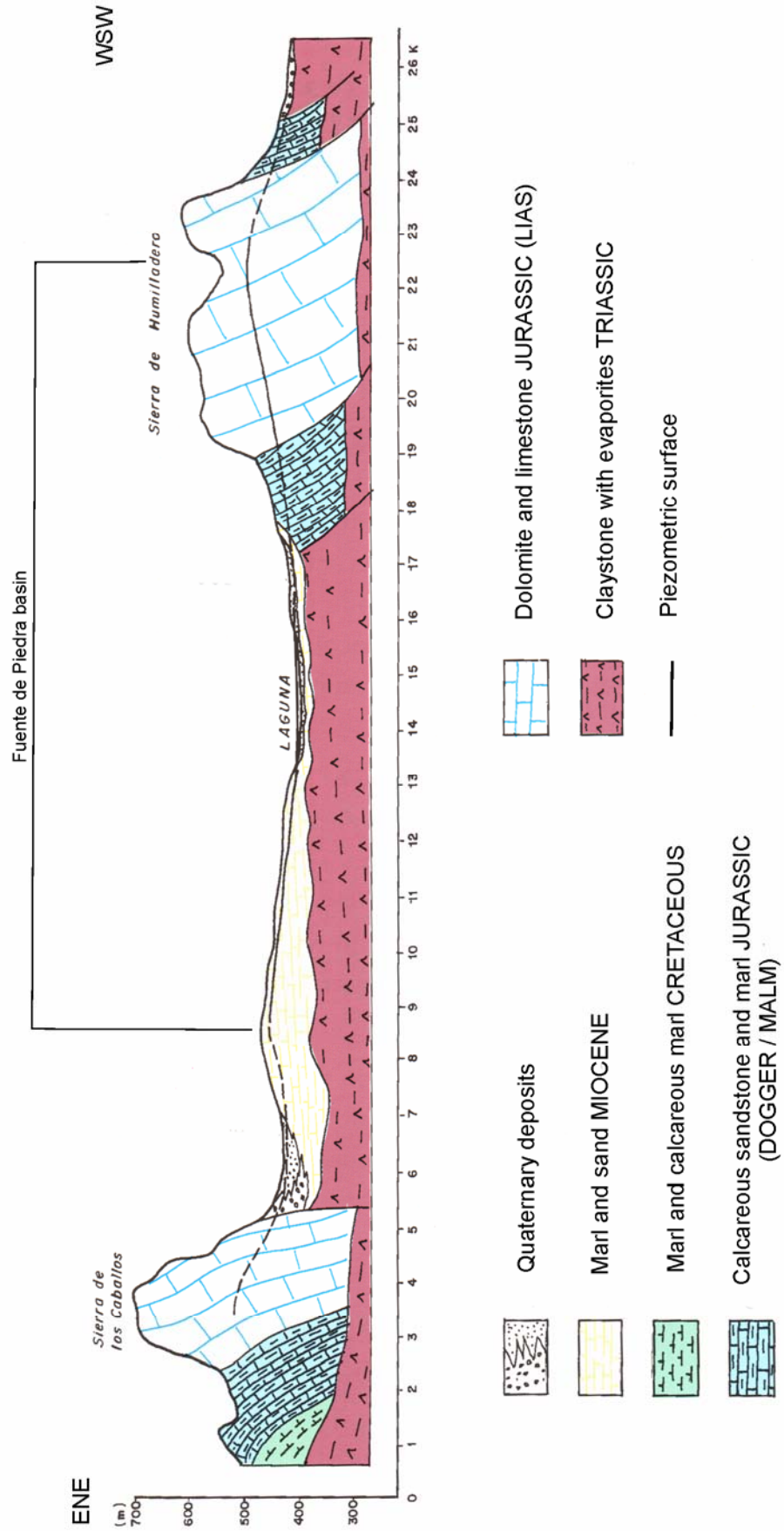


Figure 1.8: Simplified hydrogeological cross section derived from ITGE (1998) ranging from Sierra de los Caballos mountain range to Sierra de Humilladero mountain range. Course is marked in Fig. 1.4.

1.3.4 Climate and Hydrology

Southern Spain, respectively Andalusia is situated in a Mediterranean climate zone, additional the study area has a semi-arid tendency (BENAVENTE ET AL., 1996b). Mediterranean climate zones are characterized by hot and dry summers and rainy and bland winters. Semi-arid zones have annual precipitations of 250-500 mm and scanty vegetation.

The three most representative weather stations for the area of interest are Bobadilla estación, la Roda de Andalucía and la Herriza (LINARES, 1990). In this work calculations only were made with data from la Herriza and Bobadilla due to availability of data. See Tab. A1 to Tab. A8 for existing data for each weather station. LINARES (1990) correlated data from Bobadilla with la Herriza and estimated data for la Herriza from 1962 to 1973 (precipitation) and 1962 – 1977 (temperature) respectively. These estimated values were not used in this study because annual mean values decrease significantly if these data would be added.

Used climate data is distributed by the National Spanish Meteorological Service (Instituto Nacional Meteorológica, INM) and the southern Spain Commission of Water (Comisaría de Aguas del Sur de España, CASE), (Almecija Ruiz, 1997; IGME, 2001). Table 1.1 shows the inventory numbers and Tab. 1.2 the geographic coordinates of the weather stations.

Table 1.1: Inventory numbers of weather stations.

	INM	CASE	IGME
Bobadilla	106	41	
La Roda de Andalucía	582	612	56111
La Herriza	376e	270	6106

Table 1.2: Geographic coordinates for each Weather station (LINARES, 1990).

	Latitude (N)	Longitude (W)	Altitude (masl)
Bobadilla	37°02'20''	1°02'20''	380
La Roda de Andalucía	37°12'54''	1°05'23''	405
La Herriza	37°07'00''	1°06'10''	425

The annual average **temperature** is 17°C, the lowest monthly average values can be measured in January (9.6°C) and December (9.9°C), the highest monthly average degrees are reached in August (26.2°C) and July (25.7°C). These values were observed at the stations Bobadilla, la Roda and la Herriza between 1962 and 1987 (LINARES, 1990). At la Herriza the annual average values vary between 15.8°C (1983-84) and 17.6°C (1989-90) this station was set as standard by ITGE (1998). The highest temperatures are around 26.2°C in July and August, while the lowest is 8.6°C in

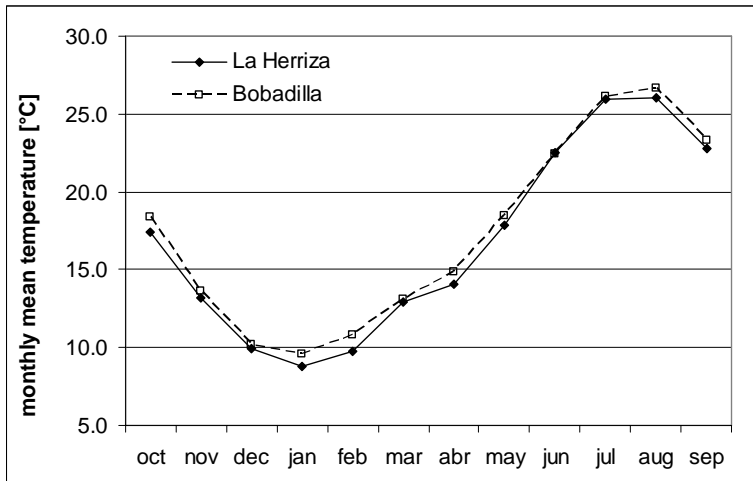


Figure 1.9: Monthly mean temperature at la Herriza from 1977/78 to 1998/99 and Bobadilla from 1964/65 to 1993/94.

January at la Herriza (Fig. 1.9). Different mean monthly temperatures can be observed due to the altitude (Fig. 1.8). The weather station at lower elevation has the higher temperatures (Bobadilla, 380 m).

During a period of 25 observed years (1962-1987)

the above-mentioned stations valued 462.8 mm per year of mean **precipitation**. The most intensive precipitations with up to 70 mm per month fall from November to February (LINARES, 1990). During the period 1973 to 2001 the average annual precipitation at the weather station la Herriza was around 440 mm. The wettest months are November (with mean precipitation of 61.9 mm) and December (with 68.5 mm). The driest is July with a mean of 2.5 mm followed by August with 7.6 mm (Fig. 1.10). At Bobadilla the mean annual precipitation is 448 mm (1964 – 1994). 90 % of the precipitations fall in five months during October and February, the other 10 % fall in the remaining seven months (ITGE, 1998).

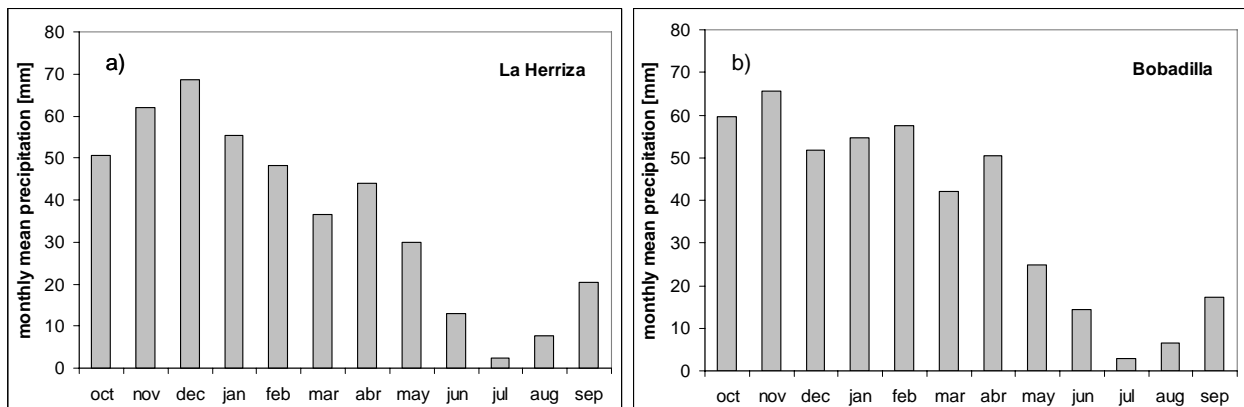


Figure 1.10: Monthly mean precipitation at a) la Herriza from 1973/74 to 2000/01; b) Bobadilla 1964/65 – 1993/94.

Evaporation takes place from soil or free water levels. Transpiration is the evaporation by plants. **Evapotranspiration** (ET) is the combination of Evaporation from free levels or soils with Transpiration.

The **potential Evaporation** E_0 describes the highest possible evaporation rate without consideration of the existing water resources. The actual Evaporation E_A considers the watermass which can be evaporated. Without water potential Evaporation E_0

can be very high but there will be no evaporation, so that the actual Evaporation E_A will be zero. Otherwise if there is very little water and a very high E_0 -value the whole water will be evaporated.

There are numerous methods to calculate the evapotranspiration. Their accuracy depends on the available data.

A method to estimate the potential evapotranspiration which needs mean monthly temperature values only is the Thornthwaite method (THORNTHWAITE, 1948) (equation 5).

$$ET_{0ThornUncor} = 1.6 \left(\frac{10t}{I} \right)^a \tag{1}$$

with

$$I = \sum_1^{12} \left(\frac{t}{5} \right)^{1.514} \tag{2}$$

$$a = \frac{0.9262188}{2.4232459 - \log I} \tag{3}$$

where

t = monthly mean air temperature [°C]

I = heat index, as sum of 12 monthly values

Equation (1) is valid without correction for months of 30 days and day length of 12 hours. Correction of days per months and hours of sunshine due to geographic latitude:

$$ET_{0Thorn} = \frac{N}{12} \times \frac{d}{30} \times d \times ET_{0ThornUncor} \tag{4}$$

with

N = maximum hours of sun due to latitude (Tab. 1.3)

d = number of days per month (Tab. 1.3)

The Thornthwaite method is valid for temperatures above 0 °C. During spring months evapotranspiration values are under estimated by this method (MATTHEß, 2003), in comparison to the Penman method. The Penman equation was set as reference for comparison with other methods by the International Commission for Irrigation and Drainage (ICID) and the Food and Agriculture Organization of the United Nations (FAO) (ALMECIJA RUIZ, 1997).

For the period 1962-87 LINARES (1990) figured po-

Table 1.3: Duration of sunshine in hours per day (N) at 37° latitude (CUSTODIO & LLAMAS, 1983).

month	N	d
jan	9.85	31
feb	10.75	28
mar	12.00	31
abr	13.20	30
may	14.25	31
jun	14.80	30
jul	14.50	31
aug	13.60	31
sep	12.45	30
oct	11.25	31
nov	10.15	30
dec	9.60	31

tential Evapotranspiration values (Thornthwaite method) (Tab.1.4). In July and August the highest potential evapotranspiration values are reached, followed by June. These three months represent nearly 50% of the annual potential Evapotranspiration. LINARES (1990) gives the average annual actual Evapotranspiration rate between 259 and 333 mm after THORNTHWAITE (1948). By subtraction of monthly average potential Evapotranspiration (Thornthwaite method) from monthly average precipitation the mean actual Evapotranspiration can be estimated graphically (THORNTHWAITE & MATHER, 1955).

Table 1.4: Potential Evapotranspiration in mm (Thornthwaite method) obtained from LINARES (1990) for the period 1962-87.

	mean annual sum	monthly mean minimum	monthly mean maximum
Average	830.8		
Bobadilla	855.0	19 (jan.)	148 (jul.)
La Herriza	818.1	17 (jan.)	148 (jul.)

Actual Evapotranspiration makes 30 – 40 % of the potential Evapotranspiration, because there is not sufficient water to reach the full potential Evapotranspiration (ITGE, 1998).

In Fig. 1.11 curves of mean monthly Precipitation and mean monthly potential Evapotranspiration (Thornthwaite method) are displayed for la Herriza and Bobadilla. Thereby actual Evapotranspiration and potential water deficit or rather water surplus can be estimated. If $P < ET_0$ there is a potential water deficit (consumption). If $P > ET_0$ potential and actual Evapotranspiration are equal. So if there is water left after evaporation, it infiltrates and refills the soil moisture until field capacity. After reaching field capacity, the water recharges the groundwater (carry over storage).

Potential and actual Evapotranspiration are only equal from November to February, so there is a water surplus and infiltration of groundwater is possible. With values between 10 and 20 mm per month a small amount of water can infiltrate into the ground. A potential water deficit can be observed from March to October.

Determination of Evaporation from the lake can not be made exactly, since there is no measuring device near to the lake to observe all necessary values for usual formulas (LINARES, 1990). Increase of Salinity lowers the water activity and therefore also the evaporation rate (SANFORD & WOOD, 2001).

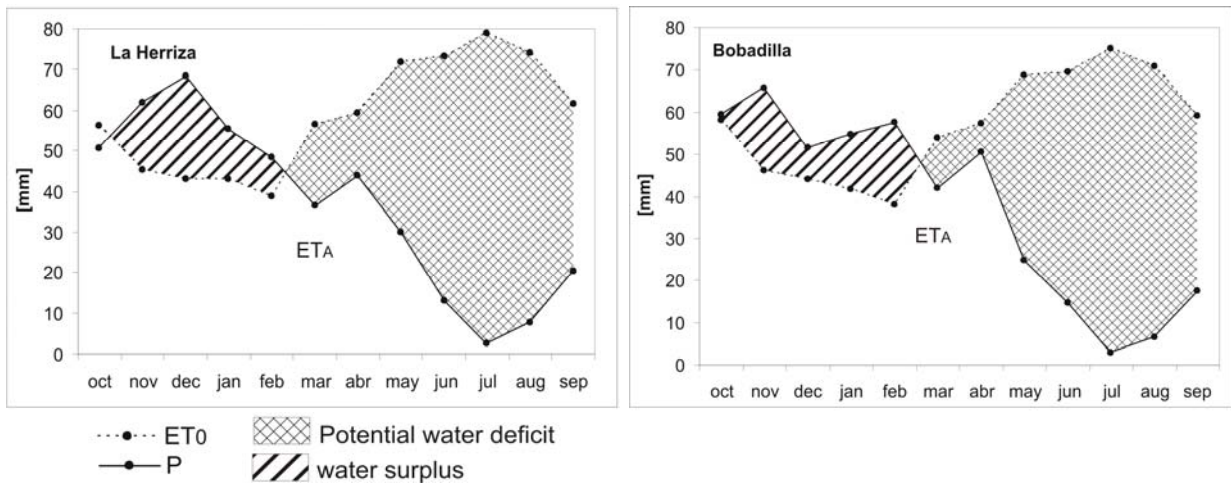


Figure 1.11: Monthly mean precipitation and evapotranspiration curves displaying potential water deficit and water surplus throughout a hydrological year at Bobadilla and la Herriza. Mean actual evapotranspiration is shown below the patterned area.

The Agencia de Medio Ambiente installed Piché-type atmometers to measure the evaporation from free water levels at the weather stations Bobadilla and La Herriza. A piece of paper is installed under a glass tube which is filled with water. One side of the paper is inside the tube, the other piece is in contact with the atmosphere, so it is constantly moist. When blotting paper gets in touch with the paper, the water can evaporate via suction by a metallic washer. The evaporation rate can be registered on a millimeter scale. Piché-type atmometers are installed inside weather stations. In comparison with evaporation pans the mean values had to be multiplied by 0.8. Great errors can be reached at Piché-type atmometers (CUSTODIO & LLAMAS, 1983). During summer there is an underestimation, only during winter the observed values are similar to other methods.

At Bobadilla station (Piché-type) evaporation measurements were held since 1950/51. For the period 1950-64 LINARES (1990) give averages of 528 mm per year and in the period 1966-87 1030 mm per year. During the second period the values range between 850 and 1300 mm per year. The monthly mean values range from 40 mm (December) to 160 mm (July). The second period seems to be more realistic due to longer time of observation. Evaporation data for Bobadilla estación was used from 1966 on due to availability of mean monthly values, for mean daily data before 1966 see LINARES (1990). Fig. 1.12 shows the distribution of monthly mean Evaporation values.

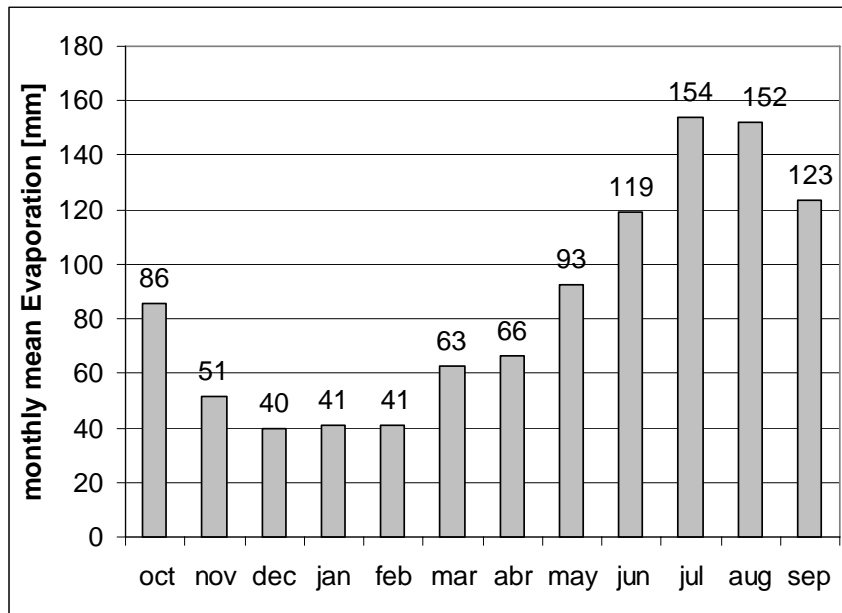


Figure 1.12: Monthly mean Evaporation (Piché atmometer) at Bobadilla for the period 1966/67 – 1986/87.

Measurement at la Herriza (Piché type) started in 1982/83. Period 1982-94 occur with 1600 mm annual average. The values range between 1250 and 2000 mm (ALMÉCJA RUIZ, 1997). For the period 1982-98 annual mean values of 1686.4 mm were given by IGME (2001). See Fig.1.13 for the monthly mean values, which range from 48 mm (December) to a maximum of 284 mm (July).

Evaporation from the lake reaches values between 1000 and 2000 mm per year.

These values occur to be higher because the lake fell dry during summer and mean depth is given with 2 m (LINARES, 1990).

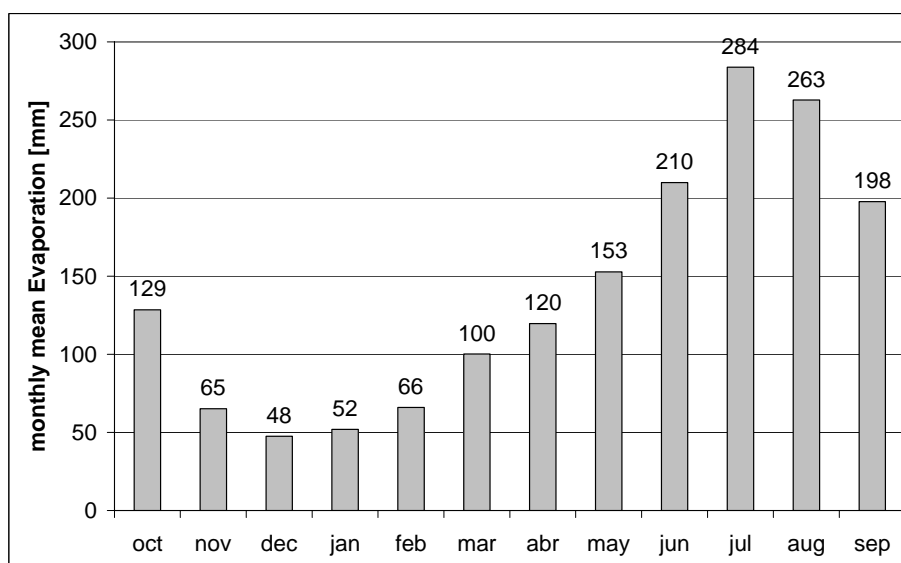


Figure 1.13: Monthly mean Evaporation (Piché atmometer) at la Herriza for the period 1982/83 – 1997/98.

The hydrological budget for an area is described by the hydrological equation 5.

$$P = R + ET + (S_+ - S_-) \quad (5)$$

where

P = Precipitation [mm]

R = Runoff (superficial, subsurface, interflow) [mm]

ET = Evapotranspiration [mm]

$S_+ - S_-$ = Change of groundwater storage [mm]

Recharge of Fuente de Piedra aquifer is made by infiltrating precipitations and reinfiltrating pumped irrigation water (LINARES, 1990). Extraction from wells and subsurface runoff into the salt lake leads to discharge of the aquifer. Tab. 1.5 shows the hydrological budget with mean values (period 1962 – 1987) obtained from LINARES (1990) and ITGE (1998).

Table 1.5: Summarization of Fuente de Piedra aquifer hydrological budget

Recharge	hm ³ /year
Infiltrating precipitations and surface runoff	11.5 - 13.4
Reinfiltrating pumped water	0.1 - 0.4
Total	11.6-13.8
Discharge	hm ³ /year
Extraction from pumping wells	3.0
Subsurface runoff into the salt lake	8.6 - 10.8
Total	11.6 - 13.8

Fig. 1.14 shows a flowchart of the hydrologic budget for Fuente de Piedra Basin. Mean values were used for development, therefore annual variations are possible.

The endoheric basin of Fuente de Piedra is situated in a water divide zone between the Guadalquivir and the Guadalhorce basin (HEREDIA ET AL., 2004). Guadalhorce river basin discharges into the Atlantic Ocean and the Guadalquivir river basin discharges into the Mediterranean Sea (HEREDIA ET AL., 2004).

Surface catchment area/watershed was calculated with Arc Hydro Tools Extension (version 1.1 Beta 3, May 2003; ESRI) for ArcGIS and verified by flow path modeling on base of Digital Elevation Model (DEM). Therefore the DEM was reconditioned and sinks (one cell that is surrounded by higher elevated cells) were filled. Flow direction, and Flow Accumulation were determined. Streams were defined and segmented. Afterwards Catchment Grid Delineation and Catchment Polygon Processing were made. The calculated size is about 148.5 km² (Fig. 1.15).

In the basin or rather to the lake three major and few smaller streams flow (Fig. 1.15). Major inflow takes place by Arroyo de Santillán and Arroyo de Marí Fernández in the extreme north and at the Middle West by Arroyo de los Arenales. Arroyo de Santillán is the most important, Arroyo Aceitera flow into it. The Spring of Arroyo de Santillán is

situated 3.5 km in the northeast of the lake. All streams inside the basin are, like the salt lake, ephemeral and therefore distribute water intermittent in winter.

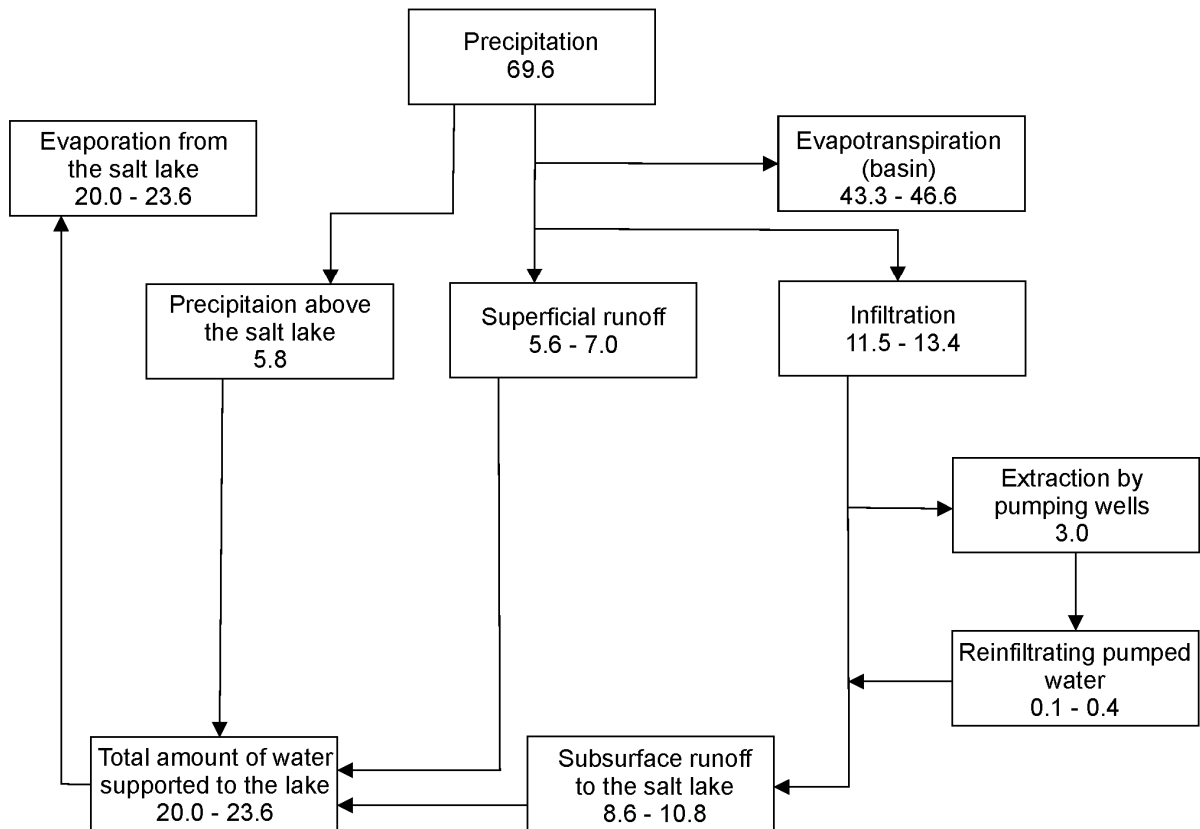


Figure 1.14: Flowchart of the hydrologic budget [hm³/year] of Fuente de Piedra Basin valid for mean conditions (of the period 1962 – 1987), modified after LINARES (1990). Assumptions: No variation in groundwater storage, in the salt lake and in the aquifer.

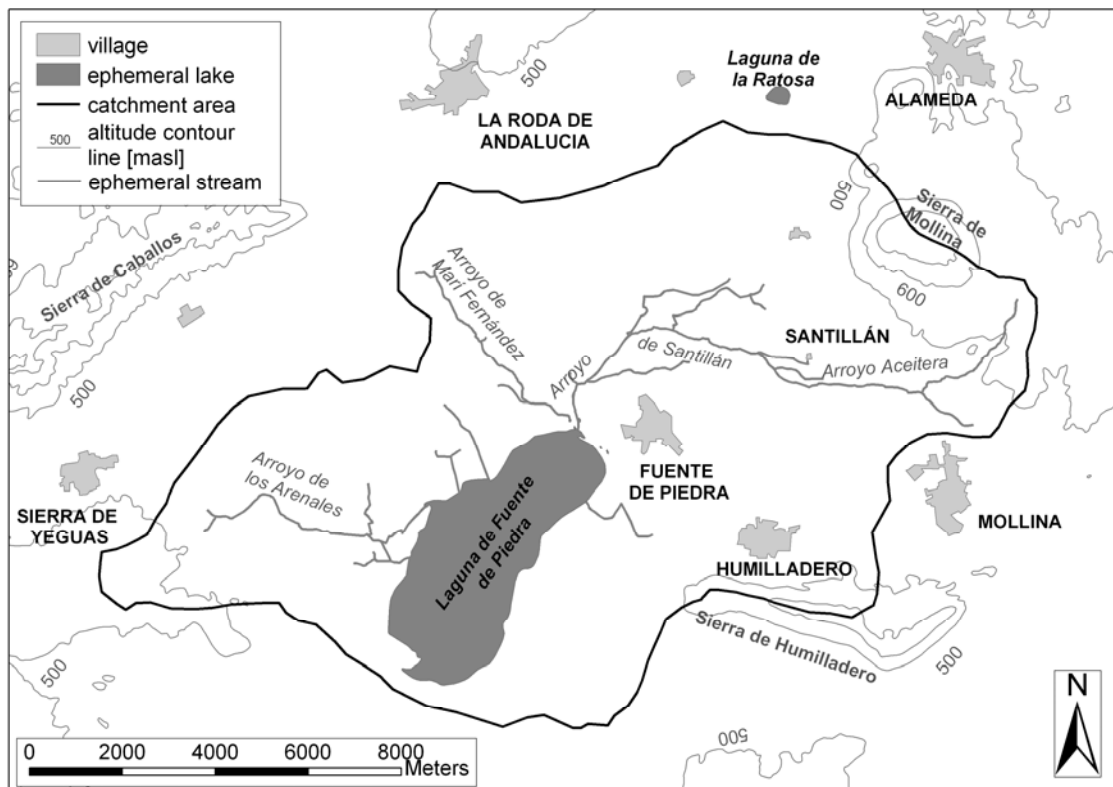


Figure 1.15: Surface catchment area for Fuente de Piedra Basin.

1.3.5 Hydrogeology

Within the Fuente de Piedra Basin aquifers are constituted of lower Jurassic carbonates (limestone and dolomite), Miocene calcareous sandstone and Miocene-Quaternary deposits (developed by eluviations and filling processes). Relatively small, isolated, highly karstified Jurassic aquifers comprise Sierra de Mollina and Sierra de Humilladero (MENGÍBAR & QUIRÓS, 1976; MOLINA, 1982).

Sierra de Mollina aquifer covers an area of 12 km². Recharge takes place only by precipitation; it discharges in the north in direction Alameda and in the south to the Santillán. Miocene-Quaternary aquifer borders on Sierra de Mollina aquifer (ITGE, 1998).

Sierra de Humilladero aquifer makes up 6 km². Precipitation is the only recharge source; the piezometric surface is located at approximately 450 masl. Like Sierra de Mollina aquifer the Sierra de Humilladero aquifer is surrounded by Miocene-Quaternary aquifer. The aquifer discharges to Humilladero in the north and to Fuente de Piedra Salt Lake in the west (LINARES, 1990).

Miocene-Quaternary aquifer is made up by Miocene calcareous sandstone and Miocene-Quaternary deposits. The granular aquifer covers the largest area of the study zone, mainly in topographically deepest parts. Hydraulic conductivity varies in horizontal and vertical direction due to lithology and facies change. Areas with coarse detritic horizons and therefore with the highest hydraulic conductivities are situated around Fuente de Piedra and north of Humilladero. Thicknesses reach 30 – 40 m. West of Fuente de Piedra Salt Lake the thicknesses are higher but detritic horizons are not as thick. Most important Quaternary formations for hydrogeologic investigation are alluvial deposits from Santillán creek bed and in minor degree alluvial deposits at mountain sides north of Sierra de Humilladero. At both cases the Quaternary aquifers have to be in hydraulic contact with subjacent Miocene or Jurassic aquifers to be relevant (LINARES, 1990).

The Fuente de Piedra aquifer is assembled by the hydraulic connection of the above named sub aquifers.

Triassic deposits are impermeable, except local permeabilities due to karstification. Evaporite contents like Gypsum and Halite are dissolved due to their high solubility. Middle and Upper Jurassic as well as Cretaceous formations can be handled like im-

permeable units. LINARES (1990) and ITGE (1998) show that the Jurassic Sierra de los Caballos aquifer is not connected to the Fuente de Piedra aquifer.

Water table levels range from 490 to nearly 400 masl (Fig. 1.17). The highest values can be found at the mountain ranges and in the southwestern part of the study area. There are 130 observation points (piezometers and wells) in the area which were used 4 times since 1983 for development of groundwater table contour maps (ITGE, 1998). Measuring period is from June 1983 to April 1994. Water table contours are constant in 1983/84 and 1995/96 period respectively. At the outer basin's region the contour lines do not change significantly during two consecutive years.

The groundwater flux is orientated towards the lower part of the basin and therefore towards the lake (ITGE, 1998; HEREDIA ET AL., submitted; LINARES, 1990). North of the village Fuente de Piedra the isopiestic surface reaches its minimum due to main pumping for water supply in this area (irrigation water, public water supply) (compare Fig. 1.18). But during the wet period, when most of the pumps stop operating, the isopiestic minimum lines are situated in the lake.

Maximum hydraulic gradients are observed west of Fuente de Piedra Salt Lake with 1.3 % and minimum values are detected at the lake's east border with 8 – 9 ‰. Mean representative hydraulic gradient is given with 1.1 % (ITGE, 1998).

1.3.6 Water supply

Due to desiccation in summer, water is pumped into the lake to avoid dying of young birds since 1985. The supply is managed by three salted wells north of the lake (ITGE, 1998). The period, in which pumping is necessary depends on climate and the amount of birds which are bred. Fig. 1.16 show the annual amount of water pumped into the lake. Otherwise wastewater from some small villages is used for water supply of the lake (BENAVENTE ET AL., 1996b). This water is collected in small canals, which flow in at the east shore of the lake (SPFP24; SPFP25). Quantity data of these canals does not exist. Maintenance with drinking water takes place from Jurassic materials. For irrigation water wells in Neogene materials are used. 300 wells exist within the basin. Pumping wells concentrate in the northern part above the lake and east of the lake around Humilladero. Fig. 1.18 shows the situation of the pumping wells and their annual pumping rate. The total annual average sum of water exploitation is 3 hm³ (ITGE, 1998).

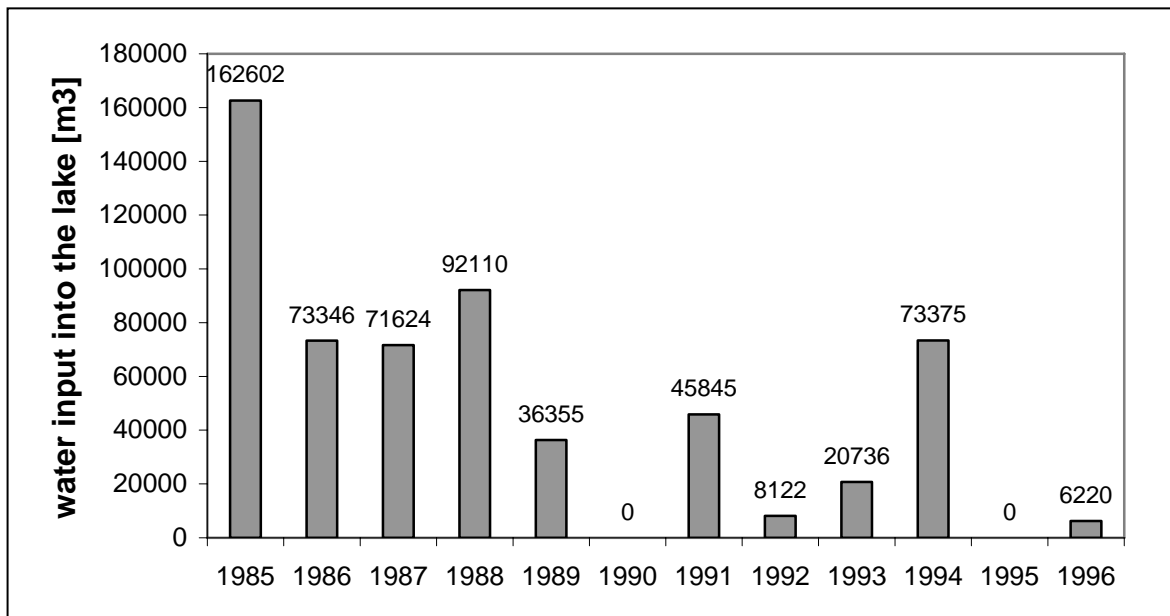


Figure 1.16: Annual artificial water supply to the lake (modified after ITGE, 1998).

1.3.7 Previous studies in Fuente de Piedra Basin

As the largest salt lake in Andalusia Laguna de Fuente de Piedra was investigated several times and therefore provides a high density of hydrogeochemical data. The Geological Survey of Spain (Instituto Geológico y Minero de España, IGME), a member of the Reserve Patronage, monitors the hydrogeological system since 1984. Since 1986 three doctoral theses were published about the Fuente de Piedra Basin at local (LINARES, 1990) and regional scale (CARRASCO, 1986; ALMÉCIJA RUIZ, 1997). CARRASCO (1986) concentrates on hydrochemical data from the Guadalquivir basin; ALMÉCIJA RUIZ (1997) compares several Salt lakes.

Hydrogeological investigations in Fuente de Piedra Basin were made by BENAVENTE ET AL. (1992, 1993, 1994, 1996B, 1998, 2003), LINARES (1990), LINARES & VALLE (1986), LINARES & RENDÓN (1998), LINARES ET AL. (1986, 1989, 2001, 2002), RODRIGUEZ-RODRIGUEZ ET AL. (2000, 2006), HEREDIA ET AL. (2004, SUBMITTED), DICHTL ET AL. (1986) and ITGE (1998). Investigations in Guadalquivir basin include BENAVENTE ET AL. (1996A, 1996B), CARRASCO & BENAVENTE (1986), CARRASCO (1978, 1979).

Karstification of Triassic materials leads to highly mineralized calcium-sulfate and sodium-chloride springs. These waters represent a hazard for the local water supply. Sodium-chloride waters are the dominant watertypes in the basin (LINARES, 1990; GUTIÉRREZ ET AL., 2001, 2002).

Close to the lake and around the northeast prolongation maxima of electric conductivity and major ions concentrations are distributed. TDS values are widely spread (till 200 mg/l) and reach up to 5 times that of seawater (LINARES, 1990, HEREDIA ET AL., 2004).

The catchment area and aquifer limits are equal at the Fuente de Piedra Basin (LINARES, 1990). LINARES (1990) made a hydrologic budget and suggest discharge is only managed by evaporation (around 830 mm) from the lake. Rainfall (around 450 mm), surface runoff and groundwater are supposed to recharge the lake.

RODRIGUEZ-RODRIGUEZ ET AL. (2006) show that groundwater is over saturated for Dolomite and surface water is over saturated for Aragonite, Calcite, Gypsum and Dolomite. Due to photosynthetic processes the CO₂ partial pressure is low (10^{-4}), this means that Calcite and Dolomite saturation are reached quickly and produce the sedimentation of calcitic and dolomitic marls (CASTELLÓN, 1970; RODRIGUEZ-RODRIGUEZ ET AL., 2006).

Transmissivity values were given by pumping tests: in Jurassic carbonates more than 800 m²/h, which pertain the karstic features; in Miocene-Quaternary materials between 2 and 80 m²/h, representative values near the lake were between 5 and 35 m²/h. Storage coefficient is given with $1.3 \cdot 10^{-2}$. Effective porosity takes values between 4 and 6 % (LINARES, 1990).

For Fuente de Piedra groundwater flow modeling was made by HEREDIA ET AL. (2004; submitted) using environmental Tracers. Vertical upflow is reported in depths of 120 – 140 m, small horizontal flow was detected in 50 - 90 m depth. HEREDIA ET AL. (2004) found that freshwater flow is linked to Jurassic and Miocene aquifers with flow lines to the lake. Piezometric observations and conductivity logs indicate time independent stable conditions for the transition zone between salt- and freshwater. Because of a sharp density contrast in shallow depths between salt- and freshwater; independent stratified flow systems are supposed. The absence of Tritium in groundwater below the lake and in shallow depths indicates long resistance times and that groundwater is older than 50 years (HEREDIA ET AL., 2004).

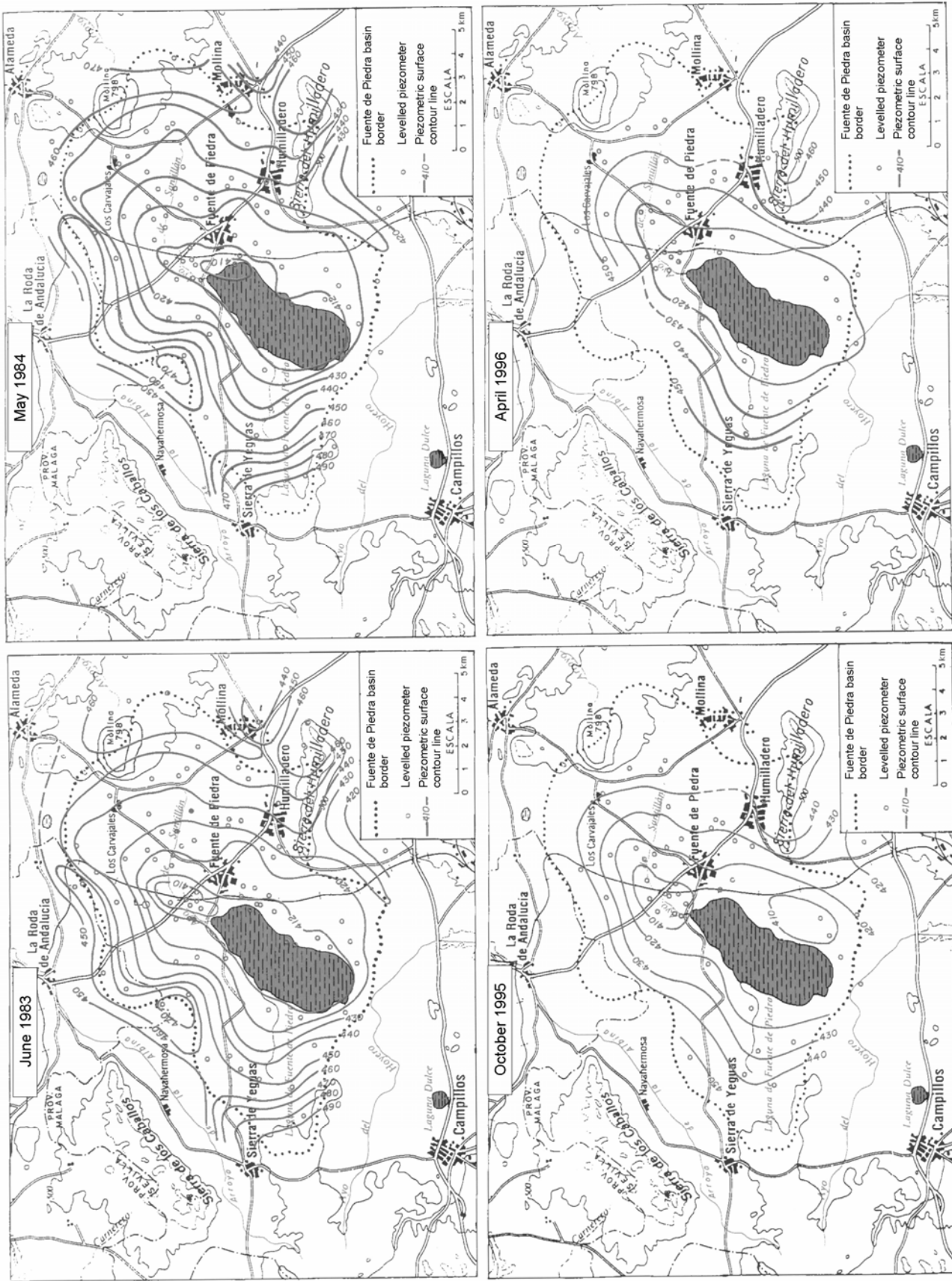


Figure 1.17: Water table contour map (modified after ITGE, 1998).

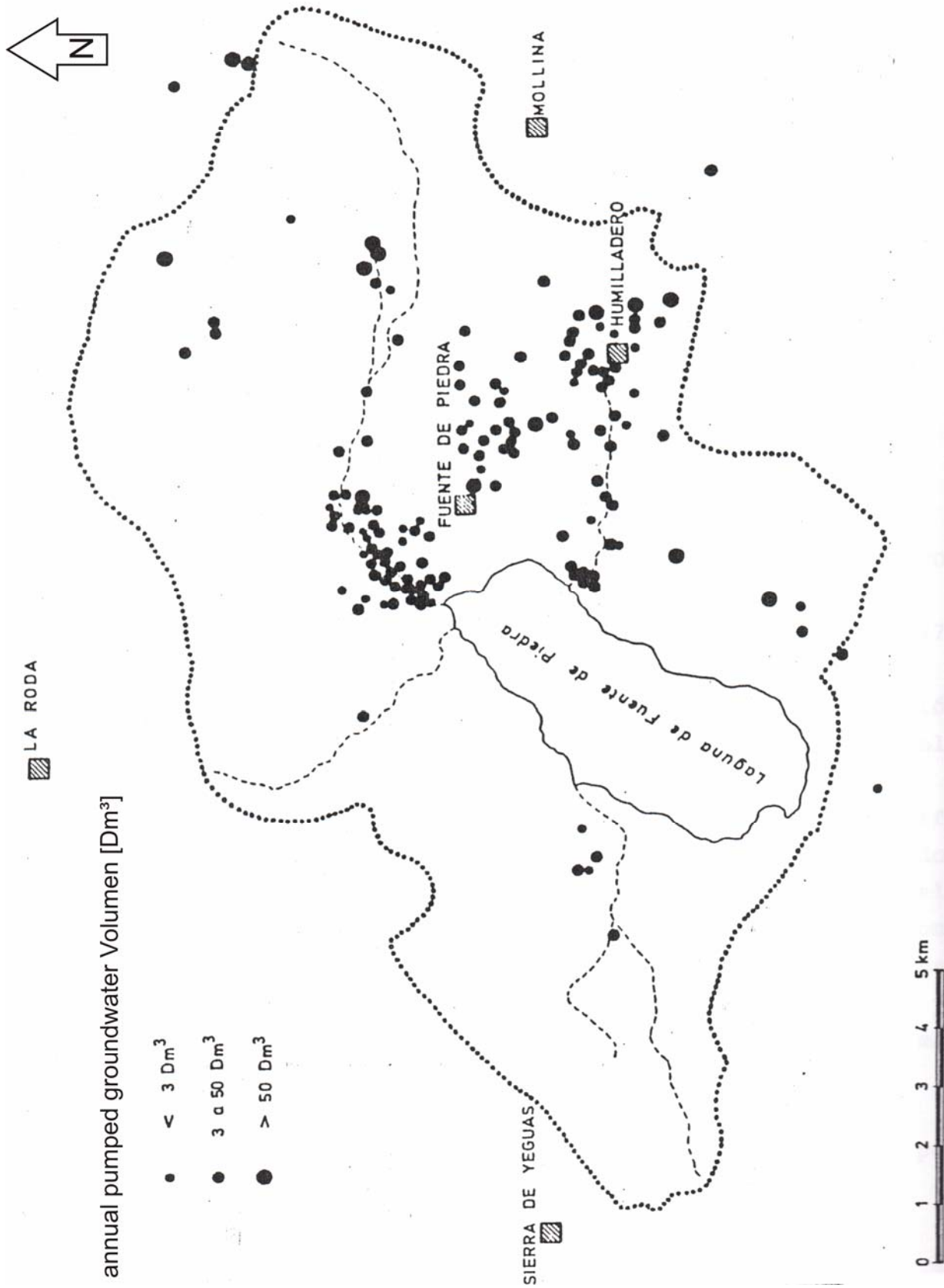


Figure 1.18: Annual pumped groundwater Volume in Fuente de Piedra Basin (modified after LINARES, 1990).

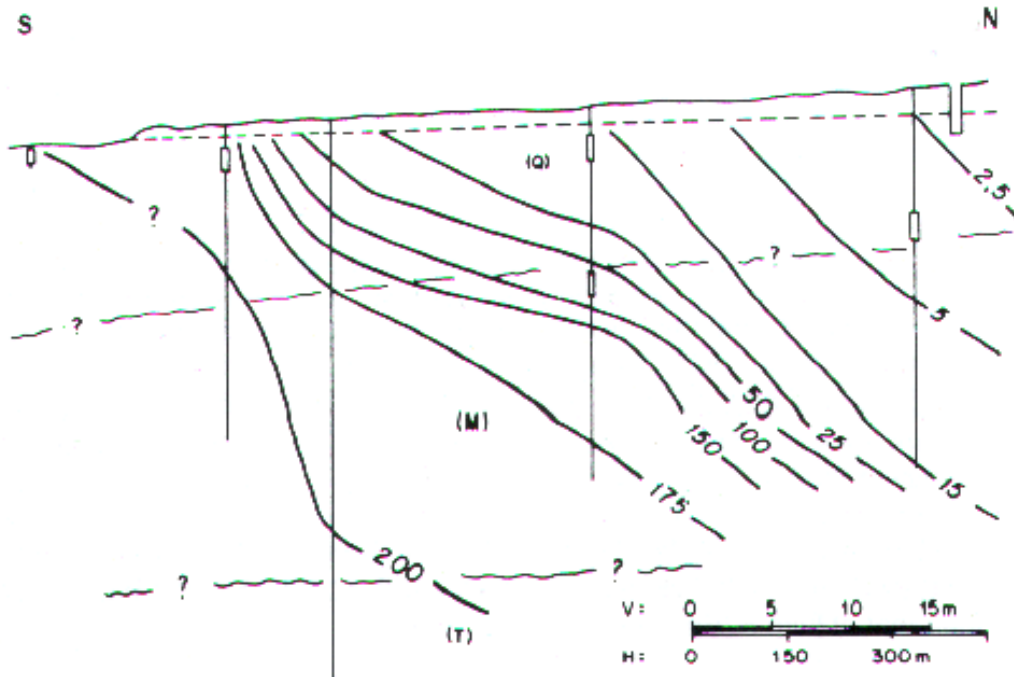


Figure 1.19: Cross section north of the lake (BENAVENTE ET AL., 1996b). The salt lake is situated at the south end of the cross section. Electric conductivity is represented in mS/cm by contour lines. Q=Quaternary materials; M=Miocene materials; T=Triassic materials.

Below the salt lake a salt wedge has evolved which is confirmed by conductivity logs. Conductivity logs that indicate almost time independent situations of the salt/freshwater transition zone were measured by ALMÉCIJA RUIZ (1997), HEREDIA ET AL. (2004), RODRIGUEZ-RODRIGUEZ ET AL. (2006) and BENAVENTE ET AL. (1993, 1994, 1996b, 2003). A cross section in the northern part of the maximum flooding area that plots the electric conductivity was published by BENAVENTE ET AL. (1993, 1994, 1996b) (Fig. 1.19).

Isotopic data shows significant evaporation signals and designate that the brines derive from surface water (HEREDIA ET AL., 2004; RODRIGUEZ-RODRIGUEZ ET AL., 2006).

1.4 Topics and aims of this study

The topic of this study is the characterization of the interaction between salt lake and groundwater on the basis of hydrogeochemical, isotopegeochemical and sedimentological investigations in Fuente de Piedra Basin, Spain.

Within the scope of this diploma thesis the hydrogeological settings of the lake and the basin are characterized. Based on the established general models, the flow pattern of salt lake brines and affiliated groundwater in Fuente de Piedra Basin are to be specified during the course of this study. Therefore the impact of density driven flows

and diffusion are to be specified with regard to brine evolution and salinization of the aquifer.

For these purposes water samples from monitoring wells and piezometers were sampled for hydrochemicals, environmental isotopes and hydraulic conditions. The Ascertainment of the spatial distribution of (former) lake sediments by borehole drillings is the aim of the geological mapping.

2. Mapping

Within the scope of the diploma mapping 28 bore holes were drilled to explore the former extension of Fuente de Piedra Salt Lake (Laguna de Fuente de Piedra) in Andalusia, SE Spain. The borehole drillings were spotted in the recent maximum flooding area and in the lake's vicinity (Fig. 2.4). Therefore two field campaigns in Fuente de Piedra Basin took place in September 2005 and in March 2006. In March 2006 the field work focuses on the basin, especially in the northern part.

Because of the bearing and shape of the salt lake and his basin, the conclusion of a notwithstanding extension of the lake in former times is standing to reason. We know that under definite conditions a certain type of salt lake is generated. Recently the Fuente de Piedra Salt Lake is of ephemeral type, which is documented in the composition of sediments and water and caused by predefined climatic and geomorphologic conditions (LINARES, 1990). If the type and, in short terms, the climatic conditions change, it is bequeathed in the soil (FÜCHTBAUER, 1988).

Drilling depths vary between 3 and 9 m, in average 5 m. To investigate the lakes setting a borehole log was erected for every bore site. Furthermore samples of the determined strata were taken for sediment analysis (Tab. 2.6).

2.1 Methods

2.1.1 Definition of mapping area

Definition of the mapping area was made using two criteria:

a) Altitude

Altitude contour map is extracted from a Digital elevation model (DEM) to define the mapping area. Digital elevation models contain X, Y and Z data respectively X and Y geographic coordinates and altitude above sea level (BURROUGH, 1987).

Longitude, Latitude and Altitude Data are exported from DEM (JUNTA DE ANDALUCÍA, 2005) as DEM.asc, this file is renamed in DEM.txt and uploaded in ArcView 3.2 (ESRI) as an Event Theme. By Spatial Analyst Extension a conversion into a grid-file was done (Gridding Method: Kriging with the adapted variogram settings). By Global Mapper 6.0 the grid-file was converted into a USGS DEM format. Now the DEM can be used for analysis. The cell size is 10 m in horizontal and vertical direction. Altitude accuracy is 0.5 m. A reasonable classification with 10 m spacing around the salt lake and 50 m steps in higher altitudes is chosen.

Contour map of elevation levels (Fig. 2.1) shows an elevation distribution of up to 410 masl inside the maximum flooding area (area I). The altitude of the lake bottom is determined as 409 masl. In the northern vicinity and at the northeast shore of the lake elevations are up to 10 m higher. This area with altitudes up to 420 masl (area II) could constitute the lake's paleo extension due to similar elevation than the lake's present maximum flooding area surface. The remaining part of the basin with altitudes > 420 masl is named as area III.

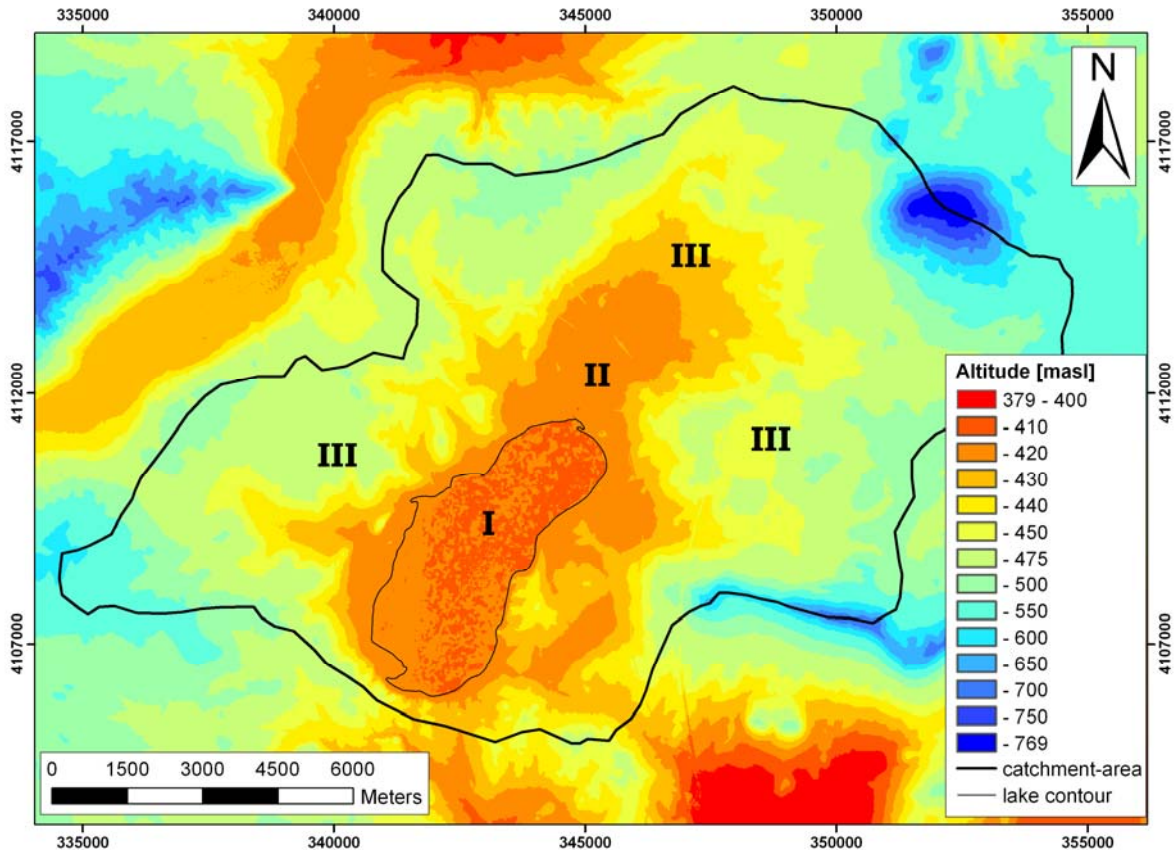


Figure 2.1: Contour map of elevation levels, indicating an elevation distribution of up to 410 masl inside the maximum flooding area (I) and in the northern part of it up to 420 masl (II). Area situated higher 420 masl is marked with III. Contours derived by DEM, spots inside the recent lake contour results from elevation boundary classification (Altitude accuracy 0.5 m).

b) Surface colour

Differentiation of surface soil colours were made by aerial colour view. In Fuente de Piedra Basin aerial colour photography shows 4 types of surface colours and therefore limits areas of colour distribution (Fig. 2.2). Type I make up the lake's water filled surface at date of record. Type II occurs inside the maximum flooding area as recent lake sediments, hues reach from white to light green, light brown and light green-brown to white. Type III is situated in the surrounding of the salt lake and mainly in the northern part of the basin below 420 masl as light hues (very light grey;

light green, light brown; light green-brown). Hues of Type III are similar to Type II. Type IV is constituted by multicolored areas.

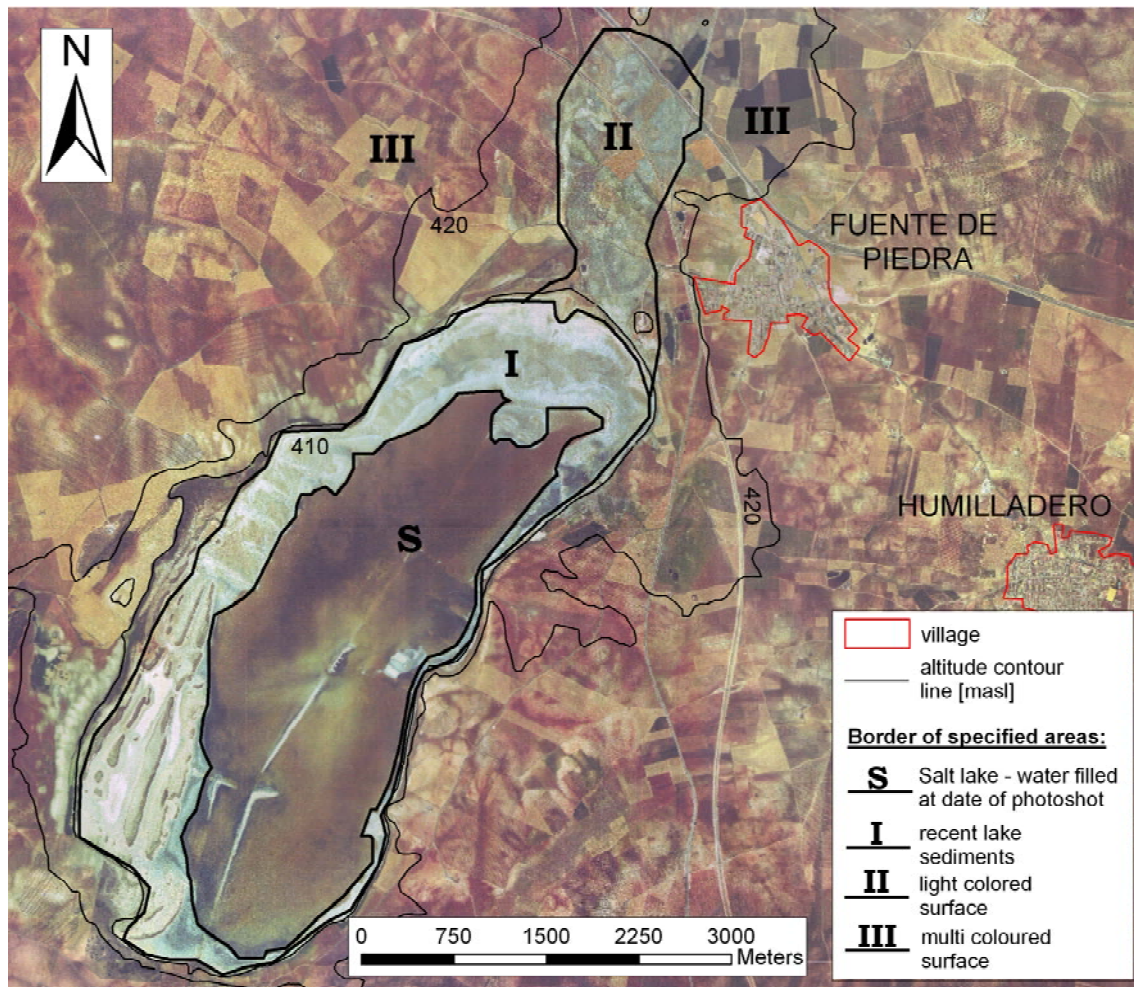


Figure 2.2: Aerial view of Fuente de Piedra Salt Lake obtained from JUNTA DE ANDALUCÍA (2003). S and I – III mark area distinguishable by surface colour. Combined presentation with altitude contour lines 410 and 420 masl.

Moreover a major region in the southwest (south of La Herriza) and a smaller part in the northeast of the salt lake is as well light colored (Type III). Laminar movement of sediments by wind (deflation) with wind strengths up to 4 m/s can move grain sizes up to 0.25 mm (fine sand) when loose, dry sediment grains or aggregates without vegetation protection appear at the surface (KUNTZE ET AL., 1994).

In Fuente de Piedra Basin main wind direction (weather station Bobadilla and Antequera) is SSE, followed by NNW. Main wind velocities range between 0.8 and 3.6 m/s with a mean of 2.1 m/s (ALMÉCIJA RUIZ, 1997; CONSEJERÍA DE AGRICULTURA Y PESCA; 2006).

In consideration of above-mentioned, the occurrence of light hues in the southwest and at the northwest shoreline at higher altitudes (> 420 masl) can be explained (compare Fig. 2.3) due to wind influenced movement of salt lake sediments.



Figure 2.3: Salty dust from the Salt lake, deposited on fields by eolian transport, east of La Herriza

By combined altitude and surface colour type illustration (Fig. 2.2) the mapping area was set between 410 and 420 masl with concentration on the northern part of the basin (Fig. 2.10).

To prove the working assumption that light colored areas mark up salt lake (paleo-) sediments due to similar hue and colour, drillings were set between 410 and 420 masl into light coloured zones and beyond.

2.1.2 Drilling network

The bore sites were chosen to achieve a good spatial distribution and with regards to accessibility by car according to the defined mapping area.

The drillings were concentrated near the lakes present coastal line and in the northern part of the basin (Fig. 2.4). The northern part of the basin is extensively used for agriculture, so bore sites mostly spotted beside farm tracks and gravel roads or placed in drainage channels. Tab. 2.1 shows the location, depth and number of samples of the drilling sites.

2.1.3 Borehole drillings

To recover drill cores for further investigations in field campaign autumn 2005 a 1 m NORDMEYER-ram probe (80 mm) and a 2 m NORDMEYER-ram probe (60 mm) were used. The NORDMEYER-ram probe is thumped for the complete length into the soil by an Electrical hammer drill and afterwards pulled out by a hydraulic puller. For drilling the first meter the 1 m NORDMEYER-ram probe was used. The following probes were carried out mainly by the 2 m NORDMEYER-ram probe, whereas the 1 m NORDMEYER-ram probe was used to extend the borehole particularly with regard to the construction of the wells. Fine grained sediments in and around the lake and

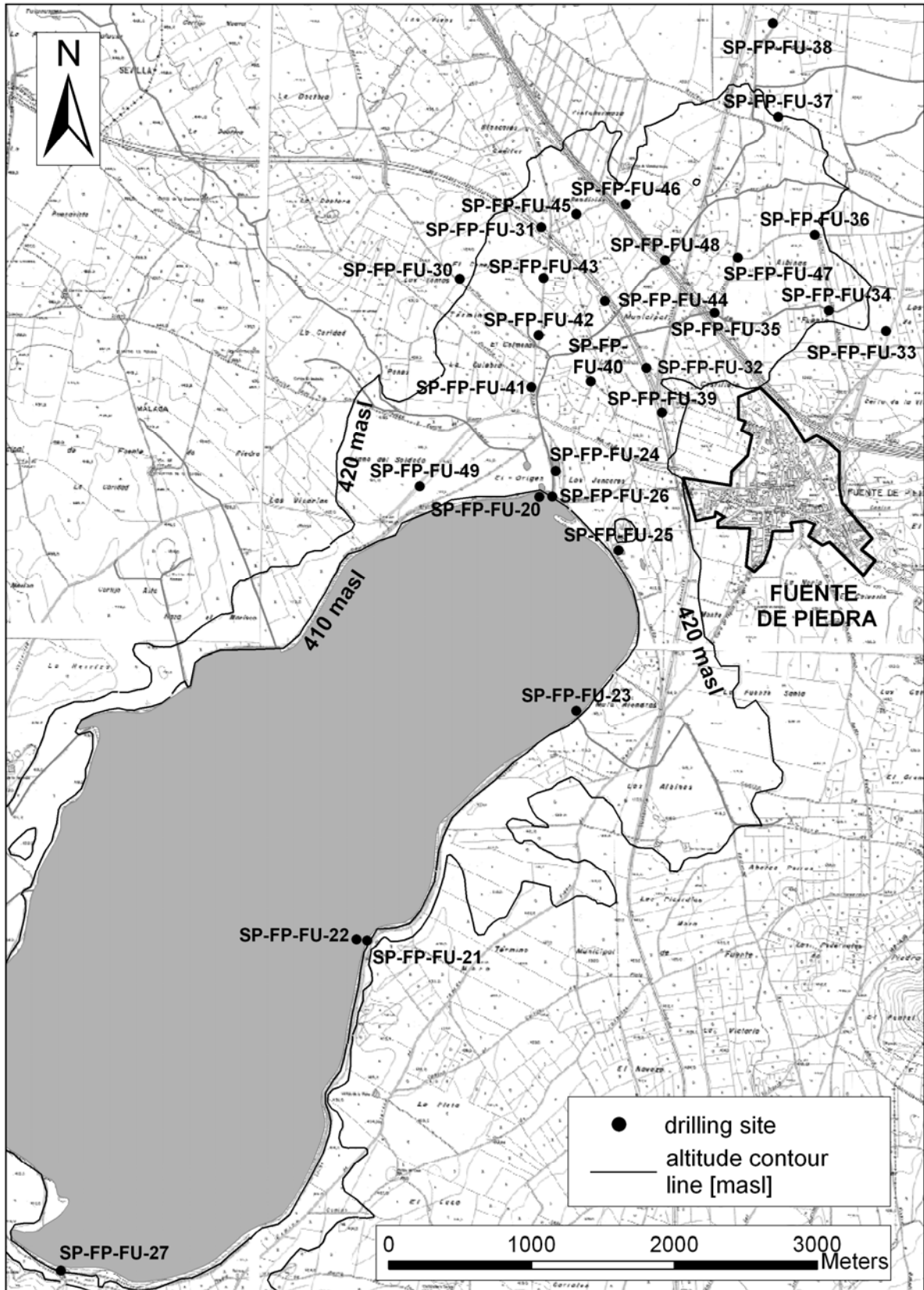


Figure 2.4: Drilling sites autumn 2005 and spring 2006 in Fuente de Piedra Basin.

land filled areas due to a brisk construction activity around the lake often complicated the drilling performance.

During the field campaign spring 2006 two different drilling systems were used. To decrease the frictional resistance of the soil in order to reduce the abrasion of the equipment to a minimum, ram probes with less diameter were used. The so called PUERCKHAUER probe and drill rods with a diameter of ½ inch is to be placed by hand or with an electrical hammer drill into the soil until 5 m and is to be pulled out by hand. The PUERCKHAUER probe recovers only a small amount of sediment sample and is only applicable for fine grained sediments. The second drilling system composed of a 1 inch probe and 1 inch drill rods is operated by an electrical hammer drill and a hydraulic puller. This system requires more time and effort, but recovers core representative samples, even for coarse sediments, until depth of 10 m.

2.1.4 Sediment characterization

Sampling and sediment characterization focus on macroscopically differentiable units. Differences in lithology result primarily in variations of grain size, colour, content of carbonate, content of fossils, organic matter and variation in penetration resistance and soil consistence. Sediment characterization occurs accordingly to directives of DIN 4022 (1987). Above directive obtains to designation and description of soil and rock and further to application for setting up borehole logs for investigations of subsoil and groundwater by drilling with (out) winning of continuous core samples.

For every drilling a required form was completed. The borehole log ensures a consistent registration of all important characteristics of the drilled soil and the identification of predominant groundwater conditions. The soil classification and description consist of varied lithological properties. Layer boundaries are mainly defined by variation of grain size and colour. Furthermore grain size distribution, material, character of mineralogical and organic composites and consolidation status are the decisive parameters for designation. Carbonate content was proved with 10% 0.1 mol HCL. The achievements were documented and processed in GeODin 3.0 as geological logs, which used for the creation of geological cross sections of the studied area.

Table 2.1: Bore sites with location, depth, no. of samples and diameter of perforation.

Site Id.	East UTM km	North UTM km	Depth below surface [m]	No. of samples	Diameter [inch]
SPFPFU20	344750	4111442	5	12	2
SPFPFU21	343545	4108333	1	-	2
SPFPFU22	343471	4108342	5,5	20	2
SPFPFU23	345008	4109947	4	12	2
SPFPFU24	344865	4111624	4	7	2
SPFPFU25	345305	4111071	2,5	-	2
SPFPFU26	344840	4111444	3	10	2
SPFPFU27	341400	4106028	4	6	2
SPFPFU30	344193	4112974	4	-	½
SPFPFU31	344764	4113336	6,5	7	½
SPFPFU32	345499	4112350	5	12	1
SPFPFU33	347175	4112604	4	7	1
SPFPFU34	346776	4112749	3	6	1
SPFPFU35	345977	4112733	7	6	1
SPFPFU36	346678	4113283	5	5	1
SPFPFU37	346422	4114109	6	10	1
SPFPFU38	346384	4114762	5	9	1
SPFPFU39	345608	4112036	5	5	1
SPFPFU40	345110	4112255	5	5	½
SPFPFU41	344694	4112216	5	7	1
SPFPFU42	344745	4112575	5	5	½
SPFPFU43	344780	4112978	5	8	1
SPFPFU44	345207	4112815	5	8	1
SPFPFU45	345008	4113426	5	5	1
SPFPFU46	345355	4113492	3	2	½
SPFPFU47	346137	4113122	6	6	1
SPFPFU48	345629	4113104	6	6	1
SPFPFU49	343913	4111518	9	13	1

2.1.5 Sediment analysis

The analysis of the sediment samples from drill cores focuses on the determination of grain size distribution. The grain size distribution describes soil, based on the medial geometrical expansion of his components, and specific soil mechanic characteristics could be derived out of it (grain size distribution; DIN/ISO 11277, 1994). Grain size distribution reflects the mass fractions of granulation fractions. Grain sizes over 0.063 mm are measured by sieving and grain sizes under 0.125 mm measured by sedimentation (elutriation). The (analyzing) soil sample is poured into a sieve set with different aperture sizes and is tared fractioned. Used aperture sizes are shown in Tab. 2.2. The data are presented in sum curves, the median grain size result from the intersection of 50 %-line with the sum curve. The standard for the classification of grain sizes is DIN 4022 (1987).

The sediment samples from the drill cores are mainly fine grained and are suitable for the analysis by sedimentation. This method based on the principle that various sized grains sink with different velocities in stagnant water. The connection between grain size, density and sink rate are specified by STROKES LAW and are only valid for spherical bodies. Because of the various sink rates of the grains (based on grain size) the (temporal) dispersal of grain size and consequently the dispersal of the density of the suspension changes with time. For quantifying the variation in defined periods a density hydrometer is used. From density values and immersion depth of the hydrometer the determination of grain size can be calculated. Before measuring grain size distribution by sedimentation certain materials have to be removed from the sample to avoid coagulation. These are primarily organic matters, soluble salts and gypsums. For the detailed proceeding see Fig. 2.5. Additionally ammonium-hydrogen ($\text{NH}_4(\text{OH})$) is added as an anti-coagulation medium.

Table 2.2: Aperture sizes of filter used for sieving.

Aperture size of filter
> 2
> 1
> 0,5
> 0,125
< 0,125

With the results for the determination of grain size from sieving and sedimentation methods, the coefficient of hydraulic conductivity can be calculated after BEYER (1964):

$$k_f = C \cdot (d_{10})^2 \tag{6}$$

where

d_{10} = effective grain size in mm, relative to which 10% of the sample is finer

C = coefficient depending on uniformity coefficient for groundwater temperature of 10 °C; Tab. 2.3

The uniformity coefficient C_U describes the grading and is given by:

$$C_U = \frac{d_{60}}{d_{10}} \tag{7}$$

where

C_U = uniformity coefficient,

d_{60} = grain size that is 60% finer by weight and

d_{10} = grain size that is 10% finer by weight (effective grain size).

The BEYER-method is valid for mean groundwater temperatures of 10 °C but is applied here in knowledge of the restriction of accuracy. Mean groundwater temperature in Fuente de Piedra Basin is 17 °C. With increasing temperature the viscosity of the groundwater decreases. The decrease from 10 °C to 17 °C is around 30 %. Typical coefficient of hydraulic conductivity values are 1E-04 to 1E-05 for fine grained sand, 1E-05 to 1E-07 for silty sand, 1E-06 to 1E-09 for clayey silt and < 1E-

09 for clay (HÖLTING, 1996). Tab. 2.4 shows the coefficient of hydraulic conductivity and related permeability.

Table 2.3: Coefficient C relating to C_U after BEYER (1964).

C_U	C
1.0 - 1.9	0.11
2.0 - 2.9	0.10
3.0 - 4.9	0.09
5.0 - 9.9	0.08
10.0 - 19.9	0.07
> 20.0	0.06

Table 2.4: Permeability related with hydraulic conductivity k_f (DIN 18130-1, 1989).

permeability	k_f
very good permeable	1E-01 - 1E-02
good permeable	1E-02 - 1E-04
permeable	1E-04 - 1E-06
less permeable	1E-06 - 1E-08
very less permeable	< 1E-08

For the determination of grain size distribution sediment samples according to a depth and bore site were chosen to figure out the change of grain size in depth.

Table 2.5: Soil texture and analysis method.

diameter [mm]	main separate	sub-separate	abbreviation	Analysis method
> 63	stone		X	sieving
20 -63	gravel	coarse gravel	gG	
6.3 – 20		medium gravel	mG	
2 – 6.3		fine gravel	fG	
0.63 – 2	sand	coarse sand	gS	
0.2 – 0.63		medium sand	mS	
0.063 – 0.2		fine sand	fS	
0.063 – 0.02	silt	coarse silt	fU	sedimentation
0.02 – 0.0063		medium silt	mU	
0.0063 – 0.002		fine silt	fU	
< 0.002	clay		T	

Another fraction of the sediment samples is handed over to the University of Malaga and will be analysed by x-ray diffractometry for crystalline structures and clay minerals. The Interpretation of these data will be subject in further investigations. Analysis for ionic composition of the sediments will be made by Liisa Majja Paul (FUB) within the scope of a diploma thesis.

The presentation of fractions is displayed as percentage in a grain size distribution graph. The determination of grain size distribution for mineral soil material is realized after DIN/ISO 11277 (1994). A schedule of the determination procedure is shown in Fig. 2.5.

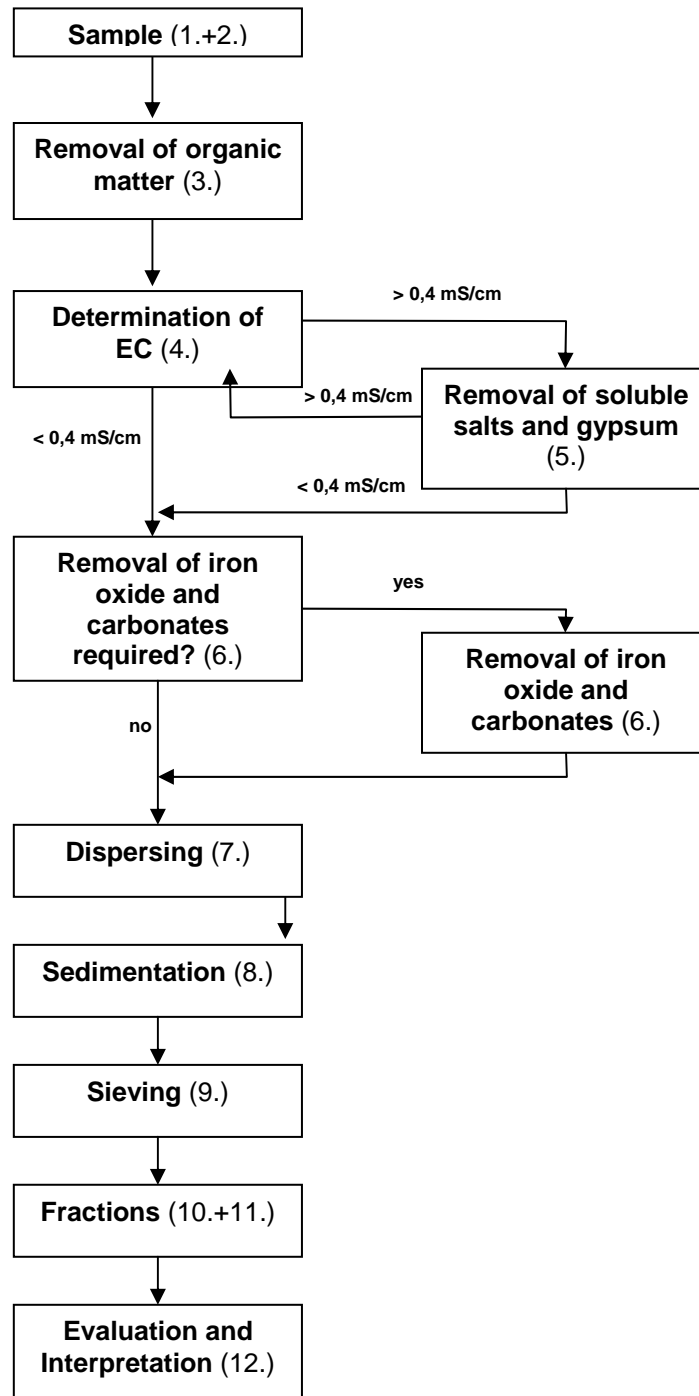


Figure 2.5: Schedule of determination of grain size distribution derived from DIN/ISO 11277 (1994).

2.2 Results

2.2.1 Sediment characterization

For the characterization of the lake sediments selected drillings with a typical and significant sequence for the lake and for the area located north of the lake are consulted and analysed. Furthermore significant drillings of the northern part are presented in four cross sections. On the basis of the data obtained by drillings and in consideration of the geological units this mapping attempt to give evidence about the deposit conditions and spread of former lake sediments.

Fine grained sediments with high gypsum content (inside the lake and at the edge) and high carbonate and sparse in organic matter are dominating the upper 5 m of the soil in the study area.

2.2.1.1 Borehole logs

For the characterization of sediments two profiles were chosen due to their representative lithologies and their location in the mapping area. As you can see in Fig. 2.6, Type 1 (SPFPFU22) is situated in the eastern marginal area of the recent salt lake. This site is yearly flooded in winter and spring time. Type 2 (SPFPFU49) is located in the northern vicinity, nearly 150 m away from the recent lake shore in a slight hillside situation. Borehole profiles of both sites are shown for SPFPFU22 (FU22) in Fig. 2.7 and for SPFPFU49 (FU49) in Fig. 2.9. Significant lithologies regarding the borehole profiles are described subsequent to them. Borehole profile SPFP20, also shown in Fig. 2.7, is discussed in type analogy.

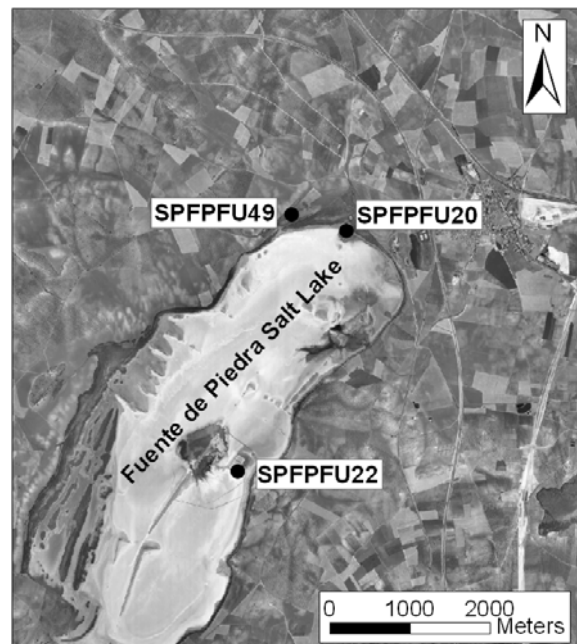


Figure 2.6: Location of selected borehole profiles for classification of types. Aerial view obtained from JUNTA DE ANDALUCÍA (2004).

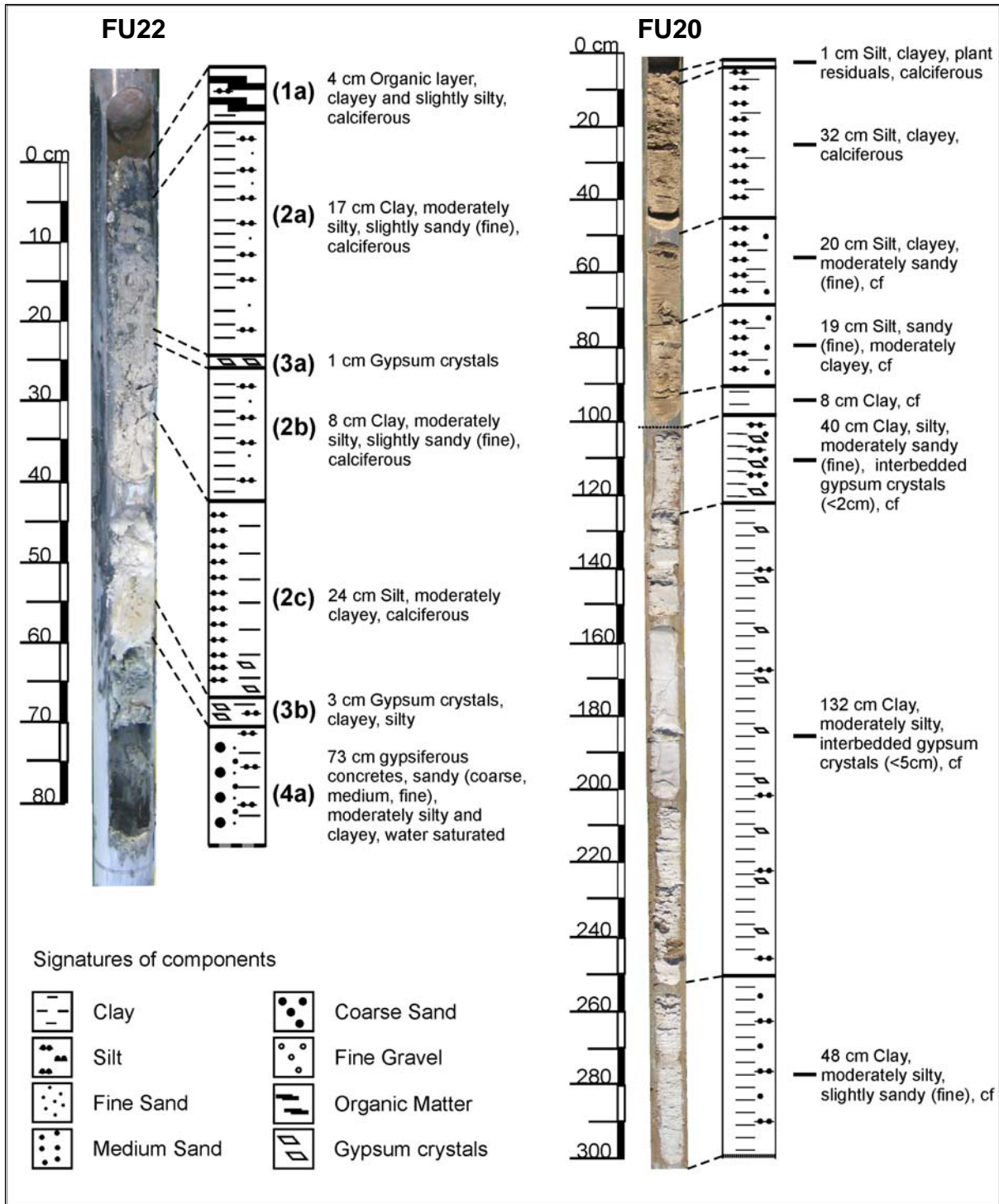


Figure 2.7: Photo and schematic borehole profile of sites FU22 (left) and FU20 (right). Type 1 lithologies are characterized on the basis of FU22 stratification.

Type 1 lithologies - SPFPFU22

(1) Organic layer

Thin organic layers were found at the surface (1a) and in a depth of 1.9 m. They consist of organic matter with a moderate content of clay and carbonate. The recurrence of this layer could mark a paleo lake floor, where organic material deposits according to slow sedimentation and a shallow water level. Due to a fast

covering, these layers can be preserved. Although high salinities limit the occurrence of organisms, they apparently are responsible, together with plant and digestive remains, for the accumulation of the organic material.

(2) Grey clays

Light-coloured (grey) clays are the dominant components of the lake sediments. Beside clay, silt and fine sands in varying contents, constitute the background sedimentation. Clay stratification thicknesses are < 1.5 m. The clays represent calm deposition conditions, associated with a high input of eolian particles. Additionally the clays include fine grained sulphates and partly carbonates. These evaporites are precipitated postsedimentary from the oversaturated brine and originate from a provenience dominated by chemical sediments. Organic matter and gypsum crystals (2c) are constantly interbedded in the clayey matrix and appear mostly combined.

(3) Gypsum crystals

Gypsum crystals appear in thin layers, few cm thick, interbedded in the clays. The crystalline gypsums are partly developed in well-defined stratifications, shown in the borehole profile (3a.) and are often imbedded in specific clay horizons (2c).

As seen in Fig. 2.7, the crystals vary in size from 1 to 5 cm and are idiomorphic shaped.

Partly they developed as typical twinning crystals. For the origin of the gypsum crystals

postsedimentary precipitation is assumed. Idiomorphic crystals develop predominantly in former desiccation cracks. They provide the space for the precipitation of gypsum and paths for the circulation of the oversaturated brine.



Figure 2.8: Idiomorphic gypsum crystals (twins) from stratification (3b).

(4) Sands

The grey-coloured sands are fine to coarse grained with a moderately fraction of silt and clay. The coarse sand grains consist mainly of subrounded gypsiferous concretes. The sand stratification is free of carbonate and water saturated. Sands seem to be turbidite deposits, sedimented due to tempest events. According to this, gypsiferous concretes could form symsedimentary by abrasion from soil or by postsedimentary precipitation processes.

2. Mapping - Results

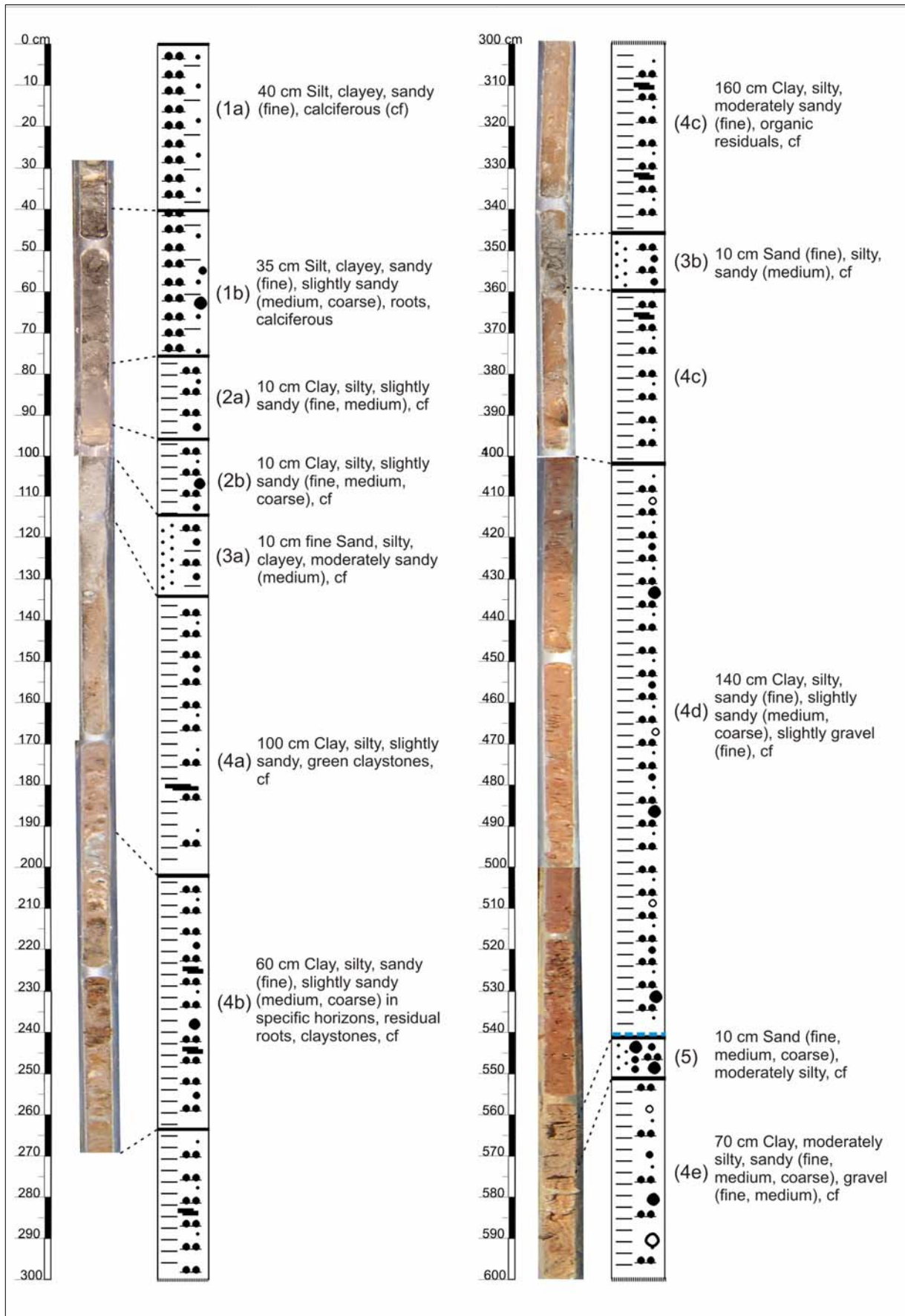


Figure 2.9: Photo and schematic borehole profile of site FU49. Type 2 lithologies are characterized on the basis of FU49 stratification. For legend of signatures see Fig. 2.7.

Type 2 lithologies - SPFPFU49

(1) Silts

The dark-coloured silts contain a minor fraction of clays and fine sands and a slightly content of medium and coarse sands. Roots appear in the first 75 cm. The grey-brown colour indicates already activated pedogenesis processes (KUNTZE ET AL., 1994). These sediments are apparently accumulations at the base of a mountainside.

(2) Light clays

The clays are characterized by light-grey colour, a minor fraction of silts and a slight fraction of fine to coarse sands. Furthermore they are calciferous. The grey clays only appear in a depth of 75 cm to 95 cm. The thickness of clay stratification in Fig. 2.9 is not veritable due to a compression of soil material in succession of drilling. The deposit of the clays can be associated with lake sedimentation under calm conditions. But contents of coarser particles indicate a slight input of clastic bulk material from the near located mountainside.

(3) Sands

Thin sandy beds appear in two depths and feature minor contents of clay and silt. The grey-coloured sands are fine grained with a varying medium grain fraction. Sand layers were found in depth of 1.0 m and 3.5 m and indicate an increased influence of periodic turbidite events with high sedimentation rates.

(4) Red clays

Red clays dominate the soil below 1.1 m. The clays have a minor fraction of silts and fine to medium grained sands. Below 5.5 m the fraction of coarse sand increase and fine to medium gravel appear sporadically. In stratification (4a) a thin horizon of plant residuals in a depth of 1.8 m indicates a former exposition with vegetation. Furthermore in stratification (4b) residual roots appear in specific horizons. Below, organic material occurs only sporadic. In addition multicoloured clays are sporadically interbedded. The red clays represent a change of provenience and deposition conditions with more clastic material and less evaporites.

(5) Red sands

Thin beds of reddish sands (fine to coarse grained) with a moderately silt fraction appear in depth of 5.6 m and 7.3 m and represent short-time periodic events of alluvial deposition. These sand layers are water-bearing and confined by the red clays.

Type analogy

As shown in Fig. 2.7 and 2.9, the dominant lithologies of type 1 and 2 are clays, representing the background sedimentation. While light clays of type 2 can be associated with type 1 clays, the type 2 reddish clays differ greatly in colour and components from type 1. Type 2 clays feature a greater and broader fraction of sands and gravel with depth and a less content of chemical sediment. In contrast to type 2, type 1 clays are abundant of gypsum and partly free of carbonates. Type 2 organic layers appear only poorly developed and are composed of plant residuals in contrast to type 1. Furthermore gypsum crystals, found in type 1 clays, are completely lacking in type 2 sediments. Interbedded clastic sand stratifications are well-defined in type 2, whereas type 1 sands are developed more inhomogeneous and mainly composed of chemical sediments.

Profile variations

Borehole profiles around the salt lake show further characteristics deviating from above-mentioned. Sites located at the lake shore are dominated by grey clay stratifications related to Type 1. In the north-eastern lake edge clays are homogenous and feature slight to moderate silt and sand fractions and are lacking of sand beds, as shown in Fig. 2.7. Roots residuals appear sporadic in horizons. In the fluctuation zone of groundwater and below crystalline gypsums are abundant. At the eastern shore clays contain greater fraction of silts and sands as well as plant residuals and sand beds in the upper zone. The southern lake shore is characterized by multicoloured clays with interbedded gypsum crystals, calcretes and claystones. Grey lake sediments are absent.

In the northern vicinity sediments are related to Type 2 stratifications. Compared to Type 2, grey clays feature a greater spectrum of grain sizes with fractions of fine sands to medium sized gravels. Furthermore chalk and clay lenses are interbedded sporadically. Red clay stratifications do not show significant variations compared to Type 2, except of a colour range from red-brown to multicoloured. Red sand beds partly feature in addition gravels as well as clay and carbonate clasts.

2. Mapping - Results

Table 2.6: Borehole-logs for drilling sites in autumn 2005 and spring 2006. Abbreviations can be seen in Tab. 2.7.

borehole-logs									
site Id.	depth [m]	type of soil material	remarks	consistency of soil material	hardness of drilling	colour	lime content	remarks2	sample Id. (sample depth)
SP-FP-FU-20	0,1	U,t	salty taste	dry	easy	light brown	++		1
SP-FP-FU-20	0,33	U,t	salty taste	dry	easy	light brown	++		2
SP-FP-FU-20	0,53	U,t,fs	salty taste	plastic	easy	brown	++		3
SP-FP-FU-20	0,72	U,fs,t	salty taste	plastic	less easier	beige	++		4
SP-FP-FU-20	0,8	T,fs	salty taste	plastic	less easier	dark brown	++		5
SP-FP-FU-20	1,2	T,u,fs,mg	salty taste, idiomorphic gypsum crystals (2cm)	plastic	less easier	grey-beige	++		6
SP-FP-FU-20	2,52	T,mg	salty taste, idiomorphic gypsum crystals (>2cm)	plastic	easy	beige	+		7(1,2-1,4);8(1,8-2,0);9(2,3-2,5)
SP-FP-FU-20	3,0	T,fs		plastic	easy	beige	++		10(2,8-3,0)
SP-FP-FU-20	4,3	T,mg,u",fs"	idiomorphic gypsum crystals	plastic	easy	beige	++		11(4,00)
SP-FP-FU-20	5,1	T,mg,u",fs"	idiomorphic gypsum crystals, brown streaks	plastic	less easier	beige	++		12(4,8-5,0)
SP-FP-FU-22	0,04	T,u'		plastic	easy	black	++		1(0,04)
SP-FP-FU-22	0,3	T,u,fs"	1cm layer of gypsum crystals in 0,21m depth	semi solid	very easy	beige	++		2(0,16)
SP-FP-FU-22	0,54	U,t,fg"	gypsum crystals on bottom	mushy	very easy	beige	+		3(0,5)
SP-FP-FU-22	1,27	gS,fs,u,t		crumble	easy	light grey	-	water saturated	4(0,64)
SP-FP-FU-22	1,4	T,fs		semi solid	easy	grey	-		5(1,3)
SP-FP-FU-22	1,75	T,fs	many gypsum crystals	crumble	easy	grey	-		6(1,4)
SP-FP-FU-22	1,79	fG,t'	gypsum crystals		easy	grey	-		7(1,78)

2. Mapping - Results

borehole-logs									
site Id.	depth [m]	type of soil material	remarks	consistency of soil material	hardness of drilling	colour	lime content	remarks2	sample Id. (sample depth)
SP-FP-FU-22	1,9	T,fg	gypsum crystals		easy	dark grey	-		7(1,9)
SP-FP-FU-22	1,92	T,u'	organic layer	plastic	easy	black			8(1,92)
SP-FP-FU-22	2,27	T,fs	with organic material	mushy	easy	grey			9(2-2,2)
SP-FP-FU-22	2,80	fG,fs,t	gypsum crystals, organic material	crumble	easy	grey	-		10(2,23-2,3);11(2,4-2,6)
SP-FP-FU-22	3,1	T	with organic material	mushy	easy	grey	-		no sample
SP-FP-FU-22	3,2	fG	gypsum crystals	semi solid	easy	grey	-		12(3,1-3,2)
SP-FP-FU-22	3,4	T,u,fs,ms		semi solid	easy	grey	+		13(3,4)
SP-FP-FU-22	3,68	T,fg,ms,gs,u,	gypsum crystals interbedded (fg)	crumble	easy	grey	+		16
SP-FP-FU-22	4,17	T,ms,gs,u,fg	gypsum crystals interbedded (fg)	plastic	less easier	grey-green	+		14(4,11)
SP-FP-FU-22	4,21	concrete	gypsum	solid	less harder	grey	+		15(4,21)
SP-FP-FU-22	4,61	T,fg	gypsum concretes and crystals	plastic	less easier	grey-green	-		17(4,45)
SP-FP-FU-22	5,0	T,ms,fg	gypsum concretes and crystals	plastic	less easier	beige-grey	-		18(4,92)
SP-FP-FU-22	5,05	mS	crystals	semi solid	less easier	light grey	-		19(5,0)
SP-FP-FU-22	5,1	T,fg,fs',ms'	gypsum crystals interbedded (fg)	plastic	less easier	dark grey	-		20(5,05)
SP-FP-FU-23	0,07	T,u,fs		dry	easy	brown-beige	++		1(0,01-0,07)
SP-FP-FU-23	0,28	mS,t,u,gs'		dry-hard	easy	beige	++		2(0,1-0,2)
SP-FP-FU-23	0,35	T,u,fs	gypsum matrix	plastic	easy	beige	++		3(0,3-0,35)
SP-FP-FU-23	0,47	fS,t,gs,u,fg	gypsum matrix	dry-hard	easy	beige	++		4(0,4-0,45);5
SP-FP-FU-23	2,0	T,u,fs	red-brown streaks	plastic	easy	brown-beige-grey	++	water saturated in 2,8m	6(0,8-0,9);7;8
SP-FP-FU-23	3,0	T,u,fs,ms	lime concretions	plastic	less easier	white-beige	++		9;10

2. Mapping - Results

borehole-logs									
site Id.	depth [m]	type of soil material	remarks	consistency of soil material	hardness of drilling	colour	lime content	remarks2	sample Id. (sample depth)
SP-FP-FU-23	3,4	T,u,fs	plants remnants	plastic	less easier	grey-green	++		11
SP-FP-FU-23	>3,4	T,u,fs	brown-red streaks	plastic	hard	brown-grey-green	++		12
SP-FP-FU-24	0,1	topsoil	roots	hard-crumble	easy	dark-brown	++		no sample
SP-FP-FU-24	0.65	U,t',fs"	roots	dry	less easier	beige	++		1(0,21-0,3)
SP-FP-FU-24	0,95	T,u,fs"		hard	less easier	beige	++		2(0,7-0,8)
SP-FP-FU-24	1,4	T,u',fs"	sporadic, small gypsum crystals	plastic	less easier	dark-white	++		3(1,2-1,4)
SP-FP-FU-24	2	T,ms,gs	gypsum concretions	plastic-crumble	less easier	dark-white	++	water saturated	4(1,6-1,7)
SP-FP-FU-24	3,05	T,u',fs'	sporadic, small gypsum crystals 2 mm diameter	plastic	less easier	dark-white	++		5(2,2-2,3);6(2,7-2,8)
SP-FP-FU-24	4	T,u'	brown spots	plastic	less easier	green-grey	++		7(3,2-3,3)
SP-FP-FU-26	0,2	fS,u,t		dry-crumble	easy	red-brown	++		1(0,2)
SP-FP-FU-26	0,5	fS,u,t		dry	less easier	grey	++		2(0,4)
SP-FP-FU-26	0,65	T,u,fs		dry	hard	grey	++		3(0,65)
SP-FP-FU-26	1,6	T,u,fs		wet	hard	beige	++		4(0,8);5(1,3)
SP-FP-FU-26	1,8	T,u,fs"	roots	plastic	easy	light beige	++		6(1,7)
SP-FP-FU-26	2,2	T,u,fs"	roots	plastic	easy	light beige-grey	++		7(1,9);8(2,2)
SP-FP-FU-26	2,75	T,u,fs"		plastic	easy	light beige-grey	++		9
SP-FP-FU-26	2,85	T,u	gypsum crystals	crumble	hard	light beige-grey	++		10(2,8)
SP-FP-FU-27	0,5	gS,ms,fs,u	top soil	dry	less easier	brown	++		1(0,5)
SP-FP-FU-27	2	mS,gs,u	gypsum crystals, carbonate fragments	plastic	less easier	light brown	++		2(0,8)

2. Mapping - Results

borehole-logs									
site Id.	depth [m]	type of soil material	remarks	consistency of soil material	hardness of drilling	colour	lime content	remarks2	sample Id. (sample depth)
SP-FP-FU-27	3,3	T,u	gypsum crystals, carbonate fragments	plastic	less easier	grey-brown-yellow	+		3(2,1);4(2,8)
SP-FP-FU-27	3,4	T,u,fg,mg	gypsum crystals, clay clasts	plastic	easy	multicoloured	++		5(3,4)
SP-FP-FU-27	3,5	T,u,fg	gypsum crystals, clay clasts	plastic	easy	multicoloured	++		no sample
SP-FP-FU-27	>3,5	T,u,fg,mg,gg	many gypsum crystals and claystones	semi solid	hard	multicoloured	+		6(3,7)
SP-FP-FU-30	0,3	T,fs'	topsoil	dry	easy	brown	++		no sample
SP-FP-FU-30	0,5	chalk,ms",fg"	ms average 1mm	crumble	less easier	orange	++		no sample
SP-FP-FU-30	3	chalk	chalk	crumble	less easier	beige	++		no sample
SP-FP-FU-30	3,30	T,fs'	brown clay	plastic	less easier	beige-brown	++		no sample
SP-FP-FU-31	0,3	topsoil	roots	dry	easy	beige-brown			1(0,2)
SP-FP-FU-31	0,35	fS,ms,u,T,gs,G	roots	dry	easy	brown			2(0,3-0,35)
SP-FP-FU-31	0,7	T,u,fs'		dry	easy	dark-brown			3(0,7)
SP-FP-FU-31	2,6	fS,ms,u,gs		dry	easy	ochre			4(2,0); 5(2,0)
SP-FP-FU-31	4,6	fS,u,ms,T,gs'		plastic	easy	ochre	++		6(4,0)
SP-FP-FU-31	6,6	T,u,ms,gs		wet	less easier	ochre	++		7(4,6-6,6)
SP-FP-FU-32	0,3	topsoil	roots	wet-solid	esay	black	+		1(0,3)
SP-FP-FU-32	1	T,u,fs"	salty taste	plastic	easy	beige	++		2(1,00)
SP-FP-FU-32	1,4	T,u,fs',fg"	chalk	crumble	easy	beige	++		3(1,4)
SP-FP-FU-32	2	T,u,fs',fg"	rust stains	semi solid	easy	ochre	++		4(1,6)
SP-FP-FU-32	2,2	T,fs,u	rust stains	plastic	easy	light grey	++		5(2,2)
SP-FP-FU-32	3,3	T,fs,u	green lentils	plastic	easy	light grey	++	water saturated: 2,3m	6(2,4)

2. Mapping - Results

borehole-logs									
site Id.	depth [m]	type of soil material	remarks	consistency of soil material	hardness of drilling	colour	lime content	remarks2	sample Id. (sample depth)
SP-FP-FU-32	3,5	T,gs,u	organic	plastic	easy	light grey	++		7(3,5)
SP-FP-FU-32	3,7	T,gs,u,fg'	rust stains	plastic	less easier	grey	+		8(3,7)
SP-FP-FU-32	4,1	mS,T,u,fg,mg"	red clay/ clay clasts(mg)	semi solid	less easier	ochre	+	schüttung?	9(4,1)
SP-FP-FU-32	4,4	Gs,ms,fg',T"		crumble	less easier	ochre	+		10(4,4)
SP-FP-FU-32	4,6	T,u,fs,ms,gs,fg		plastic	less easier	ochre- yellow	+		11(4,6)
SP-FP-FU-32	5	T,u,fs,ms',gs',fg"		plastic	less easier	multi-coloured	+		12(5,00)
SP-FP-FU-33	0,2	Hu,t,fs,u,ms		semi solid	less easier	red-brown	++		1(0-0,2)
SP-FP-FU-33	0,3	U,fs,t		plastic	easy	red-brown	++		2(0,2-0,3)
SP-FP-FU-33	0,35	T,u,fs,ms"		plastic	easy	light-brown-red	++		3(0,3-0,35)
SP-FP-FU-33	1,3	T,u,fs	light-beige clay clasts, soft	plastic	easy	light-brown/light-beige	++		4(0,35-1,3)
SP-FP-FU-33	3,3	T,fs,u,ms/T	organic: black stains and clay clasts soft in interbedded strata	semi solid/plastic	easy	reddish-brown/light-beige	++		5(1,3-2,0)
SP-FP-FU-33	3,65	mS,fs,u',mg"/T	red-brown sand with beige clay in interbedded strata	solid	less easier	reddish-brown-beige	++		6(3,3-3,65)
SP-FP-FU-33	4,0	T,u,fs,ms,gs,fg,mg	black stains, interbedded strata with fine and coarses layers	dry/ crumble	hard	light-beige	++		7(3,65-4,0)
SP-FP-FU-34	0,25	Deposit							no sample
SP-FP-FU-34	0,55	T,u,fs,hu	black stains < 2mm	dry/plastic	easy	brown	+		1(0,25-0,5)
SP-FP-FU-34	0,9	T,fs,u,ms	black stains < 2mm	dry/plastic/crumble	easy	ochre/dark red	++		2(0,6-0,9)
SP-FP-FU-34	1,3	T,fs,u,ms',gs"	black stains < 2mm	dry/plastic/crumble	easy	red-brown	++		3(0,9-1,3)
SP-FP-FU-34	2,0	T,u,fs,ms,gs,fg	black stains < 2mm/	dry/plastic/crumble	less easier	red-brown-	++/(+)		4(1,3-1,7)

2. Mapping - Results

borehole-logs									
site Id.	depth [m]	type of soil material	remarks	consistency of soil material	hardness of drilling	colour	lime content	remarks2	sample Id. (sample depth)
			clay clasts			beige			
SP-FP-FU-34	2,2	T,u,fs,ms	black stains < 2mm	dry/plastic	less easier	red-brown	(+)		5(2,0-2,2)
SP-FP-FU-34	>3	T,u,fs,ms,gs,fg,mg	black stains/clay clasts < 5cm	dry/plastic	hard	red-brown-beige	++/(+)		6(2,2-2,6)
SP-FP-FU-35	0,1	Deposit							no sample
SP-FP-FU-35	0,5	T,u,fs,gs",fg"	clay clasts	wet/crumble	very easy	dark brown	++		1(0,3-0,5)
SP-FP-FU-35	2,0	T,u,fs,fg,mg"	clay clasts,organic(black), black stones (2-3mm)	plastic/crumble	easy	light brown-beige	++		2(0,5-0,8)
SP-FP-FU-35	>7	T,u,fs,ms,gs,"fg",mg"	less clay clasts	plastic	less easier	light brown-reddish	++		3(2,0-3,0);4(4,0-4,5);5(5,3-5,6);6(6,5-7,0)
SP-FP-FU-36	0,2	deposit							no sample
SP-FP-FU-36	0,7	H,t,u,fs		dry/semi solid	easy	dark brown			1(0,3-0,5)
SP-FP-FU-36	3,0	T,u,fs,ms,gs',fg"	clay clasts, black stains	dry/semi solid/crumble	easy	brown-reddish-beige	++		2(0,7-0,9);3(2,0-2,5)
SP-FP-FU-36	4,0	U,fs,ms,t,gs,fg'	black-ochre stains	dry	hard	red-brown	++		4(3,0-3,5)
SP-FP-FU-36	4,3	T,fs,ms',gs',fg"	black stains	plastic	hard	red-brown	++		5(4,0-4,3)
SP-FP-FU-37	0,2	topsoil		plastic	easy	brown			no sample
SP-FP-FU-37	0,55	U,gs,t,fg,ms,fs		crumble	easy	beige	++		1(0,5)
SP-FP-FU-37	2,5	chalk,t		crumble	easy	withe	+++		2(0,7);3(2,5)
SP-FP-FU-37	2,6	T	multicoloured clays	plastic	easy	multicoloured	++		4(2,6)
SP-FP-FU-37	3,6	T,chalk,gs'	interbedded strata with T and chalk,gs	crumble	less easier	brown/white	++		5(2,65);6(2,8)
SP-FP-FU-37	3,88	T,u,fg"		semi solid	less easier	light-grey	++		7(4,0)
SP-FP-FU-37	3,92	T,u,fg,mg		crumble	less easier	light-grey	++		8(3,92)
SP-FP-FU-37	6,0	T,u,fg"	crumble parts	semi solid	less easier	light-grey	++		9(5,8);10(6,0)
SP-FP-FU-38	0,3	fS,u,t,ms',hu	roots	wet	very easy	brown	++		1(0,3)

2. Mapping - Results

borehole-logs									
site Id.	depth [m]	type of soil material	remarks	consistency of soil material	hardness of drilling	colour	lime content	remarks2	sample Id. (sample depth)
SP-FP-FU-38	0,8	fS,t,u,ms"	black stains	wet	very easy	dark ochre	-		2(0,8)
SP-FP-FU-38	1,6	fS,t,u,ms,gs,fg	black stains	wet	very easy	light-brown-beige	++		3(1,6)
SP-FP-FU-38	1,7	fS,t,u,ms,gs,fg,mg	coarses layers, ideomorphic Qz(diameter 4mm), black stains(organic)	wet	very easy	light-brown-beige	++		4(1,7)
SP-FP-FU-38	1,8	fS,t,ms,u,gs,chalk,fg,mg	pieces of carbon (diameter 5mm)	crumble	easy	multicoloured	++		5(1,8)
SP-FP-FU-38	3,0	chalk,t'	carbon stains (diameter 1mm), orange oxygen-stains	plastic/wet	easy	white/orange	++	water saturated at 2,80m	6(2,5);7(3,0)
SP-FP-FU-38	4,7	chalk,t',gs"	grey clay lens (diameter 5mm) without carbonat interbedded	plastic	less easier	orange	++		8(3,8)
SP-FP-FU-38	4,9	chalk,t,gs,fs,	grey clay lens without carbonat and orange chalk interbedded	plastic	less easier	orange-grey	-		9(4,9)
SP-FP-FU-39	0,15	Hu	roots, plants	dry	easy	brown	++		no sample
SP-FP-FU-39	0,35	T,u,fs	roots, organic, reddish stains	dry/plastic	very easy	brown	++		1(0,35)
SP-FP-FU-39	1,0	T,u,fs,gs',fg"		plastic	easy	red-brown	++		2(1,0)
SP-FP-FU-39	4,5	fS,u,ms,t',gs',fg',mg',gg"	black stains, clay lens, water saturated at 2,20m	wet/crumble	easy	red-brown-ochre-yellow	++		3(2,5);4(4,0)
SP-FP-FU-39	>4,5	T,fs,u,ms,gs',fg"		plastic	less easier	red-brown	++		5(5,0)
SP-FP-FU-40	0,4	U,t,fs'	roots	dry/crumble	very easy	brown	++		1(0,4)
SP-FP-FU-40	1,6	U,fs,t,ms"		crumble	very easy	beige	++		2(1,6)

2. Mapping - Results

borehole-logs									
site Id.	depth [m]	type of soil material	remarks	consistency of soil material	hardness of drilling	colour	lime content	remarks2	sample Id. (sample depth)
SP-FP-FU-40	3,5	T,u,fs'		plastic	easy	light beige	++		3(3,0)
SP-FP-FU-40	4,4	T,u,fs"		plastic	less easier	light beige	++		4(4,4)
SP-FP-FU-40	>4,4	T,u		plastic	less easier	light beige	++		5(5,0)
SP-FP-FU-41	0,2	deposit							no sample
SP-FP-FU-41	0,6	Hu:T,u,fs,ms',gs"		plastic	very easy	dark-brown-grey	++		1(0,6)
SP-FP-FU-41	1,0	U,t,fs		plastic	very easy	grey-beige	++		2(1,0)
SP-FP-FU-41	2,1	T,u,fs',ms"		plastic	very easy	beige	++		3(2,0)
SP-FP-FU-41	3,15	T,u,fs,ms',gs',fg'		plastic	easy	beige	++		4(3,0)
SP-FP-FU-41	3,8	fG,t,gs,ms,u",fs"	water saturated at 3,00m	wet/plastic	very easy	beige	++		5(3,8)
SP-FP-FU-41	4,5	T,fg,gs,ms,fs',u',mg"	red-green clay lens	wet/plastic	very easy	reddish-beige	++		6(4,5)
SP-FP-FU-41	>4,5	T,fg,gs,ms,fs',u',ms"		wet/plastic	very easy	red-brown-beige	++		7(4,9)
SP-FP-FU-42	0,3	Hu:T,u,fs		crumble	easy	brown	++		1(0,3)
SP-FP-FU-42	0,7	U,t,fs		dry	easy	brown-grey	++		2(0,7)
SP-FP-FU-42	1,4	T,u,fs		plastic	easy	beige-grey	++		3(1,4)
SP-FP-FU-42	2,5	T,u,fs,ms'		plastic	easy	beige	++		4(2,5)
SP-FP-FU-42	>4,7	T,u,fs"	at 4,4m without fs"	plastic	less easier	light beige	++		5(4,7)
SP-FP-FU-43	0,2	U,fs,ms',t'	roots	crumble	very easy	grey-beige	++		1(0,2)
SP-FP-FU-43	0,35	T,u,fs,ms'		dry/plastic	very easy	grey-brown	++		2(0,35)
SP-FP-FU-43	0,55	T,u,fs		plastic	very easy	beige	++		3(0,55)
SP-FP-FU-43	2,0	fS,u,ms',t"		dry/plastic	very easy	beige	++		4(1,7)
SP-FP-FU-43	2,3	T,u,fs,ms"		plastic	less easier	beige	++		5(2,3)
SP-FP-FU-43	3,2	T,u,fs'		plastic	less easier	beige	++		6(3,0)
SP-FP-FU-43	4,0	T,u,fs',ms",fg"		plastic	less easier	beige	++		7(4,0)

2. Mapping - Results

borehole-logs									
site Id.	depth [m]	type of soil material	remarks	consistency of soil material	hardness of drilling	colour	lime content	remarks2	sample Id. (sample depth)
SP-FP-FU-43	>4,0	T,u,fs"	some rust stains	plastic	less easier	beige	++		8(5,0)
SP-FP-FU-44	0,2	topsoil	roots	crumble	very easy	light brown	++		1(0,2)
SP-FP-FU-44	0,5	T,u,fs,ms'	roots	wet/crumble	very easy	olive-green	++		2(0,5)
SP-FP-FU-44	0,7	T,u,fs'.ms"		plastic	very easy	grey-beige	++		3(0,7)
SP-FP-FU-44	1,1	T,u,fs',ms",gs"		plastic	very easy	beige-grey	++		4(0,9)
SP-FP-FU-44	3,6	T,u',fs"	red-brown stains, organic (diameter 1-2mm)	palstic	easy	beige-ochre	++		5(2,2);6(3,0)
SP-FP-FU-44	4,3	T,u,fs',ms',gs'	clay clasts, red-brown stains	soft-crumble	less easier	beige	++		7(4,3)
SP-FP-FU-44	>4,3	T,u,fs",ms",gs"		soft-plastic	less easier	beige	++		8(5,0)
SP-FP-FU-45	0,15	deposit							no sample
SP-FP-FU-45	0,5	T,u,fs,ms'	roots	plastic	easy	grey	++		1(0,5)
SP-FP-FU-45	1,1	T,u',fs'	red-brown stains, organic	soft-crumble	easy	beige	++		2(0,8)
SP-FP-FU-45	2,0	fS,ms,t,u,gs,fg',mg"		crumble	very easy	beige	++		3(2,0)
SP-FP-FU-45	3,7	fS,ms,t,u,gs,fg"	water saturated at 2,00m	plastic	very easy	ochre-orange	++		4(3,0)
SP-FP-FU-45	>3,7	T,gg,x,mg',fs',ms',gs',u',fg',chalk		soft-plastic	very easy	white-orange	++		5(4,5)
SP-FP-FU-46	0,05	topsoil							no sample
SP-FP-FU-46	0,75	T,u,fs'		plastic	easy	grey-beige	++		1(0,3-0,75)
SP-FP-FU-46	3,0	T,u,fs'		plastic	less easy	ochre-beige	++		2(2,0-3,0)
SP-FP-FU-47	0,1	topsoil	roots,plants	dry	very easy	brown	+		no sample
SP-FP-FU-47	0,3	U,t,fs,ms	clay lens, organic lens	plastic	very easy	dark-brown	+		1(0,1-0,3)
SP-FP-FU-47	1,2	T,fs,ms',gs'		plastic	easy	brown	++		2(0,4-0,5)
SP-FP-FU-47	1,4	T,fs,ms,gs	clay lens,organic	plastic	easy	brown	++		3(1,2-1,4)

2. Mapping - Results

borehole-logs									
site Id.	depth [m]	type of soil material	remarks	consistency of soil material	hardness of drilling	colour	lime content	remarks2	sample Id. (sample depth)
			lens						
SP-FP-FU-47	4,0	T,chalk,fs',ms',gs"	at 3,40m ochre oxygen stains	semi solid	easy	light grey-beige	++		4(3,0)
SP-FP-FU-47	4,2	T,chalk,fs,ms,gs,fg,mg		semi solid	less easier	ochre-brown	++		5(4,0-4,2)
SP-FP-FU-47	>4,2	fS,ms,t,u,chalk		semi solid	less easier	red-brown	++		6(>4,2)
SP-FP-FU-48	0,23	topsoil	roots						no sample
SP-FP-FU-48	0,5	U,fs,t,ms',gs"	clay clasts (crumble	easy	beige-ochre	++		1(0,5)
SP-FP-FU-48	0,9	T,u,fs,ms',gs",fg"		plastic	easy	dark-brown/dark-grey	++		2(0,5-0,7)
SP-FP-FU-48	2,2	T,chalk,u,fs,ms",gs",fg"		plastic	easy	grey-beige	++		3(2,0)
SP-FP-FU-48	3,5	T,u,fs"	ochre stains	plastic	less easier	ochre-beige	++		4(3,0)
SP-FP-FU-48	>5,0	T,u,fs',ms'gs"		plastic	less easier	ochre-beige	++		5(3,8);6(4,7)
SP-FP-FU-49	0,4	U,t,fs	fs very dominated	crumble	easy	grey	++		1(0,3-0,4)
SP-FP-FU-49	0,75	U,t,fs,ms',gs'	roots	grey	easy	dark grey	++		2(0,6-0,75)
SP-FP-FU-49	0,85	T,u,fs',ms"		plastic/wet	easy	dark grey	++		3(0,75-0,85)
SP-FP-FU-49	0,95	T,u,fs,ms',gs"		plastic	easy	beige-grey	++		no sample
SP-FP-FU-49	1,05	fS,u,t,ms		crumble	easy	beige	++		no sample
SP-FP-FU-49	2,0	T,u,ms',gs'	green clay lens, clay stains, compression at 1,80m organic	plastic	easy	reddish-beige	++		4(1,8-2,0)
SP-FP-FU-49	2,6	T,fs,u interbedded with fs,ms,u,t,gs'	roots, green clay lens, reddish sands. Chalk	plastic	easy	multicoloured	++		5(2,0-2,6)
SP-FP-FU-49	4,0	T,u,fs',gs"	green clay lens, organic stains (diameter 1mm)	plastic	less easier	red-brown	++		6(2,6-2,9)
SP-FP-FU-49	5,4	T,u,fs',ms",gs",fg"		plastic	less easier	red-brown	++		7(4,2);8(4,8)

borehole-logs									NE
site Id.	depth [m]	type of soil material	remarks	consistency of soil material	hardness of drilling	colour	lime content	remarks2	sample Id. (sample depth)
SP-FP-FU-49	5,5	mS,gs,fs,u',t"	strong water saturated	plastic	easy	red-brown	++		9(5,4-5,5)
SP-FP-FU-49	7,2	T,u',fg',fs',ms',gs",mg"	mg (diameter 3cm)	plastic	easy	red-brown	++		10(5,5-7,0)
SP-FP-FU-49	7,3	mS,gs,fs,u',t"	water saturated	plastic	easy	red-brown	++		11(7,2-7,3)
SP-FP-FU-49	7,9	T,u',fg',ms",gs',mg'	mg (diameter 3cm)	plastic	easy	red-brown	++		12(7,7-7,9)
SP-FP-FU-49	9,0	T,u,fs',gs'		plastic	easy	red-brown	++		13(8,7-9,0)

Table 2.7: Abbreviations used in Tab. 2.6.

key grain size		
type of soil material	fraction	grain size mm
T t	clay	<0,02
U u	silt	0,02-0,063
fS fs	fine sand	0,063-0,2
mS ms	medium sand	0,2-0,63
gS gs	coarse sand	0,63-2
fG fg	fine gravel	2-6,3
mG mg	medium gravel	6,3-20
gG gg	coarse gravel	20-63
X x	stones	>63
'	few	
"	very few	
Hu	humus	
key lime content		
lime content	reaction	
-	absent	
(+)	weak foaming	
+	strong foaming	
++	very strong foaming	

2.2.1.2 Cross sections

Four cross sections were created to determine the lateral distribution of sediments in the northern mapping area; their course is shown in Fig. 2.10. The drilling sites rest on the cross sections and are not projected onto the section lines. The cross sections are scaled super elevated in different degrees for each case. Additionally the surface topography is displayed for every cross section separately with an own scale.

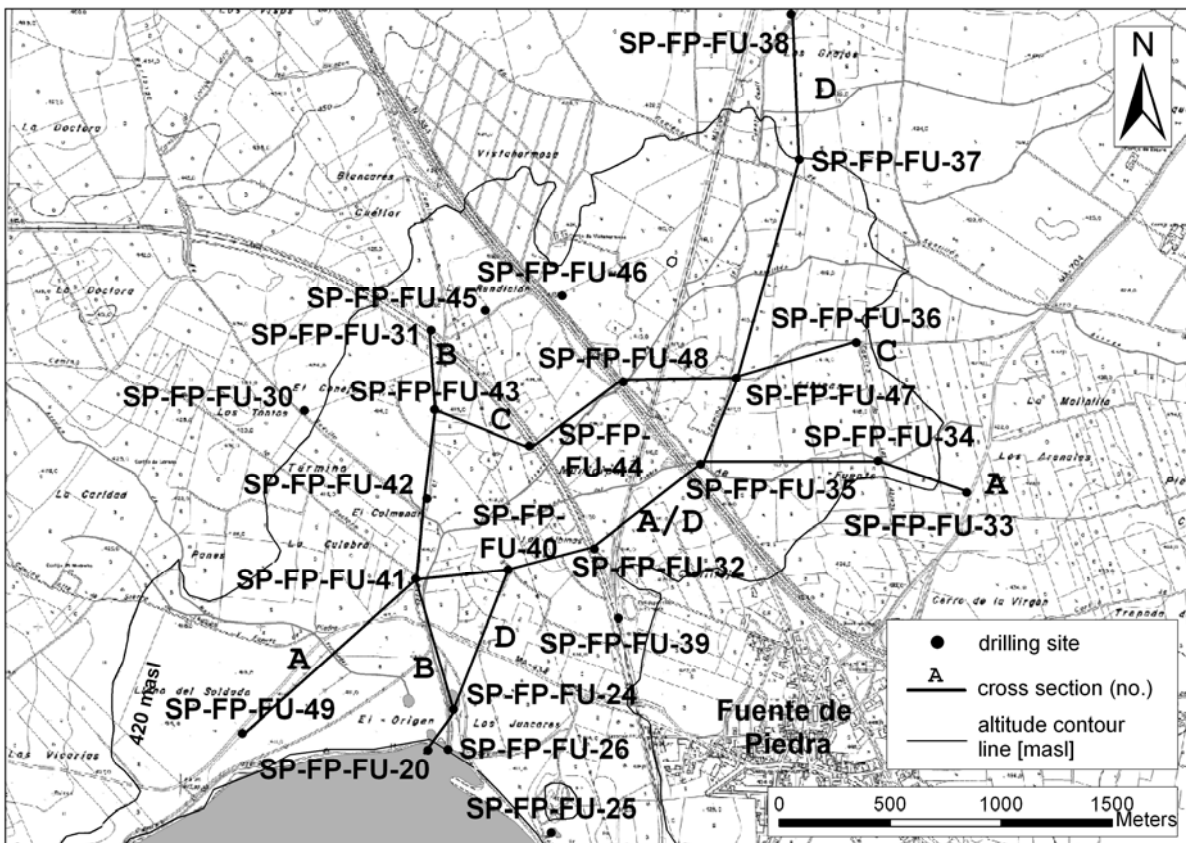


Figure 2.10: Course of cross sections A-D and bore sites.

By the **cross sections** A-D spatial distribution of the sediments and their determined types (1 and 2) can be estimated. Type 1 has thicknesses > 5 m in the central part of the northern mapping area and is decreasing in thickness to the hillsides until disappearance. Type 2 sediments are deposited below Type 1 sediments and are therefore situated in lower depths towards the hillsides. The soil is extensive covered by up to 0.2 m thick made ground. Silts are distributed close to the surface in shallow depths or as topsoil almost all over the northern mapping area.

The boundary between grey and red sediments is towards the hillsides situated in lower depths. In central situated drillings the depth of this boundary is 5 m or more. At drillings situated near the northern recent lake edge this boundary was not observed.

Coarse clastic sediment bodies occur at the northern, northeast and western edges of the northern mapping area. At central positions in this area isolated gravel or sand bodies were found in Type 2 deposits in depths below 3 m.

Macroscopically gypsum concretes and crystalline gypsum appearing in the recent lake sediments and in sites situated at the northern present lake edge. Lake marl layers are spatial discontinuous and not correspondingly retrieved in adjacent sites.

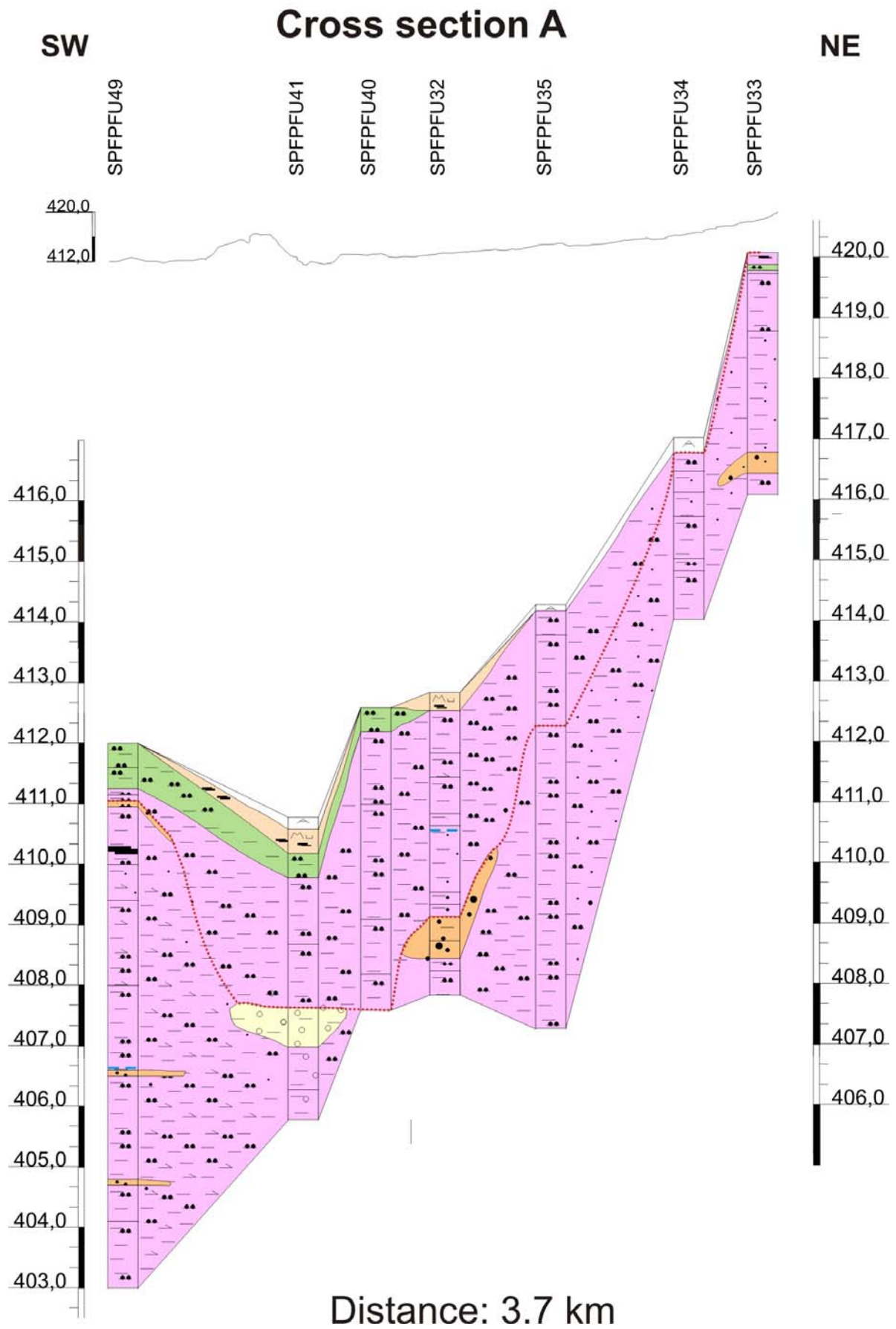


Figure 2.11: Cross section A. Legend is shown in Fig. 2.14.

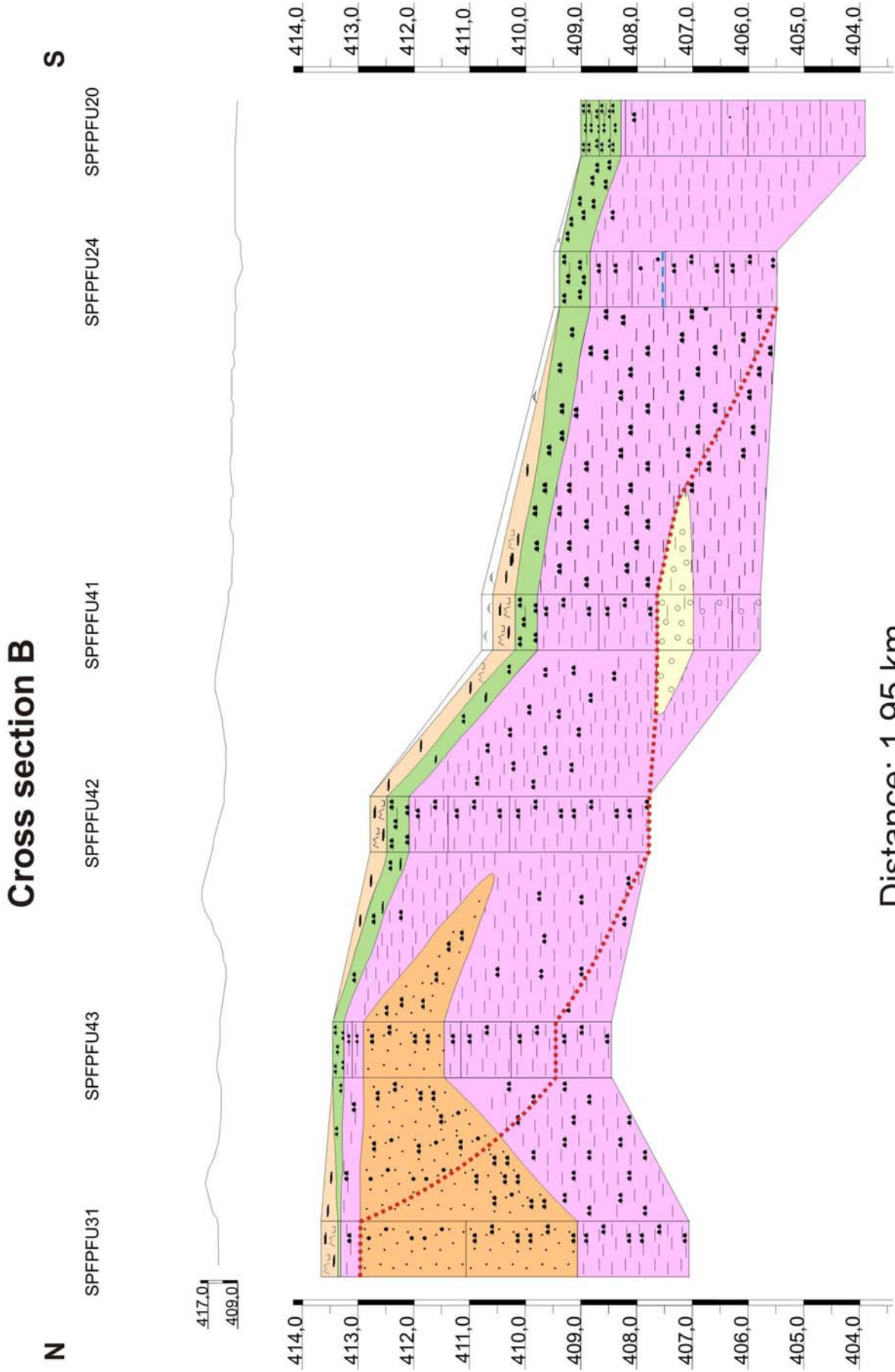


Figure 2.12: Cross section B. Legend is shown in Fig. 2.14.

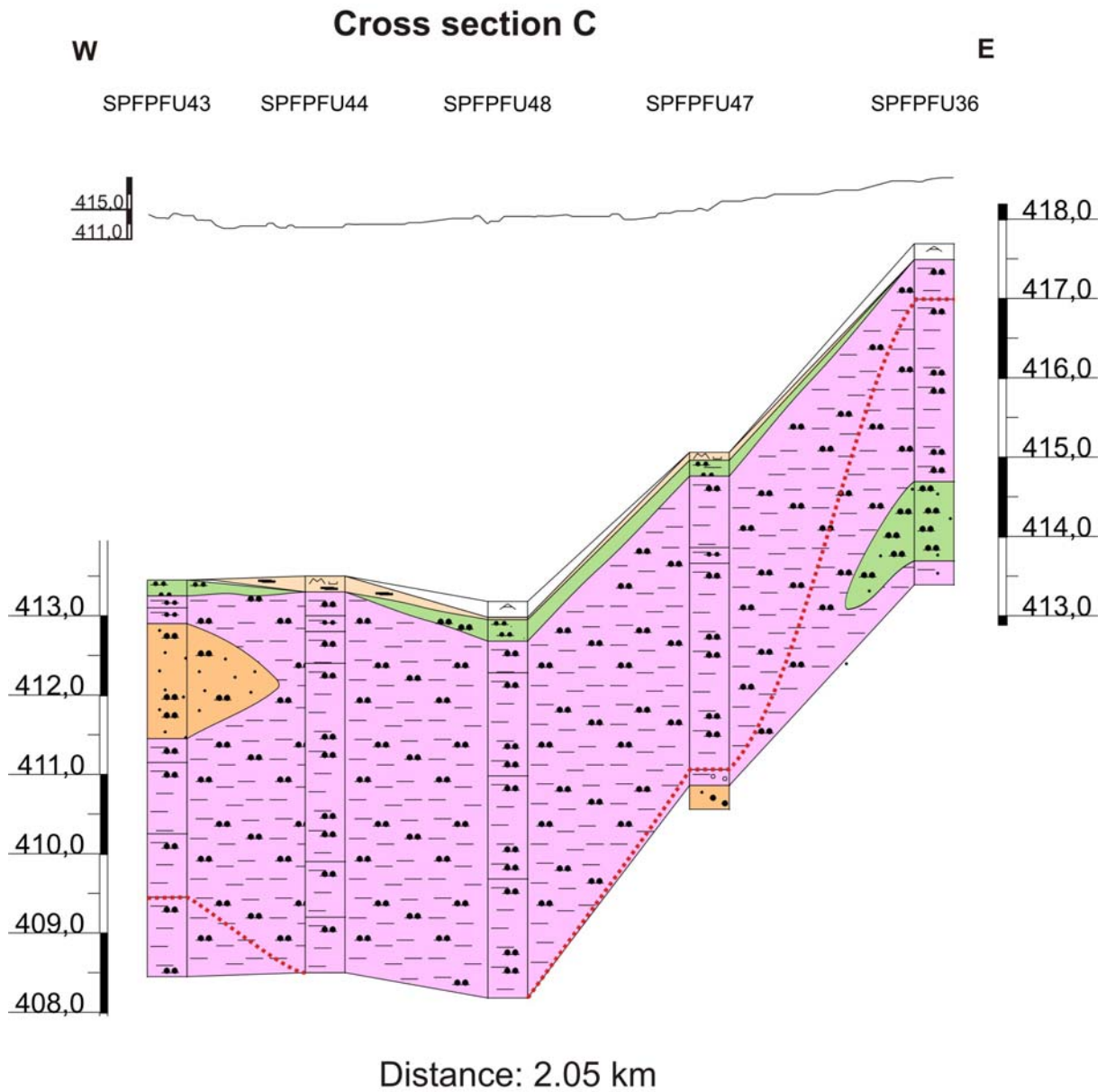


Figure 2.13: Cross section C. Legend is shown in Fig. 2.14.

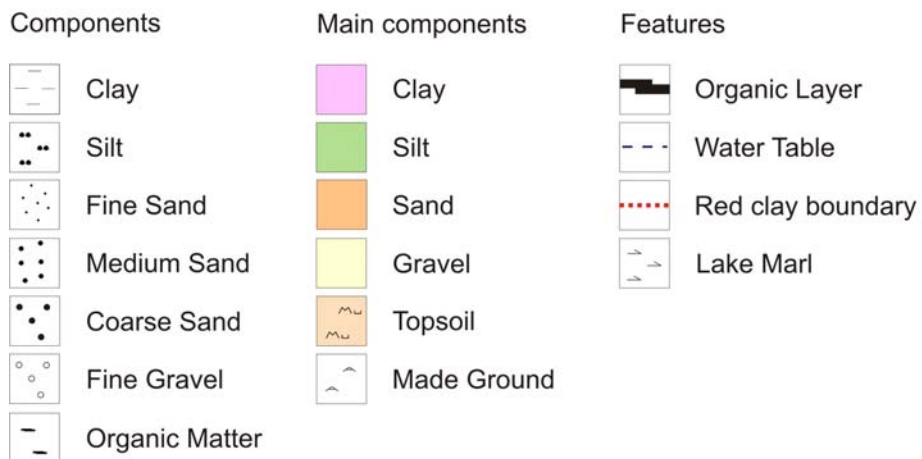


Figure 2.14: Legend of cross sections A-D.

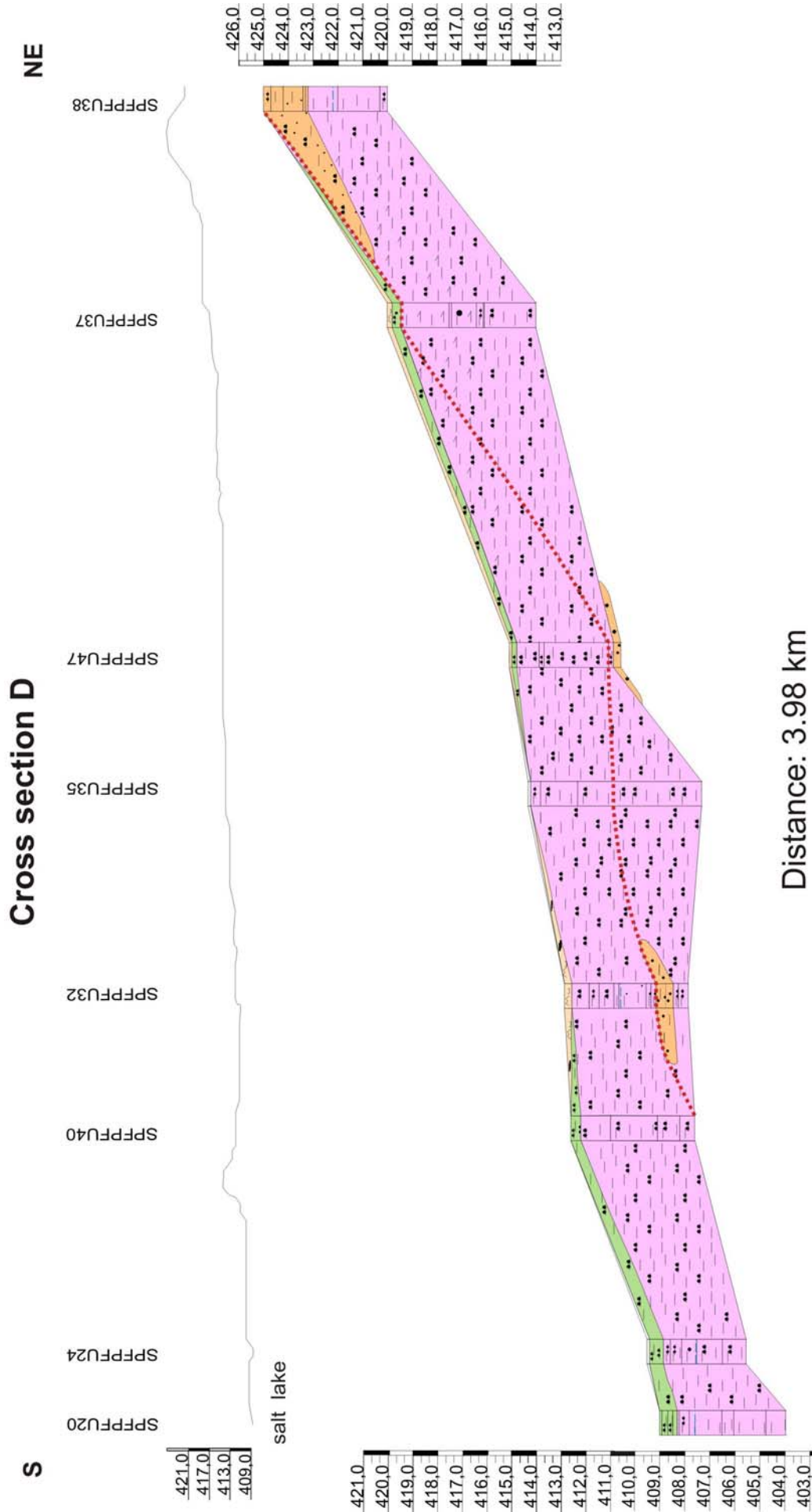


Figure 2.15: Cross section D. Legend is shown in Fig. 2.14.

2.2.1.3 Relation to stratigraphical units

By the geological map 1023 (IGME, 1986) the drilled sediments were related to stratigraphical units (Tab. 2.8). Location of drillings in the geological map with regards to associated strata and the sediment characterization were the decisive criteria for classification. Surface close sediments situated in the respective stratigraphical units, accord in the majority of drillings to descriptions made by IGME (1986). Variations appear at drillings situated on strata boundaries. Fig. 2.16 shows the drilling sites and their location in the geological map.

Table 2.8: Type profiles and the related stratigraphical units.

Type	strata after IGME (1986)	stratigraphic unit
I - Grey	(33) - (39)	Upper Pleistocene
II - Red	(14) - (32)	Upper Miocene to Upper Pleistocene
clastic	(14); (18); (29); (30)	Upper Miocene and Upper Pleistocene

2.2.1.4 Stages of lake development

Different stages of lake development can be distinguished due to variations in lithology:

a) **Type 1** sediments are allocated to the recent lake setting with hyper saline groundwaters feeding the lake and therefore precipitation of gypsum occurs. In the zone of the embouchure of river Santillán sediments do not feature a coarsening of grain size. Reasonably low flow rates and flow velocities and a catchment area dominated by fine grained sediments prevent the sedimentation of coarser particles in front of the embouchure.

Type 1 sediments in the northern area differ in constituents from recent lake sediments. The absent of hyper saline brines north of the lake avoid the occurrence of idiomorphic gypsum in the sediments. Only in brine saturated deeper parts of the soil in drillings at the northern lake edge crystalline gypsums according to the water table and salinity occur. The local occurrence of lake marl confirms the assumption of the deposition at a former lake terrace in this area.

b) A change in sedimentation conditions is primary indicated by a change in sediment colour for **Type 2** sediments. The red clays represent a change of provenience and deposition conditions with more clastic material and less evaporites. Additionally discolourations due to postsedimentary processes like iron oxidation appear in zones of groundwater fluctuation. A differentiation of Type 1 and the underlying Type 2

sediments is partly barely possible. An indication for determination is the sediment colour. The increased appearance of clastic and organic particles indicates an increased surface inflow (alluvial fan) with sporadic floods of coarser material.

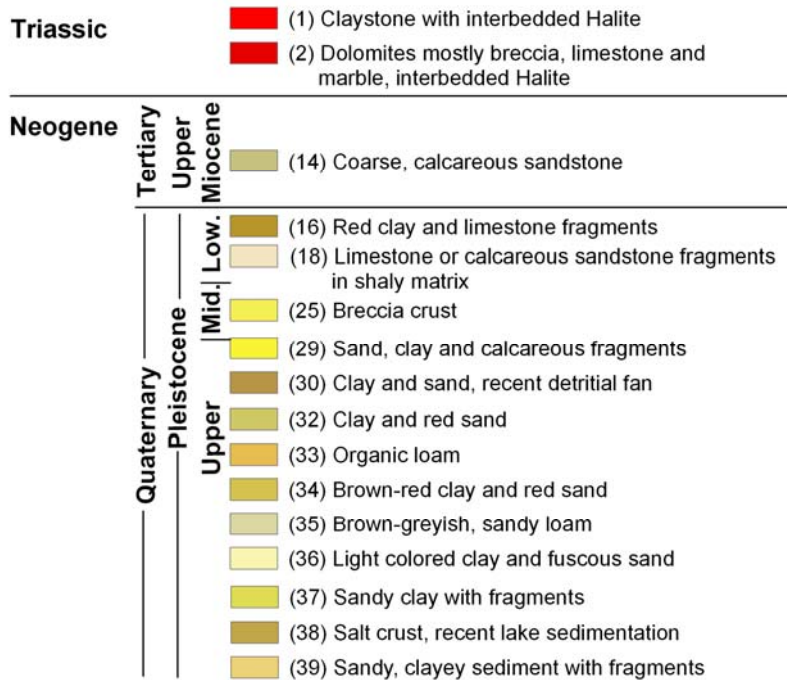
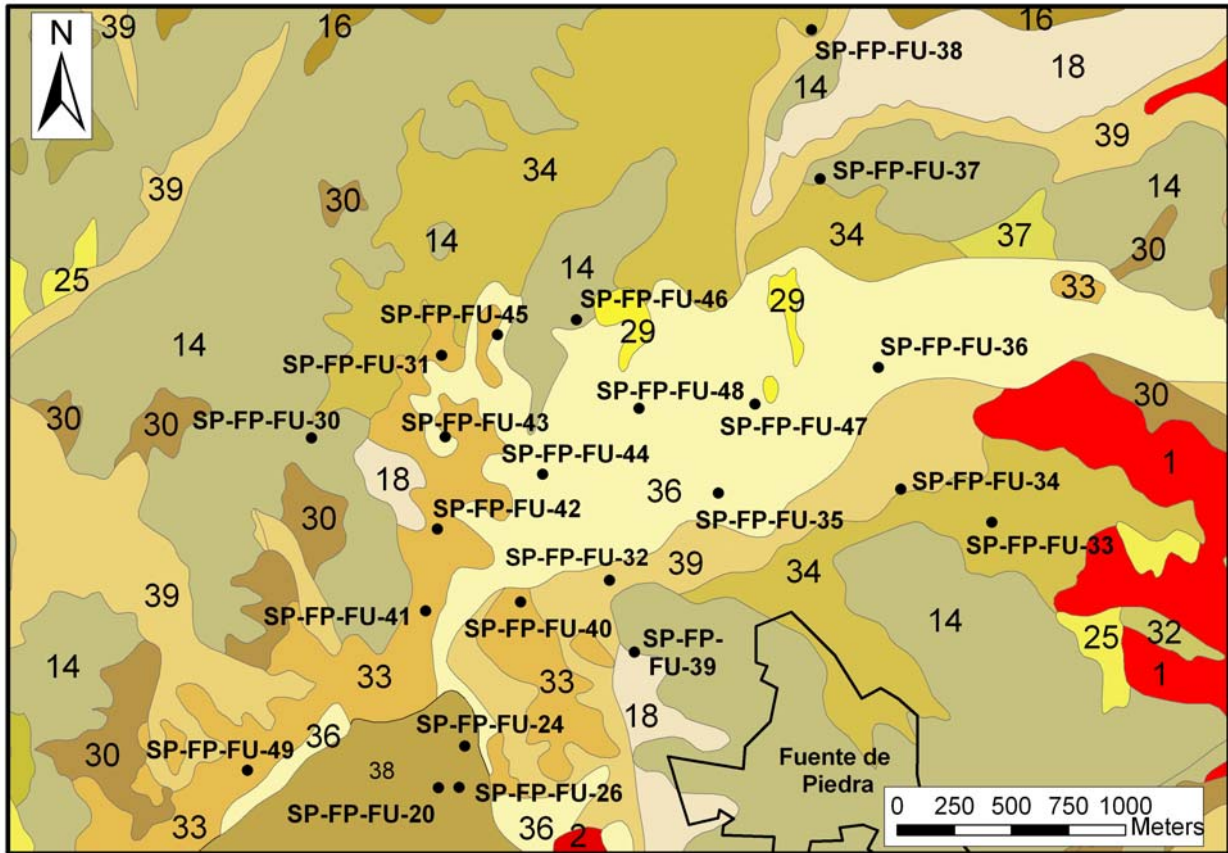


Figure 2.16: Geological situation of boreholes in the northern vicinity. Strata Id. is shown as numbers after IGME (1986).

Though for lake stratifications typical layering textures or varves respectively do not occur. The occasional appearing of sand bodies mainly concentrated at the western and northern edge fortifies the above-mentioned assumption. The strata can also be interpreted as a former lake terrace with a strong impact by clastic materials deposited as alluvial fans.

Clays represent calm sedimentation conditions (FÜCHTBAUER, 1988). After COOKE ET AL. (1993) eolian erosion is in semiarid to arid regions the predominantly process for the input of clastic sediments into playas. The grain size distribution confirms the assumption.

It can be assumed that the former Fuente de Piedra Lake spread out in the northern valley (of Santillán River) and shifted his hydrology due to regression from a former perennial lake into the recent ephemeral lake. Reasons for the change could be less rainfalls and accordingly lower water tables. The extension of the former lake was not significantly regarding to recent margins.

2.2.1.5 Proveniences

Proveniences of sediments deposited in the northern lake vicinity can be supposed as following (Fig. 2.17):

- Fine clastic materials like clay and silt originate from Triassic clays and marls and from Jurassic-Dogger marls (PI).
- Coarse clastic materials derive from Jurassic-Dogger deposits or Triassic interbedded sand strata (PI) and are widely spread in the basin as Upper Miocene alluvial deposits (PII).
- For the origin of carbonate Jurassic carbonate rocks are considered (PIII).

Beside surface erosion and fluvial transport, leaching and precipitation of soluble compounds are the dominating processes for displacement.

Salt crusts derive from leaching of Triassic materials (PI) and precipitation from ground- or surface water.

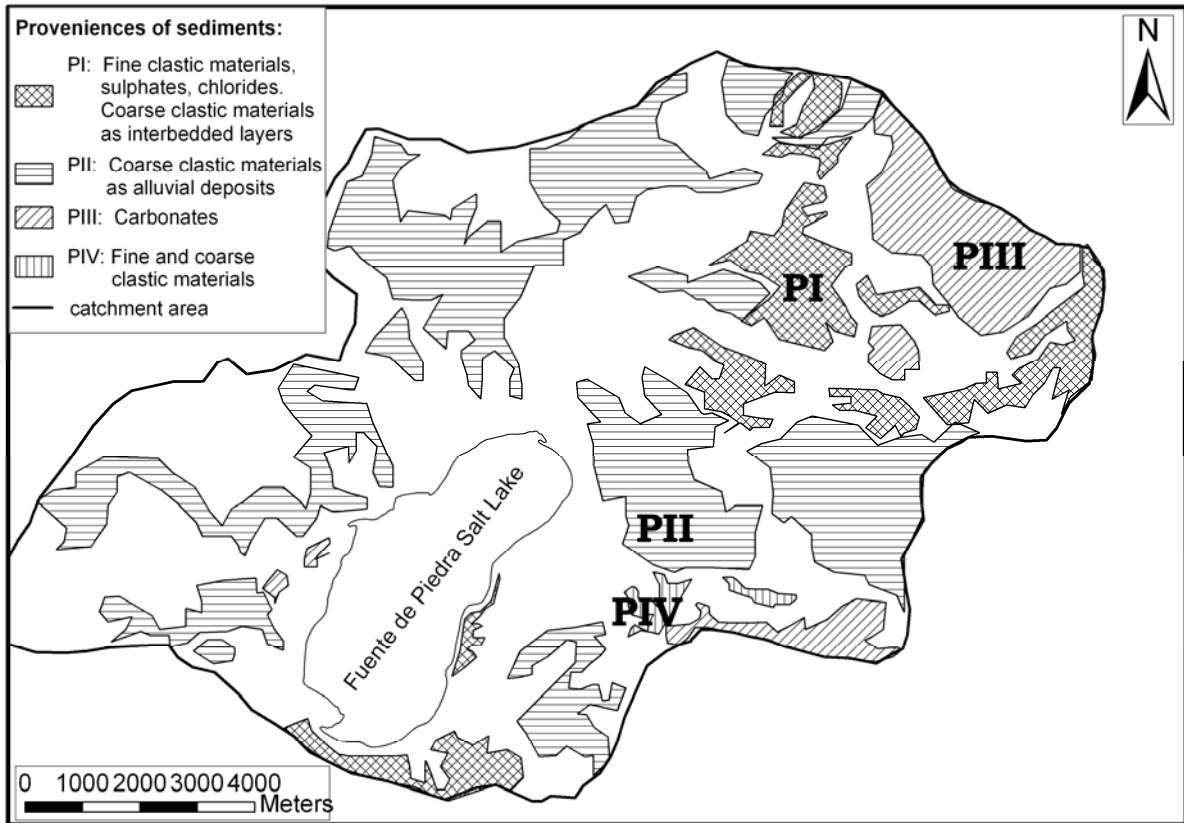


Figure 2.17: Proveniences of sediments: Fine to coarse clastic (PI); Coarse clastic (PII); carbonate (PIII).

2.2.2 Sediment analysis

Sieving and sedimentation of samples from 2 drilling sites (SPFPFU22 and -23) inside the maximum flooding area (Fig. 2.18) were realized to determine grain size distribution of soil material with depth.

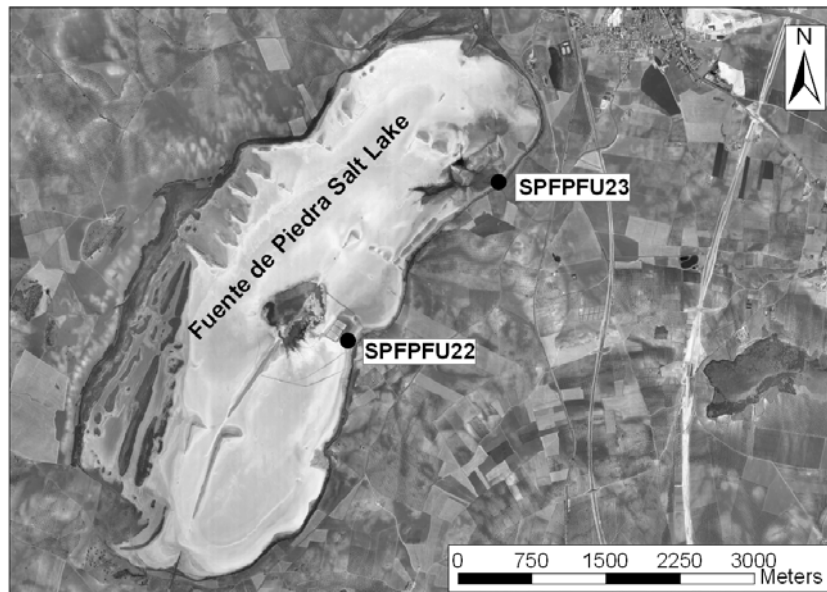


Figure 2.18: Location of drillings for analysed samples. Aerial view obtained from JUNTA DE ANDALUCÍA (2004).

Due to solution processes while leaching of sediments as part of sample preparation soluble components (salts and particular gypsum) were dissolved. Because fine grained components dissolve better than coarse grained fractions, the coarse grained particles are proportionally over-represented. Additionally to these processes loss by sieving occurs. In Tab. 2.9 the loss by leaching and sieving is shown as sieve loss.

Table 2.9: Loss by leaching and sieving of sediment samples; initial and end EC and number of leaching.

sample Id.	initial weight [g]	sieve loss [g]	sieve loss [%]	initial EC [mS/cm]	end EC [mS/cm]	no. of leachings
SPFPFU22-02	11.25	0.99	8.80	7.3	0.2	4
SPFPFU22-09	15.30	3.97	25.95	13.4	0.15	5
SPFPFU22-16	27.62	5.52	20.00	12.0	0.19	7
SPFPFU22-17	19.47	0.97	5.00	3.0	0.49	5
SPFPFU23-02	21.80	0.41	1.88	1.5	0.26	1
SPFPFU23-04	21.23	0.57	2.68	1.6	0.43	1
SPFPFU23-10	19.90	0.65	3.27	3.5	0.34	2
SPFPFU23-11	20.28	1.34	6.61	3.8	0.37	2

Sediment samples of **SPFPFU22** from different depths show similar grain size distributions. Tab. 2.10 compares sieving results with the borehole logs from field characterization. Analysis results are presented in Fig. 2.19 and Tab. A13. The relatively deeper located samples have a more fine grained composition. Gravel components found in field determination are gypsum crystals and gypsiferous concretes. Crystals do not occur in samples for sieve analysis and coagulated grains were dissolved due to preparation procedure.

Table 2.10: Type of soil material obtained from sieving results for SPFPFU22 compared with field determination.

Sample Id.	Type of soil material (sieving)	Type of soil material (field)
SPFPFU22-02	fS, ū, ms, t', gs''	T, u, fs''
SPFPFU22-09	U, fs, ms', gs''	T, fs
SPFPFU22-16	U, fs, t', ms''	T, u, fg, ms, gs
SPFPFU22-17	fS, ū, t, ms'	T, fg

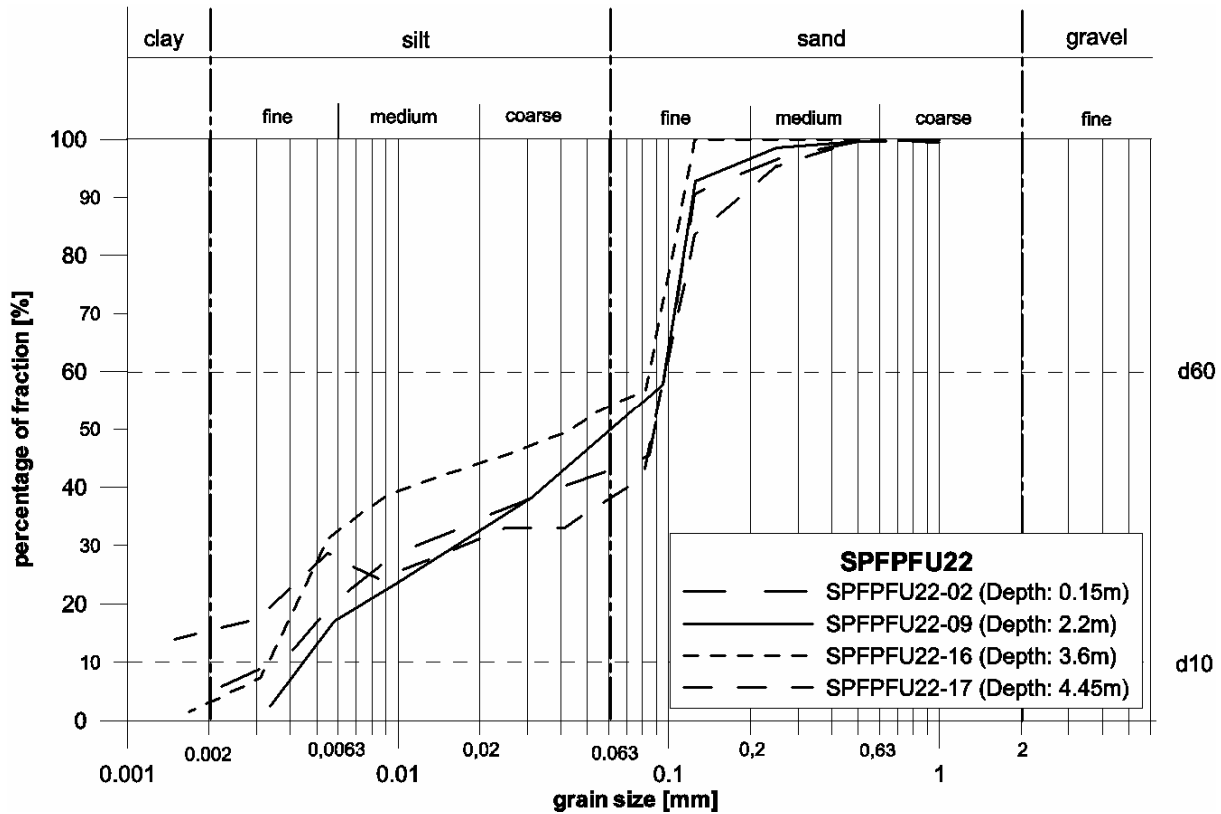


Figure 2.19: Grain size distribution curve for sediment samples from SPFPFU22.

Sediment samples from **SPFPFU23** are coarse grained in low depths and fine grained in deeper depths like shown in Fig. 2.20.

The gravel components are gypsum crystals in sample FU23-04 and lime concretions in FU23-10. In Tab. 2.11 the type of soil material is shown according to results of sieving.

Table 2.11: Type of soil material obtained from sieving results for SPFPFU23 compared with field determination.

Sample Id.	Type of soil material (sieving)	Type of soil material (field)
SPFPFU23-02	fS, ū, ms, gs	mS, t, u, gs'
SPFPFU23-04	U, fs, ms, fg, gs'	fS, t, gs, u, fg
SPFPFU23-10	U, fg', fs', ms'', gs''	T, u, fs, ms
SPFPFU23-11	U, fs, ms, gs''	T, u, fs

Dissolution of gravel components is observed at SPFPFU22, while in SPFPFU23 samples the gravel remain in sieve analysis. This can be due to a different composition of the gravel fraction or the presence of other components additionally to gypsum crystals, for example coagulated clay or carbonate fragments.

Coefficient of hydraulic conductivity is calculated after BEYER (1964); see Tab. 2.12. The coefficient of hydraulic conductivity is very low in the first sample of SPFPFU22 and low permeable in the remaining samples of SPFPFU22. Less permeable

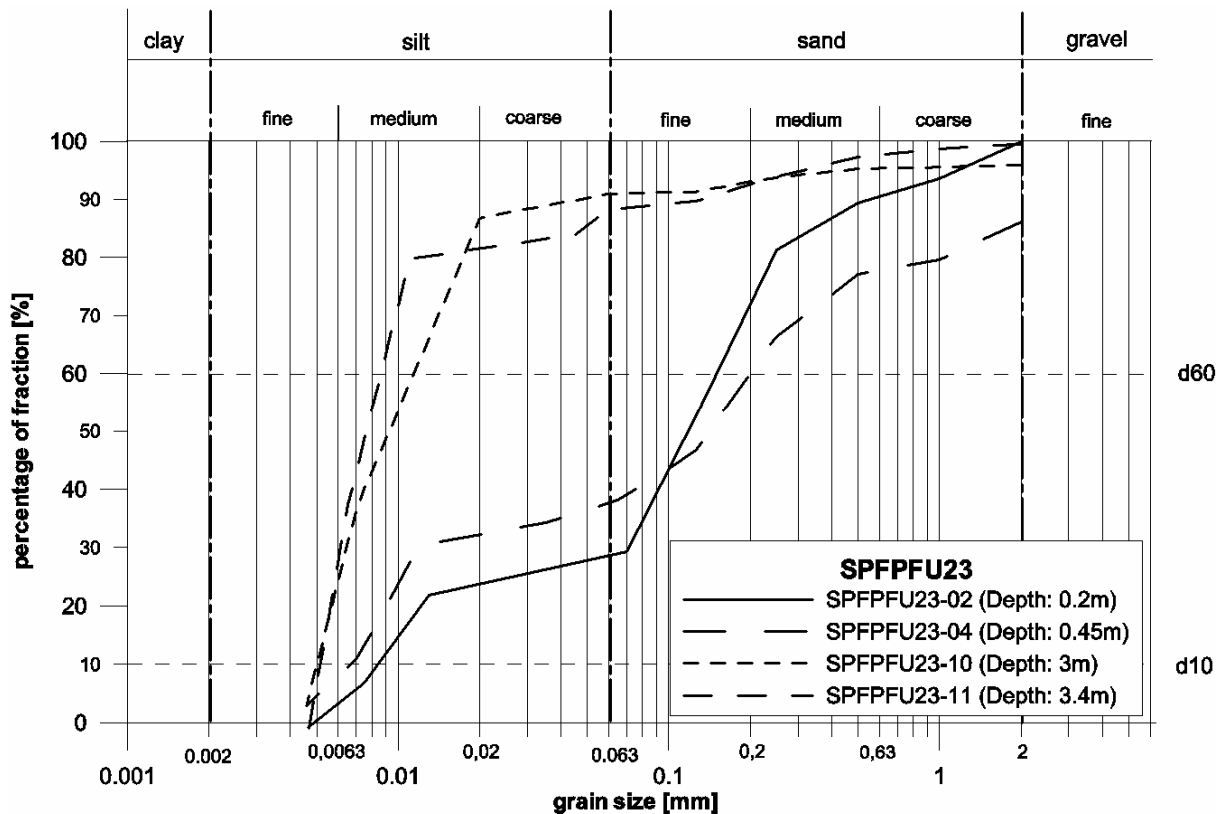


Figure 2.20: Grain size distribution curve for sediment samples from SPFPFU23.

sediments occur in SPFPFU23. At the middle of the eastern edge the permeability is less compared to the northeastern margin.

Note that the coefficient of hydraulic conductivity is overestimated due to leaching of fine particles and using the BEYER-method which is valid for a temperature of 10°C. But inaccuracy by temperature can be disregarded compared to sieve loss by leaching and sieving with up to 25 % weight loss.

Table 2.12: Uniformity coefficients (C_U) and coefficients of hydraulic conductivity (k_f) [m/s].

sample Id.	d10 [mm]	d60 [mm]	C_U	$k_{f\text{BEYER}}$
SPFPFU22-02	0.001	0.085	85	6.E-08
SPFPFU22-09	0.0045	0.098	22	1.E-06
SPFPFU22-16	0.0033	0.098	30	7.E-07
SPFPFU22-17	0.004	0.098	25	1.E-06
SPFPFU23-02	0.0085	0.16	19	4.E-06
SPFPFU23-04	0.0067	0.2	30	3.E-06
SPFPFU23-10	0.005	0.013	3	2.E-06
SPFPFU23-11	0.005	0.0085	2	3.E-07

Uncertainties in determination of grain size distribution by sedimentation analysis are caused by lack of information regarding the average density. Additionally average bulk density of sediments is set as 2.65 g/cm³ and is estimated by the assumption of a mineral composition based on quartz with a density of 2.65 g/cm³. The density of gypsum is 2.3 g/cm³. Because of the almost complete dissolution of gypsum before

sieving and sedimentation analysis, it can be disregarded. The density of carbonates can not be determined exactly without information about the compound and proportions of the carbonates. Density ranges from 2.16 to 2.93 g/cm³ for the main carbonate minerals (MATTHES, 1993). To solve these problems a determination of grain density and mineral composition is necessary.

2.3 Conclusions

Lake sediments consist of gypsum, calcite and clay minerals with interbedded layers of sand, idiomorphic gypsums and gypsum concretions. Laboratory analysis shows coefficients of hydraulic conductivity from 1E-06 to 7E-07 m/s for lake sediments. Permeabilities of salt lake sediments are presumably given by layers of former lake floor with desiccation cracks refilled by post sedimentary gypsum crystals. These layers feature a higher permeability in horizontal than in vertical direction and are distributed spatially variable. The soil in the northern marginal lake area and beyond is very homogenous and fine grained (clays and silts) in contrast to deposits at central lake margin.

To the depression edges and in greater depth the appearance of interbedded sand strata increases and indicates a more alluvial influenced deposition. Finally the previously considered lake shape on the basis of the aerial photo is nearly representing a former lake terrace (Fig. 2.21). The extension of the terrace is comprehensible by the displayed cross sections A-D and takes course along the observed boundary between unit 1 and unit 2. Unit 2 is considered to be an older terrace with a differing lake chemistry and a higher input of coarser clastic materials and organic matter.

Mapping of lake sediments in the northern vicinity of the salt lake indicates a former lake terrace with differing sedimentation conditions and an additional extension of 2 km northwards. The border of the supposed former lake extension is corresponding to an elevation of 415 to 416 m above sea level. For these reasons at the southwest shore and at the lake's northeast shore further former small flooding areas can be presumed. Thicknesses of unit 2 are > 5 m along a north-south directed axis in the central part with a decrease in thicknesses to the margins.

The distribution of lake sediments offers a high spatial variability. Whereas sediment thicknesses are great for the north-eastern lake shore and vicinity, they are small for the southern and western margins.

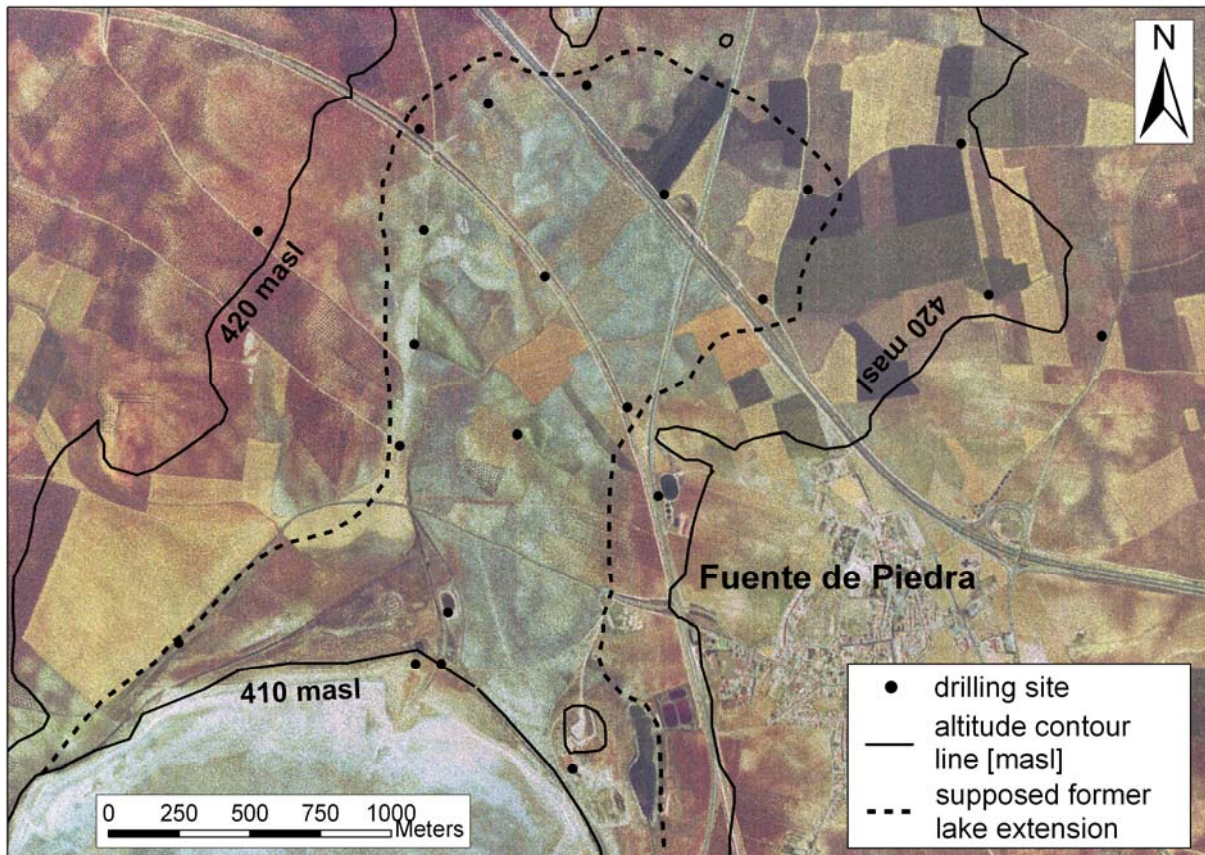


Figure 2.21: Supposed former lake extension of Fuente de Piedra Salt Lake in the adjacent northern area. Aerial view obtained from JUNTA DE ANDALUCÍA (2003).

3. Diploma thesis

3.1. Basic Principles and methods

3.1.1 Hydrogeochemistry and Isotope study

3.1.1.1 Sampling network, sampling campaigns and parameters

In the scope of 4 field campaigns within 2 years from spring 2004 to spring 2006 in Fuente de Piedra Basin ground- and surface water samples were taken and analysed for their geochemical characteristics. The sampling campaigns in spring 2004 and 2005 were attend and accomplished by Prof. J. Benavente (U Granada), Prof. A. Pekdeger and Dr. C. Kohfahl (both FU Berlin). The sampling campaign in autumn 2005 and in spring 2006 were accomplished by L. M. Paul, C. Fenk and C. Menz (all FU Berlin) with supervision of above named. Samples were taken under in situ conditions while pumping with regarding of constant values of Eh, pH, EC and O₂ in a flow through cell. All data were used in this study, whereas the main attention is on the analysis and interpretation of temperature and conductivity logs and the isotopegeochemical and hydrogeochemical investigations.

In autumn 2005 5 additional piezometers were erected to characterize the vertical flux. These additional piezometers were named SPFPFU and parameterized (Fig. 3.2). Compare chapter 3.1.3 for construction procedure.

The sampling campaign comprehends a total of 19 sampling sites. Twelve of the sites are monitoring wells around the salt lake and distributed in the catchment area. Five other piezometers, constructed within the scope of this field campaign in the salt lake or near the coastal line, were sampled. Additionally one pumping well and an artificial lake were sampled. Because of the low level of water surface in the salt lake, some sampling sites couldn't be sampled in all campaigns.

In Tab. 3.3 all used samples are displayed. Fig. 3.2 shows the location and the type of the sampling sites. Tab. A9 in Appendix specifies the properties of the sampling sites.

3.1.1.2 Sampling methods

The aim of the sampling is to gain a representative water sample due to the investigated problem for the subsequent geohydrochemical analysis.

Within the scope of the sampling of monitoring wells different types of pumps were used. For deep wells (> 5 m) with big volumes, immersion pumps of the types MP1 and Eijkelkamp were applied. The MP1 pump were screwed together with PVC tubes or hoses and were installed in depth between 8 and 40 m, dependent on water level

and volume of the well. For shallow wells (< 5 m) with small volumes a foot valve pump were used. This so called “Stucker pump” consists of a thin hose with a foot check valve connected to a modified jigsaw. In field campaigns February 2004 and February 2005 the samples were taken with a depth orientated dipper.

The values of the analysis have to represent the conditions of the sampling, so the sampled water has to correspond with the character of the groundwater body and shouldn't be influenced by the well. Attaining this, triple amount of the wells water filled volume was pumped in order to achieve stable values of field parameters. The measurement takes place in a flow-through cell. In February 2004 and February 2005 field campaigns, samples were taken without stable field parameters.

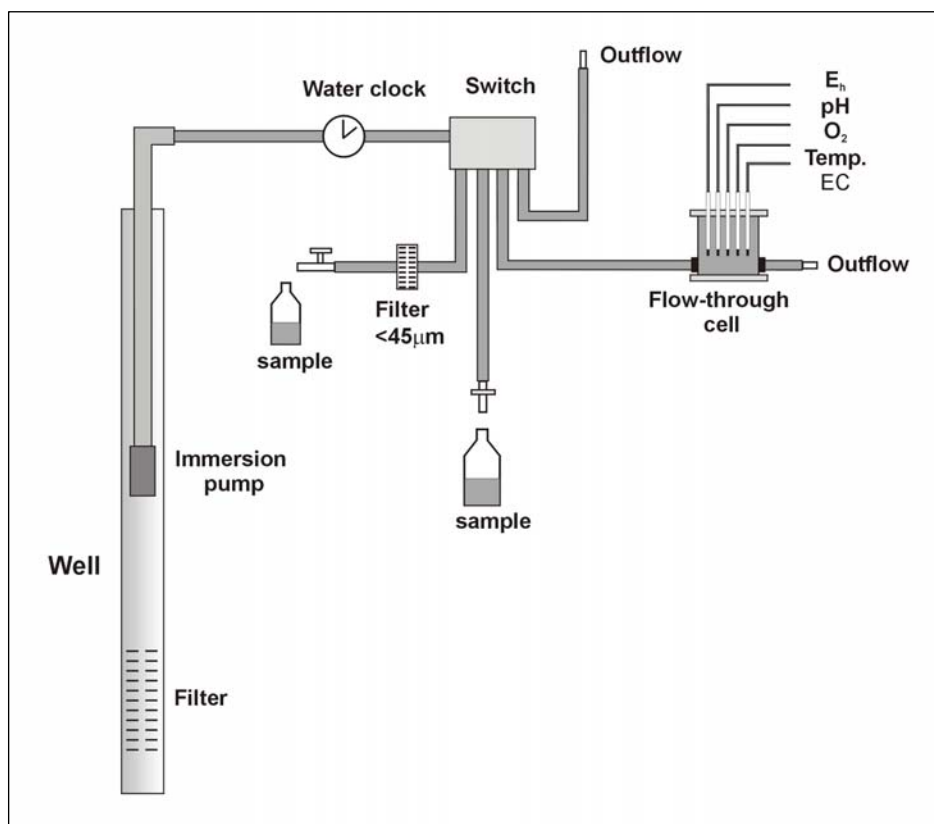


Figure 3.1: Scheme of sampling setup in the field.

Fig. 3.1 shows the sampling setup. Easily fluctuating and volatile ingredients were measured directly in the field. Ammonium (NH_4^+) and nitrite (NO_2^-) were determined with quick determination tests from the company Merck. The carbon species (HCO_3^- , CO_2) were determined by titration after DIN 38409 (1979). The values of specific electric conductivity (EC), pH and especially the redox potential (E_h) are the important parameter for orientation and were measured in situ. In Tab. 3.1 the field parameters, methods, devices and quick determination tests are listed.

Samples for anions and cations were filtered (0.45 μm) and filled into PVC-bottles (50 ml). Samples for cations were additionally acidified for the conservation with concentrated HNO_3 to a $\text{pH} < 2$.

The samples were hermetically sealed and stored refrigerated (4°C) as soon as possible. Subsequent to the field campaign the anion and cation samples were handed over for analysis to the hydrogeochemistry laboratory of the FU Berlin.

Monitoring well SPFP17 ran out of water before stable values were established. Due to the low permeability of the soil, new constructed piezometer SPFPFU22, -23, -24, -26 and -27 were also sampled without stable values of field parameter. Pumped water was stored in pvc-bottles, kept until the ebbing of the well and the last one and a half litres were taken as sample. Because of the high suspension load of the samples, they first keep calm until the load sediments and then they were filtered. This could have induced water-sediment interaction after sampling and for this reason an impact of analysis results. The sampling of pumping well SPFP23 occurred with a dipper and samplings of surface water (SPFP04) were taken without pumping.

In autumn 2005 and spring 2006 electric conductivity logs (EC-logs, Tab. 3.2) were carried out to determine the interface between superficial fresh water and subterranean saltwater. The measuring device is listed in Tab. 2.7. A series of monitoring wells (Tab. 3.2) in the surroundings of the lake is used for this task. Measuring interval was from 0.2 to 1 m, depending on the observed variations in conductivity.

These logs are used to characterize the recovery velocity of normal conditions (before pumping). Therefore several measurements at the sampling sites were made before and after pumping. Measurements in autumn 2005 were made before and af-

Table 3.1: Method and device of sampled field parameters

Parameter (effective range)	Method	Device/quick determination test
Temperature 0 to 100 $^\circ\text{C}$	Electrometric Log	Multiline P4 (WTW Inc.); Temperature probe integrated in pH probe SenTIX 41
pH-value (pH 1 to pH 13)	potentiometric Log with automatic temperature compensation	Multiline P4 + pH probe SenTIX 41 (WTW Inc.)
Spec. conductivity (10 to 10^6 $\mu\text{S}/\text{cm}$)	Electrometric Log with automatic temperature compensation (25°C)	Multiline P4 + conductivity probe TetraCon 325 (WTW Inc.)
Oxygen saturation (1 – 100%)	polarographical Log	Multiline P4 + oxygen probe CellOx 325 + calibrate vessel OxiCal-SI (WTW Inc.)
Redox potential (-200 to 1000 mV)	Potentiometric Log (Ag/AgCl-reference electrode)	Multiline P4 (WTW Inc.) + Eh probe Pt 4805 (Ingold Inc.)
Carbon species	In situ log, titration with 0,1 N HCl to pH 4,3 respectively with 0,1 N NaOH to pH 8,2	Bulb pipette (100 ml) field burette, pH meter, beaker
NO_2^- (0,005 to 0,1 mg/l)	In situ log: colorimetric	Quick test: Aquaquant 1.4408 (Merck Inc.)
NH_4^+ (0,05 to 0,8 mg/l)	In situ log: colorimetric	Quick test: Aquaquant 1.4400.001 (Merck Inc.)

ter pumping, in spring 2006 only one log per sampling site was recorded. For a couple of sites (SPFP05, -06 and -14) hydrochemical sampling was accomplished before the recording of EC-logs. For all sites the observed reestablishment times suggest a regeneration of the initial EC distribution between the samplings,

Probably most of the sampled wells are full screened, which provides good conditions for EC-logs, because the water inside the well is at each depth in contact with the surrounding water body. The maximum sampling depth of 20 m of EC-logs was limited by the given equipment.

The sampling of temperature and geothermic gradients on the basis of monitoring wells and piezometers in Fuente de Piedra Basin occurs in September/October 2005 and in March/April 2006. Concomitant conductivity-logs were recorded for selected sampling sites. For the sampling of wells > 20 m an electric contact gauge with integrated temperature gauge was used, for wells < 20 m a conductivity meter with integrated temperature gauge was used respectively (Tab. 3.2). Tab. 3.2 lists the number of respective logs.

Table 3.2: Quantity of log samples.

Site Id.	Depth of sampling (m)	Quantity of temperature logs	Quantity of conductivity logs
SPFP03	20	4	4
SPFP05	20	4	4
SPFP06	20	3	3
SPFP07	20	3	3
SPFP09	87	2	
SPFP10	100	2	
SPFP14	10,5	4	4
SPFP15	13	3	3
SPFP17	8	5	5
SPFP22	45	2	

3.1.1.3 Laboratory analytical methods

Within the scope of this project following major and minor ions were determined in FUB laboratory: Na⁺, K⁺, Mg²⁺, Ca²⁺, Li⁺, Sr²⁺, Mn²⁺, Fe²⁺, Br⁻, Cl⁻, SO₄²⁻, NO₃⁻. In Tab. 3.4 all laboratory analysis, devices and detection limits are listed.

Subsequent to the field campaign the samples for stable isotopes were handed over for analysis to the AWI Potsdam. The isotope measurements were accomplished with a Delta-S Mass spectrometer (Finigan). In Tab. 3.5 methods, devices and detection limits of the isotope analysis are shown.

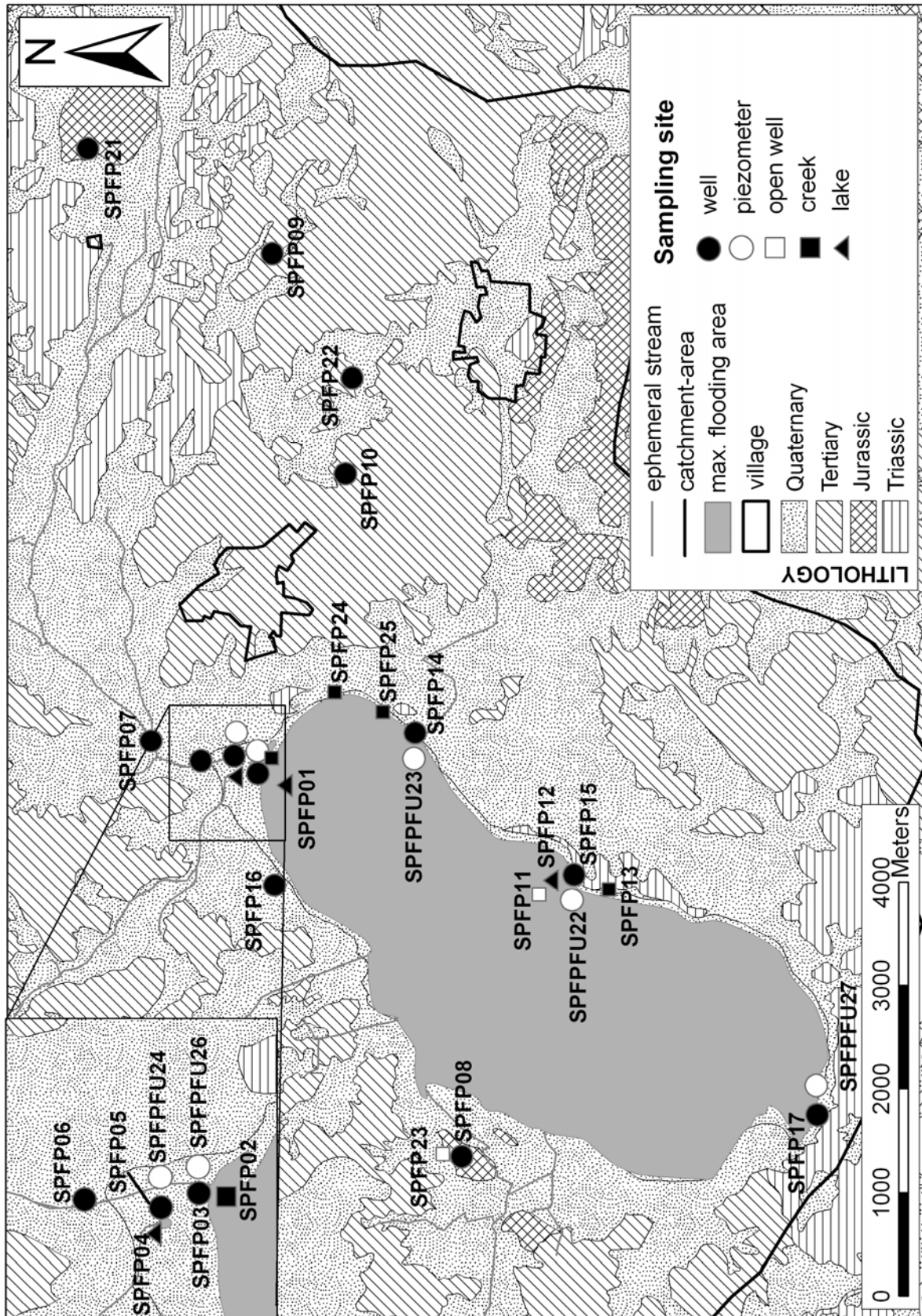


Figure 3.2: Location and type of the sampling sites.

3. Diploma thesis - Methods

Table 3.3: Overview of measured and analysed parameters of field campaigns 2004 - 2006.

Station Id.	pH	Eh	EC	T	O ₂	NO ₂	Na	K	Ca	Mg	Fe	Mn	NH ₄	Cl	HCO ₃	NO ₃	SO ₄	Br	¹⁸ O	D	³⁴ S	water table	EC log	temp log	
Winter 2004																									
SPFP01			x			x	x	x	x	x	x	x		x	x	x	x		x	x					
SPFP02			x			x	x	x	x	x	x			x	x	x	x		x	x					
SPFP03			x	x		x	x	x	x	x	x			x	x	x	x		x	x		x			
SPFP04			x	x		x	x	x	x	x	x			x		x	x		x	x					
SPFP05			x	x		x	x	x	x	x	x			x	x	x	x		x	x					
SPFP06			x	x		x	x	x	x	x	x			x	x	x	x		x	x		x			
SPFP07			x	x		x	x	x	x	x	x			x	x	x	x		x	x		x			
SPFP08			x	x		x	x	x	x	x	x			x	x	x	x		x	x		x			
SPFP09			x	x		x	x	x	x	x	x			x	x	x	x		x	x		x			
SPFP10			x	x		x	x	x	x	x	x			x	x	x	x		x	x		x			
Winter 2005																									
SPFP03			x	x		x	x	x	x	x	x			x		x	x								
SPFP04			x	x		x	x	x	x	x	x			x		x	x								
SPFP05			x	x		x	x	x	x	x	x			x	x	x	x					x			
SPFP06			x	x		x	x	x	x	x	x			x		x	x					x			
SPFP11			x	x		x	x	x	x	x	x			x		x	x					x			
SPFP12			x	x		x	x	x	x	x	x			x		x	x								
SPFP13			x	x		x	x	x	x	x	x			x	x	x	x								
SPFP14			x	x		x	x	x	x	x	x			x		x	x					x			
SPFP15			x	x		x	x	x	x	x	x			x	x	x	x					x			
SPFP16			x	x		x	x	x	x	x	x			x		x	x					x			
SPFP17			x	x		x	x	x	x	x	x			x	x	x	x					x			
Summer 2005																									
SPFP03	x	x	x	x	x	x	x	x	x	x	x	x	x	x	x	x	x	x	x	x	x	x	x	x	x
SPFP04	x	x	x	x	x	x	x	x	x	x	x			x		x	x	x	x	x		x			
SPFP05	x	x	x	x	x	x	x	x	x	x	x	x	x	x	x	x	x	x	x	x	x	x	x	x	x
SPFP06	x	x	x	x	x	x	x	x	x	x	x	x	x	x	x	x	x	x	x	x	x	x	x	x	x
SPFP07	x	x	x	x	x	x	x	x	x	x	x	x	x	x	x	x	x	x	x	x	x	x	x	x	x
SPFP08	x	x	x	x	x	x	x	x	x	x	x	x	x	x	x	x	x	x	x	x	x	x	x	x	x
SPFP09	x	x	x	x	x	x	x	x	x	x	x	x	x	x	x	x	x	x	x	x	x	x	x	x	x
SPFP10	x	x	x	x	x	x	x	x	x	x	x	x	x	x	x	x	x	x	x	x	x	x	x	x	x
SPFP14	x	x	x	x	x	x	x	x	x	x	x	x	x	x	x	x	x	x	x	x	x	x	x	x	x

3. Diploma thesis - Methods

Station Id.	pH	Eh	EC	T	O ₂	NO ₂	Na	K	Ca	Mg	Fe	Mn	NH ₄	Cl	HCO ₃	NO ₃	SO ₄	Br	¹⁸ O	D	³⁴ S	water table	EC log	temp log	
SPFP15	x	x	x	x	x	x	x	x	x	x	x	x	x	x	x	x	x	x	x	x	x		x	x	x
SPFP17	x		x	x	x	x	x	x	x	x	x	x	x	x	x	x	x	x	x	x	x		x	x	x
SPFP21	x	x	x	x	x	x	x	x	x	x	x	x	x	x	x	x	x	x	x	x	x		x		x
SPFP22	x	x	x	x	x	x	x	x	x	x	x	x	x	x	x	x	x	x	x	x	x		x		x
SPFP23	x	x	x	x	x	x	x	x	x	x	x	x	x	x	x	x	x	x	x	x	x		x		
SPFPFU22	x		x	x		x	x	x	x	x	x	x		x	x	x	x	x	x	x	x		x		
SPFPFU23	x		x	x		x	x	x	x	x	x	x		x	x	x	x	x	x	x	x		x		
SPFPFU24	x		x	x		x	x	x	x	x	x	x	x	x	x	x	x	x	x	x	x		x		
SPFPFU26	x		x	x		x	x	x	x	x	x	x		x	x	x	x	x	x	x	x		x		
SPFPFU27	x		x	x		x	x	x	x	x	x	x	x	x	x	x	x	x	x	x	x		x		
Spring 2006																									
SPFP03																							x	x	x
SPFP05																							x	x	x
SPFP06																							x	x	x
SPFP07																							x	x	x
SPFP08																							x		
SPFP09																							x		x
SPFP10																							x		x
SPFP14																							x	x	x
SPFP15																							x	x	x
SPFP17																							x	x	x
SPFP22																							x		x
SPFPFU22																							x		
SPFPFU23																							x		
SPFPFU24																							x		
SPFPFU26																							x		
SPFPFU27																							x		

Table 3.4: Method, device and detection limit of analysed ions.

Ions	Method	device	Detection limit
Na ⁺	Flame photometer	Eppendorf Elex 6361r	1,0 [mg/l]
K ⁺	Flame photometer	Eppendorf Elex 6361r	0,1 [mg/l]
Al ³⁺	ICP	Leemans	0,5 [mg/l]
Mg ²⁺	AAS	Perkin Elmer 5000	0,05 [mg/l]
Ca ²⁺	AAS	Perkin Elmer 5000	0,05 [mg/l]
Li ⁺	AAS	Perkin Elmer 5000	0,05 [mg/l]
Sr ²⁺	ICP	Leemans	0,05 [mg/l]
Mn ²⁺	AAS	Perkin Elmer 5000	0,05 [mg/l]
Fe ²⁺	AAS	Perkin Elmer 5000	0,1 [mg/l]
Br ⁻	DEV (1986)	Titration	0,01 [mg/l]
Cl ⁻	photometric	Technicon Autoanalyser	1,0 [mg/l]
SO ₄ ²⁻	photometric	Technicon Autoanalyser	0,05 [mg/l]
NO ₃ ⁻	photometric	Technicon Autoanalyser	0,05 [mg/l]

Analysis of sulphate isotopes were made by TU Bergakademie Freiberg (Tab. 3.6). For the analysis of sulphate isotopes, aqueous dissolved sulphate was precipitated with a 10% BaCl₂-solution as BaSO₄ and converted to SO₂ for the mass spectrometric determination of δ³⁴S (YANAGISAWA & SAKAI, 1983). The preparation for the determination of oxygen isotope ratios was realized after HOLT (1991).

Table 3.5: Methods, devices and detection limits of H₂O isotope analysis (AWI Potsdam).

Isotopes	Method	Device	Detection limit
δ ¹⁸ O	H ₂ -Equilibrium	Delta-S Mass spectrometer Finnigan	± 0.8 ‰
δD	CO ₂ - Equilibrium	Delta-S Mass spectrometer Finnigan	± 0.1 ‰

Table 3.6: Methods, devices and detection limits of SO₄²⁻ isotope analysis (TU Freiberg).

Isotopes	Method	Device	Detection limit
δ ³⁴ S	Element analyser	Delta plus Mass spectrometer Finnigan	± 0.3 ‰
δ ¹⁸ O	Pyrolysis	Delta plus Mass spectrometer Finnigan	± 0.5 ‰

3.1.2 Basic Principles

3.1.2.1 Hydrochemistry

The analysis of ions were proofed for their reliability by **electroneutrality** and analyzed again, if aberration was greater than ± 5 %. The electroneutrality defect was calculated with

$$\text{Electroneutrality } [\%] = \frac{\sum \text{cations } [meq/l] - \sum \text{anions } [meq/l]}{\sum \text{cations } [meq/l] + \sum \text{anions } [meq/l]} \times 100 \quad (8)$$

Hydrochemical analyses are checked for liability by plotting electric conductivity (field observation) versus Chloride (laboratory data), because both values correlate on a straight line. So analysis errors and not reliable values are barred from interpretation.

Salinity is defined as the total amount of solid materials in grams dissolved in one kilogram of sea water when all the carbonate has been converted to oxide, the bromine and iodine replaced by chlorine and all organic matter completely oxidized.

Table 3.7: Classification of watertypes due to water salinity.

Water salinity based on dissolved salts in parts per thousand (‰)			
Fresh water	Brackish water	Saline water	Brine
< 0.5 ‰	0.5 - 30 ‰	30 - 50 ‰	> 50 ‰

As you see in Tab. 3.7 water with a salt content < 0.05 % is defined as fresh water. Water with a salinity ranging from 0.05 to 3 % is regarded as brackish; whereas water with 3 to 5 % is termed as saline. Highly saline water with salt contents > 5 % is considered as brine. The average salinity of seawater is 35 ‰, which means that seawater is composed of 3.5 % salt and 96.5 % H₂O by weight.

The term **salinization** is not consistently defined. It is commonly used for waters exceeding the flavourful perception of 300 – 400 mg/l dissolved materials (GRUBE ET AL., 2000).

As critical level the values for drinking water from the water management act indicates a lead for designation.

The average salt content of sea water is about 35 g/l, in contrast to groundwater with mineralisation < 1 g/l.

Salinisation of groundwater could be effected by leaching of evaporites, ascending of existing deep brines or geothermal waters, intrusion of sea water or by infiltrating of high mineralized surface waters due to evaporation.

Evaporation removes water molecules from solutions and enriches ions. Enrichment appears until saturation (solubility product) and precipitation of certain solids. Salts precipitate in order to the solubility product; the least soluble solid precipitates first (Ca-carbonate), Mg-salts constitute the most soluble solids and represent the last precipitates. In endorheic salt lakes a zoning of these solids can be found due to precipitation sequence (see Fig. 1.2).

Groundwater can be classified due to their soluted components (in meq %) into water types. Cat- and anions that excess a certain limit, named major ion, name the water type. First cations are written and second anions in order of their proportion till a certain limit. For this study the limit has set at 10 meq % for subwater types and 20 meq % for main-water types to obtain a better differentiation.

Different plot types can be used to display the hydrochemical composition of groundwater samples.

Piper plots consist of combined triangle and quadrangle diagrams (Fig. 3.3) (PIPER, 1944). Major anions and cations [meq %] are plotted in separate triangles as a point. In the quadrangle the groundwater sample is represented. Possible water types are written at the quadrangles corners.

Piper plots display the distribution and outliers of analysed samples. Processes like mixing (mixed samples of two waters plot on a line), ion exchange, precipitation or dilution of salts can be identified.

In **Schoeller plots** the major ions are plotted in meq/l on a logarithmic scale side by side (SCHOELLER, 1935, 1938). Each point of a water sample is connected by a line. Parallel lines indicate same ion ratios of the water sample even at different concentrations. So comparison of many samples can be made very quickly regarding the genesis. Parallel courses indicate same ion ratios at different concentrations by mixing, dilution or evaporation. Due to comparatively low concentrations of K^+ and NO_3^- only Ca^{2+} , Mg^{2+} , Na^+ , Cl^- , SO_4^{2-} and HCO_3^- are plotted.

Stiff diagrams constitute a horizontal plot type for hydrochemical data (STIFF, 1951). Stiff diagrams can be used for presentation on maps to identify regional trends. Ions are presented on horizontal lines, cations and anions are separated by a vertical line

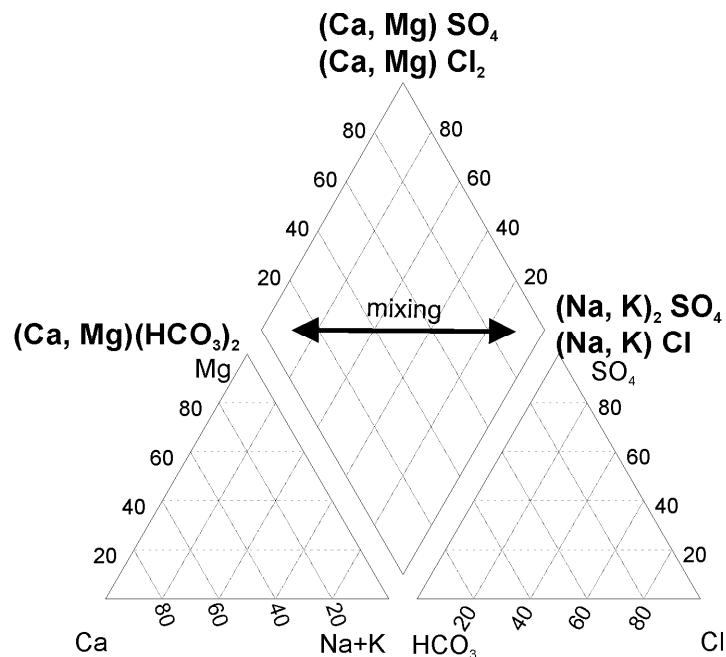


Figure 3.3: Piper plot. Major ions are plotted in meq %. Possible water types are written at the corners of the rhombus. Arrow indicates general mixing line between fresh- and saltwater.

and are situated on one site respectively. Usually groundwater samples are displayed in meq/l but Stiff diagrams are very flexible in unit and number of ions. Fig. 3.4 shows an example of a Stiff plot.

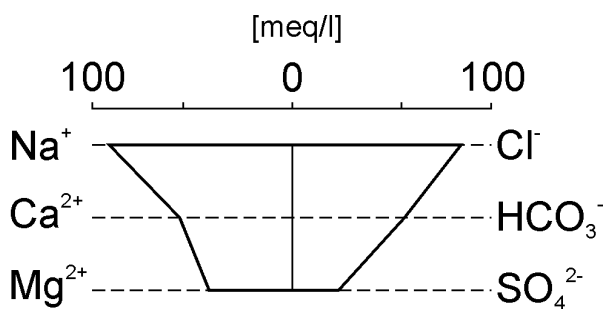
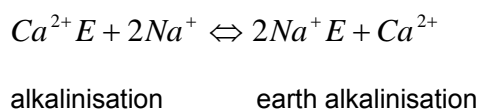


Figure 3.4: Stiff diagram.

While groundwater flows, it is in contact with absorptive effective organic and inorganic matters of the aquifer. The dissociated ions are bound by crystals, colloids surfaces or inside the lattice. This kind of bond is responsible for ion exchange processes, where ions are exchanged relative to their stoichiometric ratios. Sorbing effective compounds are clay minerals, zeolite, iron- and manganesehydroxides, humus, feldspar, mica, alumina containing augite and hornblende. With clay minerals the most intensive bond strength are reached (KRAUSKOPF, 1956). The rate of sorption depends on surface, density, porosity and grain size of the exchanger and on concentration in groundwater and exchanger of the ions. Naturally only cations will be exchanged.

Ion exchange in the saturated zone is adsorption of ions from the water into the crystal lattice and remobilization of equivalent mass of bounded ions (RENICK, 1924; RIFFENBURG, 1925; HARRASSOWITZ, 1933; SCHOELLER, 1934; ØDUM & CHRISTENSEN, 1936; SCHWILLE, 1955). This process is reversible and typical in the underground. For intruding saltwater into a freshwater saturated aquifer the exchange process is the following:



The cation exchanger is saturated with Ca^{2+} from Ca- HCO_3 freshwater. When Na-Cl saltwater flush into the freshwater aquifer Ca^{2+} is released and Na^+ occupies the ion exchanger. Ca- Cl_2 type water results as a typical exchange water type (LÖHNERT, 1966) and this process is named earth alkalinisation.

During precipitation or dissolution processes of minerals or salts in groundwater equivalent parts of ions are bound or released. The most important soluble salts are Calcium- and Magnesium-carbonates ($\text{Ca}(\text{Mg})\text{CO}_3$), Gypsum ($\text{CaSO}_4 \cdot 2 \text{H}_2\text{O}$), Sylvite (KCl) and Halite (NaCl). In thermodynamic stable groundwater which is characterized

by precipitation and dissolution processes, the following ions are present in equivalent parts, so that the difference between these pairs is 0:



Groundwater that is characterized by earth alkalinisation processes shows positive equivalent ratios and groundwater characterized by alkalinisation processes negative equivalent ratios for equation X1. For equation X2 earth alkalinisation processes have negative ratios. These relations are valuable to determine cation exchange processes.

TESMER ET AL. (2006) show these relations in a **cation-exchange diagram** with the corresponding ion pairs on the axis, the equivalent sums of the earth alkalis respectively alkalis are plotted versus their corresponding ions (Fig. 3.5). Groundwaters affected by ion exchange plot on a straight line with a slope of 1 due to an exchange of equivalent parts of cation for these processes. Samples which deviate from this straight line are not in charge balance due to analysis error or presence of not included ions. Groundwaters that are in solution equilibrium plot in the centre of the diagram.

In all samples with a pH < 8.2 the pH-dependent Carbon species CO_3^{2-} is not present and must not be considered.

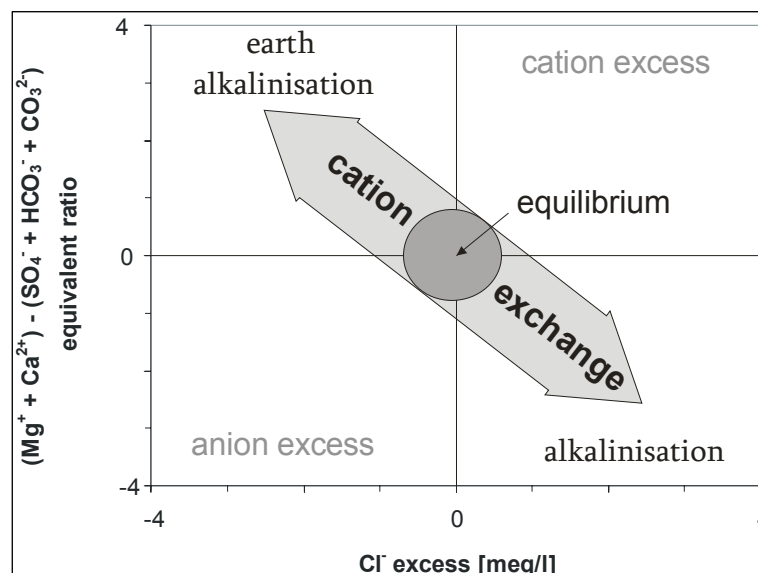


Figure 3.5: Cation-exchange diagram after TESMER ET AL. (2006).

By ion ratio analysis characteristic ratios can be determined and related with certain hydrochemical processes. **Ion ratios** are calculated in equivalent concentrations (meq/l). DEIBEL (1995) and HÖLTING (1970) give further information for ion ratio inter-

pretations of salt water. Ion ratio interpretation under influence of evaporation is made by CARPENTER (1978) and HARDIE & EUGSTER (1970). Analysis of ion ratios is made according to the above mentioned authors.

Ion ratio of $\text{Cl}^-/\text{SO}_4^{2-}$ is used for differentiation of sulfatic or chloridic sources of salinisation. Ratios > 1 indicate chloridic and ratios < 1 sulfatic influence. Chloride dominance results from anthropogenic impact or salt leaching. Sulfate dominance occurs near dumps (building rubble) or by gypsum dissolution. Sulfate concentration can be decreased by microbial reduction under conditions which include NaCl concentrations up to 200 g/l and temperatures of 80°C thus the $\text{Cl}^-/\text{SO}_4^{2-}$ ratio is not significant.

Relations between $\text{Mg}^{2+}/\text{Ca}^{2+}$ are < 0.2 in normal groundwater, values between 0.2 and 0.5 refer to a geogenic source of salinity. Values > 0.2 are characteristic for incipient cation exchange processes; clay mineral affinity for calcium is higher and leads to a relatively enrichment of magnesium in groundwater. The $\text{Mg}^{2+}/\text{Ca}^{2+}$ ratio increase because of better solubility of Mg-chlorides (MgCl_2) compared to Ca-chlorides.

Ion ratios of Cl^-/Na^+ show for non salted groundwater values < 1.0 . Ratios of 1.0 are characteristic for leaching of Halite. Values noticeable > 1.0 signify the presence of alkaline-earths-chlorides. These can derive from dissolution of Mg-chlorides or by earth alkalisation.

$\text{Ca}^{2+}/\text{Cl}^-$ ratio is an indicator for water rock interaction, if Calcium and Chloride increase in common. Associated Sulfate reduction can additionally increase the Ca^{2+} concentration. The relative loss of Mg^{2+} in brines during Dolomitization of calcite can also be responsible for increasing ratios (COLLINS, 1975). Ca^{2+} concentration can increase due to cation exchange processes. Cation exchange starts, if Na^+ concentration is high because of high chemical bond of Ca^{2+} with the cation exchanger.

For comparison of ion ratio relations the seawater evaporation curve was used for Br^- and Ca^{2+} . Table 3.8 lists the seawater evaporation stages and the mean concentrations of the ions.

Cl^-/Br^- ratio is suitable for genesis conclusions of groundwater. Both ions react sparse and appear in specific ratios in nature (THOMAS, 1994). Bromide occurs significant rarely than the geochemical similar chloride. RITTENHOUSE (1967) defined the evaluation and classification of deep waters on the basis of Cl^-/Br^- (respectively TDS/ Br^-) ratios. With incipient precipitation of halite during the process of (sea water) evaporation, an enrichment of bromide compared to chloride appears. Bromide acts

conservative and is little affected by chemical reactions such as mineral precipitation or adsorption (VALJASHKO, 1956). Mineralization sequence is Halite, Sylvite (KCl), Carnallite ($\text{MgCl}_2 \cdot \text{KCl} \cdot 6\text{H}_2\text{O}$) and Bischofite ($\text{MgCl}_2 \cdot 6\text{H}_2\text{O}$), Bromide content is increasing in this sequence (MYAGKOV & BURMISTROV, 1964).

The chloride/bromide ratio for sea water is around 300 ($\text{Cl}^-_{\text{SMOW}} = 19400 \text{ mg/kg}$; $\text{Br}^-_{\text{SMOW}} = 67 \text{ mg/kg}$), which is extensively constant for all oceans since Permian (THOMAS, 1994) and can be taken as reference value. The chloride/bromide ratio allows for higher mineralized groundwaters a determination between marine dominated water ($\text{Cl}^-/\text{Br}^- \approx 300$), leaching water ($\text{Cl}^-/\text{Br}^- > 3.000$) and residual brines, formed by evaporation processes ($\text{Cl}^-/\text{Br}^- < 300$).

Marine influenced groundwater possesses similar ratios. Bromide enriches compared to chloride due to syngenetic evaporation processes in the residual brine. The chloride/bromide ratio in residual brines is conspicuously less than 300. The precipitated salts are depleted in bromide, which causes chloride/bromide ratios for leaching water > 3000 (MAZOR, 1997). However HOTH ET AL. (1997) observes an enrichment of bromide in the groundwater due to leaching of bromide containing salts and the reaction with organic matter. Highest bromide concentrations can be found in continental salt lakes (HOTH ET AL., 1997). MATTHEß (1994) suppose that Br^- decrease in solution due to ion filtration. The greater ion ratio of Br^- compared to Cl^- leads to a preferred adsorption in clays. In organic rich sediments Bromide could be bound or released as a result of its biophil behaviour (HOTH ET AL., 1997). As said by TESMER ET AL. (2006) analysis of Chloride-Bromide ratio in surface near groundwater is complicated due to interference of various processes, like Bromide enrichment in rainwater by exhaust emissions or by anthropogenic manuring. For low mineralized waters this method is not suitable due to analysis error (TESMER ET AL., 2006).

Ca^{2+} and Br^- respectively are displayed vs. Cl^- in mg/l. These ion ratios and their comparison with seawater evaporation curve are used to determine different processes that lead to enrichment of ions in groundwater in sedimentary basins. Seawater evaporation curve data were extracted from VALJASHKO (1956); ZHEREBTSOVA & VOLKOVA (1966); HERRMANN ET AL. (1973); COLLINS (1975); HARVIE ET AL. (1980); FONTES & MATRAY (1993) and MATRAY (1988) and summarized by THOMAS (1994). Several evaporation stages were marked out on the evaporation curves, the beginning of each is defined by the incipient precipitation of a mineral-phase due to their

solubility products (Tab. 3.8). In the displayed plots only the first stage occurs: Incipient precipitation of Gypsum (1).

Table 3.8: Seawater evaporation curve data (FONTES & MATRAY, 1993).

Evaporation stage	beginning precipitation	TDS	Na ⁺	K ⁺	Mg ²⁺	Ca ²⁺	Cl ⁻	SO ₄ ²⁻	Br ⁻
		[g/l]	[mg/l]	[mg/l]	[mg/l]	[mg/l]	[mg/l]	[mg/l]	[mg/l]
0	seawater	35.8	11000	408	1320	420	19780	2770	68
1	Gypsum	124.7	37800	1470	4530	1540	69000	10100	234
2	Halite	307.9	95100	3600	13400	450	175600	19100	578
2.1		334.4	89000	5300	20900	237	188200	28900	950
2.2		332	65600	7730	35500	170	185200	36400	1327
2.3		383.8	63000	12900	50500	96	189900	65400	1830
3	Epsomite	400.2	48200	17680	56120		190500	82200	2970
4	Sylvite	410.3	22100	25900	72900		223900	56100	4770
5	Carnallite	418.2	15000	17000	85700		257600	35400	5300
5.1		462.6	8150	860	108800		304600	27100	7380
6	Bischofite	504.8	1680	860	122000	60	337300	34900	7530

Dissolution of salt stones leads to very high contents of SO₄²⁻ and Cl⁻, Na⁺, Ca²⁺ and Mg²⁺ in groundwater, so that TDS values greater 200 g/l can be reached. Because solubility of CaSO₄ increases in presence of NaCl, the equivalent ratio of Mg²⁺/Ca²⁺ for Na-Cl type water can be lower than in low mineralized groundwater.

Saturation indices (SI) indicate the degree of saturation and therefore if mineral phases in groundwater will solute or precipitate. SI is calculated by quotient of ion activity and solubility product (Form. 9) after mass action law. By the calculated activities of the soluted ions {A⁻}^m × {B⁺}ⁿ the ion activity product (IAP) is given.

$$SI = \log \frac{IAP}{SP_{AB}} = \log \frac{\{A^{-}\}^m \times \{B^{+}\}^n}{SP_{AB}} \quad (9)$$

For SI < 0 groundwater is under saturated and for SI > 0 over saturated in a specific mineral. Values of 0 +/- 0.2 form equilibrium conditions (MATTHEß, 1994). Calculation of SI was made with PHREEQC Version 2.12. For high saline groundwater activity coefficients change and therefore Pitzer equation, Pitzer database, (PITZER, 1977, 1979) was used in PHREEQC. This equation was used for samples with ionic strengths greater 0.5.

Oxidation and reduction are essential hydrogeochemical processes and affect beside the pH-value the solubility of relevant ions. Oxygen enters groundwater by diffusion and inflow and will be consumed by oxidation of Fe(II) and Mn(II) compounds and organic materials. Oxygen poor waters act reducing to less stable oxygen radicals and induce e.g. nitrate and sulphate reduction. The characteristic chemical features of reductive groundwaters are oxygen deficits, distinct contents of Fe-II and Mn-

II ions, reduced nitrates and contents of H_2S , NO_2^- and NH_4^+ . With increased depth O_2 , NO_3^- , Mn(IV) oxide, Fe(III) oxide and sulphate will be reduced successively (LEUCHS, 1988; OTTOW, 1981).

The natural temperature system of the upper earth's crust is dominated by two heat sources. On one hand the heat emission of the earth's core (5000 °C) and the radioactive decay of elements like uranium, potassium or thorium in the earth's mantle lead to a heating of the upper crust with a **geothermal gradient** of 2 to 3 Kelvin per 100 m. On the other hand this heat convection is superimposed in the most external sphere by solar radiation, which leads to high seasonal temperature fluctuations under the earth's surface. The amplitude of this fluctuation is decreasing to a depth of 20 to 25 m below surface, the so called "neutral zone", where the temperature is fluctuating less than 0.1 K (DIN 4049-3, 1994).

The spread of heat in water filled rocks occurs in two ways of heat transport: heat conduction and heat convection. Heat conduction is caused by temperature differences within a temperature field. There's no transportation of material, only an interchange on molecular level which lead to a transfer of energy from molecules of a higher energy level to molecules of a lower energy level. For heat convection the heat transport is carried out by liquids. In the subsurface layering this occurs by groundwater, there is a straight connection of groundwater dynamic and temperature field in the subsurface. Heat convection is always connected to heat conduction, whereas heat conduction could appear reclusively (DVWK, 1983).

The classification of the temperature logs for their thermodynamically properties occurs by inspection of the temperature gradients. Temperature gradients will be influenced after LUDEWIG (1981) by following factors:

- Heat flow and heat conductivity (dependent on water and quartz content)
- Temperature change on the earth's surface
- Sampling method
- Groundwater movement

Specific electrical conductivity (EC) is related to the ions in solution. At higher mineralization electrical conductivity is higher. Specific electrical conductivity depends on temperature due to Brownian molecular movement of the ions, solution viscosity (more viscose, less EC) and sort of ions (valence, ion radius) (APPELO & POSTMA, 1999; HÖLTING, 1996). The EC of an aqueous solution of one or more salts is put together of conductivity instalments of each cat- and anion. EC and salinity of

water form a linear relation. Whenever (electric) conductivity is written, specific electrical conductivity should be meant.

Between fresh water and salt water a zone of brackish water will be developed due to diffusion, the transition zone, or respectively between low and high mineralized water. The thickness of this zone is about a few meters and depends on permeability of the aquifer (Porosity, Porosity shape, etc.). Diffusion and gravity form a dynamical balance in natural conditions. Upraising of salt water in higher multiaquifer formations or until the surface can be found in Discharge areas (GRUBE ET AL., 2000).

When highly mineralized water come in contact with low mineralized groundwater the flow patterns change due to different density and viscosity of these two fluids (APPELO & POSTMA, 1999). These flow patterns that result from mixing are more complex than from diffusion only. When high mineralized saline water lies over low mineralized groundwater, the flow patterns change as an effect of salinisation. Due to this unstable situation convective motions may pertain. Non homogenous conditions in the aquifer with different permeability's influence flow patterns and therefore the distribution of concentrations in the solution (APPELO & POSTMA, 1999).

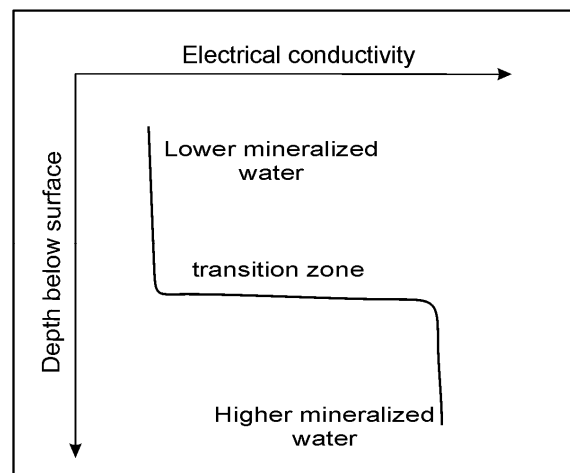


Figure 3.6: Schematic conductivity log, showing transition from low to high mineralized groundwater with transition zone.

Influence on salt water movement and movement of the fresh/salt water boundary after GRUBE ET AL. (2000):

- hydraulic conductivity of salted deep waters in higher aquifers (e.g. faults, fractures, geological window)
- morphology of the surface (high areas, depression)
- thickness of fresh water containing formations (fresh water weight)
- amount of groundwater recharge
- pressure conditions in fresh and salt water
- flow through amount, flow velocity and flow direction in fresh water
- flow through amount, flow velocity and flow direction in salt water
- anthropogenic influence:
 - groundwater drawing
 - drainage (agriculture, industry)

- recharge
- Water engineering measures

Fig. 3.6 shows a schematic conductivity log. On abscise the electrical conductivity in [$\text{mS}\cdot\text{cm}^{-1}$] is put and on ordinate depth below surface in [m]. The graph allows visualizing the change of conductivity to depth and the development of zone of dispersion in time when more than one graph exists.

3.1.2.2 Stable isotopes

Stable isotopes often used to address and solve hydrological and hydrogeological problems. The stable isotopes of **hydrogen (H) and oxygen (O)**, which represents the two components of water (H_2O), and interpretation of their ratios ($^2\text{H}/^1\text{H}$ and $^{18}\text{O}/^{16}\text{O}$) provide important information on the origin of groundwater.

Isotopes are defined as atoms whose nuclei possess the same amount of protons but a different amount of neutrons. Isotopes are divided into stable and unstable (radioactive).

As shown in Tab. 3.9 Stable isotopes are omnipresent and because of their significant differences among their physical characteristics depending on the amount of neutrons in the nuclei, they can be used for designation of sources and flows of certain substances. Lighter isotopes are situated at a higher energy level than heavier isotopes, lighter isotopes always react faster.

Table 3.9: Characteristic constants of $^1\text{H}_2^{16}\text{O}$, $^2\text{H}_2^{16}\text{O}$, $^1\text{H}_2^{18}\text{O}$ (excerped from HOEFS, 1997).

Parameter	$^1\text{H}_2^{16}\text{O}$	$^2\text{H}_2^{16}\text{O}$	$^1\text{H}_2^{18}\text{O}$
Density at 20°C [g/cm^3]	0.997	1.1051	1.1106
Boiling point	100.0	101.42	100.14
Vapour pressure at 100°C	760	721.6	?
Temperatory density max	3.98	11.24	4.30

Physical or chemical processes such as evaporation, condensation, precipitation and others and the differences of an elements isotope in their chemical properties, caused by different isotope masses, affect an isotopic fractionation. This can be either (1) equilibrium isotope exchange or (2) kinetic isotope exchange.

(1) Equilibrium isotope reactions are similar to chemical equilibrium reactions. The reaction rates of the rare isotopic species are identical to each other, as well as those of common species are identical to each other.

The partitioning of isotopes between two substances A and B is described by the isotopic fractionation factor α :

$$\alpha_{A-B} = \frac{R_A}{R_B} \quad \text{with R as the H or O ratios} \quad (10)$$

and is related to the equilibrium constant K by

$$\alpha = K^{1/n} \quad (11)$$

with n as number of atoms exchanged.

Equilibrium constants are temperature dependent. The fact that Equilibrium isotope fractionation serves as geological thermometer predicates on the temperature dependence of α .

(2) Kinetic isotope effects are of great importance in evaporation, diffusion and biological processes and base on the fact that the bonds of the lighter isotopes are broken easier than those of heavier.

In isotope geochemistry stable isotopes ratios are reported relative to a standard as δ -values in ‰.

$$\delta_x = \frac{R_x}{R_{St}} - 1 * 10^3 \text{‰} \quad (12)$$

where R_x is $^2\text{H}/^1\text{H}$ or $^{18}\text{O}/^{16}\text{O}$ of the sample and R_{St} is the standard.

δ -values and isotopic fractionation factor α are related by

$$\alpha_{A-B} = \frac{\delta_A + 10^3}{\delta_B + 10^3} \quad (13)$$

and to the isotopic content between two species or phases A and B, the Δ -value, approximated by

$$\Delta_{A-B} = \delta_A - \delta_B \approx 10^3 \ln \delta_{A-B} \quad (14)$$

because $\ln(1+x) \approx x$ for small (<10) values of x.

For stable isotope measurements of hydrogen and oxygen the ratio of H/D and $^{18}\text{O}/^{16}\text{O}$ respectively are used. The ratios measured towards V-SMOW (per definition the isotopic composition of V-SMOW – Vienna-Standard Mean Ocean Water - is taken as zero point of the δ -reference scale).

The decisive fractionation processes are the differences in vapour pressure due to evaporation and precipitation, the equilibrium fractionation and kinetic fractionation due to diffusion, bacteriogenic processes and photosynthesis.

Isotope fractionation occurs in all steps of the water cycle and is dominated by differences in vapour pressure. As in the vapour phase the light isotopes (H_2^{16}O) are enriched, in the remaining water the heavy isotopes (D_2^{18}O) enriched relatively (Fig. 3.7)

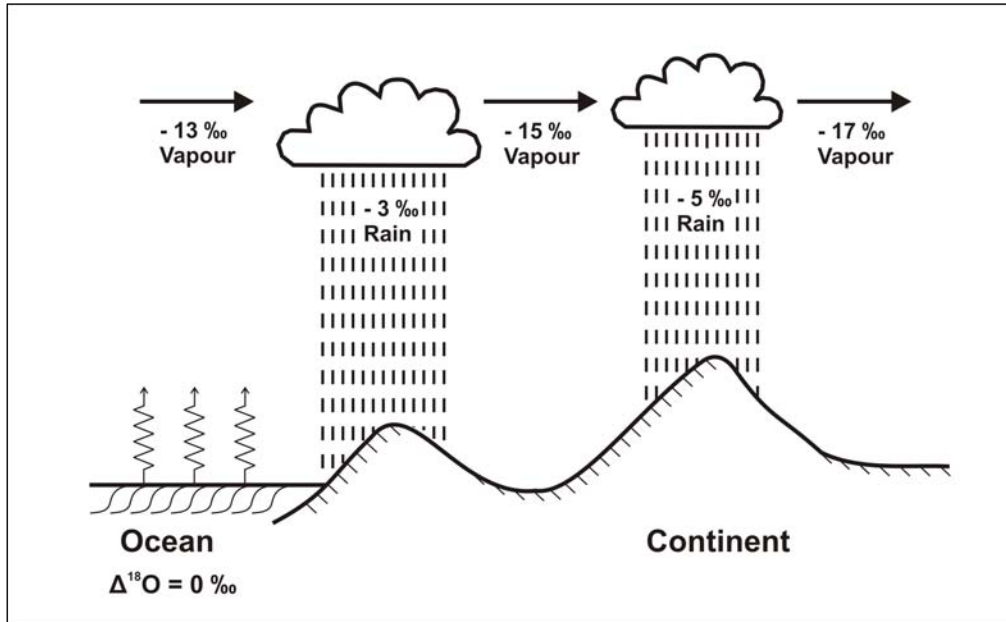


Figure 3.7: Schematic fractionation in the atmospheric water cycle (modified after SIEGENTHALER, 1979).

Continental effect: The mean isotopic composition of H and O in ocean water has a value of 0‰ as defined above. During evaporation the lighter isotopes are enriched in the vapour and transported in clouds toward the continent. When the vapour condensates the precipitation is isotopically heavier than the remaining vapour which becomes lighter than the ocean water. When the vapour in the cloud condensates again, this precipitation is lighter than the previous, and also the remaining vapour becomes lighter again. This process reoccurs until all clouds vanished by precipitation. So the D and ^{18}O contents decrease inland from a coast.

Altitude effect: As rain falls it evaporates, giving an additional altitude effect because evaporation is greater for rain drops that fall farther. So the higher the recharge altitude, the lighter is the isotopic ratio of H and O.

Temperature effect: Fractionation is temperature dependent. The colder the temperature the higher is the fractionation between vapour and condensate.

Amount effect: Evaporation increases the D and ^{18}O content of precipitation of small rainfall events more than large rainfall events.

Latitude effect: D and ^{18}O contents decrease with rain-out of air masses. Thus, D and ^{18}O contents decrease with increasing latitude.

The progressive condensation of vapour from an air mass during transport to higher latitudes with lower temperatures makes it difficult to separate latitude or altitude from temperature effects.

The hydrogen and oxygen isotopic compositions of precipitation are covariant. The relationship between δD and $\delta^{18}O$ in precipitations worldwide is described by the global meteoric water line (GMWL) and is defined by

$$\delta D = 8 \delta^{18}O + d \quad (15)$$

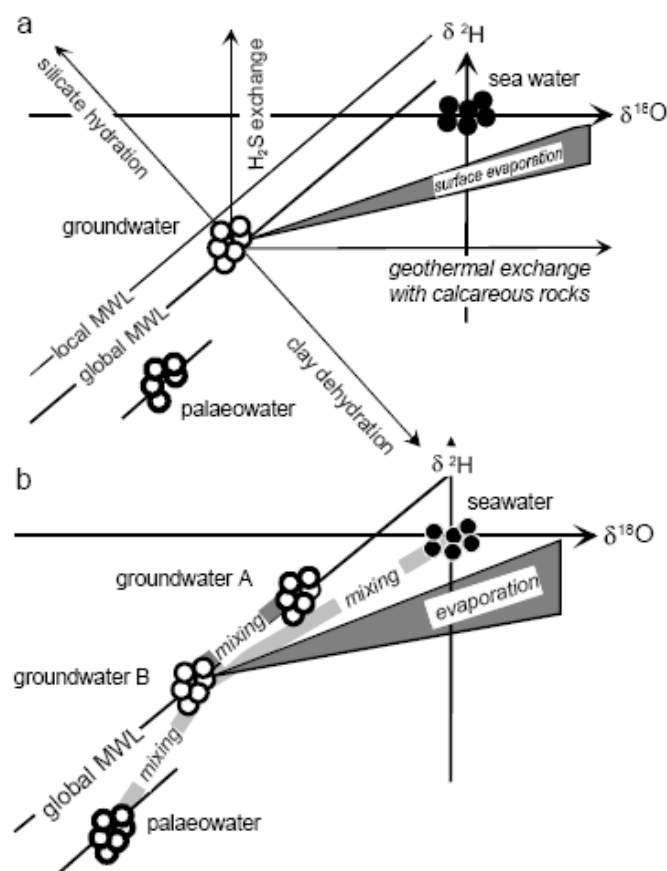
$$\text{deuterium excess } d = \delta D - 8\delta^{18}O \quad (16)$$

where d is the deuterium excess factor (for freshwater sources: $d = +10 \text{ ‰}$).

The value of d may differ significantly from area to area and over geological time. GAT & CARMICHAEL (1970) determined for the Mediterranean region (*West Mediterranean Meteoric Water Line*) a d -value greater than $+24 \text{ ‰}$.

For the interpretation of the isotopes data, δD and $\delta^{18}O$ were plotted in a curve to determine groups and mixture lines and the influence of characteristic waters and involved processes.

Figure 3.8: (a) Various processes which shift the ^{18}O and 2H values from the MWL: evaporation shifts both ^{18}O and 2H values; the former are displaced as a result of isotopic exchange with volcanic CO_2 and limestone, the latter due to exchange with H_2S and silicate hydration. (b) $^{18}O/^2H$ plot for continental precipitation (MWL = Meteoric Water Line; local corresponds to the Mediterranean precipitation) with examples of various mixing lines. The MWL of Pleistocene palaeowater may be apart from the MWL (GEYH, 2001).



Sulphur compounds appearing in nature exist basically of four stable isotopes with mass numbers from 32 to 36. These are expressed as a percentage after HOEFS (1997) shown in Tab. 3.10. The isotopes ^{32}S and ^{34}S are the most frequently appearing and commonly used.

Table 3.10: Sulphur compounds in nature.

Isotopes of S	Appearance
^{32}S	95.02 %
^{33}S	0.75 %
^{34}S	4.21 %
^{36}S	0.02%

Stable isotope ratios $^{34}\text{S}/^{32}\text{S}$ are given in the δ -notation with respect to the SF6-based Vienna-Canyon Diablo troilite (V-CDT) standard according to the following equation:

$$\delta^{34}\text{S} = \frac{R_{\text{sample}}}{R_{\text{V-CDT}} - 1} * 10^3 \text{ [‰]} \quad (17)$$

$$\text{where } R = \frac{^{34}\text{S}}{^{32}\text{S}} \quad (18)$$

The determination of sulphur isotope signatures can be realized for solved sulphates, for aquatic subspecies like H_2S and HS^- , for intermediate sulphur species (HERCH, 1997) and for solid phases like sulphide ore and gypsum (KROUSE & GRINENKO, 1991). Within the scope of this study the stable isotope ratios $^{34}\text{S}/^{32}\text{S}$ were determined for the aquatic sulphates ($\delta^{34}\text{S} - \text{SO}_4$).

The sampling occurs with 1 l glass bottles while pumping with stable values and without atmospheric contact.

Terrestrial sulphate as well as sulphate in atmospheric precipitation has isotopic ranges about:

$$d^{34}\text{S}_{\text{SO}_4} < +10\text{‰ CDT} \quad \text{and} \quad d^{18}\text{O}_{\text{SO}_4} < +4\text{‰ VSMOW}$$

The sulphate of modern seawater has a very homogeneous and well-defined isotopic composition:

$$d^{34}\text{S}_{\text{SO}_4} = 21\text{‰ CDT} \quad \text{and} \quad d^{18}\text{O}_{\text{SO}_4} = 9.5\text{‰ VSMOW}$$

Because the isotopic composition of marine sulphate was not constant over geological time, variations exist and found in all major marine evaporite deposits (Fig. 2.12).

During complex geochemical and biochemical transformations of sulphate, fractionation processes affect the stable isotopic compositions of sulphur ($^{34}\text{S}/^{32}\text{S}$) and oxygen ($^{18}\text{O}/^{16}\text{O}$). These processes are: sulphur reduction and oxidation, crystallisation of sulphate minerals and adsorption of sulphate ions in sediments. (Fig. 3.9).

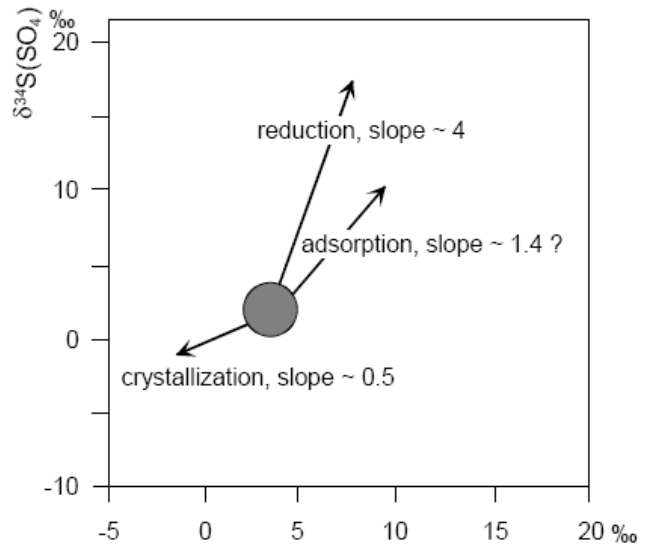


Figure 3.9: Trends in the isotopic shift of sulphur and oxygen due to the most important fractionation mechanisms (after KRAUSE, 1987).

Geogenic sources of sulphur in groundwater are evaporites (gypsum, anhydrite), sulphides and in less scale organic matter. Further sulphide sources can be sulphate intake from atmosphere (precipitation) and from agricultural fertilization.

The solution of sulphate rocks like gypsum, anhydrite or different sulphate minerals lead to an increase of sulphate concentration in groundwater. So the isotope signature of aquatic sulphur is corresponding with the signature of the solved mineral. Within this process no fractionation is occurring (CLARK & FRITZ, 1997).

Because sulphide and oxygen isotope signatures of sulphate of most evaporite series in geology are known, the source of sulphate can be reconstructed (Fig. 3.11), if reduction processes can be excluded. (CLAYPOOL ET AL., 1980).

Mixing of groundwater with modern seawater, with brines of playa lakes and with fossil formation water, modifies the isotopic composition of sulphate along the lines between the end members of mixing.

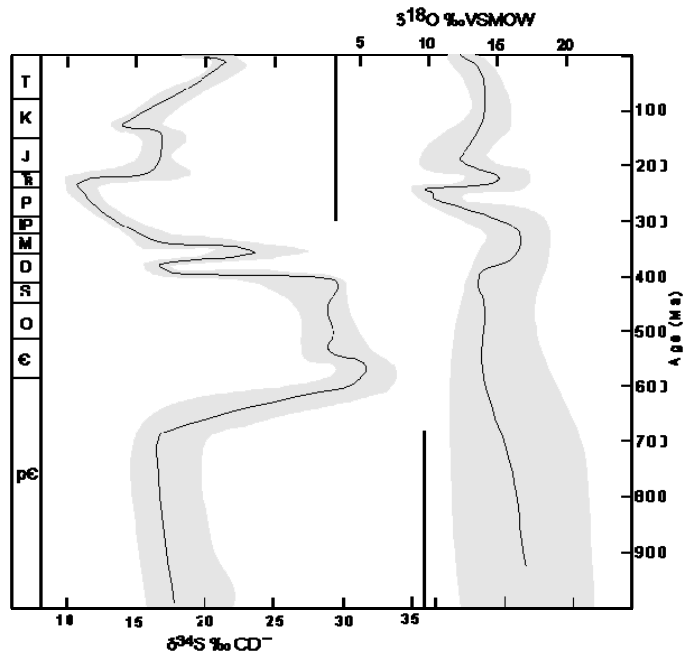


Figure 3.10: The ^{34}S and ^{18}O composition of marine sulphate through geological time (modified from CLAYPOOL ET AL., 1980, with data from FRITZ ET AL., 1988).

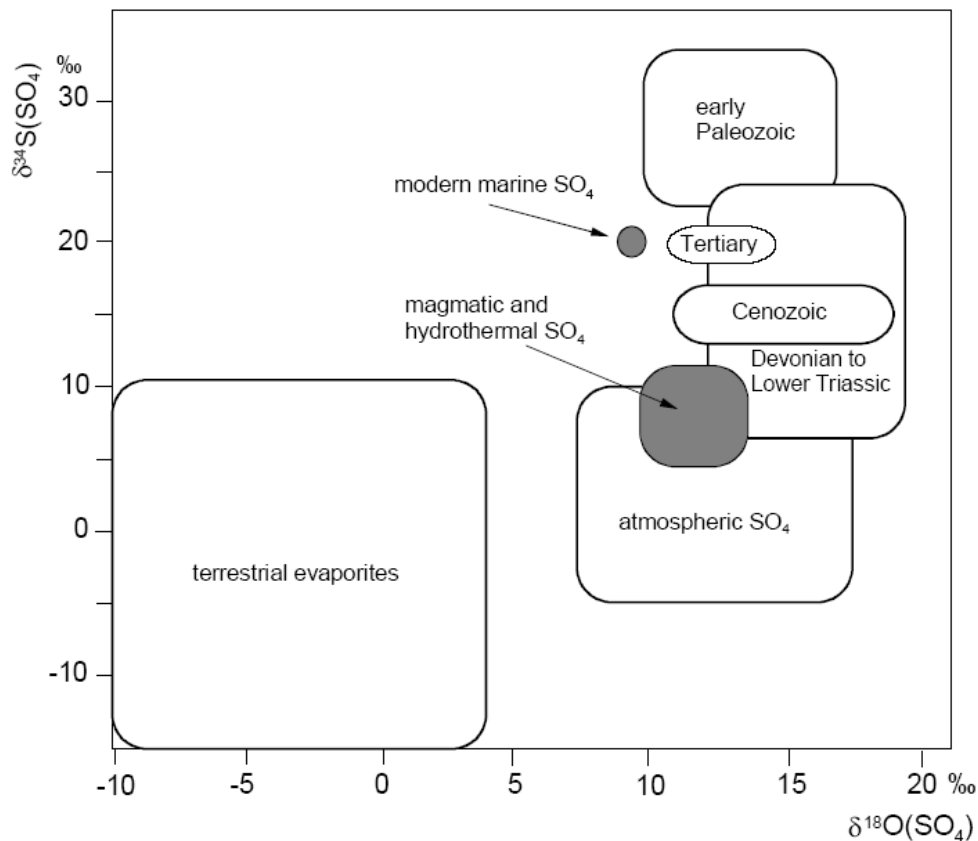


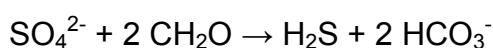
Figure 3.11: Ranges of $\delta^{34}\text{S}$ and $\delta^{18}\text{O}$ values of sulphates of various origins dissolved in groundwater (after CLARK & FRITZ, 1997).

The dissolution of evaporite minerals does not change the isotopic signature (CLARK & FRITZ, 1997).

In addition to dissolution of evaporites, marine sulphate in groundwater comes from mixing with seawater in coastal aquifers and seawater-derived sulphate that accumulates in soils by evaporation (CLARK & FRITZ, 1997). Sulphur isotopes and geochemistry can be used to distinguish between these sources.

The analysis of sulphate isotopes ^{34}S and ^{18}O primarily conduce to the estimation of aerobe respectively anaerobe conditions of the aquifer due to sulphate reduction. Groundwater samples for sulphate isotope analysis were taken for wells SPFP03 and -14 to assess reducing conditions in the lakes underlying groundwater.

The sulphate reduction can be described with the assumption of a simple organic compound completely oxidized by CO_2 by following simplified equation:



The bacterial sulphate reduction is associated with a fractionation of sulphide and oxygen isotopes. Because of a preferred conversion of sulphate reductive bacteria

for the lighter isotope, the reaction product (H_2S or sedimentary sulphides) is depleted in the heavier sulphide isotope ^{34}S (CHAMBERS & TRUDINGER, 1979).

3.1.3 Constructing monitoring wells - multilevel piezometer

Within groundwater monitoring and the aspect of a sustainable groundwater protection, the construction of monitoring wells attach great importance. The construction of monitoring wells in the basin affords measuring of amended values of piezometric levels and taking groundwater samples.

The main interest is on the determination of flow gradients by multilevel piezometers. The constructed monitoring wells set up besides or close to already existing wells, so that every new well is related to another (see chapter 3.1.3.1).

When characterization and designation of the drilled soil is finished the monitoring well has to be installed in time. For constructing monitoring wells in boreholes with at least a diameter of 60 mm, a casing, existing of HDPE-filter pipe and blank casing, with a diameter of 50 mm was used (see Appendix II). With regards to aquifer thickness and fluctuating groundwater levels, the filter tube has to be set in the investigated aquifer considering the maximum water levels. For the remaining construction seamless tubes were used. The lower ending is closed by a cone cap, the top by an unlocked closure; in the observation area unauthorized access is foreclosed. If required, the space between casing and borehole were refilled with the excavation material.

3.1.3.1 Levelling

For the levelling of the erected bore sites the surveying instrument WILD N2 from the WILD HEERBRUGG Company was used. The basic principles of surveying are portrayed by GRUBER & JOECKEL (2005). To measure altitude differences between two remote points A and W, the instrument have to be positioned with the same distance between the two points. From the location of the instrument a look back to point A is taken and the value is to be read from the levelling slat. Then a look forward to point W is taken and the elevation on the slat is to be noted. The difference between look back and look forward is the elevation difference between point A and point W. For long ranges between two points A and N, the distance has to be sectioned (Fig. 3.12). The altitude difference is to be calculating after:

$$H_N - H_A = [R - V] = [R] - [V] \quad (19)$$

where

H_N = elevation of point E

H_A = elevation of point A

R = sum of look back

V = sum of look forward

As start and checkpoint for the levelling of the bore sites the northern coastal line of the lake with an altitude of 409 m for bore site SPFPFU20 is set. All bore sites located north of this point, levelled in relation to the elevation of SPFPFU20. Knowing the level of the bore sites is essential for correlation of borehole logs and their presentation in cross sections.

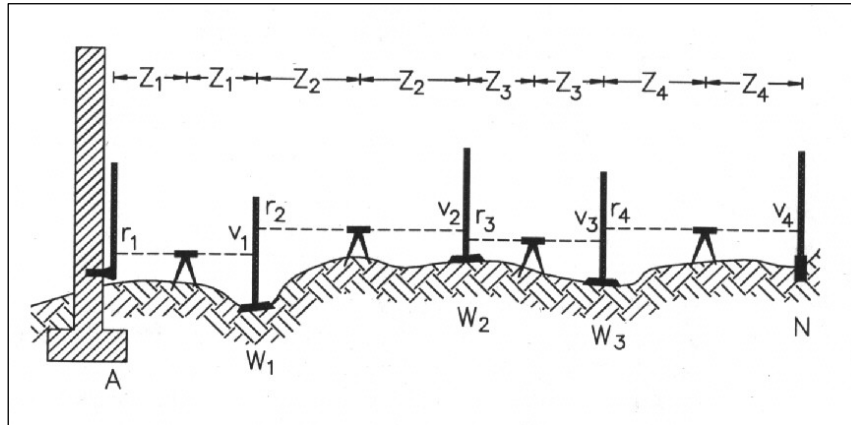


Figure 3.12: Schedule of levelling (GRUBER & JOECKEL, 2005).

The levelling is also applied for the determination of vertical and horizontal gradients of groundwater flows on the basis of multilevel piezometer. Therefore two piezometers are levelled to each other. Tab. A11 in Appendix shows levelling progression.

3.1.4 Hydraulics

3.1.4.1 Piezometer network

For the complement of the piezometer network 5 additional piezometers were built. To determine hydraulic gradients, piezometers are situated besides already existing monitoring wells and constitute a multilevel piezometer consisting of a well pair (Tab. 3.11).

Table 3.11: Well pairs.

Monitoring well	related piezometer
SPFP03	SPFPFU26
SPFP05	SPFPFU24
SPFP14	SPFPFU23
SPFP15	SPFPFU22
SPFP17	SPFPFU27

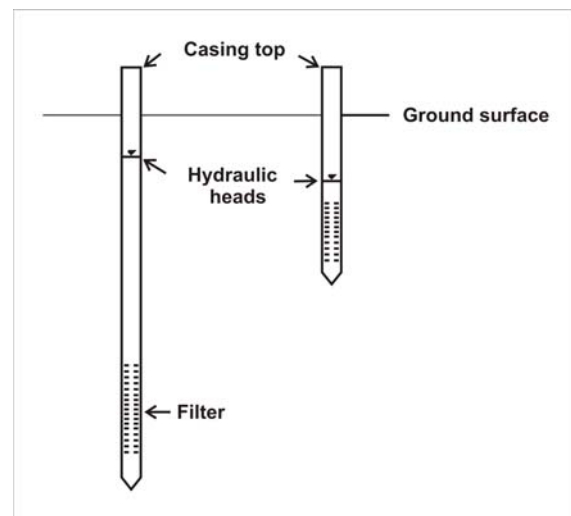


Figure 3.13: Scheme of multilevel piezometer.

The *hydraulic gradient* is a vector gradient between two or more hydraulic head measurements over the length of the flow path. A dimensionless horizontal hydraulic gradient can be calculated between two piezometers as:

$$i_h = \frac{dh}{dl} = \frac{h_2 - h_1}{\text{length}} \quad (20)$$

where

i_h is the horizontal hydraulic gradient (dimensionless)

dh is the difference between two hydraulic heads [m]

dl is the flow path length between the two piezometers [m]

3.1.4.2 Freshwater head and salt correction

The identification of the hydraulic pattern in the Fuente de Piedra Salt Lake and its vicinity is realized by the determination and interpretation of the hydraulic flow gradients. Therefore an evaluation of the piezometric heads is carried out in consideration of appearing density differences between the fresh/brine water bodies. The pressure head is dependent on the density of water, which is defined by temperature and chemical composition (salinity). Because of this dependency the fresh water head H_{fw} have to be calculated for piezometers as (LUSCZYNSKI, 1961):

$$H_{fw} = \psi \frac{\rho}{\rho_{fw}} + z \quad (21)$$

where

ψ is the water gauge pressure, in terms of the height above the piezometer bottom (m)

ρ_{fw} is the density of fresh water (kg/m³)

ρ is the density of the water (kg/m³)

z is the elevation of the piezometer bottom (m)

The density is determined after McCAIN (1991), who presents a general function for water density based on TDS, derived on the basis of published analyses of formation waters sampled by the oil industry in various sedimentary basins. The function is valid for brines under thermodynamic conditions of $P = 0.69\text{--}69$ MPa, $T \leq 127$ °C and $\text{TDS} \leq 450\,000$ mg/l. The density of saline water at 25 °C and 1 atm (Standard Temperature and Pressure, STP) is given by:

$$\rho_f = 62.368 + 0.438603S + 1.60074 \cdot 10^{-3}S^2 \quad (22)$$

where

S is TDS in wt% and ρ_f is water density at STP in lb per cubic ft ($1 \text{ lb/ft}^3 = 16.0184634 \text{ kg / m}^3$).

3.2 Results

3.2.1 Hydrogeochemistry

3.2.1.1 Major and minor ions

Hydrochemical analyses are checked by plotting electric conductivity (field observation) versus Chloride (laboratory data) because both values depend on each other (Fig. 3.14). So mistakes can be excluded. Samples must correlate and plot on a line. Except for sp13 all samples correlate, so analysis made with sp13 will be misinterpreted.

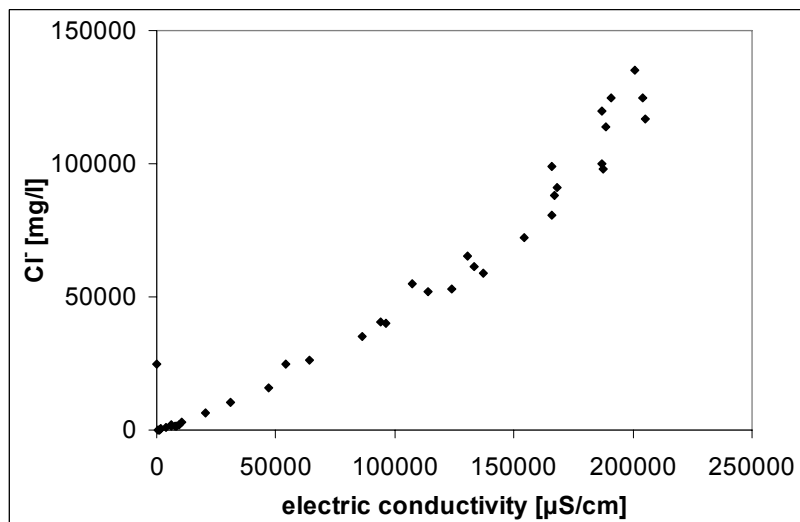


Figure 3.14: Test for sample mistakes by EC and Cl⁻.

Samples with an **Electroneutrality** $> \pm 5\%$, were excluded from further analysis. Exceptions were made for groundwater samples from piezometers built in autumn 2005 (5 samples of SP-FP-FU-22; -23, -24, -26, -27) between 5.66 and 7.55 % error) and SP-FP-06-050922 with 5.65 %

and SP-FP-23-051004 with 6.21 %. Reasons are the fact that the site ran dry during pumping and the interaction of water and suspended solids until separation by sedimentation. Electroneutrality values can be seen in Tab. 3.2. All samples analysed before autumn 2005 were measured without analysis of HCO_3^- . Therefore great errors occur. Electroneutrality values of 0 (Tab. 3.13) represent

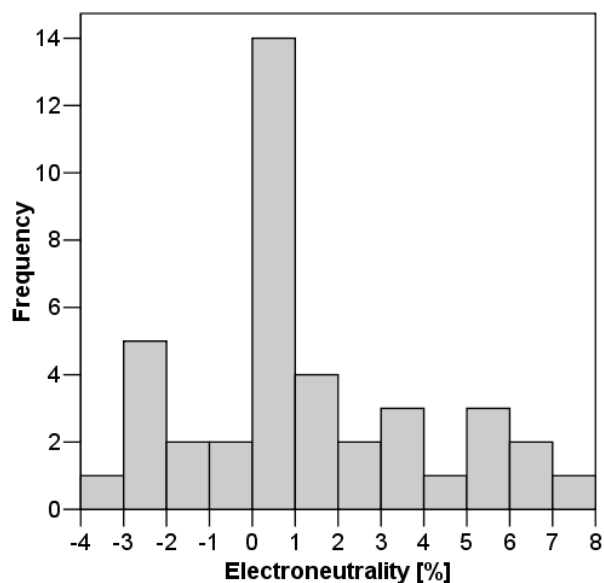


Figure 3.15: Electroneutrality [%] spread.

samples, where HCO_3^- is calculated by AquaChem 4.0 (WHI Software) using the Electroneutrality. For samples with calculated HCO_3^- values electroneutrality is $< 5\%$. Fig. 3.15 shows the Electroneutrality spread.

Major and minor ion data from laboratory analysis and field parameters are listed in Tab. 3.13 and Tab. 3.14.

An arrangement of **groups** of the sampling sites was made according to following criteria:

- location in the study area (basin – salt lake)
- ion relations according to Schoeller and Piper
- Type of water (surfacewater - groundwater).

Due to this 3 groups of groundwater sites and 2 single surface water sites are determined:

- Lake (including salt lake surface water sample)
- east/north shore
- basin (including south shore sites)
- artificial lake and
- Santillán creek (Tab. 3.12).

Table 3.12: Groups and the related samples and sampling sites.

sample Id.	site Id.	group	sample Id.	site Id.	group
sp14	SPFP09	basin	SP-FP-9	SPFP14	east/north shore
SP-FP-07-050922	SPFP07	basin	SP-FP-FU-26-050919	SPFPFU26	east/north shore
SP-FP-09-050921	SPFP09	basin	sp01	SPFP01	lake
SP-FP-10-051003	SPFP10	basin	sp03	SPFP03	lake
SP-FP-17	SPFP17	basin	sp06	SPFP05	lake
SP-FP-17-050920	SPFP17	basin	SP-FP-03-050918	SPFP03	lake
SP-FP-21-051003	SPFP21	basin	SP-FP-05-050917	SPFP05	lake
SP-FP-22-051003	SPFP22	basin	SP-FP-1	SPFP11	lake
SP-FP-23-051004	SPFP23	basin	SP-FP-4/(SP-03)	SPFP03	lake
SP-FP-FU-27-050920	SPFPFU27	basin	SP-FP-5/(SP-04)	SPFP03	lake
sp09	SPFP06	east/north shore	SP-FP-7	SPFP05	lake
sp13	SPFP08	east/north shore	SP-FP-8	SPFP05	lake
SP-FP-06-050922	SPFP06	east/north shore	SP-FP-FU-22-050915	SPFPFU22	lake
SP-FP-08-050918	SPFP08	east/north shore	SP-FP-FU-23-050916	SPFPFU23	lake
SP-FP-10	SPFP14	east/north shore	SP-FP-FU-24-050917	SPFPFU24	lake
SP-FP-11	SPFP15	east/north shore	sp02	SPFP02	Santillán creek
SP-FP-13	SPFP16	east/north shore	sp05	SPFP04	artificial lake
SP-FP-14	SPFP16	east/north shore	SP-FP-6	SPFP04	artificial lake
SP-FP-14-050916	SPFP14	east/north shore	SP-FP-3	SPFP13	surface
SP-FP-15-050918	SPFP15	east/north shore			

In **matrix scatter plot** (Fig. 3.16) major ions and total dissolved solids (TDS) relations are presented schematically. Chloride, Sodium and Magnesium show a linear correlation with TDS. Sodium and Magnesium correlate linear with Chloride, which indicates the presence of Halite and Mg-Chlorides. Chloride and Calcium show a dependency, maybe by leaching of CaCl_2 . Sulfate correlates with the alkalis and earth

Table 3.13: Results from hydrochemical analysis for major ions and belonging field parameters and Electroneutrality.

Sample ID	Station ID	Sampling date	pH	Eh [mV]	EC [µS/cm]	Temp. [°C]	O ₂ [mg/l]	Na ⁺ [mg/l]	K ⁺ [mg/l]	Ca ²⁺ [mg/l]	Mg ²⁺ [mg/l]	Cl ⁻ [mg/l]	HCO ₃ ⁻ [mg/l]	NO ₃ ⁻ [mg/l]	SO ₄ ²⁻ [mg/l]	TDS [mg/l]	E.N. [%]
sp01	SPFP01	04.02.2004			54200			13300	85	1300	1780	24800	559.51	1	4000	45826	0
sp02	SPFP02	04.02.2004			5900			725	8	320	200	1675	186.85	25	650	3790	0
sp03	SPFP03	04.02.2004			133200	13.0		33600	63	1720	4500	61400	195.20	2	6500	107987	-1.29
sp04	SPFP03	04.02.2004			200000	17.0		5400	130	1700	8000	125000	195.20	0	6500	146971	57.7
sp05	SPFP04	05.02.2004			64000	14.0		13200	60	900	2100	26400		3	3500	46163	1.5
sp06	SPFP05	04.02.2004			114200	16.0		27400	70	1000	3400	51800	216.55	4	3900	87793	0.74
sp07	SPFP05	04.02.2004			197200	17.0		4900	160	1620	8500	120000	216.55	0	7000	142434	55.93
sp08	SPFP06	04.02.2004			15600	18.0		2600	12	3400	460	5260	378.20	23	600	12734	-31.45
sp09	SPFP06	04.02.2004			168100	18.0		45800	105	1800	6000	91100	378.20	0	5500	150693	2.12
sp10	SPFP07	04.02.2004			7300	16.0		625	4	380	380	1460	366.00	0	550	3765	-13.87
sp11	SPFP07	04.02.2004			19500	17.0		2100	11	900	860	765	366.00	15	450	5468	-69.61
sp12	SPFP08	05.02.2004			1500	20.0		275	65	3	17	231		4	62	657	-31.76
sp13	SPFP08	06.02.2004				20.0		13500	20	760	1390	24900	392.00	1	1500	42463	0
sp14	SPFP09	04.02.2004			1650	20.0		100	4	244	18	324	122.00	16	290	1118	-2.04
sp15	SPFP09	04.02.2004			200000	19.0		3200	47	1500	950	8630	122.00	1	2500	16952	0.68
sp16	SPFP10	04.02.2004			990	18.0		160	10	4	4	224	311.10	1	55	769	23.78
sp17	SPFP10	04.02.2004			1140	17.0		127	2	62	27	246	311.10	17	70	862	11.47
SP-FP-03-050918	SPFP03	18.09.2005	6.28	49	204000	18.1	0	68500	120	1950	8200	125000	192.00	8	5700	209939	-1.42
SP-FP-04-051004	SPFP04	04.10.2005	6.37		116900	25.3		14400	1600	350	71000	22500		8	58000	169569	-55.57
SP-FP-05-050917	SPFP05	17.09.2005	6.46	145	188500	19.2	3.79	62500	135	1750	8400	114000	214.00		6500	193732	-2.11
SP-FP-06-050922	SPFP06	22.09.2005	6.54		107400	18.3	0	25500	55	1150	3400	55000	375.00	18	3000	88587	5.65
SP-FP-07-050922	SPFP07	22.09.2005	6.82	136	6170	16.8	0.9	460	2	430	300	1850	343.00	45	520	3956	2.22
SP-FP-08-050918	SPFP08	18.09.2005	6.7	-173	130300	19.4	1.7	32500	75	1950	3500	65500	146.92		4020	107808	3.58
SP-FP-09-050921	SPFP09	21.09.2005	6.88	-22	10520	24.3	0.1	835	18	1200	250	3000	119.00		1450	107780	-0.24
SP-FP-1	SPFP11	22.02.2005			187400	10.1		51900	224	1440	7500	98200		8	9700	169973	0.33
SP-FP-10	SPFP14	22.02.2005			187000	16.2		50300	170	1140	8400	100000		1	8250	168279	0.87
SP-FP-10-051003	SPFP10	03.10.2005	7.12	-1	1312	19.2	2.6	95	3	123	29	230	308.00	38	58	885	1.92
SP-FP-11	SPFP15	22.02.2005			31200	14.9		5750	19	300	660	10480	54.88	3	1120	18387	0
SP-FP-12	SPFP15	22.02.2005			133200	17.6		38700	124	1070	4200	57800		0.9	4750	106653	-9.34
SP-FP-13	SPFP16	22.02.2005			166000	15.6		39100	64	3900	5100	80800		2	3420	132387	0.72
SP-FP-14	SPFP16	22.02.2005			166000	17.0		46900	64	4800	6200	99100		1	3440	160507	1.34
SP-FP-14-050916	SPFP14	16.09.2005	6.52	84	166900	21.6	8.11	44000	145	1100	7100	88000	302.00		7000	147814	1.49
SP-FP-15	SPFP06	22.02.2005			26700	17.2		16700	70	670	2400	41200		7	3100	64147	12.24
SP-FP-15-050918	SPFP15	18.09.2005	6.87	96	86100	20.9	0.2	19100	71	800	2400	35000	286.00	7	3100	60838	-0.62

Table 3. 13: Results from hydrochemical analysis for major ions and belonging field parameters and Electroneutrality.

Sample ID	Station ID	Sampling date	pH	Eh [mV]	EC [μ S/cm]	Temp. [°C]	O ₂ [mg/l]	Na ⁺ [mg/l]	K ⁺ [mg/l]	Ca ²⁺ [mg/l]	Mg ²⁺ [mg/l]	Cl ⁻ [mg/l]	HCO ₃ ⁻ [mg/l]	NO ₃ ⁻ [mg/l]	SO ₄ ²⁻ [mg/l]	TDS [mg/l]	E.N. [%]
SP-FP-17	SPFP17	22.02.2005			8120	14.0		958	9	680	230	1650	165.90	55	2150	5898	0
SP-FP-17-050920	SPFP17	20.09.2005	7.33		7700	21.6		975	10	700	260	1650	387.00	52	2500	6537	3.24
SP-FP-18	SPFP17	22.02.2005			19920	14.9		3130	17	730	530	7070		27	3300	14804	10.7
SP-FP-2	SPFP12	22.02.2005			226000	13.9		271000	483	640	14500	174600		0	11950	473175	-43.14
SP-FP-21-051003	SPFP21	03.10.2005	7.26	167	654	20.2	6.9	19.5	1	75	31	40	276.00	25	55	523	-0.38
SP-FP-22-051003	SPFP22	03.10.2005	7.11	171	1815	19.2	9.6	130	1	220	17	290	177.00	200	275	1312	3.52
SP-FP-23-051004	SPFP23	04.10.2005	7.35	191	3690	25.0		430	1	210	90	1130	280.00	180	132	2457	6.21
SP-FP-3	SPFP13	22.02.2005			20400	10.4		4130	156	24	300	6400	1071.54	5	546	12632	0
SP-FP-4/(SP-03)	SPFP03	22.02.2005			154300	14.3		41300	215	1840	4800	72300			6600	127059	-2.51
SP-FP-5/(SP-04)	SPFP03	22.02.2005			205000	17.4		64400	137	1640	8800	116800			6850	198666	-2.48
SP-FP-6	SPFP04	22.02.2005			96300	11.3		20300	870	1080	3100	40100			5150	70600	0.98
SP-FP-7	SPFP05	22.02.2005			46800	14.8		8820	324	390	930	15960	268.50	1	1600	28294	0
SP-FP-8	SPFP05	22.02.2005			201000	16.9		64200	167	2090	8500	135300			7000	217288	4.77
SP-FP-9	SPFP14	22.02.2005			137000	15.9		32100	101	880	5200	59000		25	5900	103216	-2.28
SP-FP-FU-22-050915	SPFPFU22	15.09.2005			190800			58000	250	1220	9200	125000	129.00		10500	204500	5.66
SP-FP-FU-23-050916	SPFPFU23	16.09.2005	7.1		186900			56000	220	1500	7600	120000	296.00	50	10000	195839	6.81
SP-FP-FU-24-050917	SPFPFU24	17.09.2005	7.05		94200			17600	77	1350	3100	40700	271.00		5500	68679	7.55
SP-FP-FU-26-050919	SPFPFU26	19.09.2005	6.9		123800			29000	695	2050	4500	53000	259.00		6000	95617	-3.74
SP-FP-FU-27-050920	SPFPFU27	20.09.2005	7.3		9620			1280	13	640	300	2000	427.00	30	3000	7694	5.72

Table 3.14: Results from hydrochemical analysis for minor ions.

Sample ID	Station ID	Sampling Date	Fe [mg/l]	Mn ²⁺ [mg/l]	NH ₄ ⁺ [mg/l]	Br ⁻ [mg/l]	Sample ID	Station ID	Sampling Date	Fe [mg/l]	Mn ²⁺ [mg/l]	NH ₄ ⁺ [mg/l]	Br ⁻ [mg/l]
sp01	SPFP01	04.02.2004	0.4	0.05			SP-FP-17	SPFP17	22.02.2005		0.02		
sp02	SPFP02	04.02.2004	0.2	0.10			SP-FP-17-050920	SPFP17	20.09.2005		0.15	0.5	2
sp03	SPFP03	04.02.2004	1.3	5.20			SP-FP-18	SPFP17	22.02.2005	0.1	0.02		
sp04	SPFP03	04.02.2004	2.4	43.00			SP-FP-2	SPFP12	22.02.2005	1.7	0.33		
sp05	SPFP04	05.02.2004					SP-FP-21-051003	SPFP21	03.10.2005		0.05	0.1	
sp06	SPFP05	04.02.2004	1.0	1.20			SP-FP-22-051003	SPFP22	03.10.2005	1.3		0.3	1
sp07	SPFP05	04.02.2004	2.0	35.00			SP-FP-23-051004	SPFP23	04.10.2005	0.3	0.10	1.0	2
sp08	SPFP06	04.02.2004	0.2	0.16			SP-FP-3	SPFP13	22.02.2005	0.1	0.03		
sp09	SPFP06	04.02.2004	1.9	8.00			SP-FP-4(SP-03)	SPFP03	22.02.2005	0.7	3.60		
sp10	SPFP07	04.02.2004	0.0	0.10			SP-FP-5(SP-04)	SPFP03	22.02.2005	1.3	38.00		
sp11	SPFP07	04.02.2004	0.2	0.75			SP-FP-6	SPFP04	22.02.2005	0.3	0.14		
sp12	SPFP08	05.02.2004					SP-FP-7	SPFP05	22.02.2005	0.1	0.03		
sp13	SPFP08	06.02.2004					SP-FP-8	SPFP05	22.02.2005	1.2	30.00		
sp14	SPFP09	04.02.2004					SP-FP-9	SPFP14	22.02.2005	0.7	9.60		
sp15	SPFP09	04.02.2004	0.3	1.90			SP-FP-FU-22-050915	SPFPFU22	15.09.2005		0.50		200
sp16	SPFP10	04.02.2004	0.0	0.00			SP-FP-FU-23-050916	SPFPFU23	16.09.2005	1.0	1.80		170
sp17	SPFP10	04.02.2004	0.1	0.00			SP-FP-FU-24-050917	SPFPFU24	17.09.2005	0.3	0.60	0.0	80
SP-FP-03-050918	SPFP03	18.09.2005	1.3	38.00		230	SP-FP-FU-26-050919	SPFPFU26	19.09.2005	0.5	2.00		110
SP-FP-04-051004	SPFP04	04.10.2005	0.4	0.25		1700	SP-FP-FU-27-050920	SPFPFU27	20.09.2005		0.10	0.5	3
SP-FP-05-050917	SPFP05	17.09.2005	1.4	32.00		200							
SP-FP-06-050922	SPFP06	22.09.2005	0.4	3.00	0.5	85							
SP-FP-07-050922	SPFP07	22.09.2005	0.0	0.10	1.0	5							
SP-FP-08-050918	SPFP08	18.09.2005	9.0	1.70	0.5	105							
SP-FP-09-050921	SPFP09	21.09.2005	1.6										
SP-FP-1	SPFP11	22.02.2005	1.0	0.25									
SP-FP-10	SPFP14	22.02.2005	1.4	16.40									
SP-FP-10-051003	SPFP10	03.10.2005			0.2	1							
SP-FP-11	SPFP15	22.02.2005	0.1	0.03									
SP-FP-12	SPFP15	22.02.2005	0.6	7.10									
SP-FP-13	SPFP16	22.02.2005	1.2	0.24									
SP-FP-14	SPFP16	22.02.2005	1.1	0.30									
SP-FP-14-050916	SPFP14	16.09.2005	1.3	16.00		150							
SP-FP-15	SPFP06	22.02.2005	0.1	0.06									
SP-FP-15-050918	SPFP15	18.09.2005	0.3	14.00		60							
SP-FP-16	SPFP06	22.02.2005	0.9	6.30									

alkalis, except for Potassium the samples spread around correlation lines. The presence and ablation of Na-; Mg- and K-Sulfates could explain the dependency. Solute Gypsum is proved in the most samples by correlation of Calcium and Sulphate. Hydrogencarbonate indicates no dependency with any parameter. Chloride and Sulfate correlate linear but spread around the correlation line. Chloride and Potassium correlate at low Potassium concentrations. Sodium and Magnesium mark out a linear correlation in all samples.

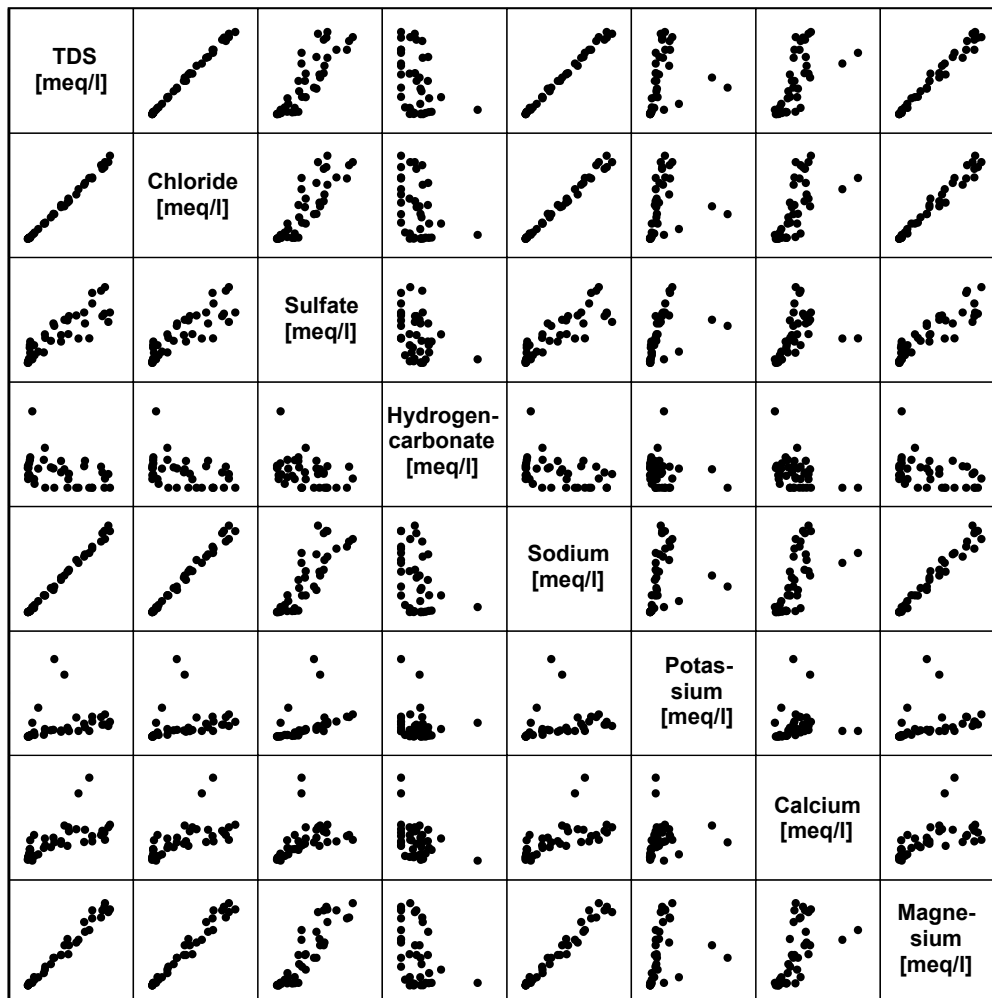


Figure 3.16: Matrix scatter plot of major ions and TDS in equivalent concentrations.

In **Piper diagram** (Fig. 3.17a) basin group samples plot in cation diagram and in square diagram well-defined from east/north shore and lake group samples. Sulphate and Chloride equivalent concentrations are at 4 samples similar to east/north shore and lake samples. Different mixing lines between basin and lake samples can be supposed. End members are SP-FP-03-050918, SP-FP-21-051003, sp14 and SP-FP-09-050921.

Schoeller Plots show the variation of major ion content among the groups (Fig. 3.17b). Samples of lake and east/north shore groups tend to show the same ion ra-

tios, whereas lake group samples are predominantly higher concentrated. This indicates mixing, dilution or evaporation of waters of these groups. Basin group samples vary strongly among each other in ion ratio relations and show significant differences in course compared to the other groups. Samples from the artificial lake correspond with samples from the lake group.

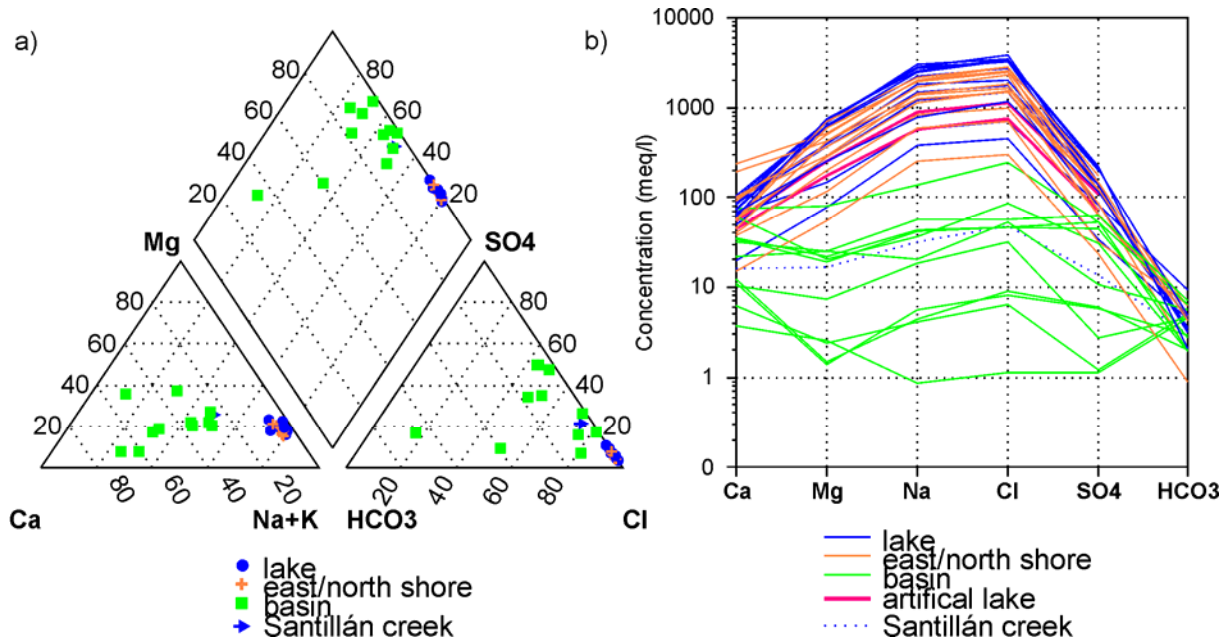


Figure 3.17: a) Schoeller Plot b) Piper Plot of samples from 2004/2005 sampling campaigns with EN < 8%.

By displaying the water types combined with sampling depth and TDS (Fig. 3.18) dependencies can be identified. Lake and surface near, at the east shore and in the northern part, Na-Cl and Na-Mg-Cl type water dominate. In low depths between 3 and 5 m Na-Mg-Cl type water dominates. The enrichment of Mg^{2+} leads possible from precipitation of Calcite and Gypsum, which removes Ca^{2+} and SO_4^{2-} and enriches relatively Mg^{2+} , or by evaporation from soil. Additionally dilution of Mg^{2+} from pore water, respectively dolomite, occurs. At the west shore where Ca^{2+} is enriched in lower depths mixing from brine with over layering low mineralized water through pumping and therefore beginning cation exchange processes can be the origin of Na-Ca-Cl type water.

Samples show at the south shore compared with the remaining sampling sites around the lake low mineralized. The type water differs significantly from the other with Na-Ca-Mg- SO_4 -Cl.

Main-water types in the eastern part of the basin are Ca-Cl. Ca-Cl type waters are significant for cation exchange processes and therefore for salinisation of the aquifer. The additional presence of Na^+ and SO_4^{2-} indicates the continuous exchange proc-

esses in this area. SPFP21 marks the only freshwater sample (523 mg/l TDS) and is thus Ca-Mg-HCO₃ type water.

For a better visualization of **regional distribution** of hydrochemical data, maps with **Stiff diagrams** were created. For varying co-domains two maps were made. Water samples with comparatively low concentrations are displayed in Fig. 3.19. Water samples with the lowest TDS content, respectively electric conductivity, show the

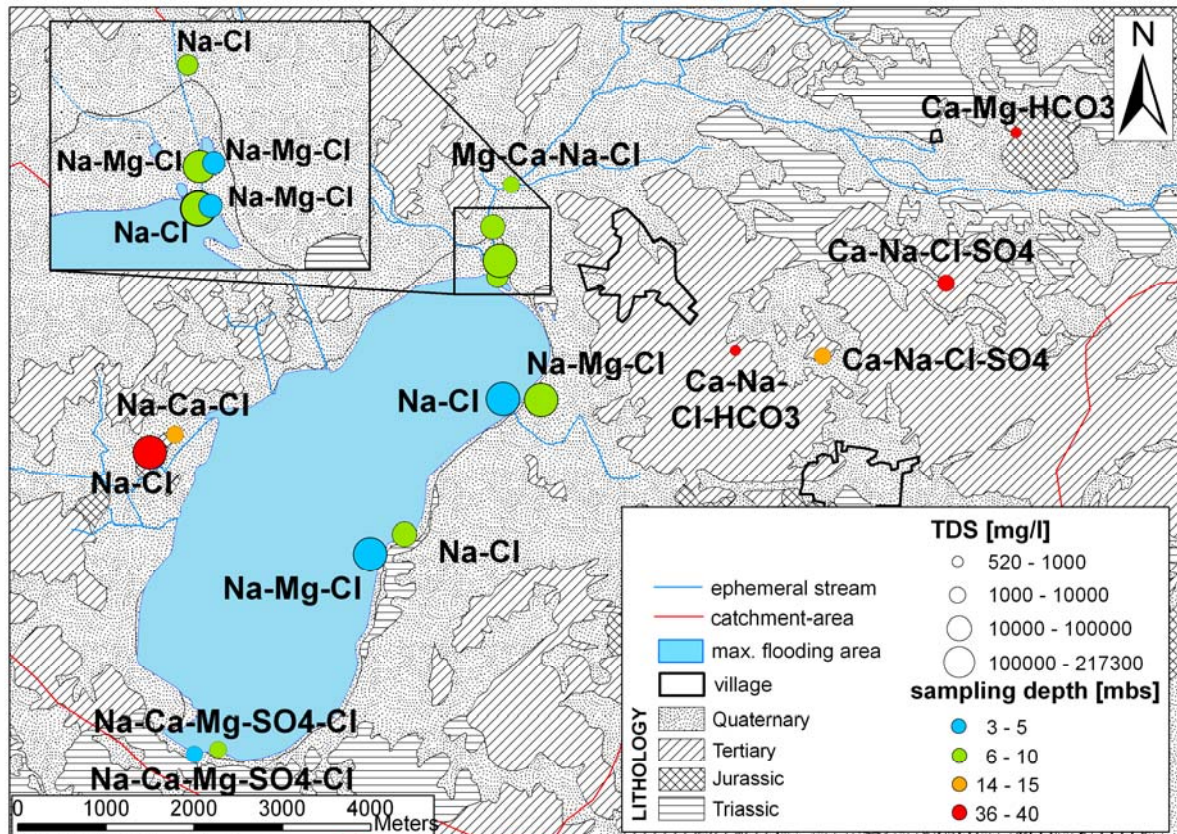


Figure 3.18: Distribution of water types of autumn 2005 samples (major ion > 10 equiv.%). Combined presentation with TDS [mg/l] and sampling depth [m below surface].

smallest amount of soluted ions as expected. Values reach up to 85 meq/l. These water samples are of Ca-HCO₃ and Ca-Cl water type. The water sample of SPFP07 has nearly the same amount of Mg²⁺, Ca²⁺ and Na⁺ which corresponds to the amount of Cl⁻ and SO₄²⁻. Multilevel piezometers show similar forms (polygons) and therefore similar ion ratio relations as shown before in Schoeller plots (Fig. 3.21 – 3.28).

Comparatively high mineralized water samples are displayed in Fig. 3.20. In the northern area, inside the salt lake and at the west and south shore mineralization of groundwater reaches values up to 3525 meq/l. Na⁺ and Cl⁻ are the dominating ions, the main water type is Na-Cl.

By these Stiff plots it can be seen easily that the type of salinisation is chloridic. Sulfatic salinisation only becomes important at less mineralized samples in comparison

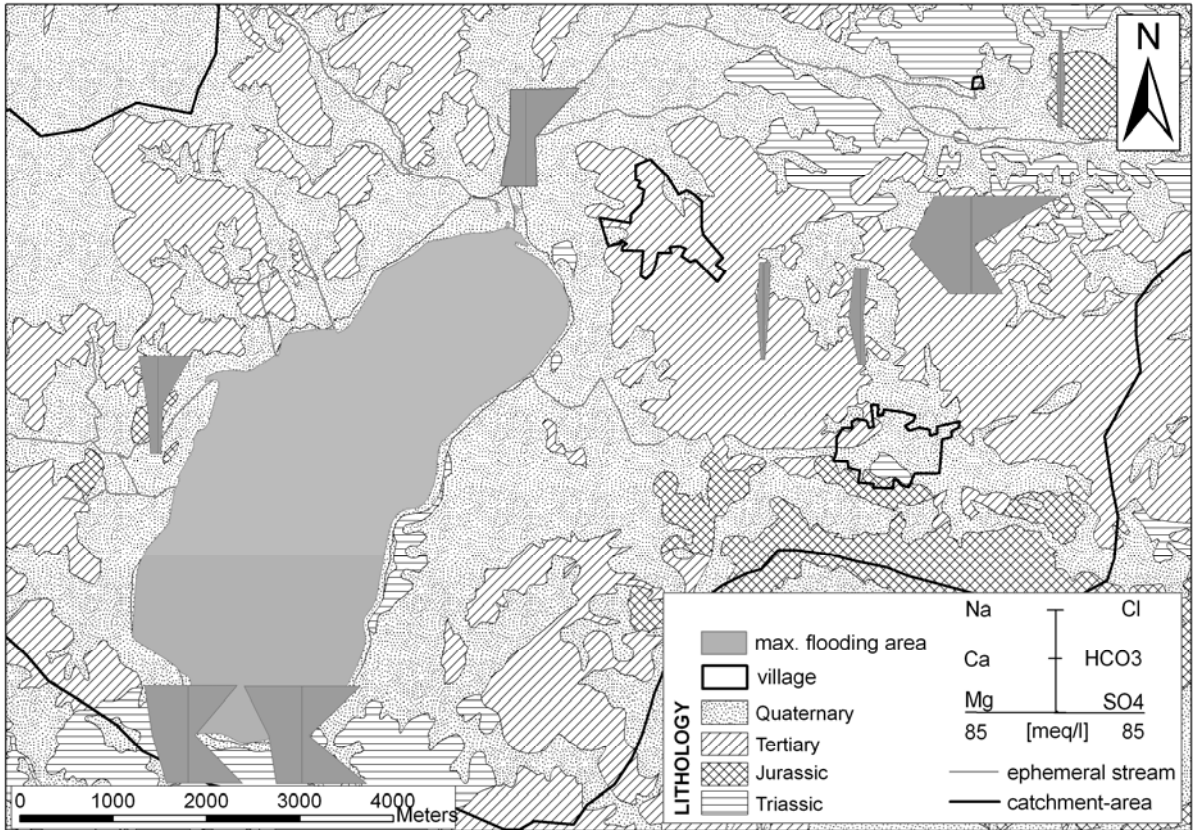


Figure 3.19: Stiff diagrams displayed of autumn 2005 samples on the map. Concentrations till 85 meq/l.

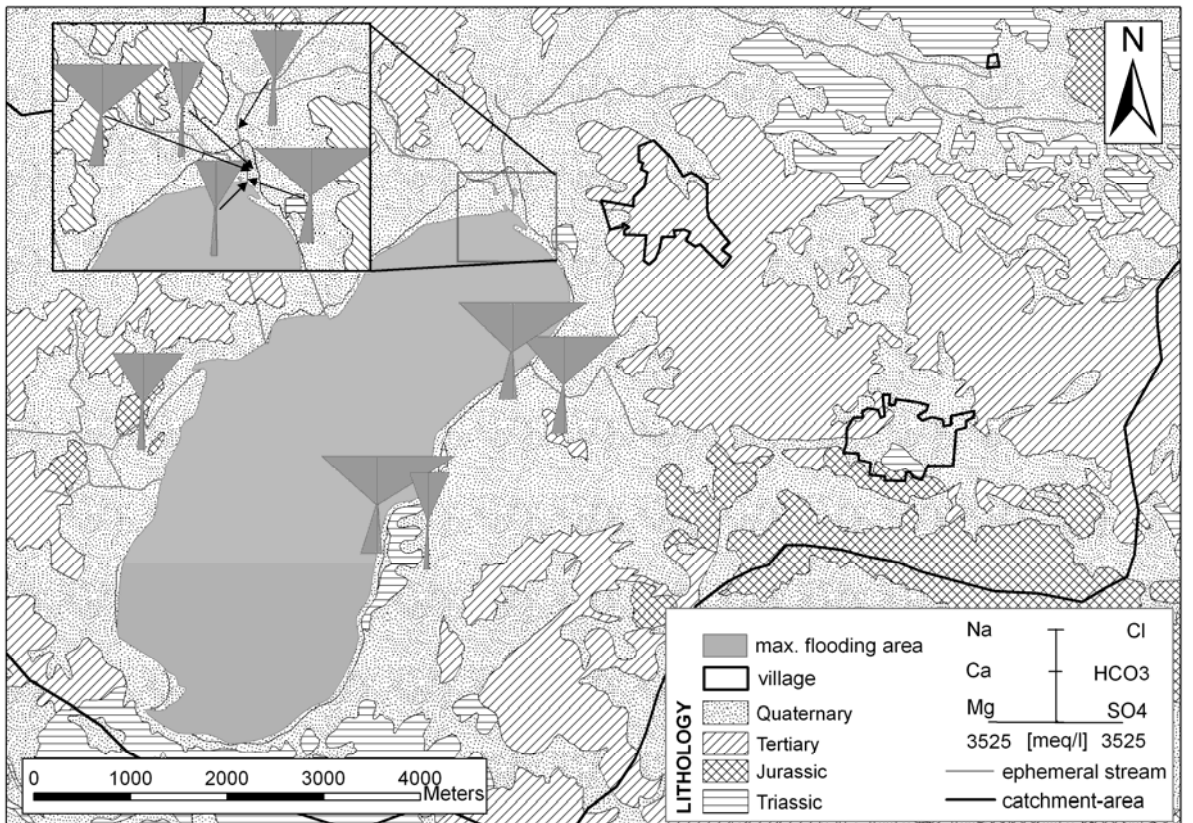


Figure 3.20: Stiff diagrams of autumn 2005 samples displayed on the map. Concentrations till 3525 meq/l.

to chloridic salinisation. Main leaching of salts is assumed at SPFP09 due to highest mineralizations in basin group and deviating composition. In the following Piper and Schoeller plots (Fig. 3.21 – 3.28) groundwater samples from the different sampling campaigns were used to visualize the concentration spread over depth and to characterize variations in concentration over time. In case of multilevel piezometers, samples of the shallow wells are added. Some samples without HCO_3^- equivalent concentration were excluded from presentation because implausible results were calculated. For comparison of samples in these plots, the HCO_3^- content can be neglected due to comparatively low concentrations.

Comparison of groundwater samples from SPFP03 show that Mg^{2+} , Na^+ and Cl^- contents are higher concentrated in autumn 2005 sample and in greater depth; the other major ions occur in the same concentrations (Fig. 3.21). Sampling depth declaration for winter 2003/2004 sample is missing but it seems to be 3 m due to congruence with SPFPFU24.

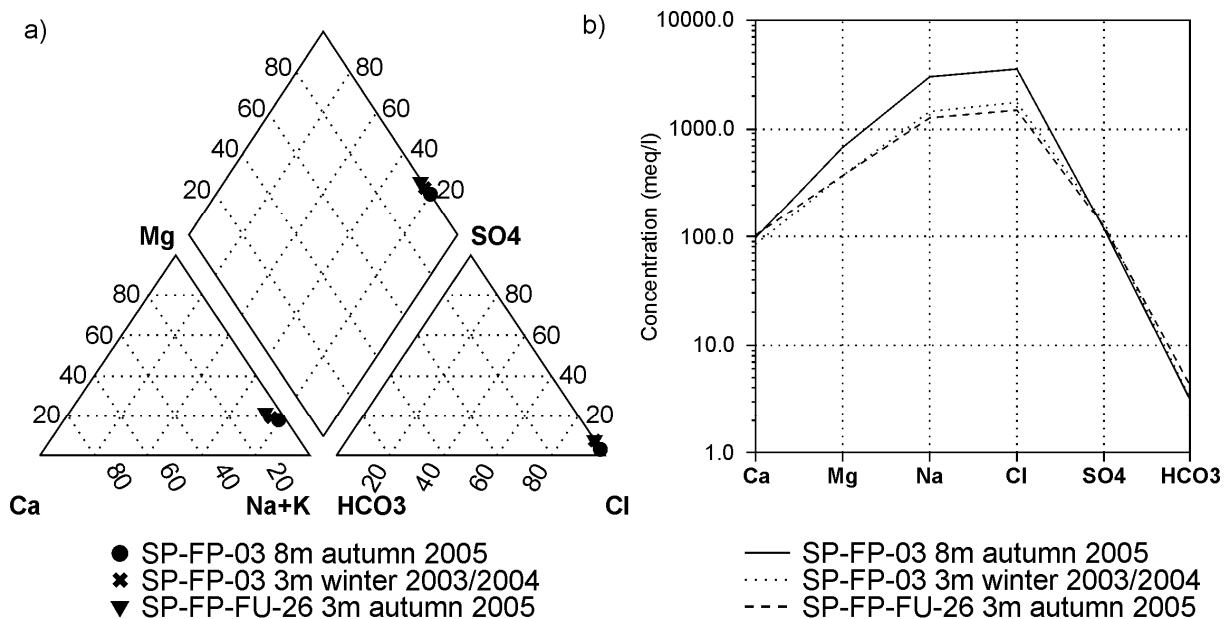


Figure 3.21: a) Piper Plot b) Schoeller Plot of groundwater from SPFP03 and SPFPFU26.

Groundwater of SPFP05 indicates same ratios of major ions at all samples (Fig. 3.22a/b). SPFPFU24 shows the same course as winter 2003/2004 except for Na^+ . Ion concentrations increase with depth. Both samples from 3 m show different concentrations maybe caused by watertable fluctuation, which is 0.84 m in winter 2005 (for winter 2004 no data exist). The movement of the salt/freshwater interface is distinctly associated with watertable fluctuations. Salinity increases with depth; Schoeller Plot verifies the salinity stratification recorded by conductivity logs (Fig. 3.40; Fig. 3.22b).

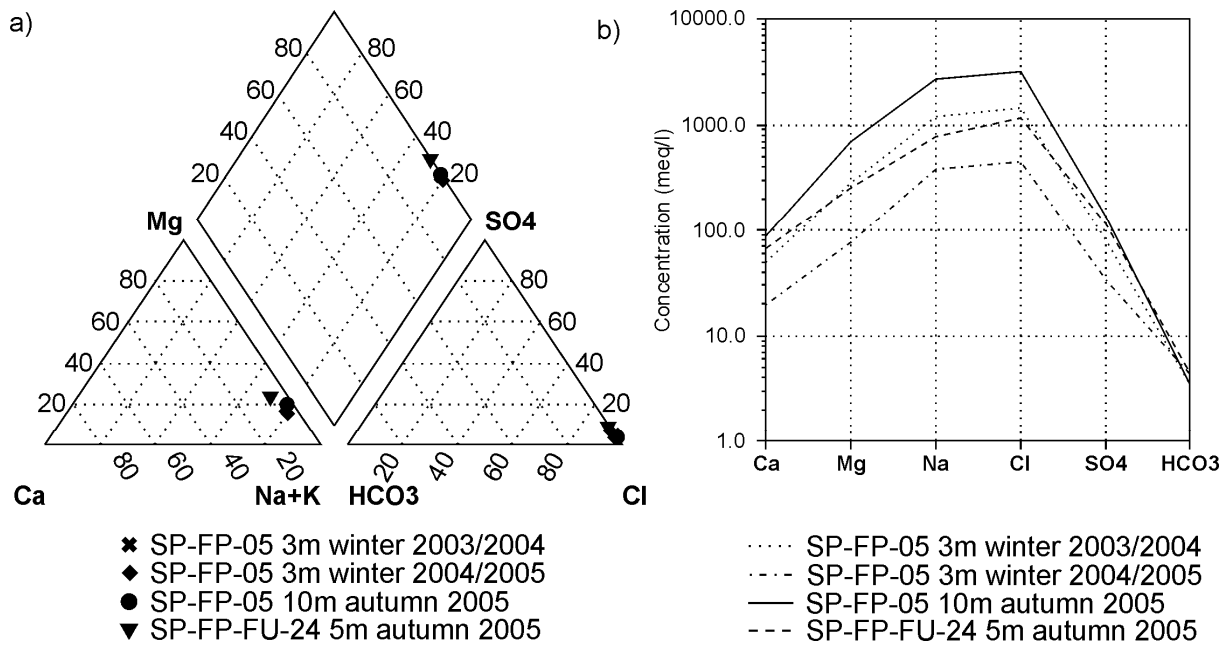


Figure 3.22: a) Piper Plot b) Schoeller Plot of groundwater from SPFP05 and SPFPFU24.

Samples from winter 2003/2004 and autumn 2005 of SPFP06 have the same ion ratios (Fig. 3.23a/b). With increasing depth the concentrations of the certain ions increase proportionally. Like shown in Fig. 3.10a, samples have the same equivalent composition, which leads to the conclusion that dilution or mixing is active. Regarding the time dependence conclusions are not possible due to missing suitable samples from same depth.

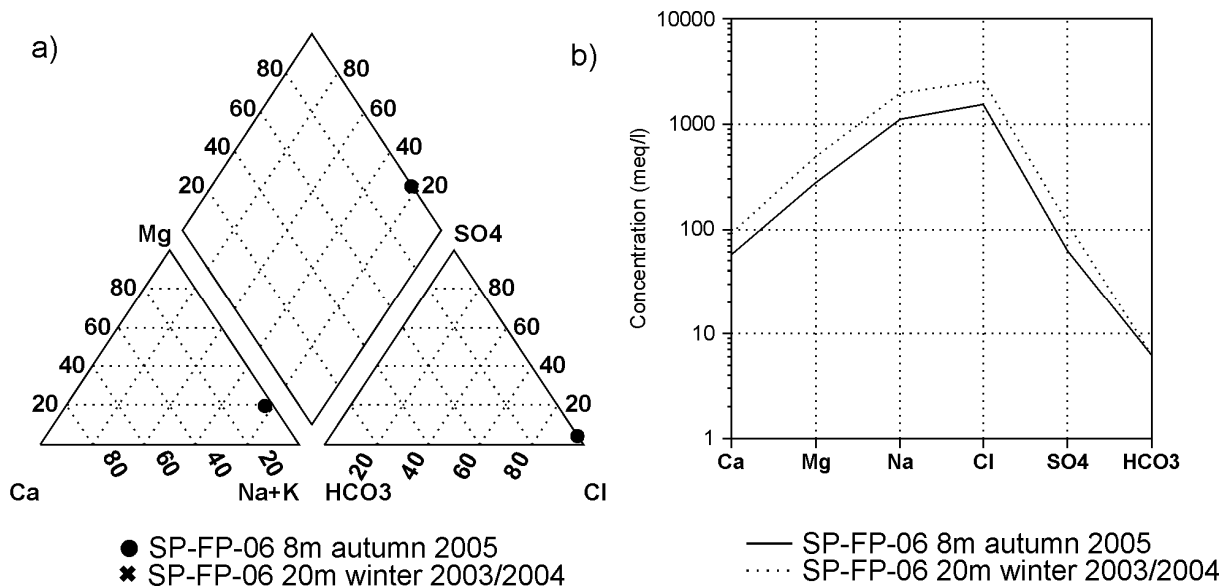


Figure 3.23: a) Piper Plot b) Schoeller Plot of groundwater from SPFP06.

Groundwater from 60 and 34 m depth in SPFP08 show equivalent compositions (Fig. 3.24a/b). The higher concentrated sample is situated in lower depth compared to the lower mineralized sample. Waterlevel below casing top was 27.2 m in winter 2003/2004 and 28.4 m in autumn 2005. A movement of the salinity stratification can be observed.

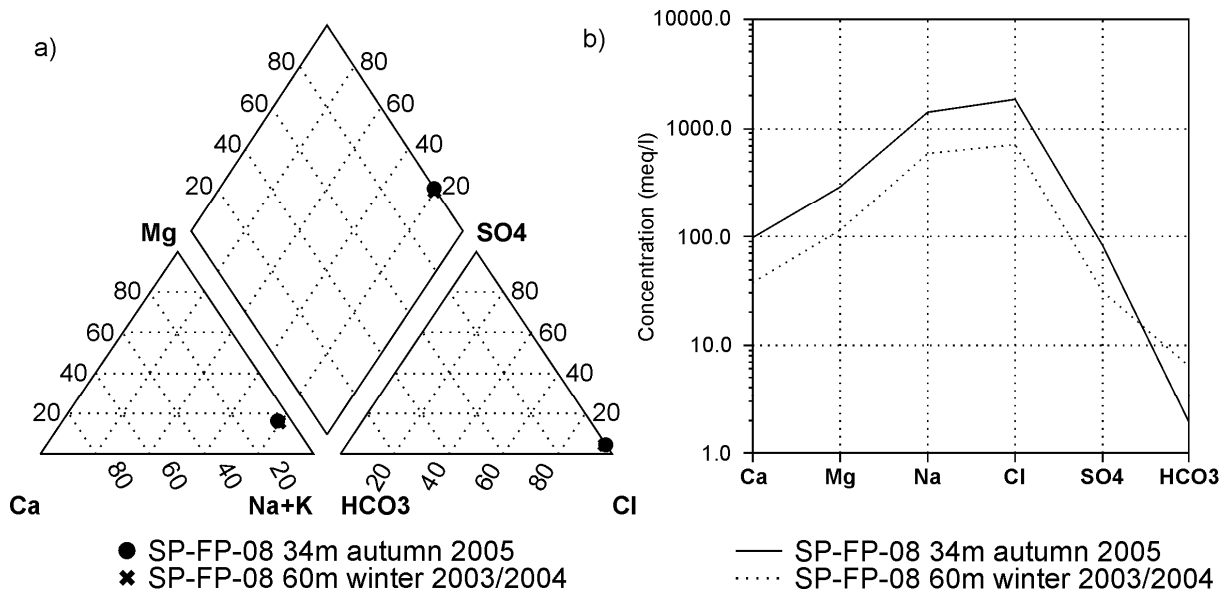


Figure 3.24: a) Piper Plot b) Schoeller Plot of groundwater from SPFP08.

Samples from SPFP09 show a parallel course in Schoeller Plot (Fig. 3.25b) except for SO_4^{2-} concentration. For winter 2003/2004 sample HCO_3 was calculated. A stratification of higher and lower mineralized water of same origin can be identified.

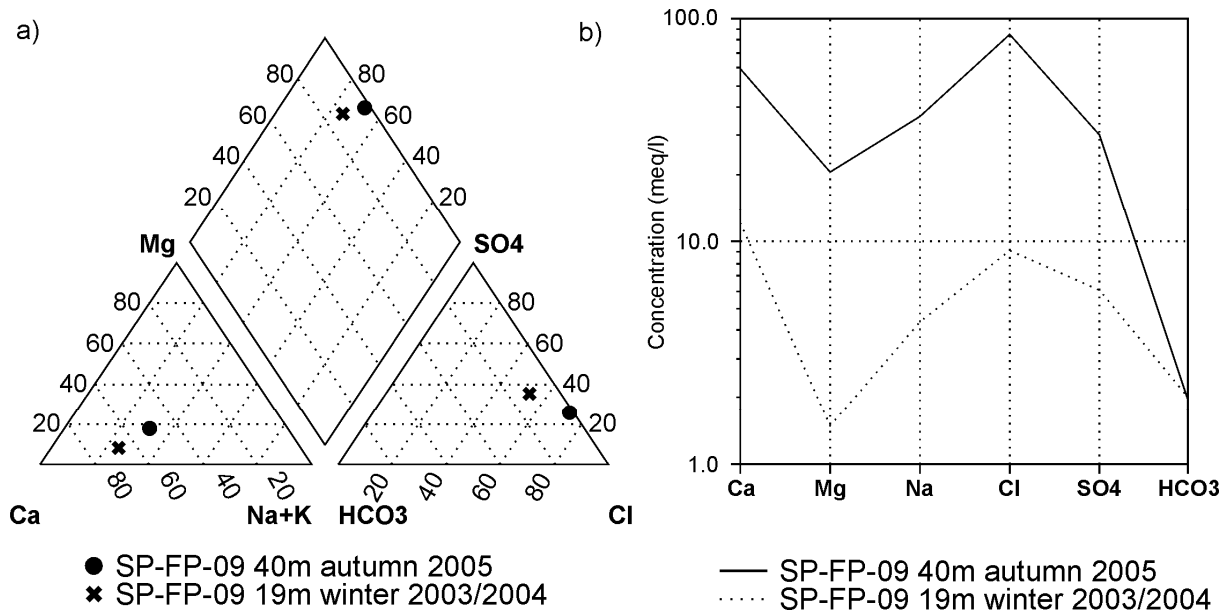


Figure 3.25: a) Piper Plot b) Schoeller Plot of groundwater from SP-FP-09.

Groundwater samples at SPFP14 and SPFPFU23 have nearly the same equivalent composition except for Na^+ and Cl^- (Fig. 3.26a/b). Sampling depth is 5 m at SPFP14 as well as at SPFPFU23. Depth dependencies can not be observed.

Like seen in Fig. 3.27a groundwater samples from SPFP15 have the same equivalent composition in different depths in winter 2004/2005 and autumn 2005 samples, but differing concentrations. The increase of soluted compounds with depth is also shown in Fig. 3.41. The shallow piezometer SPFPFU22 is higher mineralized due to

location in the salt lake. Therefore a comparison with shoreline samples is not veritable.

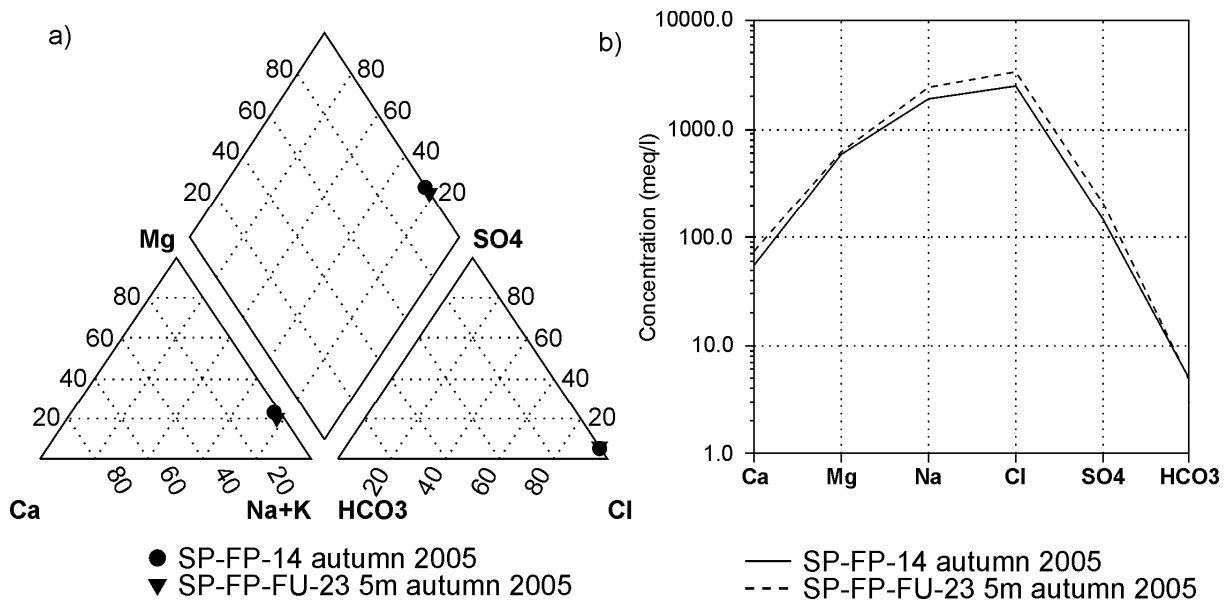


Figure 3.26: a) Piper Plot b) Schoeller Plot of groundwater from SPFP14 and SPFPFU23.

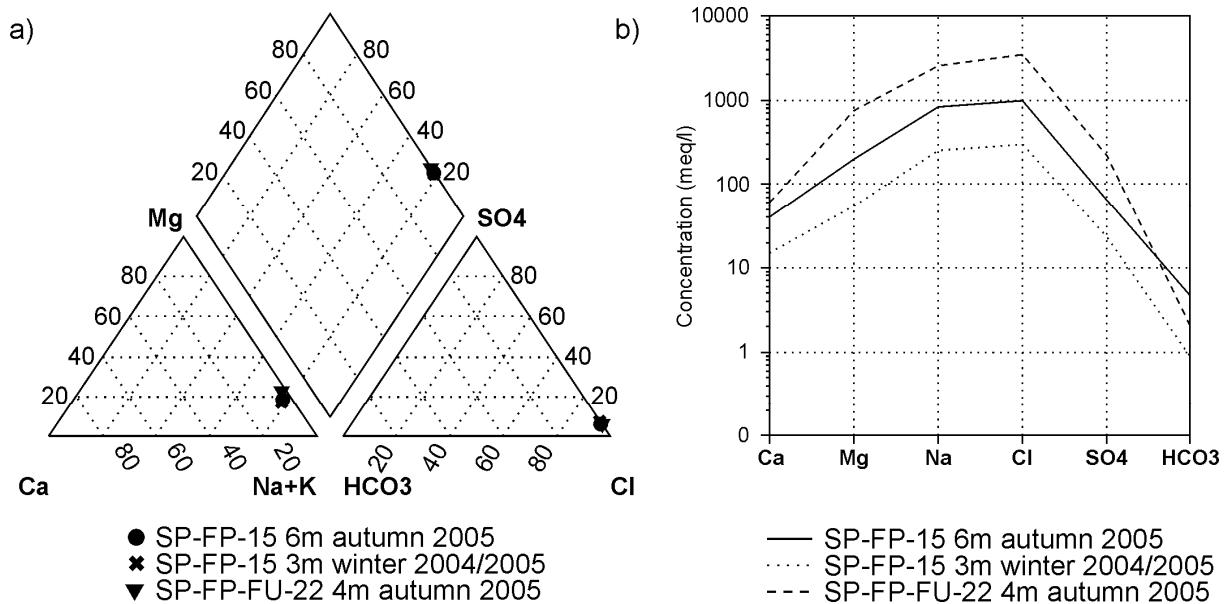


Figure 3.27: a) Piper Plot b) Schoeller Plot of groundwater from SPFP15 and SPFPFU22.

Groundwater samples from SPFP17 show the same course in Schoeller Plot (Fig. 3.28b), except for SO₄²⁻ concentration. Samples were taken in different depths. Due to different sampling methods a deviation at this sampling site is possible, because of the fact that the well ran out of water while pumping at SPFP17 in autumn 2005. Note that the HCO₃⁻ value was calculated for winter 2004/2005 sample, therefore the deviation is not significant. SPFPFU27 has a slightly higher mineralization.

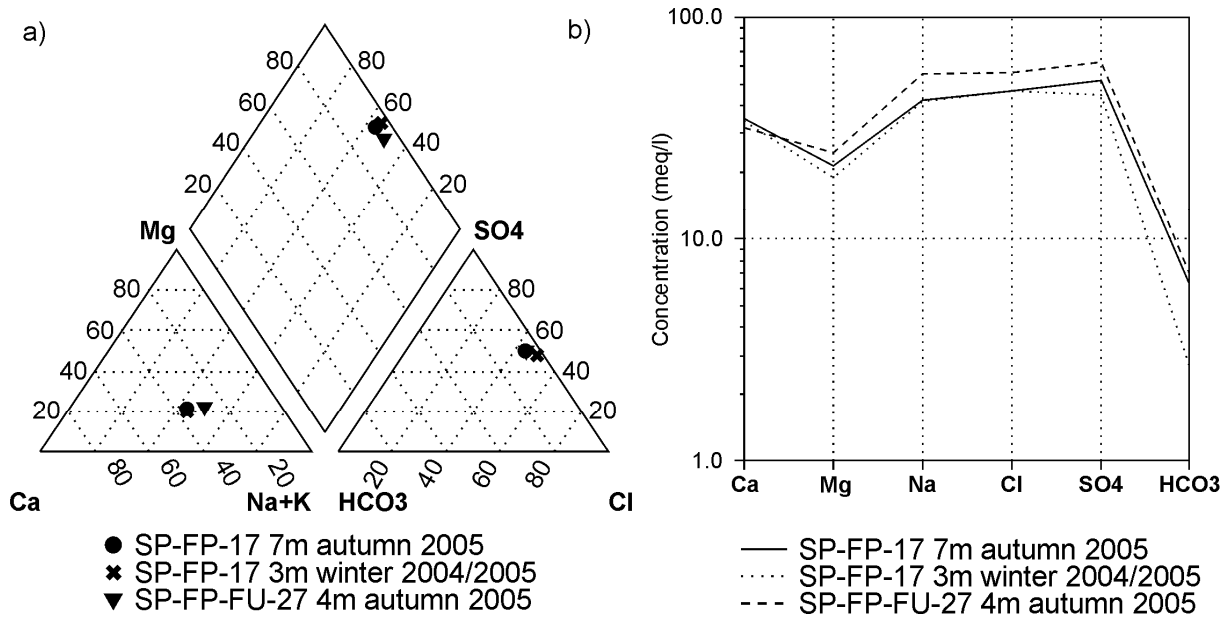


Figure 3.28: a) Piper Plot b) Schoeller Plot of groundwater from SPFP17 and SPFPFU27.

The distribution of **Saturation indices** is shown in Fig. 3.29, 3.30 and 3.31. Tab. 3.15 lists the calculated values.

Halite is under saturated in groundwater within the whole study area. Magnesite ($MgCO_3$) precipitates at samples from the lake group and the shore group.

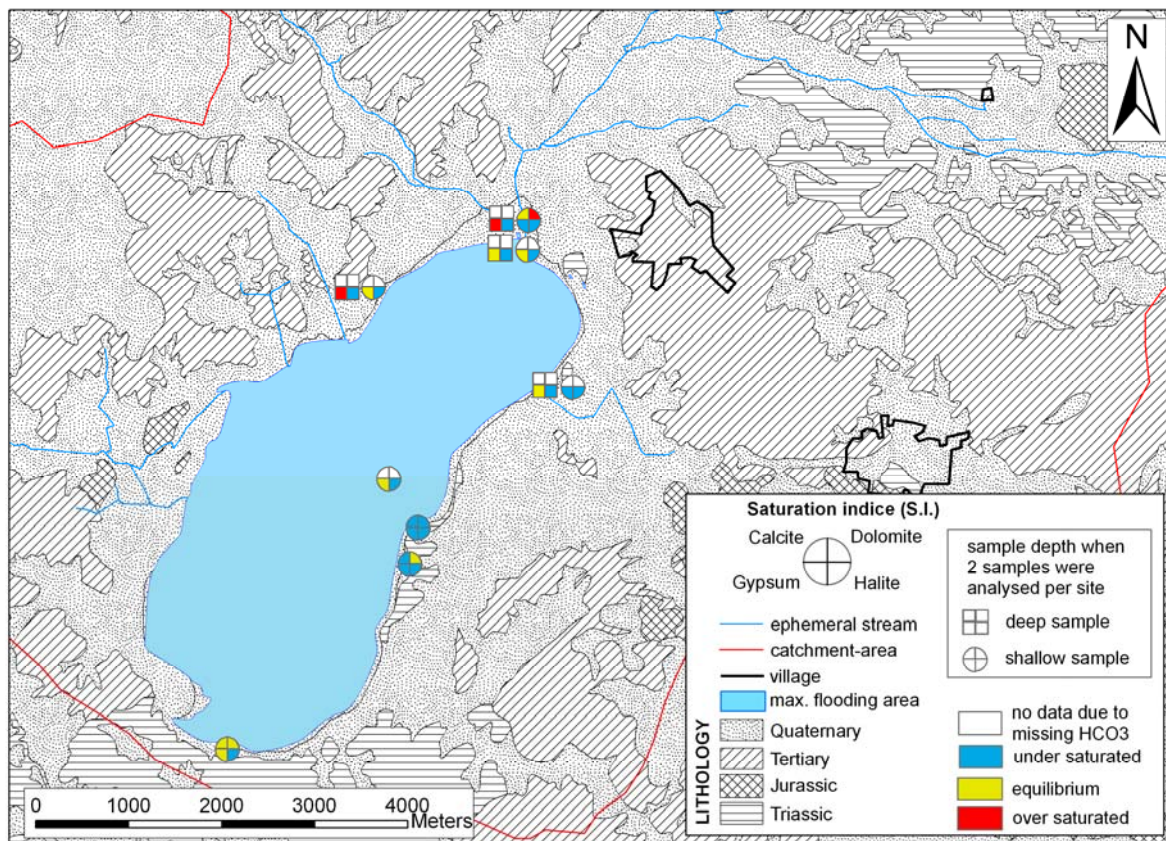


Figure 3.29: Distribution of saturation indices of February 2005 samples.

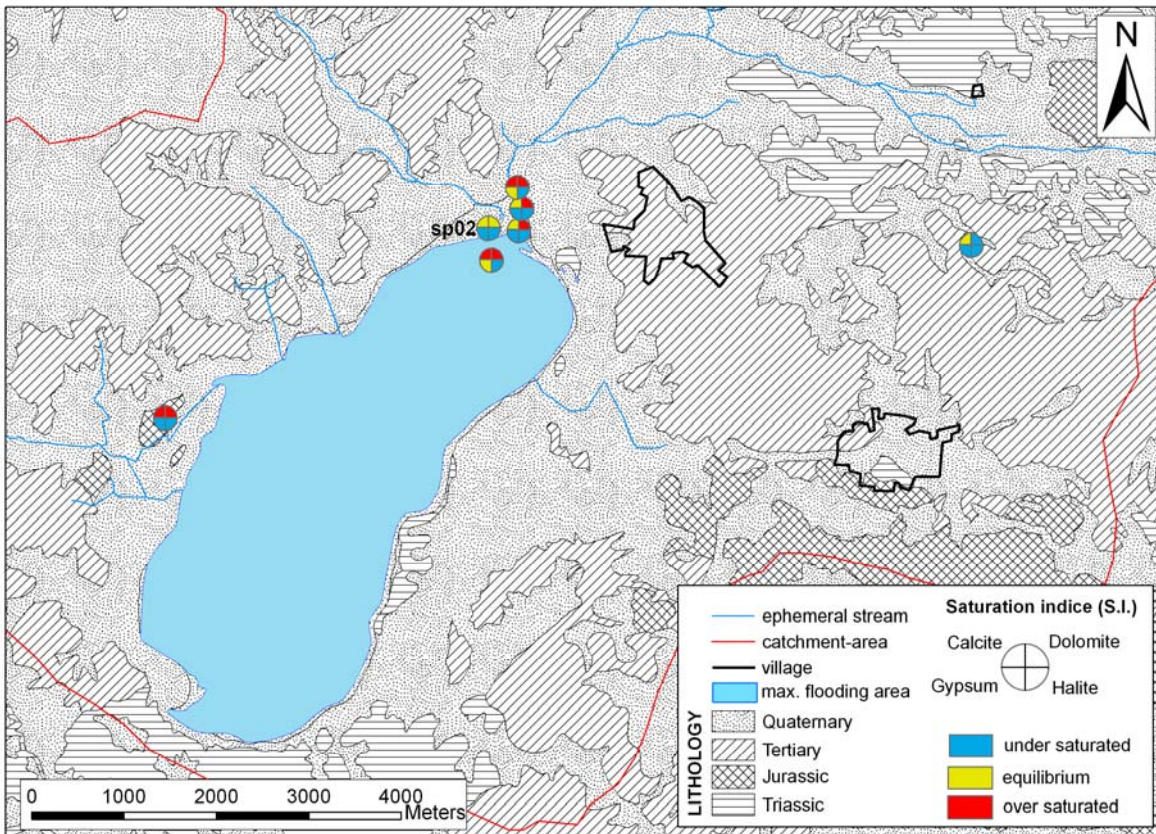


Figure 3.30: Distribution of saturation indices of winter 2004 samples.

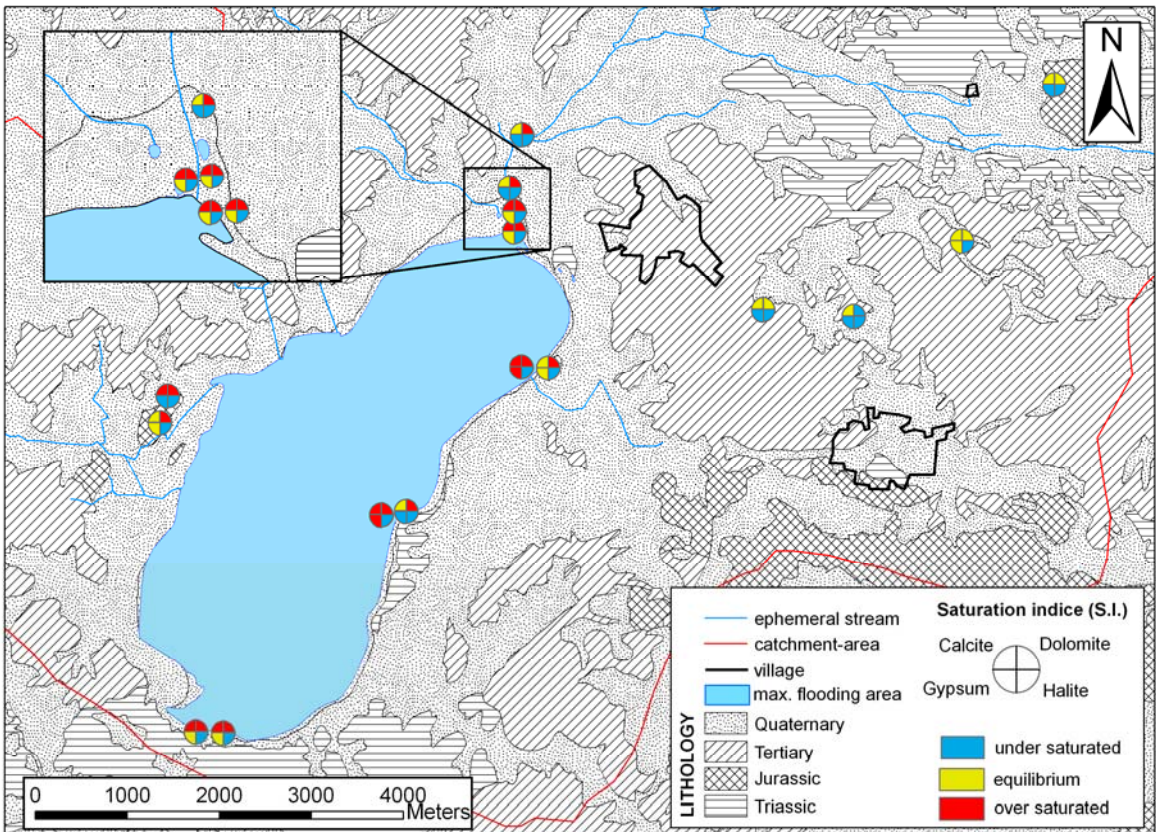


Figure 3.31: Distribution of saturation indices of autumn 2005 samples.

Comparison of deep and shallow samples in autumn 2005 shows that deeper samples have higher SI for comparable minerals (gypsum and calcite) due to a higher mineralization with depth (Fig. 3.31).

For autumn 2005 groundwater is super saturated for gypsum in the shallow piezometers inside the maximum flooding area. The remaining multilevel piezometers show a similar behavior in SI. The present precipitation of gypsum explains the occurrence of idiomorphic gypsum minerals found in boreholes near the lake shore. Calcite precipitates in close vicinity to the maximum flooding area.

Table 3.15: Saturation indices. Values up to ionic strength of 0.5 are calculated by PHREEQC using the phreeq.dat database, for higher ionic strength the Pitzer.dat database had been used. Shaded values indicate precipitation of the mineral.

sample id	ionic strength	Calcite	Halite	Gypsum	Dolomite	Magnesite	Aragonite	Anhydrite
sp01	0.99	0.68	-2.28	-0.08	1.97	0.52	0.49	-0.31
sp02	0.08	-0.01	-4.60	-0.70	0.06		-0.16	-0.94
sp03	2.46	0.36	-1.39	0.03	1.55	0.54	0.16	-0.18
sp05	1.00		-2.24	-0.29				-0.54
sp06	1.91	0.17	-1.60	-0.36	1.32	0.44	-0.02	-0.58
sp09	3.51	0.95	-0.98	0.02	2.96	1.27	0.76	-0.14
sp13	0.84	0.34	-2.28	-0.65	1.30		0.20	-0.86
sp14	0.02	-0.14	-6.10	-0.85	-1.12		-0.29	-1.09
SP-FP-03-050918	5.25	0.31	-0.44	0.18	1.84	0.79	0.12	0.09
SP-FP-05-050917	4.82	0.39	-0.59	0.13	2.05	0.90	0.20	0.02
SP-FP-06-050922	1.90	0.10	-1.60	-0.39	1.16	0.31	-0.09	-0.60
SP-FP-07-050922	0.09	0.14	-4.75	-0.71	0.37		-0.01	-0.96
SP-FP-08-050918	2.36	0.15	-1.39	-0.08	1.06	0.15	-0.04	-0.27
SP-FP-09-050921	0.15	0.16	-4.34	-0.04	-0.01		0.02	-0.26
SP-FP-1	4.10		-0.83	0.17				0.01
SP-FP-10	4.12		-0.83	0.00				-0.15
SP-FP-10-051003	0.02	0.15	-6.25	-1.73	-0.06		0.00	-1.97
SP-FP-11	0.36	-0.87	-2.99	-0.89	-1.16		-1.02	-1.13
SP-FP-13	3.08		-1.14	0.12				-0.07
SP-FP-14	3.86		-0.88	0.24				0.09
SP-FP-14-050916	3.51	0.19	-1.02	-0.11	1.78	0.79	0.01	-0.26
SP-FP-15-050918	1.29	0.08	-1.96	-0.47	1.12	0.26	-0.11	-0.69
SP-FP-17	0.11	0.04	-4.50	-0.01	-0.18		-0.11	-0.26
SP-FP-17-050920	0.12	0.82	-4.52	0.00	1.52		0.68	-0.23
SP-FP-21-051003	0.01	0.09	-7.68	-1.88	0.08		-0.06	-2.11
SP-FP-22-051003	0.02	0.08	-6.03	-0.90	-0.68		-0.07	-1.14
SP-FP-23-051004	0.05	0.51	-4.98	-1.40	1.01		0.37	-1.62
SP-FP-3	0.23	-0.67	-3.31	-2.11	-0.09		-0.82	-2.36
SP-FP-4/(SP-03)	2.92		-1.19	0.05				-0.14
SP-FP-5/(SP-04)	4.99		-0.54	0.13				0.02
SP-FP-6	1.54		-1.86	-0.17				-0.41
SP-FP-7	0.57	-0.19	-2.63	-0.78	0.37	-0.12	-0.38	-1.03
SP-FP-8	5.44		-0.42	0.38				0.29
SP-FP-9	2.37		-1.44	-0.30				-0.51
SP-FP-FU-22-050915	5.11	0.36	-0.55	0.25	2.23	1.10	0.17	0.16
SP-FP-FU-23-050916	4.76	1.09	-0.63	0.31	3.51	1.65	0.90	0.20
SP-FP-FU-24-050917	1.50	0.48	-1.93	-0.04	1.81	0.57	0.29	-0.25
SP-FP-FU-26-050919	2.20	0.51	-1.55	0.06	1.86	0.59	0.32	-0.14
SP-FP-FU-27-050920	0.14	0.74	-4.33	0.01	1.44		0.59	-0.23

For **cation exchange processes** basin group shows the lowest values on X-axis with -0.25 to -47.84 and on Y-axis with -12.95 to 47.86 (Fig. 3.32). Only groundwater sampled in the northernmost well, the Santillán spring, is in solution equilibrium, which indicates recent water. Except two samples from the south shore, which show an anion excess, probably caused by unusual high HCO_3^- concentrations due to an analysis error¹. All remaining samples indicate earth alkalinisation (Fig. 3.32), which means that Na-Cl-type water is intruding into a Ca- HCO_3 -type water aquifer and is therefore responsible for the salinisation. Earth alkalinisation in lake group samples though develops due to the inflowing earth alkalinised water from the basin.

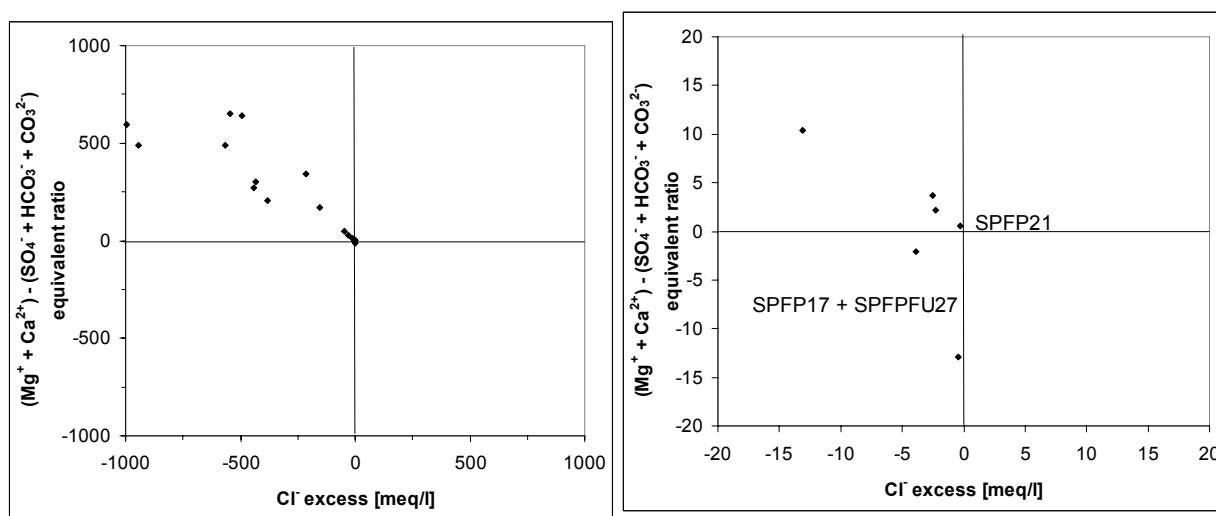


Figure 3.32: Cation exchange diagram after TESMER ET AL. (2006) plotting autumn 2005 samples. Right: all samples. Left: zoom in left plot with axis values ranging from -20 to 20.

All samples show **ion ratios** >1 for $\text{Cl}^-/\text{SO}_4^{2-}$, except for the south shore (Tab. 3.16) and therefore indicate salt leaching and a chloridic source of salinisation. Gypsum dissolution can be assumed for the south shore in autumn 2005 due to sulphate dominated salinisation. $\text{Cl}^-/\text{SO}_4^{2-}$ ratio tends to increase with increasing chloride concentration in basin and east/north shore groups (Fig. 3.33). Basin group shows the lowest ratio because of lower mineralization and lower chloride concentration. Artificial lake water correlates with the lake group and Santillán creek water with basin group due to similar environmental conditions.

Basin group has $\text{Mg}^{2+}/\text{Ca}^{2+}$ ratios from 0.13 to 1.15 (Tab. 3.16); four samples indicate incipient cation exchange with values up to 0.6 for the basin group. East/north shore samples vary from 2.13 to 12.15. The highest ratios are observed for the lake group

¹ Groundwater samples from shallow piezometers containing high contents of suspended load (clay and carbonate particles). Remaining carbonate increases HCO_3^- concentrations, which lead to an increase of the consumption of hydrogen acid for titration.

due to precipitation of sulphates and a relatively enrichment of Mg^{2+} in groundwater. The Mg^{2+}/Ca^{2+} ratio versus chloride concentrations spread wide along a

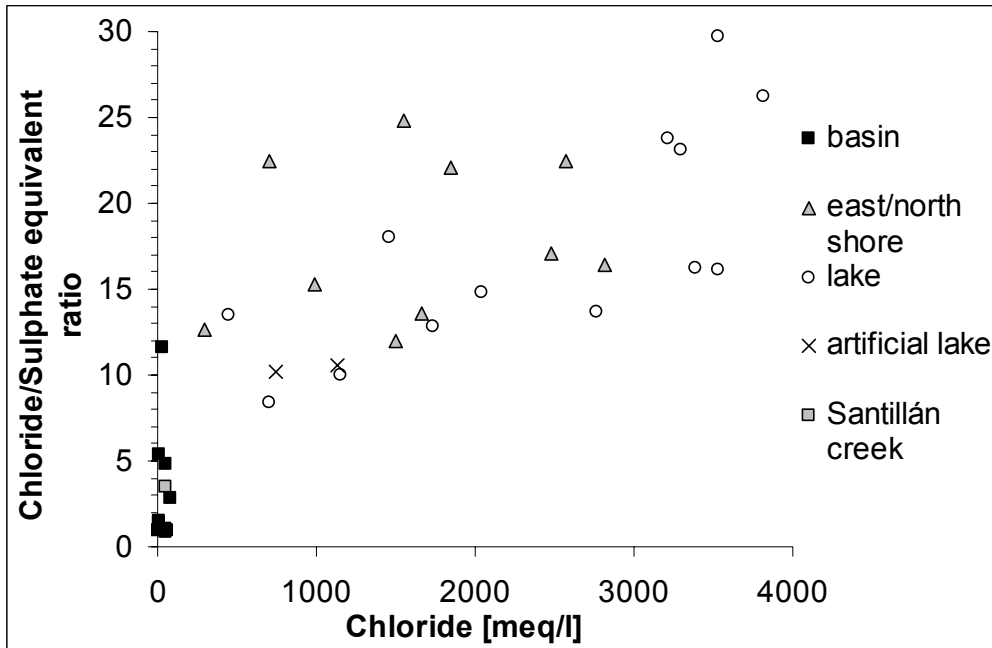


Figure 3.33: Cl^- vs. Cl^-/SO_4^{2-} .

straight line. It tends to increase with increasing chloride concentration (Fig. 3.34). Due to ratios > 0.2 (incipient) cation exchange is detected in almost all samples.

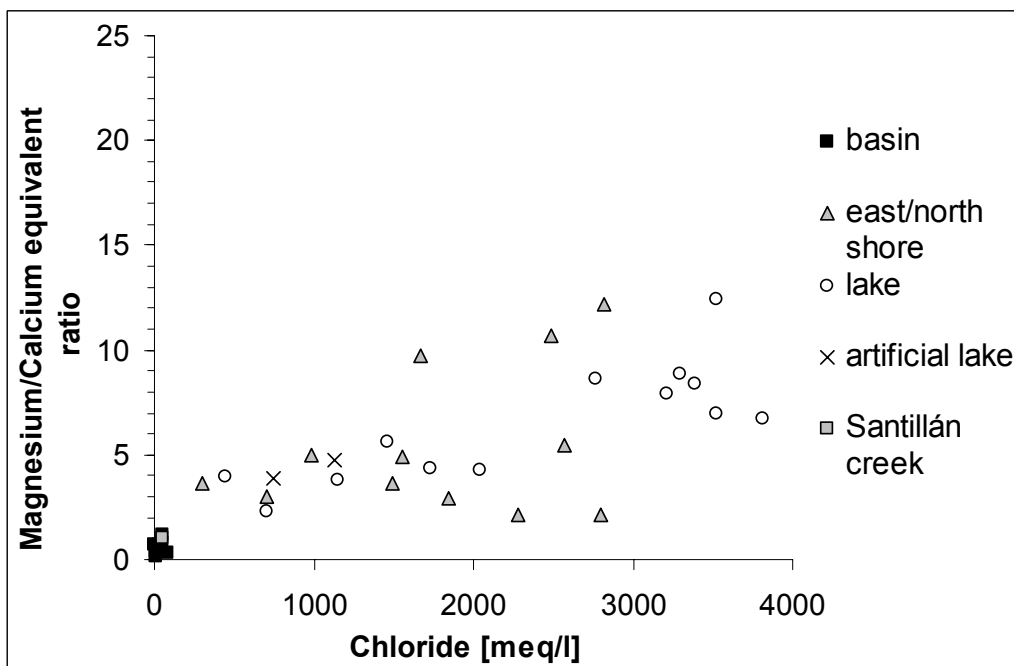


Figure 3.34: Chloride vs. Magnesium/Calcium equivalent ratio.

Cl^-/Na^+ ratios > 1 (Tab. 3.16) and simultaneous high Mg^{2+}/Ca^{2+} ratios, which additionally indicate the leaching of Mg- and Ca-chlorides, are present in salt lake and shorelines samples. Thus leaching of halite as well as of Mg-chlorides is the source of salinisation. An ion ratio of 1.01 can only be observed at the south shore and in

creek in the close vicinity to the lake (SPFP13). Lake, east/north shore and artificial lake groups show no significant increase in Cl^-/Na^+ ratio with increasing chloride concentration. The highest Cl^-/Na^+ ratios are observed in the south and west shore shallow groundwaters and in deep groundwaters in the eastern basin (SPFP09). This indicates that alkaline-earth-chloride leaching is very dominant at these sites. Fig. 3.35 displays the spread of Chloride/Sodium ratio versus Chloride concentration. No significant variation of Cl^-/Na^+ ratios with increasing Chloride indicate a dilution of leaching water (basin group) by fresh water.

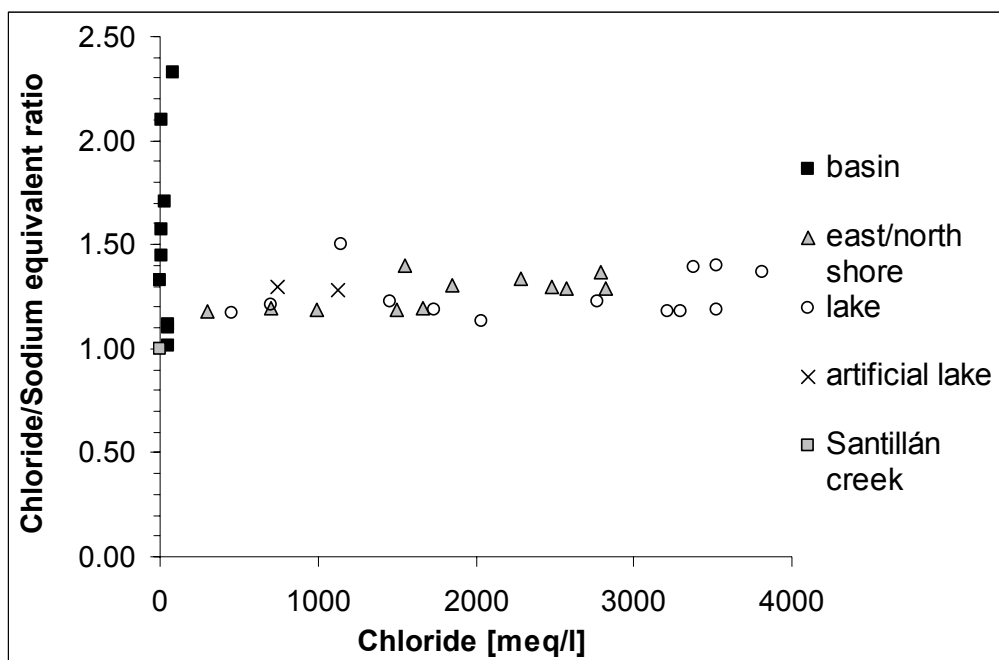


Figure 3.35: Chloride vs. Chloride/Sodium equivalent ratio.

Samples of basin group show a parallel evolution on a straight line of Ca^{2+} and Cl^- and thus indicate water rock interaction (Fig. 3.36). For lake and east/north shore groups earth alkalisation can be suggested as a result of high Na^+ concentrations which are concomitant with high Cl^- concentrations. Gypsum should precipitate from groundwaters situated right of the gypsum precipitation point in Fig. 3.36. Super saturation by saturation indices is only observed for western basin samples and a multi-level piezometer near the artificial lake. Table 3.16 lists the $\text{Ca}^{2+}/\text{Cl}^-$ ratios.

Bromide has been analysed only in autumn 2005 samples. Samples from Fuente de Piedra Basin higher mineralized than seawater show an enrichment of Bromide compared with the seawater evaporation curve. According to THOMAS (1994) and RIDDENHOUSE (1967) this is indicating a leaching of Halite (Fig. 3.37).

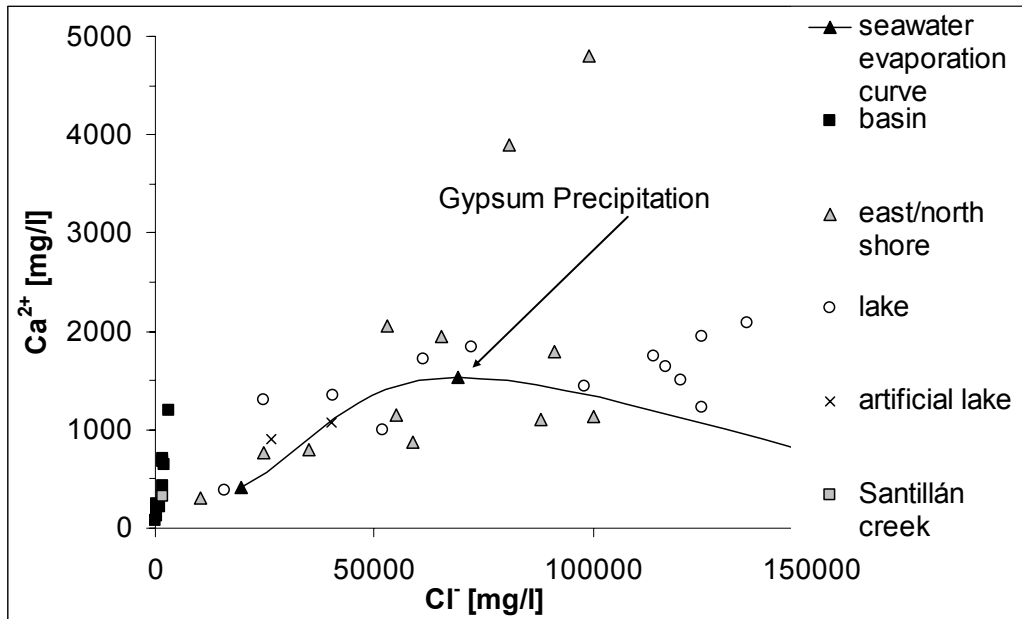


Figure 3.36: Chloride vs. Calcium in mg/l plotted with the seawater evaporation curve (FONTES & MATRAY, 1993).

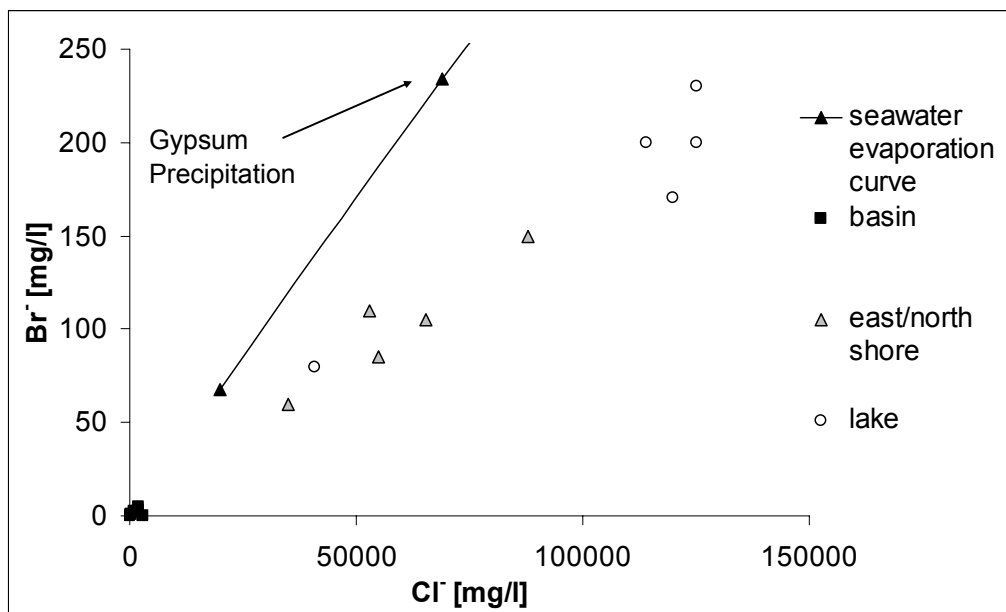


Figure 3.37: Chloride vs. Bromide in mg/l plotted with seawater evaporation curve (FONTES & MATRAY, 1993).

The values of chloride/bromide ratios (Tab. 3.16) range from 13 (artificial lake) to 825 (SPFP17), whereas the mean is represented by 552.

For further graphical analysis the Cl^-/Br^- ratios (y-coordinate) were plotted against the Chloride concentration (x-coordinate). This affords a coeval interpretation for the source and degree of salinisation (Fig. 3.38).

For groundwater with Chloride concentrations around the natural background level (< 40 mg/l) no Chloride/Bromide ratios are available. Groundwater with < 300 mg/l Chloride content shows Cl^-/Br^- ratios < 300. Chloride/Bromide ratios for groundwaters with > 300 mg/l range from 370 to 825.

Maximum Chloride/Bromide ratios around 800 for groundwaters at the south shore indicate a leaching of evaporites as source of salinisation in this area.

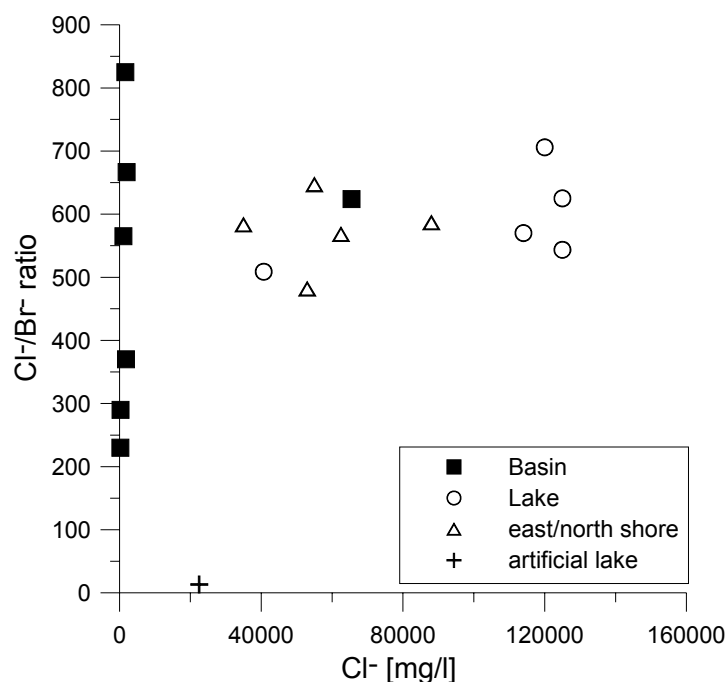


Figure 3.38: Chloride vs. Chloride/Bromide ratio, indicating equal ratios in samples around the lake.

Most groundwaters show Cl^-/Br^- ratios between 540 and 650 with increasing salinisation for decreasing distance to the lake. These groundwaters can be determined as multicomponent waters, where evaporative effects, along with leaching processes, cause the salinisation.

Reducing or oxidizing conditions are indicated by redox potential, O_2 , Mn^{2+} , Fe^{3+} , NH_4^+ , NO_2^- and NO_3^- . The redox potential for the sampled groundwater ranges from -173 mV in deep groundwaters to +191 mV in shallow groundwaters at the western basin. The groundwater in the western and northern lake margins is almost free of O_2 (SPFP03 - 08), whereas the groundwater in Santillán creek is saturated with O_2 . Therefore the spatial variation of O_2 contents is great. Also high contents of NO_3^- in conjunction with a high redox potential argues against reductive processes in the aquifer. High concentrations of Fe and Mn in conjunction with low or negative redox potentials and the absence of O_2 for deep groundwaters in western and eastern basin (SPFP09) might suggest reductive processes.

3. Diploma thesis - Results

Table 3.16: Ion equivalent ratios. Cl/Br and Ca/Cl are calculated with values in mg/l.

sample Id.	site Id.	group	Cl/Na	Mg/Ca	Cl/SO4	Cl/Br	Ca/Cl
			by meq/l			by mg/l	
sp05	SPFP04	artificial lake	1.30	3.85	10.22		0.060
SP-FP-6	SPFP04	artificial lake	1.28	4.73	10.55		0.048
sp02	SPFP02	Santillán creek	1.50	1.03	3.49		0.338
sp14	SPFP09	basin	2.10	0.12	1.51		1.332
SP-FP-07-050922	SPFP07	basin	2.61	1.15	4.82	370.00	0.411
SP-FP-09-050921	SPFP09	basin	2.33	0.34	2.80		0.708
SP-FP-10-051003	SPFP10	basin	1.57	0.39	5.37	230.00	0.946
SP-FP-17	SPFP17	basin	1.12	0.56	1.04		0.729
SP-FP-17-050920	SPFP17	basin	1.10	0.61	0.89	825.00	0.751
SP-FP-21-051003	SPFP21	basin	1.33	0.68	0.99		3.317
SP-FP-22-051003	SPFP22	basin	1.45	0.13	1.43	290.00	1.342
SP-FP-23-051004	SPFP23	basin	1.70	0.71	11.60	565.00	0.329
SP-FP-FU-27-050920	SPFPFU27	basin	1.01	0.77	0.90	666.67	0.566
SP-FP-3	SPFP13	creek	1.00	20.61	15.88		0.007
sp09	SPFP06	east/north shore	1.29	5.50	22.44		0.035
sp13	SPFP08	east/north shore	1.20	3.02	22.49		0.054
SP-FP-06-050922	SPFP06	east/north shore	1.40	4.88	24.84	647.06	0.037
SP-FP-08-050918	SPFP08	east/north shore	1.31	2.96	22.07		0.053
SP-FP-10	SPFP14	east/north shore	1.29	12.15	16.42		0.020
SP-FP-11	SPFP15	east/north shore	1.18	3.63	12.68		0.051
SP-FP-13	SPFP16	east/north shore	1.34	2.16	32.01		0.085
SP-FP-14	SPFP16	east/north shore	1.37	2.13	39.03		0.086
SP-FP-14-050916	SPFP14	east/north shore	1.30	10.64	17.03	586.67	0.022
SP-FP-15-050918	SPFP15	east/north shore	1.19	4.95	15.30	583.33	0.040
SP-FP-9	SPFP14	east/north shore	1.19	9.74	13.55		0.026
SP-FP-FU-26-050919	SPFPFU26	east/north shore	1.19	3.62	11.97	481.82	0.068
sp01	SPFP01	lake	1.21	2.26	8.40		0.093
sp03	SPFP03	lake	1.18	4.31	12.80		0.050
sp06	SPFP05	lake	1.23	5.61	17.99		0.034
SP-FP-03-050918	SPFP03	lake	1.18	6.93	29.71	543.48	0.028
SP-FP-05-050917	SPFP05	lake	1.18	7.92	23.76	570.00	0.027
SP-FP-1	SPFP11	lake	1.23	8.59	13.72		0.026
SP-FP-4/(SP-03)	SPFP03	lake	1.14	4.30	14.84		0.045
SP-FP-5/(SP-04)	SPFP03	lake	1.18	8.85	23.10		0.025
SP-FP-7	SPFP05	lake	1.17	3.93	13.51		0.043
SP-FP-8	SPFP05	lake	1.37	6.71	26.19		0.027
SP-FP-FU-22-050915	SPFPFU22	lake	1.40	12.43	16.13	625.00	0.017
SP-FP-FU-23-050916	SPFPFU23	lake	1.39	8.35	16.26	705.88	0.022
SP-FP-FU-24-050917	SPFPFU24	lake	1.50	3.79	10.03	508.75	0.059

3.2.1.2 Temperature logs

In Fig. 3.39 the temperature distribution with depth is displayed for an overall of 10 monitoring wells in the Fuente de Piedra Basin. Therefore the temperature was recorded in 7 wells to a maximum depth of 20 m and in 3 wells to a maximum depth of 100 m. The deep wells are located in the eastern basin, whereas the shallow wells are situated at the lakes shoreline and in the northern edge. The shallow wells show a resembling distribution of temperature for the autumn logs, where temperatures of the uppermost waterlayer range from 19.5 to 24.5 °C. In depth around 10-15 m temperatures settle to a stable level with fluctuations < 0.1°C and mark the beginning of the “neutral zone”. For wells SPFP07, -14 and -17 the temperature of the “neutral zone” is with around 17°C at the level of the annual average temperature (17.5°C), whereas for wells SPFP03, -05, -06 and -15 the temperature is nearly 18°C. This increase could indicate exothermal reactions due to a reductive environment below the lake, but hydrochemical and ³⁴S-isotope data do not confirm this assumption. The temperature distributions in shallow wells after pumping are completely re-established in short times and except a temperature layering of water. Conspicuous fluctuations in spring logs, appearing in the uppermost groundwater layer, are ascribed to seasonally increasing air temperatures. Lowest temperatures for spring logs are around 15°C in depth of 2-4 m, except of SPFP06 with 17.5°C.

The deep wells show a similar distribution of temperature during the seasons. The temperature fluctuations within the wells are less with a maximum of 1°C, and it first seems that the “neutral zone” is first developed in depth of 20-25 m. But the upper waterlayer show high temperatures around 19°C and the decrease of temperature with depth are probably indicating a lateral flux of colder water. Another conclusion for the first decreasing and then with increasing depth stagnating or less increasing temperatures is not become apparent. The observed temperature gradients for the deep wells are with 1°C/100 m less than the expected (2-3°C/100 m). This leads to the assumption of a lateral groundwater flow for the drilled thickness of the aquifer in the eastern basin. The temperature crack in the autumn log of SPFP22 is caused by the exchange of thermometers in 20 m depth. The increased temperature (19°C) in the “neutral zone” in well SPFP09 could be provoked by reductive reactions in the groundwater. A low Eh-value and the relatively high contents of Fe, Mn, NH₄⁺ and NO₂⁻ could confirm these. In contrast groundwater observed in well SPFP22, with an analog temperature in the upper waterlayer, is oxygen saturated.

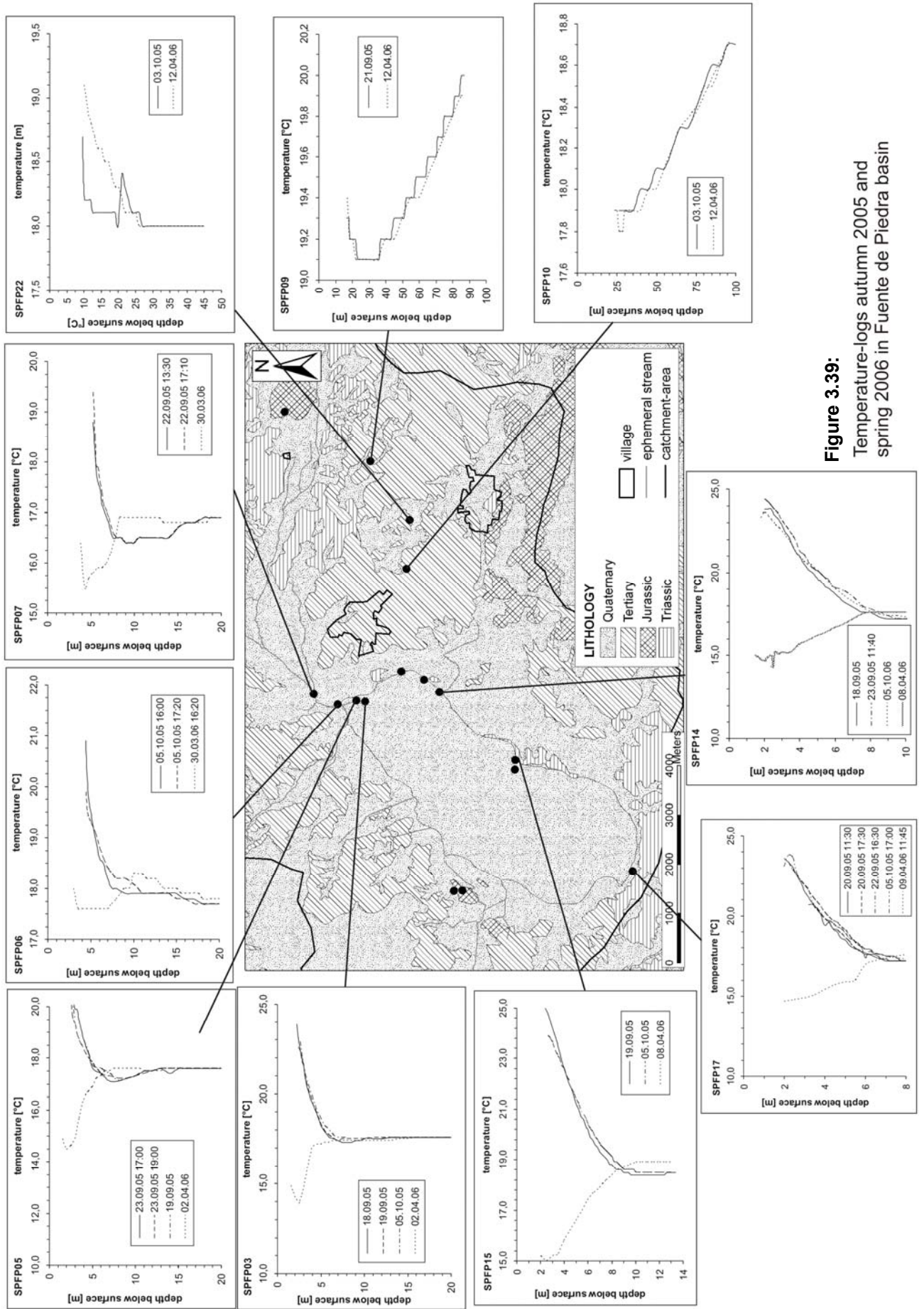


Figure 3.39:
Temperature-logs autumn 2005 and
spring 2006 in Fuente de Piedra basin

3.2.1.3 Electric conductivity logs

Conductivity logs were measured at 7 sampling sites at the lake's shoreline (SPFP03, -05, -06, -07, -14, -15, -17) and at one site in the basin (SPFP22) in autumn 2005 and spring 2006 (Tab. 3.2). Measurements in autumn 2005 (1 to 4 times) were made before and after pumping, in spring 2006 only one log was recorded. The first measured logs (before pumping) are set as initial conditions and are used for comparison with situations after pumping and determination of recovering times. Pumping depth and constant end conductivity is represented by a rectangle in the charts (Fig. 3.40 and 3.41).

The electric conductivity ranges from 654 to 205000 $\mu\text{S}/\text{cm}$. The highest values are observed in the edges of the salt lake. Conductivity increases with decreasing distance to the lake over the water column in the observation sites. Position of the transition zone is situated in lower depths with decreasing distance to the lake (Fig. 3.40 and 3.27).

Different salinity stratifications can be identified by the EC logs. Between the upper and the lowermost stratification smaller salinity layers are observed. These layers particularly divide the main transition zone.

By the recovering times of the transition zone three groups can be identified: a) < 4 hours (SPFP06, SPFP07, SPFP15); b) > 14 days (SPFP03, SPFP14, SPFP17) and c) < 4 days (SPFP05) (Fig. 3.40 and 3.41). Existing borehole-log data had been added schematically in the graphs (SPFP05, -15, -17). By recovering times and by borehole-log data conclusions for sampling sites without borehole-log information can be made. Additionally sampling sites with less permeable sediments have greater

Table 3.17: Drawdown [m] after 30 min. pumping at the sampling sites.

site Id	drawdown [m]
< 4 hours	
SPFP06	0.30
SPFP07	0.20
SPFP15	0.06
< 4 days	
SPFP05	1.37
> 14 days	
SPFP03	not measured
SPFP14	not measured
SPFP17	> 5

drawdowns, shown in Tab. 3.17. Analysis of the EC-logs before and after pumping shows that the required recovering time varies and depends on the permeability of the sediments. At SPFP17 much bygone time after pumping is necessary to re-establish the normal situation in the groundwater body at this measuring point, 15 days are insufficient (Fig. 3.41). Due to these long recovering times very low permeability can be assumed. Above a depth of 2 m sand and from 2 to 8.5 m clay with gypsum interbeddings is present so that this assumption is validated. At SPFP15 no change after pumping with regard to the initial condition can be observed due to good permeable sandy

strata (Fig. 3.40)). In probably good permeable materials, recovering time < 4 hours (SPFP06, SPFP07, SPFP15), in very less permeable materials (clay) recovering time > 14 days (SPFP03, SPFP14, SPFP17), compare Fig. 3.40 and Fig.3.41. An exception is SPFP05 with a recovering time of < 4 days.

Measurements of EC conditions in spring 2006 had been very similar to conditions after pumping at SPFP03, SPFP06 and SPFP14 in autumn 2005. At these sites the transition zone between low and high mineralized groundwater was observed in spring in a lower depth than in autumn. The upraising is associated with an increasing groundwater flow from east and an influence of evaporation which advantage arise of the brine. The only sampling site which shows a decrease in conductivity in spring in the upper 7 m is SPFP05 (beside the artificial lake) which can probably be related to the comparably good permeability and therefore lateral inflow of less mineralized water in the upper water column.

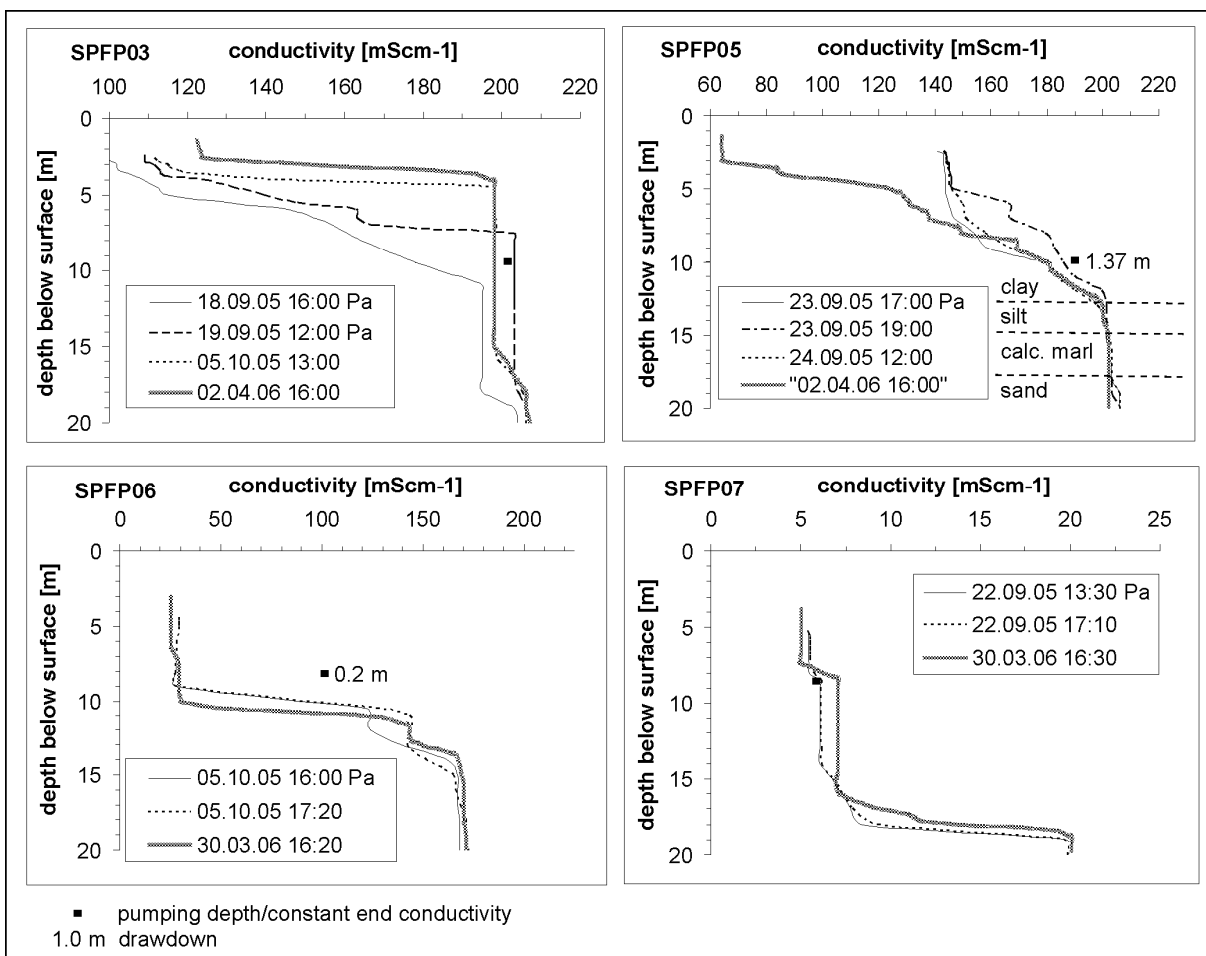


Figure 3.40: Electric conductivity logs with simplified borehole-logs. Pa: Pumping made after log. Depth of the pump and constant end conductivity are represented by a rectangle, drawdown is placed beside the pump-symbol.

Sites at the southern edge of the lake indicate a vertical downward displacement of 1 m of the transition zone in April 2006, compared to the situation before pumping in autumn 2005. This downward displacement can be assumed as a result of infiltrating precipitation or low mineralized groundwater flux from the upper sandy strata. At SPFP15 no seasonal and no change by pumping was observed due to good permeable strata.

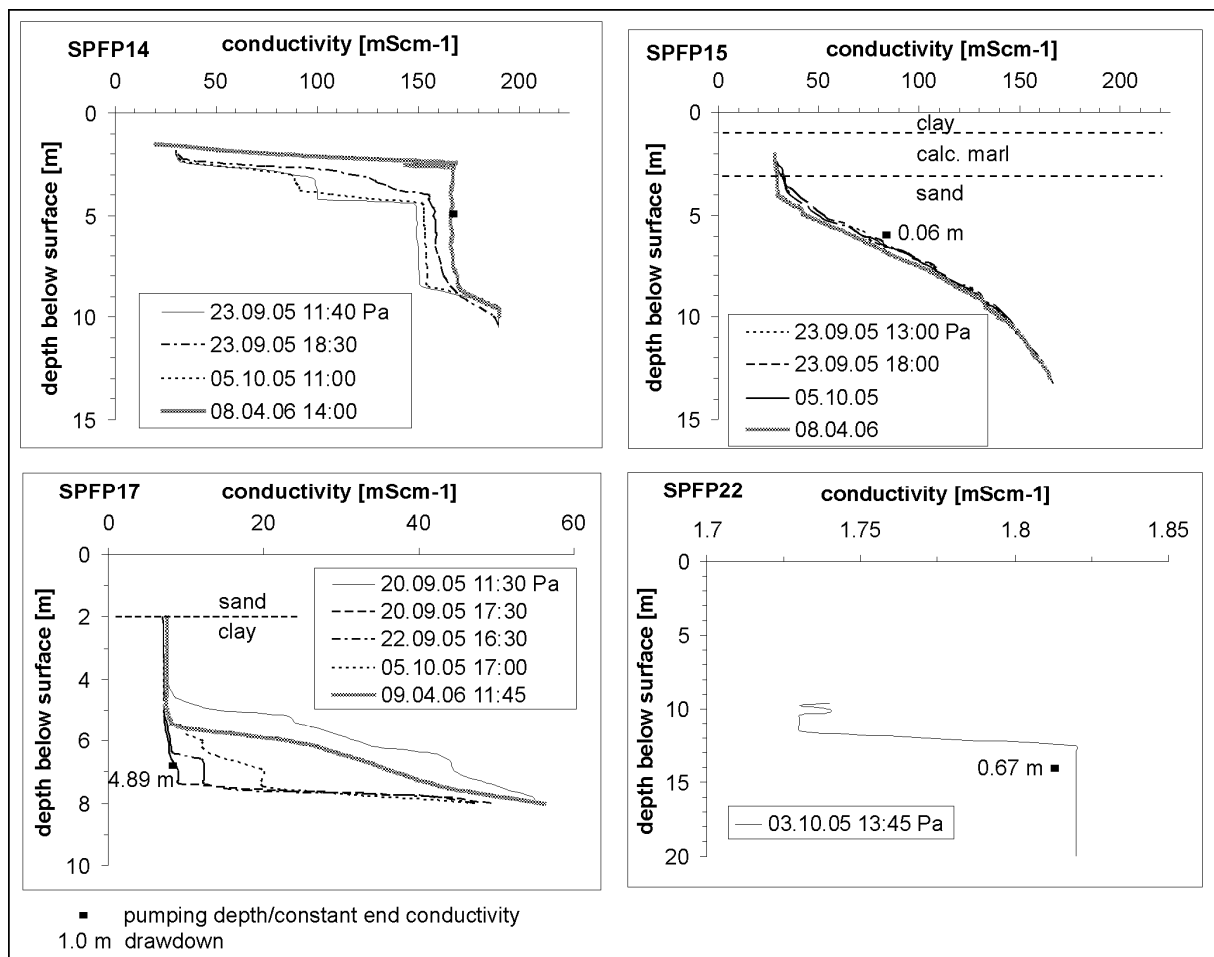


Figure 3.41: Electric conductivity logs with simplified borehole-logs. Pa: Pumping made after log. Depth of the pump and constant end conductivity are represented by a rectangle, drawdown is placed beside the pump-symbol.

EC logs at a series of monitoring wells show the existence of an interface between fresh and saltwater, respectively low and high mineralized water. The wedge shape of the interface between low and high mineralized water indicates that the salinisation derives from the salt lake (Fig. 1.19, Fig. 3.40 and 3.41).

3.2.2 Stable isotopes

3.2.2.1 Oxygen and Hydrogen of H₂O

In Fig. 3.28 isotopic ratios of ¹⁸O and D from ground- and surfacewater samples of Fuente de Piedra Basin, taken from 2004-2005, in comparison with isotope data of precipitation from the GNIP-stations Barcelona and Gibraltar are plotted. As you can

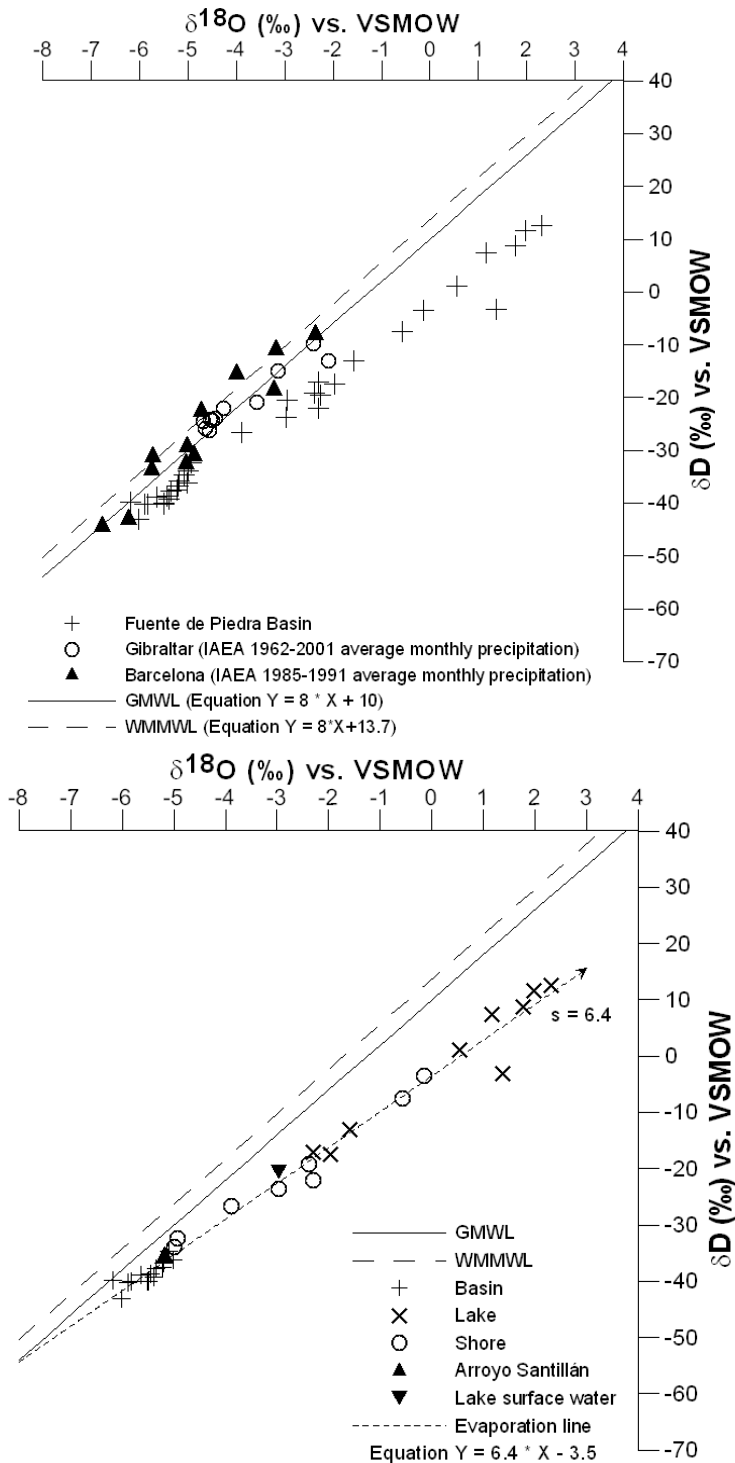


Figure 3.42: Scatter plots of isotopic ratios of ¹⁸O and δD from ground water samples of Fuente de Piedra Basin, autumn 2005.

seen in Fig 3.42, isotope ratios of precipitation in Gibraltar are situated around the GMWL and representing Atlantic influenced rainfalls, whereas for isotope ratios in Barcelona rainfalls are stronger influenced by the Mediterranean. Groundwater isotope data for Fuente de Piedra are located at a local waterline and plotting near the GMWL.

In Fig 3.42 isotope ratios for samples, distinguished by location, and the evaporation line are displayed. The samples plotted as + near the GMWL with $\delta^{18}\text{O}$ -values of around -6 ‰ and δD -values of around -40 ‰, common for this region, taken from wells in the northeastern part of the basin and in the south, where the salt lake's shore forms the basins boundary as well.

Samples and isotope signatures are below-mentioned in Tab. 3.18. Wells are distinguished by their location and divided into groups (see chapter 3.2.1).

The sampled ground waters with the heaviest isotopic signatures ($\delta^{18}\text{O}$ -values -3 to +2.5 ‰ and δD -values -21 to +12.5 ‰) are located in the salt lake (x) and along the northern shore line, where the lake regresses appreciably. The samples from wells in the area of the recent and former shoreline (o) show $\delta^{18}\text{O}$ -values ranging from -5 to 0 ‰ and δD -values from -35 to 0 ‰. These ground waters seem to be a mixture of freshwater, streaming from recharge areas in the north and east of the basin and the evaporative enriched lake water, which infiltrates lake sediments. Sampled lake surface water features $\delta^{18}\text{O}$ and δD -values of -3 and -20.5 ‰ respectively and plots among the shore group groundwaters. The most important surface inflow, the Santillán Creek, plots among the basin group. The regression line for the sampled groundwaters shows a strong evaporation trend with a slope of $s \approx 6.4$. The slope for evaporative enrichments less than 5 is typical for evaporation from open surfaces.

Table 3.18: Salt-corrected isotope data for D and ^{18}O .

Sample Id.	$\delta^{18}\text{O}$ [‰]	$\delta^{18}\text{O}$ corrected [‰]	δD [‰]	δD corrected [‰]	EC [$\mu\text{S}/\text{cm}$]	D-excess [‰]	D-excess corrected [‰]	group
sp05	-2,32	-2,27	-21,20	-19,51	64000	-2,64	-1,38	artificial lake
sp02	-5,19	-5,19	-35,90	-35,79	5900	5,62	5,70	Santillán Creek
sp10	-5,20	-5,20	-36,90	-36,81	7300	4,7	4,77	basin
sp11	-5,09	-5,09	-34,70	-34,65	19500	6,02	6,06	basin
sp14	-5,39	-5,39	-39,30	-39,28	1650	3,82	3,84	basin
sp16	-5,44	-5,44	-38,70	-38,69	990	4,82	4,83	basin
sp17	-5,64	-5,64	-38,90	-38,88	1140	6,22	6,23	basin
SP-FP-07-050922	-5,22	-5,22	-37,70	-37,58	6170	4,06	4,15	basin
SP-FP-09-050921	-5,96	-5,83	-44,30	-40,11	10520	3,38	6,50	basin
SP-FP-10-051003	-5,89	-5,89	-40,30	-40,29	1312	6,82	6,83	basin
SP-FP-17-050920	-5,51	-5,51	-40,20	-40,09	7700	3,88	3,96	basin
SP-FP-21-051003	-6,18	-6,18	-39,90	-39,90	654	9,54	9,54	basin
SP-FP-22-051003	-5,35	-5,35	-37,80	-37,78	1815	5	5,01	basin
SP-FP-23-051004	-5,02	-5,02	-36,20	-36,13	3690	3,96	4,01	basin
SP-FP-FU-27-050920	-5,49	-5,49	-40,20	-40,07	9620	3,72	3,82	basin
sp01	-3,01	-2,96	-22,10	-20,51	54200	1,98	3,16	lake surface
sp03	-1,71	-1,58	-16,90	-12,97	133200	-3,22	-0,29	lake
sp04	1,72	1,98	3,60	11,60	200000	-10,16	-4,20	lake
SP-FP-05-050917	0,93	1,16	0,20	7,50	188500	-7,24	-1,80	lake
SP-FP-FU-22-050915	2,06	2,32	4,50	12,50	190800	-11,98	-6,02	lake
SP-FP-FU-23-050916	0,30	0,54	-6,50	1,18	186900	-8,9	-3,18	lake
SP-FP-FU-24-050917	1,28	1,36	-5,80	-3,20	94200	-16,04	-14,10	lake
sp06	-2,41	-2,30	-20,30	-16,98	114200	-1,02	1,45	shore
sp08	-5,01	-5,00	-34,30	-33,96	15600	5,78	6,03	shore
sp09	-0,33	-0,14	-9,30	-3,47	168100	-6,66	-2,32	shore
sp12	-4,93	-4,93	-32,40	-32,39	1500	7,04	7,05	shore
sp13	-3,94	-3,89	-28,20	-26,61		3,32	4,51	shore
SP-FP-06-050922	-2,49	-2,38	-22,60	-19,08	107400	-2,68	-0,06	shore
SP-FP-08-050918	-2,31	-2,30	-22,20	-22,01	130300	-3,72	-3,58	shore
SP-FP-14-050916	-0,75	-0,57	-13,20	-7,57	166900	-7,2	-3,00	shore
SP-FP-15-050918	-3,04	-2,97	-25,90	-23,66	86100	-1,58	0,09	shore
SP-FP-FU-26-050919	-2,07	-1,96	-20,90	-17,51	123800	-4,34	-1,81	shore

In Fig. 3.43 the isotopic composition for groundwater samples from different depth for the wells SPFP05 and SPFP06 is shown. The samples for medium depth were taken after pumping and with stable values. The endmembers of a mixture line, with the main surface reflux of the lake, the Arroyo Santillán (with $\delta^{18}\text{O} = -5\text{‰}$ and $\delta\text{D} = -36\text{‰}$), and the groundwater sampled in SPFPFU22 ($\delta^{18}\text{O} = 2\text{‰}$ and $\delta\text{D} = 4.50\text{‰}$) are shown additionally. The isotopic signature of the lakes surface water with $\delta^{18}\text{O}$ -values around -3‰ and δD -values around -22‰ in Feb 2005 already shows a light evaporative enrichment. The increase of the values of isotopic ratios with depth leads to the conclusion that lake water is descending and mixing with fresh groundwater. Lower isotope ratios in the upper waterlayer are probably caused by a dilution with superficial groundwater. The convection of lake brines is possibly induced by density driven flows and responsible for the groundwater layering at the lake. Piezometer SPFP05 and SPFP06 reveal an increasing influx of freshwater in the first 5 to 10 m below surface with increasing distance to the lake, while the brine's bottom out wedge shaped into the basin. In well SPFP06 in 2 m depth the isotopic composition is nearly the same than those of the Arroyo Santillán. In 8 m depth $\delta^{18}\text{O}$ - and δD -values are correlating with the isotopic values for a depth of 3 m in well SPFP05. These conclusions are confirmed by the results of the analysis of conductivity-logs discussed in chapter 3.2.1.3.

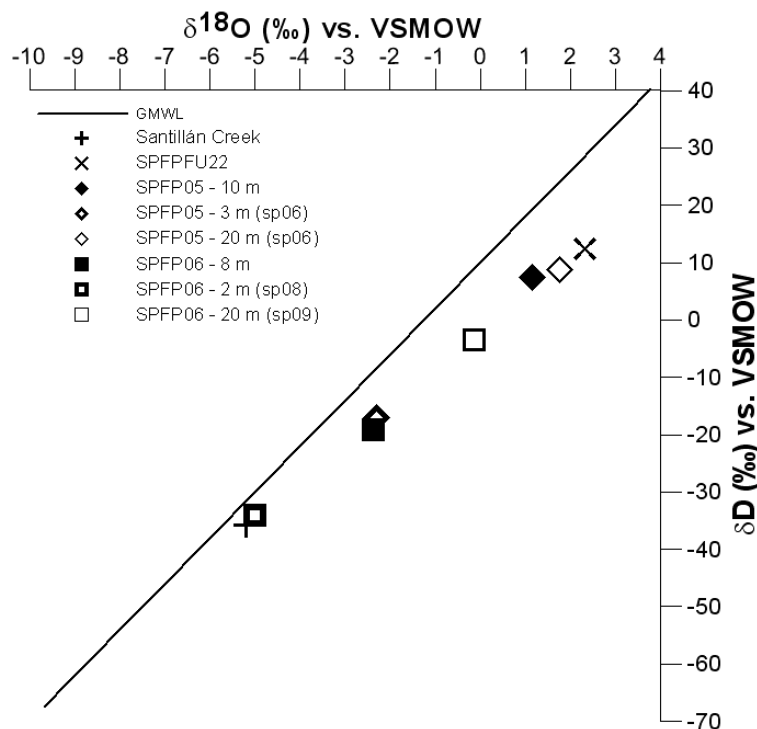


Figure 3.43: Isotopic ratios of $\delta^{18}\text{O}$ and δD in different depth for wells SPFP05, -06, -FU22 and selected surface water.

Fig. 3.44 identifies different sources of salinisation in the Fuente de Piedra Basin. Positive isotopic values indicate a strong influence of evaporation.

The wells with light isotopic signature ($\delta^{18}\text{O} = -5$ to -6 ‰) and less salinity (< 10 mS/cm) are situated in the northern part of the basin and are not influenced by the lake.

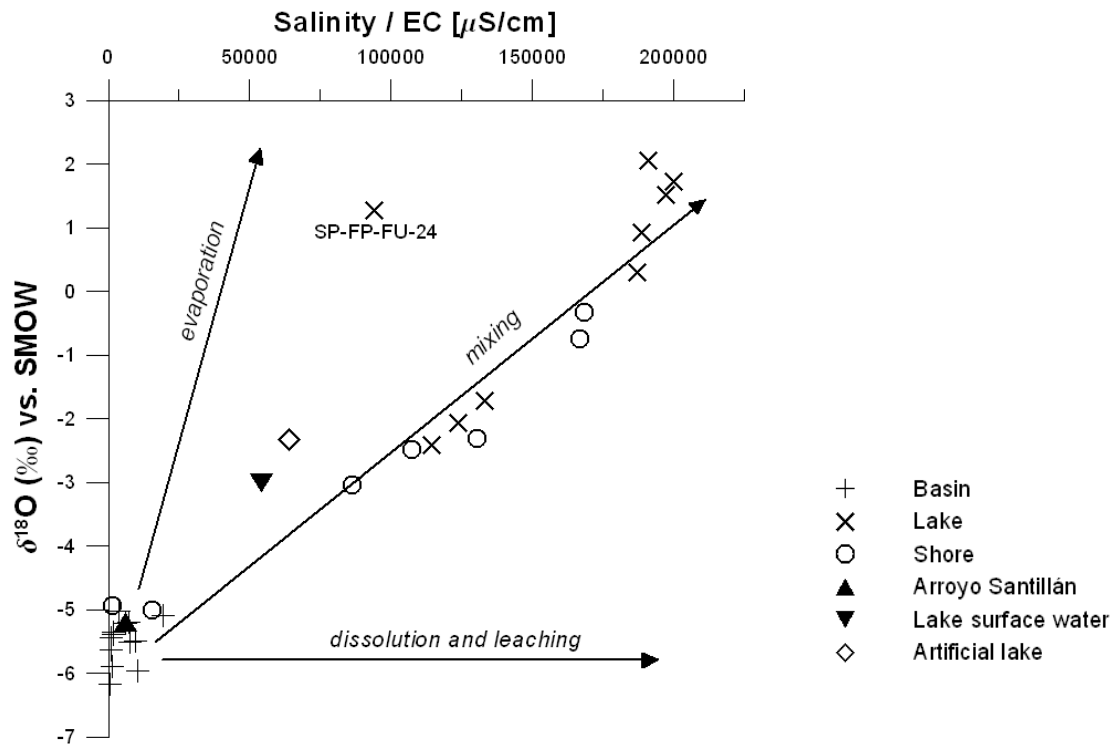


Figure 3.44: Scatter plot d18O (salt corrected) versus Salinity after GEYH (2001).

Furthermore lake brines and groundwaters from the shoreline show a correlation of $\delta^{18}\text{O}$ and salinity in terms of a mixing line between dissolution, leaching processes and evaporation. The endmembers of this line are SPFPFU22 and groundwaters in the recharge area (SPFP21). In the course of time the high mineralized brines passed different stages of evaporative enrichment to get concentrated. Brine samples on the mixing line additionally indicate an influence of leaching processes for the salinisation. So the groundwater forming the brine had initially to be enriched by leaching and dissolution processes, before it concentrated due to evaporation. The wells in the lake, near the Salinas (SP-FP-FU-22) and in the north, near the embouchure of Arroyo Santillán (SP-FP-03 / 1st well of section) show the most positive isotopic values and the highest salinity induced by a concentration of uprising groundwater in the lake area. Additionally a mixing of strong evaporative enriched groundwaters with superficial groundwater occurs, that enriched in the course of dissolution and leaching of evaporite Triassic material (e.g. SPFP09). The lake surface water, like the artificial lake water, shows a stronger evaporative trend than groundwater

samples. Groundwater in piezometer SPFPFU24 is strongly influenced by the artificial lake and plots on a line with the surface water from the salt lake and the small artificial lake. A reason could be a deviating composition of water due to the discharge of waste water. This is reflected in the isotopic signature of SPFPFU24.

In an $\delta^{18}\text{O}$ - Cl^- -plot this significant deviation is not existing. Because dissolution of Triassic evaporites, mainly gypsum, is contributing to the salinization, for the interpretation of the data, an $\delta^{18}\text{O}$ -EC-plot was chosen to consider the different salinization processes.

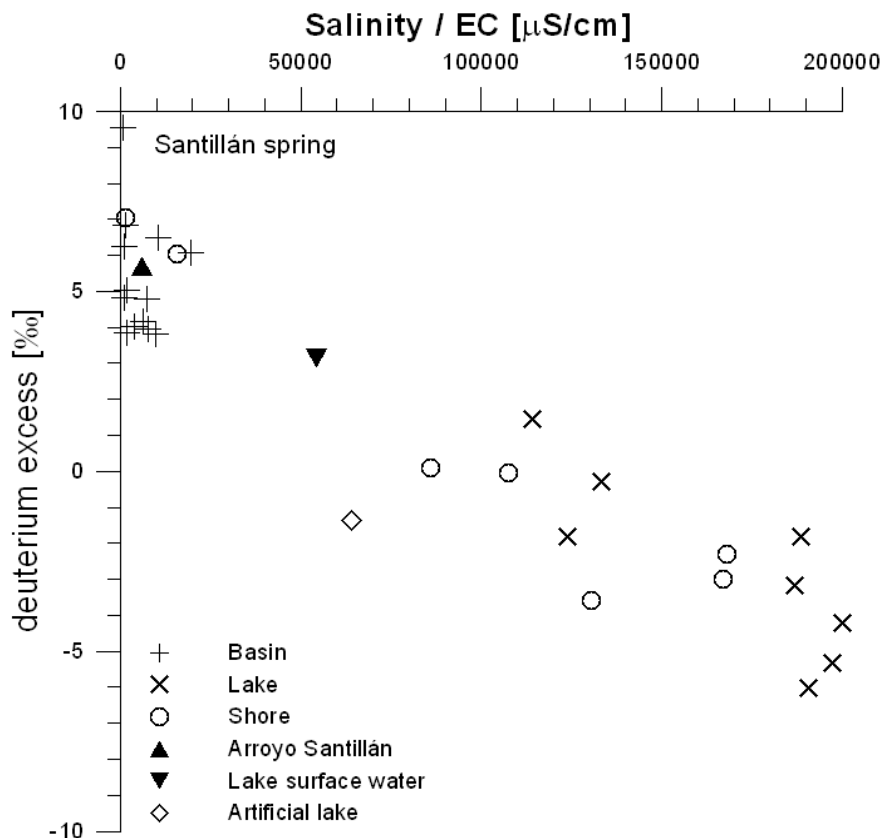


Figure 3.45: Deuterium excess data for Fuente de Piedra Basin.

Converting stable isotope data into "deuterium excess" is a useful way to show the extent of groundwater movement. The deuterium excess is defined by $\delta\text{D}-\delta^{18}\text{O}$ and the deviation compared to the MWL's deuterium excess of 10 yields information about the impact of evaporation (SIMMONS ET AL., 2002). A greater degree of evaporation is indicated by a more negative deuterium excess (Fig. 3.45). For Fuente de Piedra Basin the deuterium excess for regional groundwater is about 10 ‰, which corresponds to Atlantic influenced precipitation (CELLE-JEANTON, 2001), and for the lake brine about -10 ‰. The cluster of points with a deuterium excess from 3 to 7 ‰ represents the regional groundwater located in the northern area of the basin which is only marginally influenced by the salt lake brine. The deuterium excess for lake

brine is $< -5 ‰$ and indicates a greater influence of hypersaline water. Values ranging from -5 to $0 ‰$ represent various mixtures between regional groundwater and lake brine. After SIMMONS ET AL. (2002) mixing fractions can be calculated for any groundwater sample by using deuterium excess values of the end members. The two shore samples (sp08 and sp12) plotting among the basin samples representing superficial groundwater in wells SPFP06 and -08, which indicates a defined transition zone between lake brine and superficial groundwater.

3.2.2.2 Sulphate isotopes

The sampled wells are located at the present coastal line and show very high mineralized groundwaters with conductivities around 200

Table 3.19: Analysis of sulphate isotopes

Sample (weight of BaSO ₄)	$\delta^{18}\text{O}$ (‰) V-SMOW	$\delta^{34}\text{S}$ (‰) CDT
SP-FP-03 (18g)		14.8
SP-FP-14 (19g)		14.4
SP-FP-14 (4g)		14.2
SP-FP-14 (11g)	20.1	
SP-FP-03 (12g)	18.4	

mS/cm (SPFP03) and 180 mS/cm. Both wells are situated in gypsum clay material of salt lake sediments and have depth of 22 m (SPFP03) and 14 m (SPFP14). In Tab. 3.19 the analysis results of the sulphate isotopes $\delta^{18}\text{O}$ (V-SMOW) and $\delta^{34}\text{S}$ (CDT) are shown.

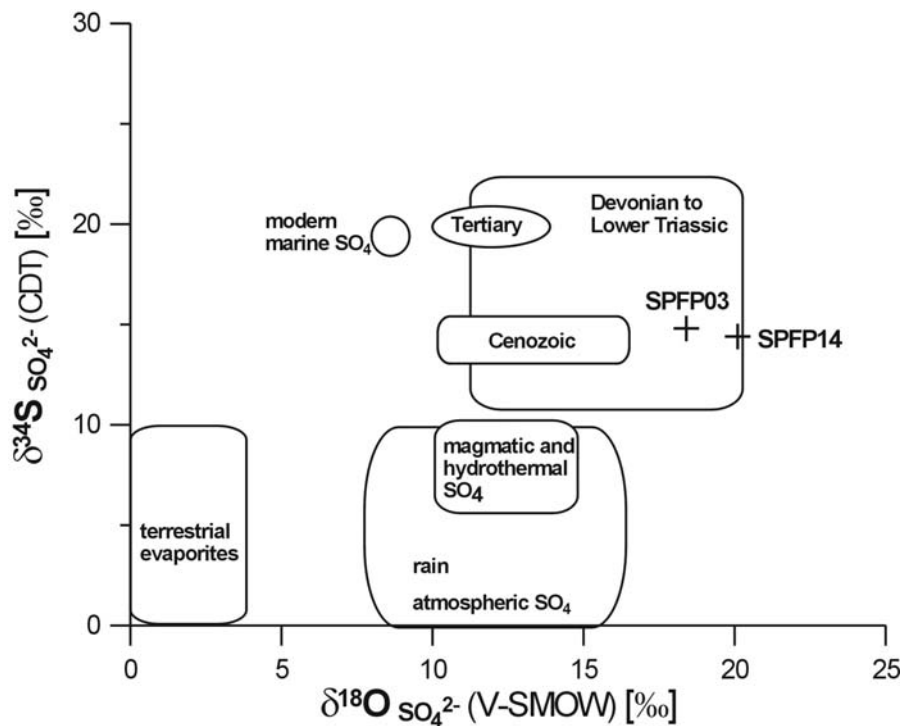


Figure 3.46: Isotope ratios of $\delta^{18}\text{O}_{\text{sulphate}}$ and $\delta^{34}\text{S}_{\text{sulphate}}$. (background isotope data derived from CLARK & FRITZ, 1997).

The isotopic signatures of sulphide and oxygen of the sulphates are relatively heavy according to modern marine SO_4^{2-} , terrestrial evaporites and atmospheric SO_4^{2-} . The values for $\delta^{18}\text{O}_{\text{sulphate}}$ (V-SMOW) range from 18 to 20 ‰ and for $\delta^{34}\text{S}_{\text{sulphate}}$ (CDT) from 14 to 15 ‰ and confirm the expected conclusion of a Triassic evaporite source (Fig. 3.46) of the SO_4 for well SPFP03 and -14.

In Fig 3.47 $\delta^{34}\text{S}$ is plotted against $\delta^{18}\text{O}$ and SO_4^{2-} respectively. On the basis of this assumption the isotope ratios of $\delta^{34}\text{S}_{\text{sulphate}}$ and $\delta^{18}\text{O}_{\text{sulphate}}$ do not show a shift from the primary composition, and for this reason an isotope fractionation due to sulphate reduction is not indicated. The analysis of the characteristic ions operating as indicator for reductive groundwater conditions accord the interpretation of sulphate isotopes.

For a more explicit interpretation with regard to reductive and oxidizing conditions further samplings in different depth of the groundwater story are required.

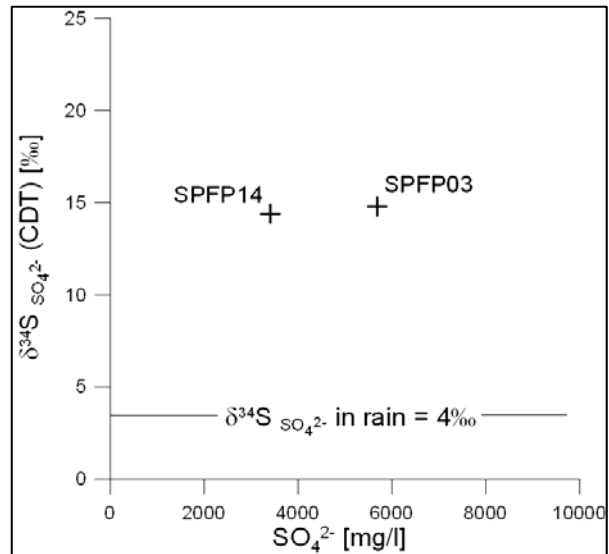


Figure 3.47: $\delta^{34}\text{S}_{\text{sulphate}} / \text{SO}_4^{2-}$ plot for Fuente de Piedra Basin (precipitation data from PEARSON & RIGHTMIRE, 1980).

3.2.3 Hydraulic pattern in Fuente de Piedra Basin

All piezometric data used here originate from the period February 2005 to March 2006. For the plausibility of water tables in a high saline aquifer, the freshwater heads were calculated for each site. The piezometric and freshwater heads are displayed in Tab. 3.20.

The water table is fluctuating over the year with maxima in spring and minima in autumn (Tab. 3.20 and Fig. 3.48). The highest water table is located in the northeast and observed in SPFP09, whereas the shallowest water table is located in the northern vicinity of the salt lake and observed for SPFP07. In autumn 2005 the water level in Fuente de Piedra Basin range from 446.30 m, observed in the Eastern margin in piezometer SPFP09, to 407.08 m observed north of the lake in piezometer SPFP07. In spring shallowest water tables migrate south in approximation to the lake level. Due to intensive agriculture and pumping in the hot dry month in the northern lake vicinity, the water table decreases comparatively very strong in this area (1.98 m). The

Table 3.20: Water table and calculated freshwater heads for field campaigns 2005-2006.

Site Id.	Density McCain [g/cm ³]	February 2005		Sept. / Oct. 2005		March / April 2006	
		Piezometric head [masl]	Freshwater head [masl]	Piezometric head [masl]	Freshwater head [masl]	Piezometric head [masl]	Freshwater head [masl]
SPFP03	1.158	408.56	411.88	407.43	410.57	408.39	411.68
SPFP05	1.145	409.08	414.70	407.71	413.13	408.87	414.46
SPFP06	1.063			411.13	412.48	412.62	414.07
SPFP07	1.002			407.02	407.08	408.99	409.06
SPFP08	1.078			413.23	424.10	413.74	424.65
SPFP09	1.078			446.30	451.95	446.40	452.06
SPFP10	1.000			427.12	427.25	429.50	429.63
SPFP14	1.108	409.12	410.64	408.58	410.05	408.89	410.38
SPFP15	1.043	408.40	408.92	407.97	408.47	408.33	408.84
SPFP17	1.003	408.96	409.00	408.22	408.25	408.73	408.76
SPFP21	0.999			428.04	428.06	459.36	459.42
SPFP22	1.000			430.43	430.50	430.20	430.27
SPFP23	1.001			407.83	407.83	421.68	421.72
SPFPFU22	1.154			407.42	409.65	408.25	410.61
SPFPFU23	1.146			407.68	407.77	408.71	408.96
SPFPFU24	1.048			407.31	407.39	408.81	408.97
SPFPFU26	1.068			407.49	407.56	408.55	408.69
SPFPFU27	1.004			408.30	408.31	408.78	408.80

inflow to the lake from eastern, western and southern margins is seasonally less fluctuating than in the north. In the eastern basin the water table change is variable for the piezometers SPFP09 (0.11 m), SPFP10 (2.38 m) and in case of SPFP22 the water table is actually rising during summer. This indicates the influence of local effects (pumping, irrigation) on the groundwater. Furthermore the distribution of temperature shows for these wells a constant groundwater flow.

Data for calculation of freshwater heads is shown in Tab. A10 and for calculation of density after MCCAIN (1991) in Tab. A12.

In considering of the multilevel piezometers, the seasonal change is greater for the shallow piezometers than for the deep, except for SPFP17/SPFPFU27 (see Fig. 3.48). This indicates a stronger groundwater flow in low depth beneath the surface, which is correlating with EC-logs and support the assumption of inhomogeneous horizontal permeabilities in different depths. Freshwater heads of multilevel piezometer shown in Fig. 3.48 may indicate an upward directed vertical flux component in the north-eastern lake margin. For a further conclusion environmental heads have to be calculated after Lusczynski (1961).

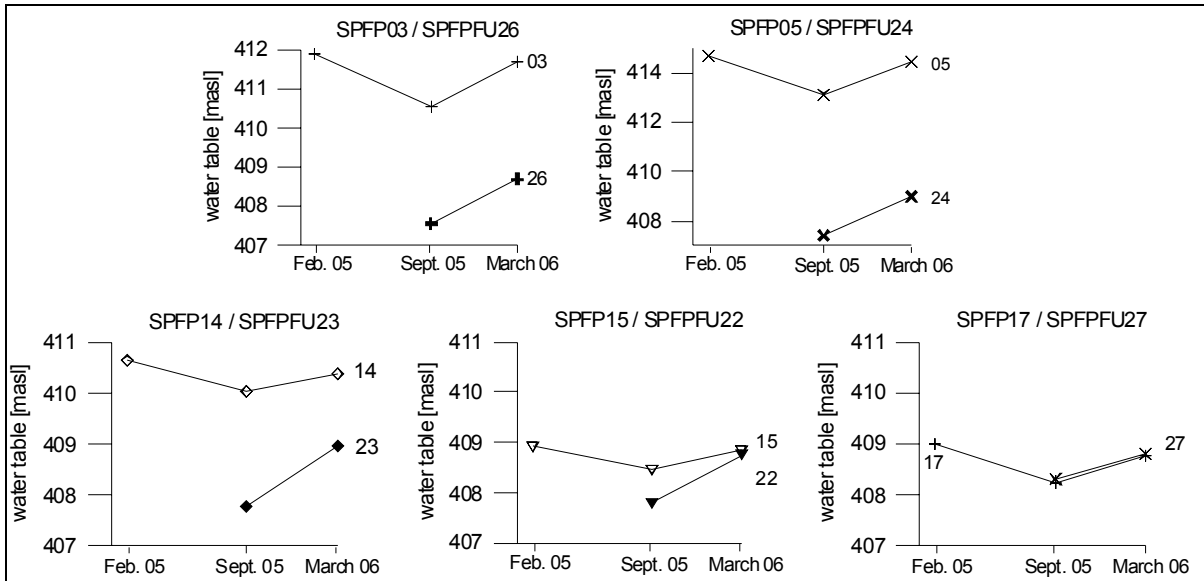


Figure 3.48: Hydrograph curves (freshwater heads) of multilevel piezometers for the period February 2005 to March 2006.

The water table rise in springtime compared to autumn is for the eastern shore site SPFPFU23 greater than for SPFP14, which attributes to an increased superficial groundwater flux into the lake. Water tables for northern shore wells SPFP03 and -05 and associated piezometers show nearly similar increases in spring compared to autumn.

Vertical gradients are calculated for the northern basin on the basis of freshwater heads. The groundwater flow is directed to the lake and gradients are ranging from 0.2 to 0.8 % (Tab. 3.21). Groundwater streaming from Nacimiento de Santillán (SPFP21) to the northern lake area (SPFP03) features the smallest gradient, whereas between SPFP03 and SPFP09 the steepest groundwater slope is observed. This indicates an inhomogeneous composition and spread of sediments in the north-eastern basin. However small flow gradients indicate a good permeability of the Fuente de Piedra Basin aquifer, especially in the northern part.

Table 3.21: Horizontal flow gradients for selected sites in Fuente de Piedra Basin.

Sites		Altitude difference [m]	Distance [m]	Gradient [%]
SPFP03	SPFP21	14.85	6098	0.24
SPFP03	SPFP10	14.04	2820	0.5
SPFP03	SPFP09	38.74	4868	0.8

3.3 Conclusions

The interaction between Salt lake and groundwater and the estimation of solute transport were the decisive aims for the realisation of this study.

On the basis of ion composition and ion relations sites can be classified as basin, lake shore and lake groups. Lake and shore group samples have the same ion relations, but differ in concentration possibly due to evaporative processes. Groundwater at the southern margin is not influenced by Salt lake brines; water chemistry varies in ion ratios significantly from Lake Group samples due to inflowing groundwater from east and west.

In the lake's vicinity Na-Cl type water dominates. Type water at the eastern basin is Ca-Cl₂ which indicates earth alkalisation and therefore a transition zone between salt- and freshwater which point to salinization of the aquifer by Na-Cl type water. This process is additionally indicated by Cl⁻ excess and ion ratios.

Cation exchange, earth alkalisation, is detected in all samples. Earth alkalisation signals at lake group samples does not originate from intruding saltwater into a freshwater aquifer but develops due to evaporative concentration of earth alkalised inflowing groundwater from the basin.

Chloride, Sodium and Magnesium are along with Sulphate responsible for the salinisation. Halite and Gypsum are the mainly leached salts as indicated by Cl⁻/Na⁺ and Cl⁻/SO₄²⁻ ratios. Gypsum is dissoluted at the basin group and precipitates at the lake group, which is also indicated by saturation indices. Saturation indices indicate precipitation of Calcite, Dolomite and Magnesite inside the maximum flooding area and at the south and north shore.

Cl⁻/Br⁻ ratio show a mixing of evaporative enriched water and leaching water and therefore mark multicomponent water.

Strong evaporative enriched isotope signatures of D and ¹⁸O in depth around 20 m at the margins of the Salt lake indicate a descent of brines originated in the Salt lake and their responsibility for salinization of the aquifer by mixing with freshwater.

Deuterium excess data show the mixing of freshwater from the north-eastern part of basin and Salt lake brine. The influence of the brine is decreasing with distance to lake, but groundwater samples of SPFP09 in the eastern basin still bearing traces of evaporative influence.

The progression of isotope ratios and salinity indicates that recycling of lake water is effecting the brine evolution.

For the source of salinity, Triassic evaporates are supposedly responsible. These evaporites are mainly located in the eastern basin and are observed due to hydro-chemical data in well SPFP09. Along the horizontal flow gradient this groundwater is streaming towards the salt lake. A groundwater flow across the overall aquifer thickness is observed in temperature and conductivity logs. However this groundwater flow is locally bound to certain levels in the direct proximity of the lake.

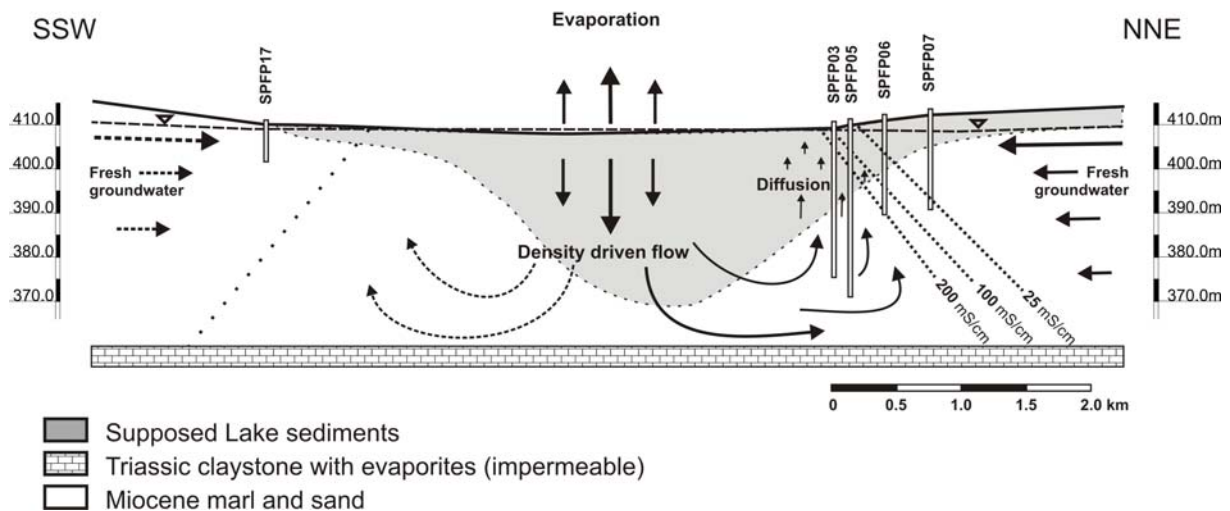


Figure 4.1: Schematic cross section of Fuente de Piedra Lake. Controlling processes on the flow regime in the salt lake and transition zone between brine/freshwater are shown. Deposit thicknesses are not full-scale.

Electric conductivity logs at a series of monitoring wells identify the existence of an interface between less and high mineralized water. A shallow brackish waterbody cover high saline water. With decreasing distance to the lake conductivity increases and the salt / freshwater transition zone is situated in lower depth, so that the distribution of conductivity shows the formation of a cone-shaped brine body beneath the Salt lake. This cone-shaped body can only be well defined by EC-logs in the northern part of the Salt lake. In Fig. 4.1 processes controlling the flow regime and the character of the transition zone between salt and freshwater are shown in a schematic cross section.

The transition zone in the southern and eastern lake margins is not considered as well-defined compared to the northern area. To give evidence about the development of a transition zone in the western margin additionally groundwater data are required.

A comparison with groundwater samples over time and depth shows a constant position of the salinity stratification. A movement of this stratification is only locally docu-

mented in low depth at the lake's edge. Increasing groundwater flow from east and an influence of evaporation on the arise of brines is associated with upraising.

Recovering times of initial groundwater stratifications show a high variability. Long time Re-establishment times of initial situation of the transition zone after pumping indicate low permeable sediments. Due to low permeability of fine grained lake sediments the ascent of brines must be very slow and is presumably partly driven by diffusion. In SPFP05 the horizontal groundwater flow is proved by short re-establishment times which specify relatively good permeabilities. Additional a surface close decrease in conductivity in spring 2006 indicates a lateral groundwater inflow. However re-establishment times of groundwater layerings after pumping for SPFP15 located at the lakes east margin in contrast to the lakes north margin indicate greater permeabilities and a main water supply of the lake by groundwater from east as well as borehole logs did.

4. Future prospects

Future prospects could include construction of piezometers in the western part of the basin and at the western shoreline to improve the spatial comprehension in this area. Modeling of density driven flow combined with gained conclusions of this study would advance understanding of hydraulics and hydrogeological settings. With more samples of Sulphate isotopes better comparison would be possible. Detailed chemical analysis of lake sediments with analysis of minerals and measurement of their amounts would help to verify the described mechanisms of precipitation and zoning of evaporites. By analysis of organic material from the lake's deeper sediments determination of age and therefore sedimentation rates should be feasible. Development of a better analysis method for sediments grain size distributions would be helpful to obtain more accurate coefficients of hydraulic conductivity. Better spatial conclusions could be made with additional borehole drillings inside the maximum flooding area concerning permeabilities, mineral composition and sediment thicknesses.

Abbreviations

°C	degree centigrade (Celsius scale)
‰	per mil
AAS	Atomic Absorption Spectroscopy
cond	specific electrical conductivity
(V)CDT	(Vienna) Canyon Diablo Troilite
cf	calciferous
D	Deuterium
d-excess	deuterium excess
EC	specific electrical conductivity
ET ₀	potential evapotranspiration
ET _A	actual evapotranspiration
FUB	Freie Universität Berlin
GMWL	Global Meteoric Water Line
IGME	Instituto Geologico y Minero España
masl	meter above sea level
max.	maximum
med.	medium, average
min.	minimum
MWL	Meteoric Water Line
SI	saturation index
temp	temperature in °C
UGR	Universidad Granada
vs.	versus
VSMOW	Vienna Standard Mean Ocean Water
WMMWL	Western Mediterranean Meteoric Water Line

- ALMECIJA RUÍZ C (1997). Estudio hidrológico e hidroquímico de los sistemas lagunares del norte de la provincia de Málaga. PhD (unedited), University of Granada, Granada. 518 pp.
- APPELO CAJ, POSTMA D (1993). *Geochemistry, Groundwater and Pollution*. Balkema, Rotterdam, Brookfield, 552 pp.
- BENAVENTE HERRERA J, CARRASCO CANTOS F (1985). Influence of Evaporite Karst in the streamwater quality of Guadalhorce river (Andalusia, Spain). 4 (XII) - Proc. Int. Symp. on Evaporite Karst, Le grotte d` Italia, 39-48
- BENAVENTE J, ALMÉCIJA C, CARRASCO F, RODRÍGUEZ-JIMÉNEZ P, CRUZ SAN JULIÁN JJ (1992). Reconocimiento hidroquímico de zonas endorreicas del Karst evaporítico de Antequera (Málaga). *Geogaceta* 12: 50-51
- BENAVENTE J, CARRASCO F, ALMÉCIJA C, RODRÍGUEZ-JIMÉNEZ P, CRUZ SAN JULIÁN J (1993). La zona de transición agua dulce-salmuera bajo el borde norte de la laguna de Fuente de Piedra (Málaga). *Geogaceta* 14: 6-8
- BENAVENTE J, ALMÉCIJA C, CARRASCO F (1994). Características físico-químicas de las aguas subterráneas en la proximidad da lagos salados. Algunos ejemplos del norte de la provincia de Málaga. Análisis y evolución de la contaminación de aguas subterráneas en España, Alcála de Henares, AIH-GE, t II: 111-122
- BENAVENTE J, CRUZ-SAN JULIÁN J, LINARES L (1996a). Use of groundwater for the maintenance of a protected wetland (Fuente de Piedra salt lake, Andalusia, Spain). *Wetlands: A Multiapproach Perspective. Hydrological and Ecological Studies applied to Wetlands Managment in Semiarid Climate*, Granada, Water Research Institute, University of Granada, 13-24
- BENAVENTE J, ALMÉCIJA C, CARRASCO F (1996b). Origin and significance of saline waters in the Antequera region (southern Spain). *Wetlands: A Multiapproach Perspective. Hydrological and Ecological Studies applied to Wetlands Managment in Semiarid Climate*, Granada, Water Research Institute, University of Granada, 55-68
- BENAVENTE J, REYES J, RODRÍGUEZ M (1998). Aporte de solutos por cursos superficiales a la laguna de Fuente de Piedra (Malága). *Geogaceta* 21: 51-54
- BENAVENTE J, RODRÍGUEZ-RODRÍGUEZ M, ALMÉCIJA RUIZ C (2003). Aguas subterranas salinas en el entorno de la laguna Fuente de Piedra: Revisión, Interrogantes y datos experimentales. In: *Tecnología de la intrusión de agua de mar en acuíferos costeros: Países mediterráneos*. 555-560
- BEYER W (1964). Zur Bestimmung der Wasserdurchlässigkeit von Kiesen und Sanden aus der Kornverteilung. *Wasserwirtschaft – Wassertechnik (WWT)* 14: 165-169
- BRIERE PR (2000). Playa, playa lake, sabkha: Proposed definitions for old terms. *J. Arid. Environ.* 45: 1-7
- BURROUGH A (1987). *Principles of Geographical Information Systems for Land Resources Assessment. Monographs on soil and resources survey*. Clarendon Press, Oxford, 193
- CALAFORRA JM, PULIDO-BOSCH A (1999). Gypsum karst features as evidence of diapiric processes in the Betic Cordillera, Southern Spain. *Geomorphology* 29: 251-264
- CARPENTER AB (1978). Origin and chemical evolution of brines in sedimentary basins. *Okl. Geol. Surv. Bull.* 79: 60-77
- CARRASCO F (1978). Variación de la salinidad de las aguas del río Guadalhorce. Influencia de la litofacies. *Tecniterrae* 22: 35-41
- CARRASCO F (1979). Captación de manantiales salinos subacuáticos en el fondo de embalses: manantial de Meliones. *Hidrogeol. y Rec. Hidraul.* IV: 465-479

- CARRASCO F (1986). Contribución al conocimiento de la cuenca alta del río Guadalhorce: el medio físico, hidrogeoquímica. PhD (unedited), University of Granada, Granada. 435 pp.
- CARRASCO F, BENAVENTE J (1986). Estimación de la aportación salina al río Guadalhorce en el sector Bobadilla-Gobantes (prov. Málaga). II Simp. Agua en Andalucía, Granada, I: 273-277,
- CASTELLÓN SERRANO L (1970). Sobre la sedimentación en la laguna salada de Fuente de Piedra. Tesis de Licenciatura, University of Granada, Granada. 82 pp.
- CELLE-JEANTON H, TRAVI Y, BLAVOUX B (2001). Isotopic typology of the precipitation in the Western Mediterranean region at three different time scales. *Geophys. Res. Lett.*, 28: 1215-1218
- CHAMBERS LA, TRUDINGER PA (1979). Microbiological fractionation of stable sulfur isotopes: a review and critique. *Geomicrobiology J.* 1: 249-293
- CLARK D, FRITZ P (1997). *Environmental Isotopes in Hydrogeology*. Lewis Publishers, Boca Raton, 328 pp.
- CLAYPOOL GE, HOLSER WT, KAPLAN IR, SAKAI H, ZAK I (1980). The age curves of sulfur and oxygen isotopes in marine sulfate and their mutual interpretation. *Chem. Geol.* 28: 199-260
- COLLINS AG (1975). *Geochemistry of oilfield waters*. Elsevier, Amsterdam, 496 pp.
- CONSEJERÍA DE AGRICULTURA Y PESCA (2006). <http://www.juntadeandalucia.es/agriculturaypesca/estacionesAgroclimaticas/ElEgirMedidas.jsp?CODPROVINCIA=29&CODESTACION=3&ORDEN=DESC&FECHAINI=21-11-2000&FECHAFIN=28-06-2006>. Visited: 29.06.06
- CUSTODIO E, LLAMAS MR (1983). *Hidrología Subterránea*. Omega, Barcelona, 1157 pp.
- DAVIS SN, DE WIEST RJM (1967). *Hydrogeology*. New York, 463 pp.
- DEIBEL K (1995). Grundwasserchemismus im Südosten von Mecklenburg-Vorpommern - Zur Unterscheidung anthropogener und geogener Einflüsse. *WWt* 1 (6/95): 35-42
- DEWEY JF, HELMAN ML, TURCO E, HUTTON DHW, KNOTT SD (1989). Kinematics of the western Mediterranean. In: Coward MP, Dietrich D, Park RG (eds) *Alpine Tectonics*. *Geol. Soc. Lon. Spec. Publ.* 45: 265-283
- DICHTL L, LINARES L, VALLE M (1986). Hidrogeología de la laguna de Fuente de Piedra y su entorno (prov. de Málaga). II. Simp. Agua en Andalucía, Granada, II: 357-366
- DIN/ISO 11277: 1994-06 (1994). Bodenbeschaffenheit - Bestimmung der Partikelgrößenverteilung in Mineralböden - Verfahren durch Sieben und Sedimentation nach Entfernen der löslichen Salze, der organischen Substanz und der Carbonate (ISO/ DIS 11277: 1994) - Soil quality - Determination of particle size distribution in mineral soil material - Method by sieving and sedimentation
- DIN 18130-1 (1989). Bestimmung des Wasserdurchlässigkeitsbeiwerts, Laborversuche
- DIN 4022-1: 1987-09 (1987). Subsoil and groundwater; classification and description of soil and rock; borehole logging of soil and rock not involving continuous core sample recovery (FOREIGN STANDARD)
- DIN 4049-3: 1994-10 (1994). Hydrologie - Teil 3: Begriffe zur quantitativen Hydrologie
- DIN 38409-H7: 1979-05 (1979). Bestimmung der Säure- und Basenkapazität

- DÚRAN JJ, VAL J (1984). El karst yesífero en España: condicionantes geológicos y problemática territorial, ambiental y geotécnica. Congreso Español de Geología, 1: 623-634
- DVWK (1983). Beiträge zu tiefen Grundwässern und zum Grundwasserwärmehaushalt. Grundlagen und Beispiele. Schriftenreihe des DVWK. Hamburg, 166 pp.
- FAN Y, DUFFY CJ, OLIVER DS (1997). Density-driven groundwater flow in closed desert basins: field investigations and numerical experiments. J. Hydrol. 196: 139-184
- FONTES JC, MATRAY JM (1993). Geochemistry and origin of formation brines from the Paris basin, France, 1: Brines associated with Triassic salts. Chem. Geol. 109: 149-175
- FRITZ P, LAPCEVIC A, MILES M, FRAPE SK, LAWSON DE, O'SHEA KJ (1988). Stable isotopes in sulphate minerals from the Salina formation in southwestern Ontario. Can. J. Earth Sci. 25: 195-205
- FÜCHTBAUER H (1988). Sedimente und Sedimentgesteine. Sediment-Petrologie. Schweizerbart, Stuttgart, 1141 pp.
- GARCÍA JIMÉNEZ CM (1991). Estudio de un medio acuático fluctuante: la laguna atalasoalina de Fuente de Piedra (Málaga). PhD (uneditado), University of Málaga, Málaga, 300 pp.
- GAT JR, CARMÍ I (1970). Evolution of the isotopic composition of atmospheric waters in the Mediterranean Sea area. J. Geophys. Res. 75: 3039-3048
- GEYH M (2001). Environmental Isotopes in the Hydrological Cycle Principles and Applications. IAEA, IV: Groundwater
http://www.iaea.org/programmes/ripc/ih/volumes/vol_four/cht_iv_05.pdf.
Visited 15.6.2006
- GHYBEN WB (1889). Nota in verband met de voorgenomen putboring nabij Amsterdam. Tijdschrift van het Koninklijk Inst. van Ingenieur (The Hague) 21: 8-22
- GIBBONS W, MORENO MT (2002). The geology of Spain. Geological Society. London, 649 pp.
- GREER DC (ed.) (1977). Desertic Terminal Lakes. Utah Water Research Laboratory, Utah State University, Logan, 448 pp.
- GRUBE A, WICHMANN K, HAHN J, NACHTIGALL KH (2000). Geogene Grundwasserversalzung in den Porengrundwasserleitern Norddeutschlands und ihre Bedeutung für die Wasserwirtschaft. Technologiezentrum Wasser Karlsruhe (TZW), Karlsruhe, 203 pp.
- GRUBER FJ, JOECKEL R (2005). Formelsammlung für das Vermessungswesen. 179 pp.
- GUTIÉRREZ F, ORTÍ F, GUTIÉRREZ M, PÉREZ-GONZÁLEZ A, BENITO G, GRACIA PRIETO J, DURÁN VALSERO JJ (2001). The stratigraphical record and activity of evaporite dissolution subsidence in Spain. Carbonates and Evaporites 16: 46-70
- GUTIÉRREZ F, ORTÍ F, GUTIÉRREZ M, PÉREZ-GONZÁLEZ A, BENITO G, GRACIA J, DURÁN JJ (2002). Paleosubsidence and active subsidence due to Evaporite dissolution in Spain. Carbonates and Evaporites 17: 121-133
- HARDIE LA, EUGSTER HP (1970). The evolution of closed basin brines. Miner. Soc. Am. Spec. Pap. 3: 273-290
- HARRASSOWITZ H (1933). Die alkalischen Quellen in ihrer geochemischen Bedeutung. Z. Kurortwiss. 2: 211-216
- HARVIE CE, WEARE JH, HARDIE LA, EUGSTER HP (1980). Evaporation of seawater: calculated mineral sequences. Science 208: 498-500

- HERCH A (1997). Untersuchungen zur hydrogeochemischen Charakteristik der Spurenelemente und Schwefelspezies im Aachener Thermalwasser. *Mittlg. Ingenieurgeol. Hydrogeol.* 64: 164 pp.
- HEREDIA DÍAZ J, ARAGUAS ARAGUAS L, RUIZ JM (2004). Use of environmental Tracers to characterize a complex system under variable Density conditions: Case of the subsurface brine of Fuente de Piedra (SW Spain). 18. SWIM, IGME, 1-14
- HEREDIA DÍAZ J, ARAGUAS ARAGUAS L, RUIZ JM (submitted). Definición del modelo conceptual del flujo del sistema hidrogeológico de densidad variable en la laguna de Fuente de Piedra, sur de España.
- HERRMANN AG, KNAKE D, SCHNEIDER J, PETERS H (1973). Geochemistry of Modern Seawater and Brines from Salt Pans: Main Components and Bromine Distribution. *Contr. Mineral. Petrol.* 40: 1-24
- HERZBERG B (1901). Die Wasserversorgung einiger Nordseebäder. *J. Gasbel. Wasservers.* 44: 815-819, 842-844
- HOEFS J (1997) *Stable Isotope Geochemistry*. Springer, Berlin, Heidelberg, New York, 201 pp.
- HÖLTING B (1970). Beiträge zur Hydrochemie der Tiefenwässer. *Z. dt. Geol. Ges.* 121: 19-44
- HÖLTING B (1996). *Hydrogeologie*. Ferdinand Enke Verlag, Stuttgart, 441 pp.
- HOLT BD (1991). Oxygen isotopes. In: Krouse HR, Grinenko VA (eds): *Stable Isotopes: Natural and anthropogenic sulphur in the environment*. Chichester, 55-64
- HOLZBECHER E (2005). Groundwater flow patterns in the vicinity of a salt lake. *Hydrobiologica* 532: 1-8
- HOTH P, SEIBT A, KELLNER T, HUENGES E (1997). Geothermie Report 97-1: *Geowissenschaftliche Bewertungsgrundlagen zur Nutzung hydrogeothermaler Ressourcen in Norddeutschland*. Scientific Technical Report. GFZ Potsdam, Potsdam, 149 pp.
- IGME (1986). *Mapa Geológico de España – Antequera 16-42: 1023*. 1:50 000. Madrid
- IGME (2001). Informe annual sobre la hidrogeología de la laguna de Fuente de Piedra. aguas.igme.es/zonas_humedas/laguna/medio_fisico/ev_piezo_lib99/pdf/lib99/in_03.pdf. Visited: 27.12.2005
- ITGE: LÓPEZ GETA J, RUBIO CAMPOS J, GONZÁLEZ RAMÓN A, LUQUE ESPINAR J, MORENO MERINO L, GÓMEZ LÓPEZ J, RODRÍGUEZ PADILLA J (1998). *Hidrogeología de la reserva natural de la laguna Fuente de Piedra (Málaga)*. 79 pp.
- JUNTA DE ANDALUCÍA (2003). *Ortofotografía digital en color*. Provincia de Málaga. DVD-ROM
- JUNTA DE ANDALUCÍA (2004) *Ortofotografía digital de Andalucía*. Provincia de Málaga. DVD-ROM
- JUNTA DE ANDALUCÍA (2005). *Modelo digital del terreno de Andalucía. Relieve y Orografía*. DVD-ROM
- KRAUSE HR (1987). Relationships between the sulphur and oxygen isotope composition of dissolved sulphate. In: *Studies on Sulfur Isotope Variations in Nature*. Panel Proc. Series, IAEA Vienna: 31-47
- KRAUSKOPF KB (1956). Factors controlling the concentrations of thirteen rare metals in sea-water. *Geochim. Cosmochim. Acta* 10: 1-32
- KROUSE HR, GRINENKO VA (1991). *Stable isotopes: natural and anthropogenic sulphur in the environment*. John Wiley & Sons, Chichester. 440 pp.

- KUNTZE H, ROESCHMANN G, SCHWERDTFEGER G (1994). *Bodenkunde*. Eugen Ulmer, Stuttgart, 424 pp.
- LA GAL LA SALLE C, HOWES N, HERZEG A (2006). <http://www.scieng.flinders.edu.au/cpes/research/hydrology/saltlakes.html>. Visited 30.11.07
- LAST WM, VANCE RE (1997). Bedding characteristics of Holocene sediments from salt lakes of the northern Great Plains, Western Canada. *J. Paleolimnology* 17: 297-318
- LEUCHS W (1988). Vorkommen, Abfolge und Auswirkungen anoxischer Redoxreaktionen in einem pleistozänen Porengrundwasserleiter. *Besond. Mitt. Dt. Gewässerk. Jahrb.* 25: 106 pp.
- LHENAFF R (1981). *Recherches geomorphologiques sur les Cordillères Bétiqes centro - occidentales (Espagne)*. PhD, University of Lille, Lille. 713 pp.
- LINARES L (1990). *Hidrogeología de la laguna de Fuente de Piedra (Málaga)*. PhD, University of Granada, Granada. 343 pp.
- LINARES L, ANDREO NAVARRO B, CARRASCO CANTOS F, FÉRNANDEZ DEL RÍO G (2002). El balance hídrico de la cuenca de Fuente de Piedra (Málaga) en un año húmedo (1997-98). *Geogaceta* 31: 95-98
- LINARES L, ANDREO NAVARRO B, CARRASCO CANTOS F, FERNÁNDEZ DEL RÍO G, VADILLO PÉREZ I (2001). La Escorrentía superficial en la cuenca de la laguna de Fuente de Piedra (Málaga) durante un año húmedo (1997-98). 195-198
- LINARES L, LOPEZ GETA JA, RUBIOS JC (1989). Consecuencias hidrologicas de la explotación de los acuíferos en la cuenca de Fuente de Piedra (Málaga). In: *La Sobreexplotación de Acuíferos*. 561-575
- LINARES L, RENDÓN MARTOS M (1998). La laguna de Fuente de Piedra (Málaga), un área edorreica de interés ecológico ligada al karst yesífero-salino. In: *Karst en Andalucía*. 165-172
- LINARES L, RIVERA A, TRENADO L (1986). Hidroquímica de los acuíferos de la cuenca de Fuente de Piedra (Málaga). II. *Simp. Agua en Andalucía, Granada, II*: 113-124
- LINARES L, VALLE M (1986). Relaciones entre la laguna de Fuente de Piedra y la piezometría de los acuíferos de la Cuenca (Málaga). II. *Simp. Agua en Andalucía, Granada, II*: 345-355
- LÖHNERT EP (1966). Die Beschaffenheit des tieferen Grundwassers und die Grenze Salzwasser / Süßwasser im Staatsgebiet von Hamburg. *Geol. Mitt.* 6: 29-36
- LUDEWIG H (1981). Zur Auswertung vom Temperaturmessungen im tiefen Grundwasser. *Z. dt. Geol. Gesell.* 132: 799-809
- LUSCZYNSKI NJ (1961). Head and flow of ground water of variable density. *J. Geophys. Res.* 66: 4247-4256
- MATRAY JM (1988). *Hydrochimie et géochimie isotopique des eaux de réservoir pétrolier du Trias et du Dogger dans de le bassin de Paris*. PhD, Université de Paris-Sud, Paris. 119 pp.
- MATTHES S (1993). *Mineralogie – Eine Einführung in die spezielle Mineralogie, Petrologie und Lagerstättenkunde*. Springer, Berlin, 461 pp.
- MATTHEß G (1994). *Die Beschaffenheit des Grundwassers*. Lehrbuch der Hydrogeologie Band 2. Gebr. Bornträger, Berlin-Stuttgart, 499 pp.
- MATTHEß G (2003). *Allgemeine Hydrogeologie – Grundwasserhaushalt*. Lehrbuch der Hydrogeologie Band 1. Gebr. Bornträger, Berlin-Stuttgart, 575 pp.
- MAZOR E (1997). *Chemical and isotopic groundwater hydrology*. Dekker, New York, 413 pp.

- MCCAIN WDJ (1991). Reservoir fluid property correlations - state of the art. SPE Reservoir Engineering 6: 266-272
- MEES F (1999). Distribution patterns of gypsum and kalistrontite in a dry lake basin of the southwestern Kalahari. Earth Surf. Proc. Landf. 24: 731-744
- MENGÍBAR JL, QUIRÓS R (1976). La Cueva de los Órganos. Jábega 16: 7-12
- MOLINA JA (1982). Los karst en yesos de la provincia de Málaga. Publicación conmemorativa 75 Anivers. Soc. Excurs. de Málaga, 95-112
- MUÑOZ F, GARCÍA AR (1983). Historia de Fuente de Piedra. 206 p. Madrid
- MYGAKOV VF, BURMISTOV DF (1964). Distribution of bromine in the carnallite beds of the Verkhnekamsk deposit. Geochem. Int. 1: 701-703
- ØDUM H, CHRISTENSEN W (1936). Danske Grundvandstyper og deres geologiske sptraeden. Danmarks Geol. Undersøg. Kopenhagen, 184 pp.
- OTTOW JC (1981). Mechanisms of bacterial iron reduction in flooded soils. In: Proc. Symp. Paddy Soil 1980, Inst. Soil Sci. Academia Sinica, Science Press, Springer, Berlin, 330-345
- PEARSON FJ, RIGHTMIRE CT (1980). Sulphur and oxygen isotopes in aqueous sulphur compounds. In: Fritz, P, Fontes J (eds.): Handbook of environmental geochemistry, 1: The terrestrial environment. Amsterdam, 227-258
- PEYRE Y (1974). Geologie d'Antquera et sa region (Cordilleres Bétiques, Espagne). PhD, University of Paris, Paris. 528 pp.
- PIPER AM (1944). A graphic procedure in the geochemical interpretation of water analyses. Trans. Amer. Geophys. Union 25: 914-928
- PITZER KS (1977). Electrolyte theory-improvements since Debye-Hückel. Acc. Chem. Res. 10: 371-377
- PITZER KS (1979). Theory: ion interaction approach. In: Pytokowicz RM (ed) Activity Coefficients in Electrolyte Solutions. 1: 157-208
- PLATT JP, VISSERS RLM (1989). Extensional collapse of thickened continental lithosphere: A working hypothesis for the Alboran Sea and Gibraltar arc. Geology 17: 540-543
- RENDÓN MARTOS M (1996). La laguna de Fuente de Piedra en la dinámica de la población de flamencos (*Phoenicopterus ruber roseus*) del Mediterráneo occidental. PhD, University of Málaga, Málaga. 369 pp.
- RENICK BC (1924). Base exchange in ground water by silicates as illustrated in Montana. US Geol. Surv. Water Supply Pap. 520: 53-72
- RIFFENBURG HB (1925). Chemical character of ground waters of the Northern Great Plains. US Geol. Surv. Water Supply Pap. 560: 31-52
- RITTENHOUSE G (1967). Bromine in oilfield waters and its use in determining possibilities in the origin of these waters. Bull. Am. Ass. Petr. Geol. 51: 2430-2440
- RODRÍGUEZ RODRÍGUEZ M, BENAVENTE HERRERA J, CRUZ SAN JULIÁN J, TORRES RUIZ F (2000). Análisis multivariable aplicado a datos hidroquímicos de las zonas húmedas de la provincia de Málaga. Geogaceta 28: 125-128
- RODRÍGUEZ-JIMÉNEZ P, CARRASCO F, BENAVENTE J, ALMÉCIJA C (1993). Mineralogía de los sedimentos de la laguna de Fuente de Piedra (provincia de Málaga). Geogaceta 14: 18-20
- RODRÍGUEZ-RODRÍGUEZ M, BENAVENTE HERRERA J, MORAL MARTOS F (2005). High Density Groundwater Flow, Major-ion Chemistry and Field Experiments in a Closed Basin: Fuente de Piedra Playa Lake (Spain). Am. J. Environ. Sci. 1: 164-171

- RODRIGUEZ-RODRIGUEZ M, BENAVENTE J, CRUZ SAN JULIAN JJ, MORAL MARTOS F (2006). Estimation of ground-water exchange with semi-arid playa lakes (Antequera region, southern Spain). *J. Arid Environ.* 66: 272-289
- RODRÍGUEZ-RODRÍGUEZ M, MORAL MARTOS F (2005). Cartografía geológica de la Reserva Natural Lagunas de Campillos. *Hidroquímica y dinámica hidrológica. Geogaceta* 37: 87-90
- SANFORD WE & WOOD WW (2001). Hydrology of the coastal Sabkhas of Abu Dhabi, United Arab Emirates. *Hydrogeol. J.* 9: 358– 366
- SCHOELLER H (1934). Les échanges des bases dans les eaux souterraines vadoses: trois exemples en Tunisie. *Bull. Soc. Géol. France* 4: 389-420
- SCHOELLER H (1935). Utilité de la notion des échanges des bases pour la comparaison des eaux souterraines. *Bull. Soc. Géol. France* 5: 651-657
- SCHOELLER H (1938). Notions sur la corrosion intere des canalisations d'eau. *Ann. Ponts et Chaussées Mém.* 8: 199-282
- SCHOELLER H (1962). *Les Eaux Souterraines*. Masson, Paris, 642 pp.
- SCHWILLE F (1955). Ionenumtausch und der Chemismus von Grund- und Mineralwässern. *Z. dtsh. Geol. Ges.* 106: 16-22
- SIEGENTHALER U (1979). Stable hydrogen and oxygen isotopes in the water cycle. In: Jaeger E (ed) *Isotope geology*. 265-273
- SIMMONS CT, NARAYAN KA (1997). Mixed convection processes below a saline disposal basin. *J. Hydrol.* 194: 263-285
- SIMMONS CT, NARAYAN KA, WOODING RA (1999). On a test case for density-dependent groundwater flow and solute transport models: the salt lake problem. *Water Resources Research* 35: 3607-3620
- SIMMONS CT, NARAYAN KA, WOODS JA, HERCZEG AL (2002). Groundwater flow and solute transport at the Mourquong saline-water disposal basin, Murray Basin, southeastern Australia. *Hydrogeol J.* 10: 278-295
- SMOOT JP, LOWENSTEIN TK (1991). Depositional environments of non-marine evaporites. In: Melvin JL (ed) *Evaporites, Petroleum and Mineral Resources. Developments in Sedimentology*. 50: 189-347
- STIFF HAJ (1951). The interpretation of chemical water analysis by means of patterns. *J. Petrol. Techn.* 3: Sect. 1: 15-16; Sect 2: 3
- STRAHLER A, STRAHLER A (1994). *Introducing Physical Geography*. John Wiley & Sons, Chichester, 537 pp.
- TESMER M, KÖHLER S, LORENZEN G (2006). Untersuchungen zur Genese und Dynamik der Grundwasserversalzung im Großraum Lübeck. F & E Vorhaben. Report. Free University of Berlin, Berlin, 228 pp.
- THOMAS L (1994). Hydrogeochemische Untersuchungen an den Ölfeldwässern aus NW-Deutschland und dem Oberrheingraben und ihre Modellierung unter dem Aspekt der Entwicklung eines Expertensystems für Fluid-Rock-Interactions (XPS FROCKI). PhD, Berliner Geowissenschaftliche Abhandlungen Reihe A. Selbstverlag Fachbereich Geowissenschaften, Berlin. 165: 167 pp.
- THORNTONWAITE CW (1948). An approach toward a rational classification of climate. *Geogr. Rev.* 38: 55-94
- THORNTONWAITE CW, MATHER JR (1955). The water balance. *Publ. Climat.* 8: 104 pp.
- VALJASHKO MG (1956). The geochemistry of bromine in halogenesis processes and the use of bromine content as a genetic and prospecting criterion. *Geochem. Int.* 1: 33-49
- WOODING RA, TYLER SW, WHITE I, ANDERSON PA (1997). Convection in groundwater below an evaporating salt lake. 2 - Evolution of fingers and plumes. *Water Resources Research* 33: 1219-1228

- YANAGISAWA F, SAKAI H (1983). Thermal decomposition of barium sulfate - vanadium pentoxide – silica glass mixtures for preparation of sulfur dioxide in sulfur isotope ratio measurements. *Anal. Chem.* 55: 985-987
- YECHIELI Y, WOOD WW (2002). Hydrologic Processes in saline systems: playas, sabkhas and saline lakes. *Earth-Science Rev.* 58: 343-365
- ZHEREBTSOVA IK, VOLKOVA NN (1966). Experimental study of the behaviour of microelements in the process of natural solar evaporation of Black Sea water and brine of lake Sasyk-Sivash. *Geochem. Int.* 4: 656-670